DESIGN AND DEVELOPMENT OF NOVEL SMALL MOLECULE INHIBITORS TARGETING TUBULIN AND AUTOTAXIN FOR CANCER THERAPY

By

Joshua Thammathong

A Thesis Submitted in Partial Fulfillment

of the Requirements for the Degree of

Master of Science in Chemistry

Middle Tennessee State University

2025

Thesis Committee:

Dr. Souvik Banerjee

Dr. Kevin Bicker

Dr. Scott Handy

Acknowledgements

I would like to thank my family who have given me the support and encouragement I needed when I was going through my rock bottom lows and my mightiest highs throughout this degree. I would also like to thank my fellow classmates for giving me the support to keep pushing with this degree and not giving up on it.

I also want to thank Dr. Banerjee for giving me the opportunity to work on these projects, being able to work together for the past 5 years and being my mentor throughout my academic life. I also thank Dr. Weissmiller and her lab for our collaboration together on the tubulin paper and for teaching me more about the biological aspects of research. I also want to thank Dr. Bicker and Dr. Handy for being patient with me throughout these years, for the times when I needed help when I could not find a solution and the times where I thought I was at my wits end. I would also like to thank Dr. Iriarte-Gross for allowing me to volunteer for TGIS and be a part of WI-STEM.

I would like to thank my senior lab members for the time we spent together in the lab. Christopher Clark was the first friend I made when I moved to Tennessee. He showed around the Murfreesboro area and has been great at coming up with ideas when the lab equipment was not working. Prateek Rai and Tanya Garain have both been wonderful people to meet and talk to; being able to bounce ideas back and forth with each other while allowing me to bother them with any of the absurd questions that I had, as well as providing support when times got rough.

I would also like to thank the Department of Chemistry, the Department of Graduate Studies, as well as the S-STEM program and MTI-Go, for helping with funding this degree and the projects during this time.

ABSTRACT

Overcoming drug resistance remains a critical barrier in the effective treatment of many cancers. Resistance to chemotherapeutic agents—such as tubulin inhibitors—significantly reduces treatment efficacy and contributes to relapse and poor patient outcomes. This work addresses this challenge through two complementary strategies aimed at disrupting key mechanisms of cancer survival and resistance.

First, a series of novel fused imidazopyridine and imidazopyrazine analogues were designed, synthesized, and evaluated for their ability to act as colchicine-binding site inhibitors (CBSIs). These compounds demonstrated potent inhibition of cancer cell viability, disrupted tubulin polymerization, and interfered with cell division and cytoskeletal integrity, supporting their function as intracellular tubulin inhibitors with the potential to overcome resistance to existing microtubule-targeting agents. Second, the study explores the role of the Autotaxin–lysophosphatidic acid (ATX–LPA) signaling axis, a pathway increasingly implicated in promoting tumor survival, immune evasion, and resistance to chemotherapy and radiation. A focused library of 21 pyrazolo[5,1-b]quinazolin-8(4H)-one compounds targeting ATX was synthesized and screened. Two lead compounds exhibited low micromolar IC_{50} values in comparison to the known ATX inhibitor BMP-22, underscoring the importance of specific functional groups in retaining inhibitory potency.

By targeting both microtubule dynamics and resistance-promoting lipid signaling pathways, this work proposes a dual-acting therapeutic strategy to combat drug-resistant cancers and lays a foundation for the development of more effective treatment options.

TABLE OF CONTENTS

Chapter I

LIST OF TABLES

Chapter I

LIST OF SCHEMES

Chapter I

Chapter II

LIST OF FIGURES

Chapter I

Chapter II

CHAPTER I

Fused Imidazopyrazine-Based Tubulin Polymerization Inhibitors Inhibit Neuroblastoma Cell Function

1.A. Introduction

α and β-tubulin dimers make up the extremely dynamic intracellular structures known as microtubules (MTs), which are essential to many basic cellular functions such as spindle pole formation, cell division, and cytoskeleton maintenance.[1-4] The polymerization and depolymerization of tubulin dimers are necessary for the construction and deconstruction of MTs.[5-7] Given that MTs are intimately involved in proper cell division, disruption of MT dynamics has been a well-established approach in anticancer therapy.[8-11] Taxanes, vinca alkaloids, and epothilones are three primary types of tubulin inhibitors that have been widely utilized to treat cancer clinically.[6, 7, 12] However, the effectiveness of these medications in the clinic is frequently constrained by the emergence of multidrug resistance (MDR), peripheral neuropathy, and constrictive therapeutic indices.[13-19] As such, targeting of the colchicine binding site, located at the interface of the α and β-tubulin dimer, has gained attention as a novel tubulin inhibition approach that may overcome these challenges.

The small molecule named colchicine and other small compounds that bind to the colchicine site prevent tubulin dimers from polymerizing and forming useful microtubules.[3, 20] Colchicine binding site inhibitors (CBSIs) consequently show significant cytotoxicity in a variety of experiments.[21-23] Importantly, unlike colchicine, small molecule CBSIs are known to be less susceptible to drug resistance mechanisms, including efflux transporters and β3 tubulin overexpression mediated MDR.[4, 20] However, the significant adverse effects against normal cells, low solubility, and low oral bioavailability of small-molecule CBSIs have limited their practical applicability.[24, 25] Thus, in recent years, there has been extensive research on developing new

classes of CBSIs with wider therapeutic window, including PAT[26], SAIs[27] (substituted-2-aryl imidazoles), ABI (2-aryl-4-benzoyl-imidazoles)[28], SMART (4-substituted methoxybenzoyl-aryl-thiazoles)[29], and verubulin[9, 20] (**Figure 1A**). In human melanoma and prostate cancer xenograft models, the SMART, ABI, and PAT analogues demonstrate extremely potent *in vivo* effectiveness.[29] However, it has been observed that the carbonyl group linking the B and C rings in ABI and SMART counterparts makes them metabolically unstable.[30, 31] New fused 1H - imidazo[4,5-c]pyridine analogues (**Figure 1B**) were reported to improve metabolic stability with moderate $t_{1/2}$ values (45 to 56 min) against human liver microsome.[30] Thus, in an attempt to derive new colchicine-site tubulin polymerization inhibitors with improved metabolic stability while enhancing or retaining potency, we designed a series of fused imidazo[1,2-a]pyridine and pyrazine analogues (**Figure 1B**). Imidazo[1,2-a]pyridine and pyrazine scaffolds are known have broad range of applications in medicinal chemistry, including anticancer, antiviral, and antimicrobial activities.[32] Therefore, these new series of compounds were tested for their efficacy against a panel of two neuroblastoma cell lines with *MYCN* amplification. Neuroblastoma is one of the most prevalent extracranial solid cancers in children and infants.[33] Amplification of the *MYCN* gene, which encodes the N-MYC oncoprotein transcription factor, is associated with high-risk cases and metastasis, resulting in poor prognosis and a higher fatality rate.[34] Because of this, *MYCN* amplification is associated with advanced disease and failure to respond to chemotherapy. Importantly, as it relates to this study, tubulin inhibitors such as vincristine are commonly used as a chemotherapeutic agent to treat neuroblastoma.[35, 36] Additional pre-clinical studies are also actively being performed using colchicine binding site inhibitors.[37] Unfortunately, vincristine-resistance is common in neuroblastoma patients[36, 38] and not all tubulin inhibitors are yet effective against neuroblastoma. Although novel therapies to treat neuroblastoma have been proposed or are

progressing to phase I and/or phase II clinical trials, their true impact is yet to be determined.[39-41] Thus, there remains a demand in improving current therapeutics used to treat this childhood cancer. Here, we report the design, synthesis, and biological evaluation of new fused imidazopyridine and pyrazine CBSIs against two *MYCN* amplified neuroblastoma cell lines. Our findings demonstrate that fused imidazopyrazine analogues inhibit both neuroblastoma cell viability and *in vitro* tubulin polymerization. Additional experimental evidence suggests that these analogues can also block cell division and disrupt cytoskeletal structures within cells suggesting that at least some of these analogues can act as *bona fide* tubulin inhibitors within cells.

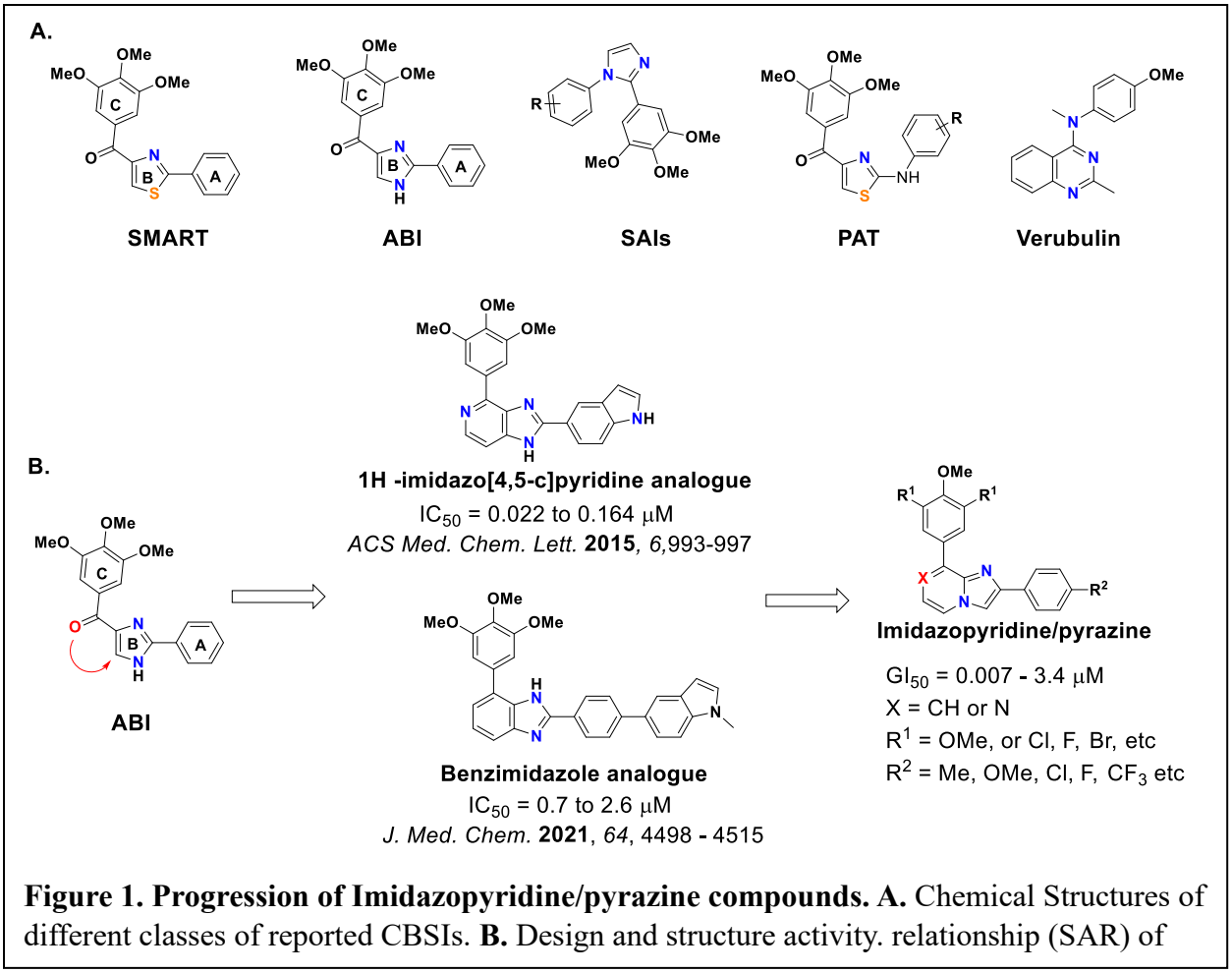

Figure 1. Progression of Imidazopyridine/pyrazine compounds. A. Chemical Structures of different classes of reported CBSIs. **B.** Design and structure activity. relationship (SAR) of

1.B. Results and Discussion

1.B.1. Synthesis and cytotoxicity screening

First, we synthesized six fused imidazo[1,2-a]pyridine analogues with fused A and B rings as demonstrated in **Scheme 1**. We started with commercially available para-substituted α-bromoacetophenone (**1**) and allowed it to react with commercially available 3-bromo-5-substituted-pyridine-2-amine derivatives (**2a-2b**) in presence of scandium (III) triflate catalyst and acetonitrile as a solvent to obtain the imidazo[1,2-a]pyridine core (**3a-3f**) with para-substituted C-ring. Finally, 3,4,5-trimethoxyphenyl ring (ring-D) was installed using a Suzuki coupling to achieve the desired imidazo[1,2-a]pyridine derivatives. This first set of compounds was evaluated for their ability to decrease cell viability in the Kelly and CHP-134 *MYCN*-amplified neuroblastoma cell lines over the course of three days. Commercially available colchicine was included as a comparison. Sensitivity of cells to each compound, including colchicine, was assessed by calculating the GI_{50} across cell lines monitored. As reported in **Table 1**, the para-methyl substituent on C-ring was most tolerated making **4a** the most potent (GI_{50} ~ 200 nM) compared to **4b-4f**. Neither the activating methoxy substituent nor the deactivating halogen substituents (Cl or F) at para position of ring-C were tolerated resulting in deterioration in GI_{50}. Compound **4f** with a methyl substituent on the 6-position lost cellular potency, though, not to the same extent as **4b**, **4c**, and **4d**.

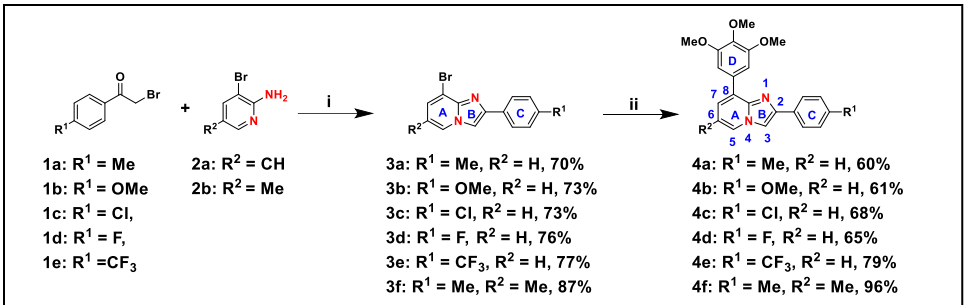

Scheme 1. Synthesis of imidazo[1,2-a]pyridine analogues.

Next, we synthesized the reverse imidazo-pyridine analogue **4g** following **Scheme 2** to assess the effect of location of nitrogen atoms in the imidazopyridine core on cellular activity. Cell viability screening demonstrated that location of nitrogen atoms in the core is crucial and N-1 nitrogen on the same side as trimethoxy phenyl ring is imperative for biological efficacy (**Table 1**). Finally, we synthesized six imidazo[1,2-a]pyrazine analogues following **Scheme 3** for comparison.

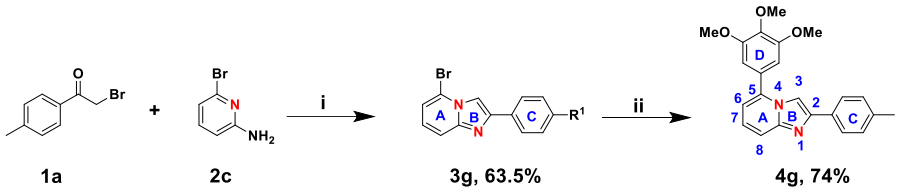

i. $Sc(OTf)_3$, ACN (sol) 80^{O}C, 16 hrs; ii. 3,4,5-trimethoxyphenylboronic acd, $Pd(PPh_3)_4$, dioxane (sol), reflux, 16 hrs.

Scheme 2. Synthesis of reverse imidazopyridine derivative.

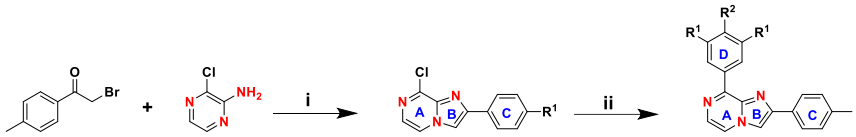

4h: $R^1 = R^2 = R^3 = OMe$, 63.4%
4i: $R^1 = R^2 = F$, $R^2 = H$, 78%
4j: $R^1 = R^2 = F$, $R^2 = OMe$, 78%
4k: $R^1 = R^2 = Cl$, $R^2 = OMe$, 61%
4l: $R^1 = R^2 = Br$, $R^2 = OMe$, 44%
4m: $R^1 = R^2 = Cl$, $R^2 = F$, 68%

i. $Sc(OTf)_3$, ACN (sol) 80^{O}C, 16 hrs; ii. 3,4,5-trimethoxyphenylboronic acd, $Pd(PPh_3)_4$, dioxane (sol), reflux, 16 hrs.

Scheme 3. Synthesis of imidazo[1,2-a]pyrazine derivatives

Our goal in the comparison was to assess the effect of the N-7 nitrogen of the imidazopyrazine core, as well as different substituents at 3,4, and 5 positions of ring-D on the biological efficacy. Cell viability screening showed that the N7 nitrogen on the imidazopyrazine core and 3,4,5-trimethoxyphenyl D-ring enhances cellular potency and compound **4h** was as potent as colchicine in decreasing cell viability with an average GI_{50} of ~ 10 nM (**Table 1**). Additional

structure-activity relationship results indicate that the dichloromethoxyphenyl ring-D was well-tolerated resulting in compound **4k** having a double digit nanomolar efficacy against CHP-134 cell line and that at least one methoxy group at the 4-position of ring-D is important yielding **4j,** which is significantly more active than **4i**. Surprisingly, **4l**, with bulkier dibromomethoxyphenyl ring-D, was found to be detrimental to antiproliferative activity. These findings indicate that combination of imidazo[1,2-a]pyrazine core with trimethoxyphenyl ring-D (**4h**) is the best followed by dichloromethoxyphenyl (**4k**), difluoromethoxyphenyl (**4j**), and difluorophenyl (**4i**) ring-D.

Table 1. Antiproliferative activities of fused-imidazopyridine and imidazopyrazine analogues in neuroblastoma cancer cell lines. The *MYCN*-amplified Kelly and CHP-134 neuroblastoma cells were treated with a nine-point serial dilution of each compound for 3 days. Cell viability was determined by CellTiter-Glo assay. All values were normalized to DMSO-treated cells and then used to calculate a GI_{50} value. GI_{50} values are shown with the standard error of the mean. The values "> 5.00" and "> 2.50" mean that this was the highest dose (μM) tested and this dose did not decrease cell viability below 50%.

Compounds	GI_{50} (μM)	
	Chp-134	Kelly
4a	0.152 ± 0.043	0.217 ± 0.046
4b	0.511 ± 0.119	1.371 ± 0.291
4c	1.623 ± 0.310	3.420 ± 0.450
4d	1.611 ± 0.365	2.995 ± 0.415
4e	2.088 ± 0.483	> 5.000
4f	0.381 ± 0.089	0.717 ± 0.136
4g	3.320 ± 0.865	4.915 ± 1.276
4h	0.007 ± 0.002	0.012 ± 0.002
4i	0.474 ± 0.108	0.438 ± 0.081
4j	0.175 ± 0.038	0.402 ± 0.102
4k	0.079 ± 0.017	0.165 ± 0.048
4l	0.469 ± 0.101	0.504 ± 0.129
4m	> 2.500	> 2.500
Colchicine	0.008 ± 0.002	0.009 ± 0.002

1.B.2. Tubulin polymerization inhibition assay

To determine if the compounds with the lowest GI_{50} values across both cell lines were capable of inhibiting tubulin polymerization, we tested compounds **4a**, **4h**, **4j**, and **4k** in an *in vitro* tubulin polymerization assay using purified tubulin. Colchicine was used as a control to inhibit and destabilize microtubule formation, while paclitaxel was used as a microtubule enhancer control. All four compounds sampled inhibited tubulin polymerization comparably and were as effective as colchicine in destabilizing microtubule formation (**Figure 2**). The overall cell viability and *in vitro* tubulin polymerization results suggest that many of the imidazo[1,2-a]pyrazine class of compounds (**4h**, **4j**, **4k**, and **4l**) may be capable of tubulin inhibition as their mechanism of action.

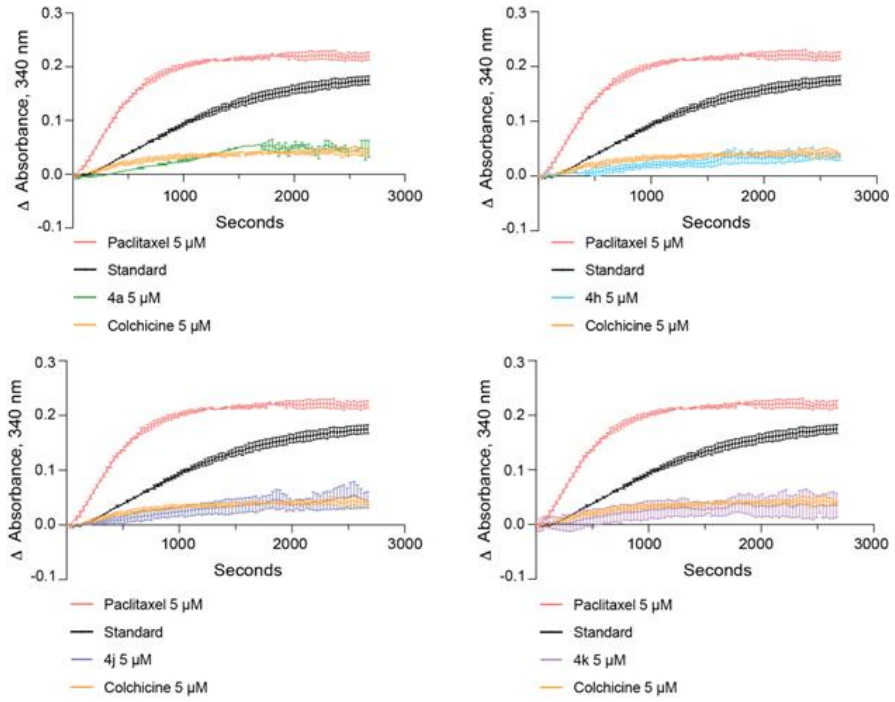

Figure 2. Compounds inhibit tubulin polymerization *in vitro*. *In vitro* tubulin polymerization was monitored in the absence of any compound ("standard"), with the addition of 5 μM paclitaxel, 5 μM colchicine, or 5 μM of the indicated compounds. The same curve generated from the standard, paclitaxel, and colchicine reactions are superimposed on all four graphs for comparison with each of the indicated compounds. All compounds tested inhibit microtubule formation as compared to the standard and colchicine reactions.

1.B.3. Cell cycle analysis

To specifically compare their ability to act as tubulin inhibitors within neuroblastoma cells we tested whether compound treatment inhibits the process of mitosis, a cellular activity dependent on active microtubule dynamics, by performing cell cycle phase distribution

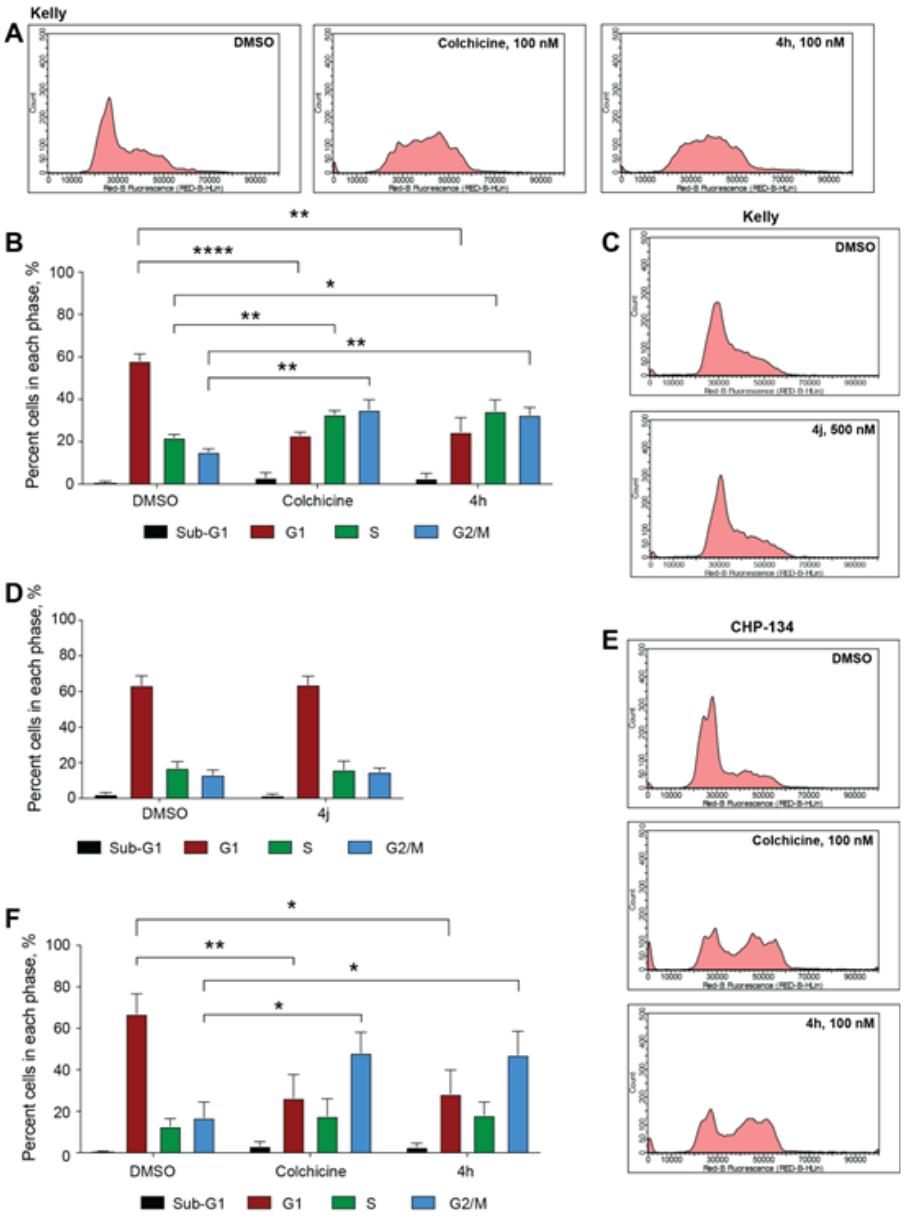

Figure 3. Cell cycle progression is impaired with compound 4h. A. Cell cycle profile images of Kelly cells treated with DMSO, 100 nM colchicine, or 100 nM compound **4h** for 24 hr. **B.** Quantification of cell cycle phase distributions for cells treated as in (A). **C.** Cell cycle profile images of Kelly cells treated with DMSO or 500 nM compound **4j** for 24 hr. **D.** Quantification of cell cycle phase distributions for cells treated as in (C). **E.** Cell cycle profile images of CHP-134 cells treated with DMSO, 100 nM colchicine, or 100 nM compound **4h** for 24 hr. **F.** Quantification of cell cycle phase distributions for cells treated as in (E). (n = 3 biological replicates, error bars are standard error, **P = 0.0089, *P < 0.019 using unpaired t-test, two-tailed).

analysis. In Kelly cells, a 24 hr treatment with 100 nM compound **4h** revealed that this compound mirrors colchicine in its ability to block cell cycle progression and promote an accumulation of cells in the G2/M phase of the cell cycle (**Figure 3A, B**). Interestingly, compound **4j** did not cause any overt changes in cell cycle phase distribution, even at a 500 nM dose (**Figure 3C, D**). In CHP-134 cells, compound **4h** was also as effective as colchicine (**Figure 3E, F**) and the overall effect was similar to that of Kelly cells, suggesting that **4h** acts as an anti-mitotic in these neuroblastoma cells.

1.B.4. Effect of top compounds on mitotic markers

As a second approach to compare the impact on cell cycle progression, we analyzed the level of two proteins that increase in cells during mitosis—cyclin B1 and histone 3 phosphorylated at serine residue 10 (p-S10 H3)—and therefore can act as mitotic markers [42, 43]. In both Kelly and CHP-134 cells, compound **4h** mirrored colchicine in its ability to induce an increase in the level of both cyclin B1 and p-S10 H3 compared to the dimethyl sulfoxide (DMSO) vehicle control (**Figure 4**), indicative of these two compounds causing an enrichment of the cell population in the mitotic phase. In line with cell cycle phase distribution analysis (**Figure 3C, D**), protein levels of both mitotic markers following treatment with compound **4j** were not overtly different in comparison to DMSO-treated

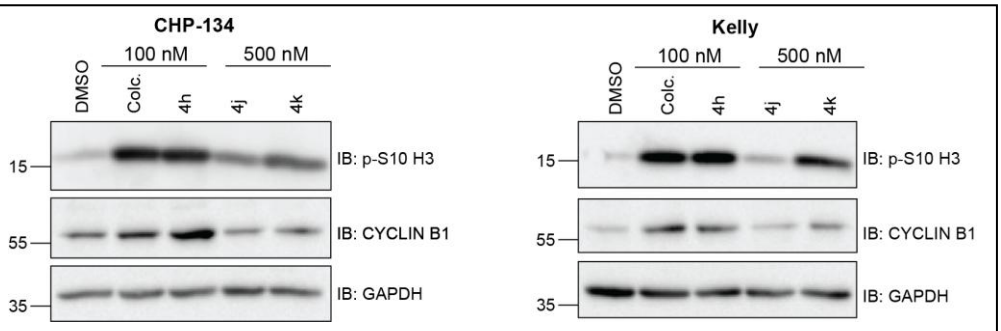

Figure 4. Compounds cause induction of mitotic protein markers. Western blot of protein lysates collected following treatment of indicated cells with DMSO, 100 nM colchicine, 100 nM compound **4h**, or 500 nM compound **4j** and **4k** for 24 hr. GAPDH is used as a loading control.

cells (**Figure 4**). However, in both cell lines, compound **4k** treatment resulted in a moderate increase in level of both mitotic markers, which was present in each cell line, suggesting that compound **4k** may function as a weaker mitotic inhibitor than compound **4h** and colchicine.

1.B.5. Immunofluorescence staining

Microtubule dynamics are also important in maintaining cytoskeletal structures within cells grown in culture. Therefore, we examined the ability of compounds **4h**, **4j**, and **4k** to disrupt the microtubule network using immunofluorescence. We first focused these experiments on Kelly cells due to their larger cytoplasmic area for visualization. DMSO treatment, followed by immunostaining for α-tubulin, revealed an intact microtubule network that extended from the cell nuclei, which were co-stained with DAPI. Colchicine treatment, as expected, caused a dramatic disruption to the microtubule

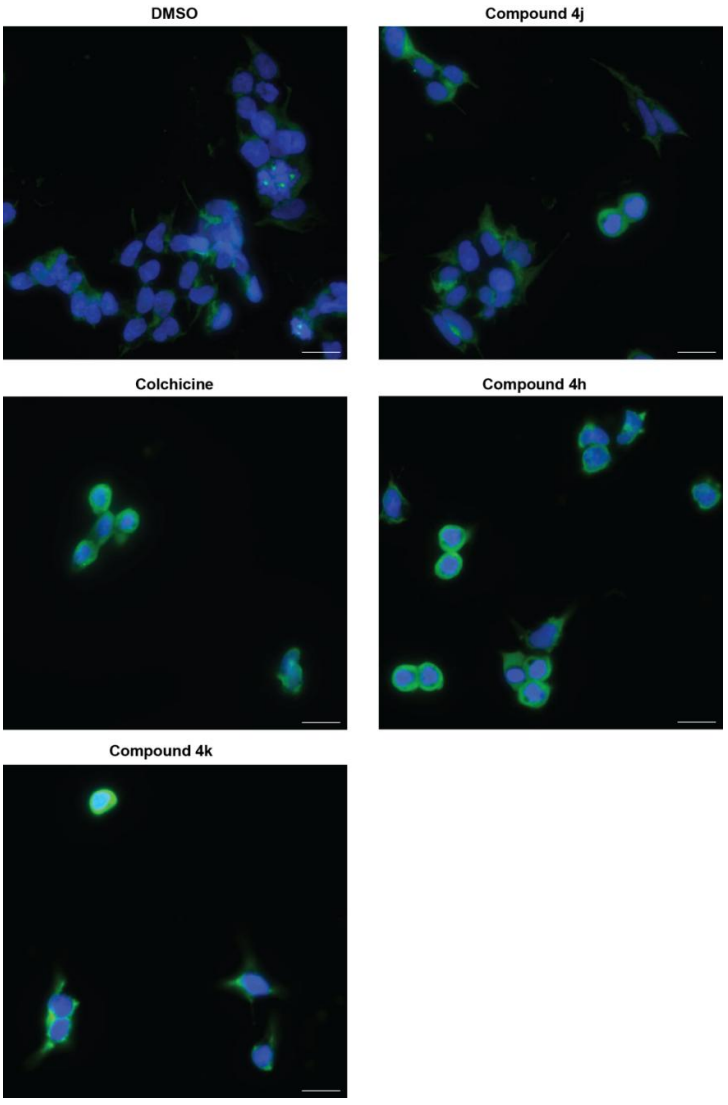

Figure 5. Intracellular tubulin is impacted by compound treatment. Immunostaining images of Kelly cells treated with DMSO, 100 nM colchicine, 100 nM compound **4h**, or 500 nM compound **4j** and **4k** for 24 hr. Nuclei are stained with DAPI in blue and α-tubulin is stained with Alexa-488 in green. Scale bar = 20 μm

network with tubulin compacting around the nuclei of cells, indicative of the rounded morphology cells acquire when microtubule dynamics are impacted [44]. Compound **4h** was as effective as colchicine at promoting the same effect, indicating again that compound **4h** mirrors the effects of colchicine (**Figure 5**). Consistent with the cell cycle phase distribution assay and mitotic marker analysis, compound **4k** showed a moderate effect on disruption of the microtubule network and compound **4j** appearing closer to DMSO-treated cells than those treated with colchicine. As a second point of confirmation, we also visualized tubulin in another *MYCN*-amplified cell line, Be(2)C, which also shows high cellular sensitivity to **4h**, **4j**, and **4k** (**Table 1**) and has a large cytoplasmic area for visualization. Compared to Kelly cells, the response of Be(2)C cells was very similar and tubulin compaction was evident with **4h** and **4k**, compared to colchicine (**Figure 1**).

Overall, these results indicate that compound **4h** functions as a potent tubulin inhibitor in *MYCN*-amplified neuroblastoma cells. In addition, these results suggest that other compounds containing an imidazo[1,2-a]pyrazine scaffold structure, such as compound **4k** (**Table 1**), may function as less potent but effective inhibitors of tubulin.

1.B.6. *In vitro* metabolic stability of top compounds

To determine if compounds **4h**, **4j**, and **4k** differ in their metabolic stability, each was evaluated in a human liver microsomal assay. As shown in **Table 2**, compounds **4k** and **4j** have improved stabilities ($t_{1/2}$ ~

Table *2*. *In vitro* human liver microsomal stability. The half-lives of indicated compounds in human liver microsomes are shown with standard deviation of the mean. The value > 60 means that this was the longest time point (min) tested and the sample was almost intact.

Compound	*t*1/2 (min)
4h	25.99 ± 0.4
4j	36.1 ± 1.0
4k	51.96 ± 1.15
Colchicine	> 60
Verapamil	26.3 ± 1.35

52 min and 36 min, respectively) than compound **4h** ($t_{1/2}$ ~ 26 min), indicating that addition of the 3,4,5-trimethoxyphenyl D-ring improves cellular potency but reduces metabolic stability.

1.B.7. Molecular modeling studies

To gain further insight into structure-activity relationships of the biologically evaluated hits, a molecular docking analysis was performed to envisage binding interactions within the

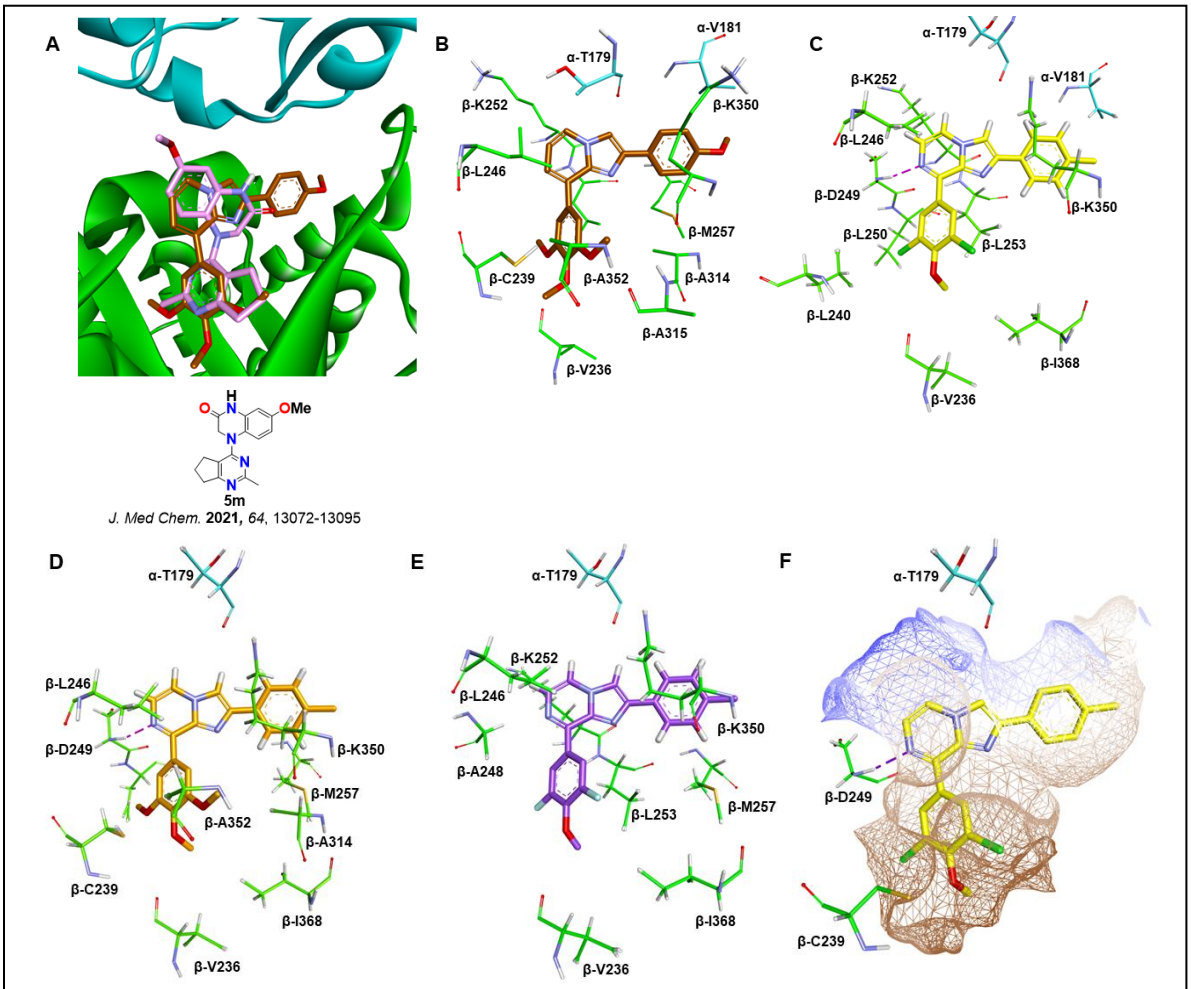

Figure 6. **Molecular docking. A**. Docking of **4b** (brown) at the colchicine binding site of tubulin (PDB: 6X1F). α-tubulin monomer is shown in cyan and β-tubulin monomer is shown in green. Native ligand (SB-216/5m) is shown in pink. **B**. Amino acid residues within 5Å of the docked ligand **4b**. **C**. Docked pose of **4k** (yellow) at the colchicine binding site. **D**. Docked pose of **4h** (gold) at the colchicine binding site. **E**. Docked pose of **4j** at the colchicine binding site. **F**. Binding surface (hydrophobic) around the ligand **4k**. Hydrogen bonding has been shown by purple dotted line.

colchicine binding site. As demonstrated in **Figure 6**, compound **4b** (imidazopyridine) binds nicely at the colchicine binding while overlapping well with the native ligand **5m** (PDB: 6X1F, **Figure 6A**). It is evident from **Figures 6A** and **6B** that **4b** is occupying deep within the hydrophobic β-tubulin pocket consisting of amino acid residues of Cys239, Val236, Leu240, Ala314, Ala352, Ile316, Met257, Leu253, Leu240, and Leu246. The imidazopyridine core is located close to the α-Thr179, and α-Val181 residues suggesting that the molecule is binding at the colchicine binding site, which is at the interface of α- and β-tubulin monomer of α- and β-tubulin heterodimer. **Figure 6C** and **6D** show that the N-7 nitrogen of imidazo[1,2-a]pyrazine core of **4k and 4h** form hydrogen bonding (2.29 Å and 2.23 Å respectively) with the β-Asp249 NH backbone. However, this hydrogen bond is not observed with **4j** (**Figure 6E**). Taken together, the docking results suggest that **4h** and **4k** may bind at the colchicine binding site with higher binding affinity resulting in an enhanced inhibitory effect against tubulin polymerization.

We also carried out MD simulation of the top two compounds, **4h** and **4k**, in complex with tubulin to assess their binding stabilities. Root mean square deviation (RMSD) of protein and ligand movement were analyzed

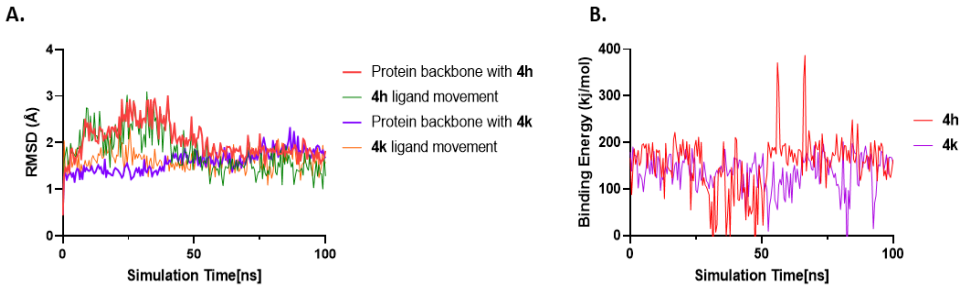

Figure 7. **RMSD and binding energy time plot for 4h and 4k. A.** RMSD vs simulation time plot for (**A**) protein backbone atoms with **4h** as ligand in red, movement of **4h** in its binding site in green, protein backbone atoms with **4k** as ligand in purple, and movement and **4k** in its binding site in orange. **B**. Binding energy of protein-ligand interactions of colchicine binding site of tubulin with **4h** and **4k**. Binding energy was calculated by analyzing MD trajectory using the BoundaryFAST method in YASARA. Based on the YASARA algorithm, hinger binding energy values means stronger binding.

(**Figure 7A**). The protein structure's conformational flexibility is represented by the RMSD, and higher deviations denote a more flexible protein structure. The MD simulation of tubulin-**4h** system (red) shows a sudden increase in RMSD value for the backbone and eventually stabilizes at an average 2.03 Å around 50 ns. Tubulin-**4k** complex demonstrates a gradual increase in RMSD value and finally stabilizes at 1.59 Å around 50 ns. The backbone RMSD calculations of the tubulin-ligand complexes suggest that ligand binding seems to decrease backbone flexibility of tubulin. We also analyzed ligand movement RMSD values for **4h** (green, **Figure 7A**) and **4k** (orange, **Figure 7A**). As evident from **Figure 7A**, both ligands maintain a closer proximity with the binding site over the course of simulation. Binding free energy calculations demonstrate that **4h** has higher average binding energy (red, **Figure 7B**, 153.44 $\pm$ 5.8 kj/mole) than **4k** (purple, **Figure 7B**, 135.46 $\pm$ 3.7 kj/mole) suggesting stronger binding of **4h** to the colchicine binding site.

1.C. Conclusion

In summary, we designed and synthesized a series of novel fused imidazopyridine and pyrazine CBSIs and evaluated their efficacy against two neuroblastoma cell lines with increased levels of N-MYC, a potent transcription factor implicated in diverse types of cancers.[45] Among this series, the imidazo[1,2-a]pyrazine class of compounds showed best potency in cell viability assays (compound **4h**, **4j**, **4k**, and **4l**). Mechanism of action studies support that this class of compounds can inhibit tubulin polymerization *in vitro* and **4h**, along with **4k**, have the ability to impair microtubule-dependent processes in cells. Interestingly, although **4h**, **4k**, and **4j** can each inhibit tubulin polymerization *in vitro* (**Figure 2**), **4j** fails to promote robust tubulin inhibition in cells. This discrepancy may be due to the use of purified tubulin in the *in vitro* assay, a form of tubulin that most likely does not fully resemble tubulin *in vivo*, which may be bound by other proteins or cargoes or have access restricted depending on the state of the cell. Additional evidence from molecular docking, MD simulation, and metabolic stability assays help to refine the structure-

activity relationship, showing that a combination of imidazo[1,2-a]pyrazine core with trimethoxyphenyl ring-D (**4h**) results in highest cellular activity and stronger binding to the colchicine binding site compared to combination with a dichloromethoxyphenyl (**4k**) or difluoromethoxyphenyl (**4j**) ring-D. Importantly, however, while **4k** and **4j** show less potency and weaker binding, they have significantly improved metabolic half-lives. Future studies that aim to optimize these lead compounds should prove useful in identifying novel compounds that have improved metabolic stability while retaining cellular potency.

1.D. Experimental protocols

1.D.1 Chemistry- General Methods

All nonaqueous reactions were performed in oven-dried glassware under an inert atmosphere of dry nitrogen. All the reagents and solvents were purchased from Aldrich (St. Louis, MO), Alfa-Aesar (Ward Hill, MA), Combi-Blocks (San Diego, CA), Ark Pharm (Libertyville, IL) and used without further purification. Analytical thin-layer chromatography was performed on silica gel GHLF 10 cm × 20 cm Analtech TLC Uniplates (Analtech, Newark, DE) and were visualized by fluorescence quenching under UV light. Combiflas flash chromatography purification system (Teledyne) was used to purify the compounds. ^{1}H NMR and ^{13}C NMR spectra were recorded on a JEOL spectrometer (500 MHz). Chemical shifts are reported in ppm on the δ scale and referenced to the appropriate solvent residual peaks ($CDCl_3$, 7.26 ppm for ^{1}H and 77.23 ppm for ^{13}C; DMSO-d6, 2.50 ppm for ^{1}H and 39.51 ppm for ^{13}C). High resolution mass spectrometer (HRMS) data were acquired on a Waters Synapt G1 HDMS high-definition mass spectrometer system. Porcine brain tubulin (catalog no. T238P) was purchased from Cytoskeleton, Inc. The purity of all tested compounds was determined to be ≥95% by ^{1}H NMR and HPLC. The HPLC method used to determine purity is as follows: Compound purity was analyzed using a

Thermo-Fisher UltiMate 3000 instrument with a Restek Ultra C18 5µM column (250 x 4.6 mm). Mobile phases consist of water with 0.1% formic acid (A) and acetonitrile with 0.1% formic acid (B). A flow rate of 0.6 mL/min was used. The run was conducted over a timespan of either 45 or 60 minutes, with solution A at 100% elution for 5 minutes. Solution B was then slowly increased to 100% in gradience in 30 mins. Solution B stayed at 100% elution for another 20 minutes for pyrazine-based samples. Solution B was then set to 0% elution while increasing Solution A to 100% for 5 minutes. Compound purity was monitored with a UV detector set at 254 nm.

1.D.2. Chemical synthesis

General Procedure for the Preparation of 3a-3h. A solution of 3-bromopyridin-2-amine analogue (**2a** or **2b**, 1 eq), or 6-bromopyridine-2-amine (**2c**, 1 eq), or 3-chloropyrazine-2-amine (**2d**, 1 eq) with 2-bromo-1-(4-substitutedphenyl) ethane-1-one **(1a-1e**, 1.2 eq) in anhydrous acetonitrile was placed in a three necked round bottom flask under argon atmosphere. Catalytic amount of Scandium (III) triflate (0.05 eq.) was added, and the reaction was refluxed at 85-95°C over the night. The reaction was then cooled to room temperature and transferred to a single neck round bottom flask. Acetonitrile was evaporated to dryness using a rotary evaporator. The remaining solid inside the round bottom flask was then transferred into a separatory funnel upon dissolving in ethyl acetate (30-50 mL). The ethyl acetate layer was washed with water (3 X 50 mL), organic layer was collected, dried over $MgSO_4$, and evaporated under reduced pressure to provide access to the crude. Crude was then purified using flash chromatography (ethyl acetate/hexanes: 3: 10) providing access to pure product.

Synthesis of 8-bromo-2-(p-tolyl) imidazo[1,2-a]pyridine (3a). Compound **3a** was synthesized following the general procedure to prepare intermediates **3a-3h**. An amount of 200 mg of 3-bromopyridin-2-amine (1.15 mmol) and 295 mg of 2-bromo-1-(p-tolyl) ethan-1-one (**1a**,

1.39 mmol) in presence of catalytic amount of scandium (III) triflate yielded 230 mg of pure product (0.80 mmol, 70%) as a white solid upon purification (30% EtOAc/hexanes). ^{1}H NMR (500 MHz, DMSO-d6) δ 8.77 – 8.20 (m, 2H), 7.98 – 7.66 (m, 2H), 7.55 (dd, J = 8.0, 3.3 Hz, 1H), 7.32 – 7.04 (m, 2H), 6.96 – 6.49 (m, 1H), 2.32 (s, 3H). ESI-MS: $[C_{14}H_{12}BrN_2]^+$ calculated: 287.0184, observed: 287.0283.

Synthesis of 8-bromo-2-(4-methoxyphenyl) imidazo[1,2-a] pyridine (3b). Compound **3b** was synthesized following the general procedure to prepare intermediates **3a-3h**. An amount of 200 mg of 3-bromopyridin-2-amine (1.15 mmol) and 318 mg of 2-bromo-1-(4-methoxyphenyl) ethan-1-one (**1b**, 1.39 mmol) in presence of catalytic amount of scandium (III) triflate yielded 255 mg of pure product (0.84 mmol, 73%) as a white solid upon purification (30% EtOAc/hexanes). ^{1}H NMR (500 MHz, $CDCl_3$) δ 8.07 (ddd, J = 6.7, 3.3, 1.9 Hz, 1H), 8.02 – 7.69 (m, 3H), 7.55 – 7.33 (m, 1H), 7.11 – 6.83 (m, 2H), 6.77 – 6.49 (m, 1H), 3.84 (s, 3H). ESI-MS: $[C_{14}H_{12}BrN_2O]^+$ calculated: 303.0133, observed: 303.0688.

Synthesis of 8-bromo-2-(4-chlorophenyl) imidazo[1,2-a] pyridine (3c). Compound **3c** was synthesized following the general procedure to prepare intermediates **3a-3h**. An amount of 200 mg of 3-bromopyridin-2-amine (1.15 mmol) and 324 mg of 2-bromo-1-(4- chlorophenyl) ethan-1-one (**1c**, 1.39 mmol) in presence of catalytic amount of scandium (III) triflate yielded 260 mg of pure product (0.84 mmol, 73%) as a white solid upon purification (30% EtOAc/hexanes). ^{1}H NMR (500 MHz, $CDCl_3$) δ 8.10 (dd, J = 6.7, 1.1 Hz, 1H), 8.01 – 7.67 (m, 3H), 7.61 – 7.29 (m, 3H), 6.77 – 6.48 (m, 1H). ESI-MS: $[C_{13}H_9BrClN_2]^+$ calculated: 306.9638, observed: 307.0137.

Synthesis of 8-bromo-2-(4-fluorophenyl) imidazo[1,2-a] pyridine (3d). Compound **3d** was synthesized following the general procedure to prepare intermediates **3a-3h**. An amount of 200 mg of 3-bromopyridin-2-amine (1.15 mmol) and 302 mg of 2-bromo-1-(4- fluorophenyl)

ethan-1-one (**1d**, 1.39 mmol) in presence of catalytic amount of scandium (III) triflate yielded 252 mg of pure product (0.87 mmol, 76%) as a white solid upon purification (30% EtOAc/hexanes). ^{1}H NMR (500 MHz, $CDCl_3$) δ 8.10 (dd, J = 6.7, 1.1 Hz, 1H), 8.00 – 7.92 (m, 2H), 7.88 (d, J = 0.9 Hz, 1H), 7.44 (dd, J = 7.3, 1.0 Hz, 1H), 7.16 – 7.07 (m, 2H), 6.66 (dd, J = 7.4, 6.7 Hz, 1H). ESI-MS $[C_{13}H_9BrFN_2]^+$ calculated: 290.9933, observed: 291.0395.

Synthesis of 8-bromo-2-(4-(trifluoromethyl) phenyl)imidazo[1,2-a]pyridine (3e). Compound **3e** was synthesized following the general procedure to prepare intermediates **3a-3h**. An amount of 200 mg of 3-bromopyridin-2-amine (1.15 mmol) and 371 mg of 2-bromo-1-(4-fluorophenyl) ethan-1-one (**1e**, 1.39 mmol) in presence of catalytic amount of scandium (III) triflate yielded 300 mg of pure product (0.88 mmol, 77%) as a white solid upon purification (30% EtOAc/hexanes). ^{1}H NMR (500 MHz, $CDCl_3$) δ 8.63 – 8.08 (m, 3H), 8.00 (d, J = 5.0 Hz, 1H), 7.68 (d, J = 8.9 Hz, 2H), 7.47 (d, J = 7.3 Hz, 1H), 6.89 – 6.54 (m, 1H). ESI-MS $[C_{14}H_9BrF_3N_2]^+$ calculated: 340.9901, observed: 341.0241.

Synthesis of 8-bromo-6-methyl-2-(p-tolyl) imidazo[1,2-a] pyridine (3f). Compound **3f** was synthesized following the general procedure to prepare intermediates **3a-3h**. An amount of 200 mg of 2-amino-3-bromo-5-methylpyridine (1.1 mmol) and 277 mg of 2- bromo-1-(p-tolyl) ethan-1-one (**1a**, 1.3 mmol) in presence of catalytic amount of scandium (III) triflate yielded 310 mg of pure product (1.0 mmol, 87%) as a white solid upon purification (30% EtOAc/hexanes). ^{1}H NMR (500 MHz, $CDCl_3$) δ 8.09 – 7.78 (m, 3H), 7.77 (s, 1H), 7.30 – 7.09 (m, 3H), 2.37 (s, 3H), 2.28 (s, 3H). ESI-MS $[C_{15}H_{14}BrN_2]^+$ calculated: 301.0340, observed: 301.0613.

Synthesis of 5-bromo-2-(p-tolyl) imidazo[1,2-a] pyridine (3g). Compound **3g** was synthesized following the general procedure to prepare intermediates **3a-3h**. An amount of 200 mg of 2-amino-6-bromopyridine (1.15 mmol) and 294 mg of 2-bromo-1-(p-tolyl) ethan-1-one (**1a**,

1.38 mmol) in presence of catalytic amount of scandium (III) triflate yielded 210 mg of pure product (0.73 mmol, 63.5%) as a white solid upon purification (30% EtOAc/hexanes). ^{1}H NMR (500 MHz, $CDCl_3$) δ 7.95 (dd, J = 9.3, 4.4 Hz, 2H), 7.31 (t, J = 8.4 Hz, 1H), 6.76 (dd, J = 8.6, 4.6 Hz, 1H), 6.47 (dd, J = 9.3, 4.6 Hz, 1H), 5.69 (s, 1H), 4.96 – 4.49 (m, 2H), 2.44 (s, 3H). ESI-MS $[C_{14}H_{12}BrN_2]^+$ calculated: 287.0184, observed: 287.0907.

Synthesis of 8-chloro-2-(p-tolyl) imidazo[1,2-a] pyrazine (3h). Compound **3h** was synthesized following the general procedure to prepare intermediates **3a-3h**. An amount of 500 mg of 2-amino-3-chloropyrazin (3.9 mmol) and 1 gm of 2-bromo-1-(p-tolyl) ethan1-one (**1a**, 4.7 mmol) in presence of catalytic amount of scandium (III) triflate yielded 750 mg of pure product (0.31 mmol, 79.5%) as a white solid upon purification (30% EtOAc/hexanes). ^{1}H NMR (500 MHz, $CDCl_3$) δ 8.08 – 7.93 (m, 2H), 7.90 (dd, J = 8.1, 2.0 Hz, 2H), 7.66 (dd, J = 5.7, 4.0 Hz, 1H), 7.27 (d, J = 8.2 Hz, 3H), 2.41 (s, 3H). ESI-MS $[C_{13}H_{11}ClN_3]^+$ calculated: 244.0642, observed: 244.1124.

General Procedure for the Preparation of 4a-4m. A solution of intermediate compound (**3a-3h**), 3,4,5-trisubstitutedphenylboronic acid (1.2 eq.), K_2CO_3 (4.0 eq.) and Pd (0) $[PPh_3]_4$ (.05 eq) in purged dioxane (22.5 mL dioxane and 7.5 mL DI-H_2O, purged with Argon) was refluxed at 85-95˚C overnight under Argon atmosphere. The reaction was then cooled to room temperature and then transferred to a round bottom flask. Dioxane was evaporated under a high vacuum. The remaining solid inside the round bottom flask was then transferred into a separatory funnel with ethyl acetate. The ethyl acetate layer was washed with DI-H_20 multiple times, the organic layer was then transferred into an Erlenmeyer flask, dried over $MgSO_4$, and evaporated to dryness. The solid was then purified by using flash column chromatography with a solution of ethyl acetate and hexanes to obtain pure product.

Synthesis of 2-(p-tolyl)-8-(3,4,5-trimethoxyphenyl) imidazo[1,2-a] pyridine (4a). Compound **4a** was synthesized following the general procedure to prepare compounds **4a-4m**. A solution of 100 mg **3a** (0.35 mmol), 89 mg of 3,4,5-trimethoxyphenylboronic acid (0.42 mmol), 193.5 mg (1.4 mmol) of K_2CO_3, 47 mg of Pd (0) $[PPh_3]_4$ in dioxane was refluxed to obtain the crude product. An amount of 80 mg (60%, 0.21 mmol) of pure product was obtained as a light brown wax after purification (30% EtOAc/hexanes, Rf = 0.3). ^{1}H NMR (500 MHz, $CDCl_3$) δ 8.08 (d, J = 6.7 Hz, 1H), 7.89 (s, 3H), 7.52 (s, 2H), 7.36 – 7.00 (m, 3H), 6.83 (t, J = 6.9 Hz, 1H), 3.96 (d, J = 25.3 Hz, 9H), 2.39 (s, 3H). ^{13}C NMR (126 MHz, $CDCl_3$) δ 153.18, 137.81, 131.96, 131.18, 129.46, 126.00, 124.54, 122.23, 112.46, 108.25, 106.53, 61.03, 56.34, 21.42. HRMS $[C_{23}H_{23}N_2O_3]^+$ calculated: 375.1709, observed: 375.1703. HPLC purity: 98.04% (Rt = 28.4 min)

Synthesis of 2-(4-methoxyphenyl)-8-(3,4,5-trimethoxyphenyl) imidazo[1,2-a] pyridine (4b). Compound **4b** was synthesized following the general procedure to prepare compounds **4a-4m**. A solution of 100 mg **3b** (0.33 mmol), 85 mg of 3,4,5-trimethoxyphenylboronic acid (0.4 mmol), 182.4 mg (1.32 mmol) of K_2CO_3, 47 mg of Pd (0) $[PPh_3]_4$ in dioxane was refluxed to obtain the crude product. An amount of 77 mg (61%, 0.2 mmol) of pure product was obtained as a light brown wax after purification (30% EtOAc/hexanes, Rf = 0.22). ^{1}H NMR (500 MHz, $CDCl_3$) δ 8.18 – 8.00 (m, 1H), 7.99 – 7.88 (m, 2H), 7.84 (d, J = 2.0 Hz, 1H), 7.50 (d, J = 2.0 Hz, 2H), 7.30 (dt, J = 7.1, 1.0 Hz, 1H), 7.04 – 6.90 (m, 2H), 6.90 – 6.66 (m, 1H), 3.98 (s, 6H), 3.92 (s, 3H), 3.84 (s, 3H). ^{13}C NMR (126 MHz, $CDCl_3$) δ 159.64, 153.19, 145.69, 144.34, 138.40, 131.98, 129.56, 127.35, 126.77, 124.47, 122.18, 114.17, 112.40, 107.69, 106.55, 61.03, 56.36, 55.41. HRMS $[C_{23}H_{23}N_2O_4]^+$ calculated: 391.1658, observed: 391.1652. HPLC purity: 96.47% (Rt = 27.74 min)

Synthesis of 2-(4-chlorophenyl)-8-(3,4,5-trimethoxyphenyl) imidazo[1,2-a] pyridine (4c). Compound **4c** was synthesized following the general procedure to prepare compounds **4a-4m**. A solution of 100 mg **3c** (0.325 mmol), 82.7 mg of 3,4,5-trimethoxyphenylboronic acid (0.39 mmol), 179.7 mg (1.3 mmol) of K_2CO_3, 47 mg of Pd (0) $[PPh_3]_4$ in dioxane was refluxed to obtain the crude product. An amount of 87 mg (68%, 0.22 mmol) of pure product was obtained as an off white solid after purification (30% EtOAc/hexanes, Rf = 0.27). MP = 137.0 – 138.8 ˚C. ^{1}H NMR (500 MHz, $CDCl_3$) δ 8.10 (dd, J = 6.7, 1.2 Hz, 1H), 7.93 (dd, J = 6.9, 1.6 Hz, 3H), 7.47 (s, 2H), 7.39 (d, J = 8.6 Hz, 2H), 7.33 (dd, J = 7.1, 1.2 Hz, 1H), 6.87 (t, J = 7.0 Hz, 1H), 3.98 (s, 6H), 3.93 (s, 3H). ^{13}C NMR (126 MHz, $CDCl_3$) δ 153.23, 144.65, 144.50, 138.54, 133.69, 132.54, 131.73, 129.95, 128.93, 127.32, 124.58, 122.61, 112.81, 108.68, 106.54, 61.04, 56.36. HRMS $[C_{22}H_{20}ClN_2O_3]^+$ calculated: 395.1162, observed: 395.1157. HPLC purity = 98.44% (Rt = 35.95 min)

Synthesis of 2-(4-fluorophenyl)-8-(3,4,5-trimethoxyphenyl) imidazo[1,2-a] pyridine (4d). Compound **4d** was synthesized following the general procedure to prepare compounds **4a-4m**. A solution of 100 mg **3d** (0.34 mmol), 87 mg of 3,4,5- trimethoxyphenylboronic acid (0.41 mmol), 188 mg (1.36 mmol) of K_2CO_3, 47 mg of Pd (0) $[PPh_3]_4$ in dioxane was refluxed to obtain the crude product. An amount of 84 mg (65%, 0.22 mmol) of pure product was obtained as a light brown oil after purification (30% EtOAc/hexanes, Rf = 0.27). ^{1}H NMR (500 MHz, $CDCl_3$) δ 8.11 (d, J = 6.7 Hz, 1H), 8.01 – 7.90 (m, 2H), 7.90 – 7.78 (m, 1H), 7.47 (d, J = 1.3 Hz, 2H), 7.36 – 7.27 (m, 1H), 7.11 (t, J = 8.2 Hz, 2H), 6.87 (t, J = 6.7 Hz, 1H), 4.09 – 3.80 (m, 9H). ^{13}C NMR (126 MHz, $CDCl_3$) δ 149.76, 141.37, 140.98, 134.99, 128.43, 126.34, 124.31, 121.24, 119.26, 112.33, 112.15, 109.29, 104.99, 103.09, 57.60, 52.91. HRMS $[C_{22}H_{20}FN_2O_3]^+$ calculated: 379.1458, observed: 379.1452. HPLC purity: 97.56% (Rt = 31.91 min)

Synthesis of 2-(4-(trifluoromethyl)phenyl)-8-(3,4,5-trimethoxyphenyl)imidazo[1,2-a]pyridine (4e). Compound **4e** was synthesized following the general procedure to prepare compounds **4a-4m**. A solution of 100 mg **3e** (0.29 mmol), 74 mg of 3,4,5-trimethoxyphenylboronic acid (0.35 mmol), 160 mg (1.16 mmol) of K_2CO_3, 47 mg of Pd (0) $[PPh_3]_4$ in dioxane was refluxed to obtain the crude product. An amount of 100 mg (79%, 0.23 mmol) of pure product was obtained as an off-white solid after purification (30% EtOAc/hexanes, Rf = 0.27). MP = 167.0 – 167.8 ˚C. ^{1}H NMR (500 MHz, $CDCl_3$) δ 8.13 (dd, J = 15.1, 7.3 Hz, 3H), 8.03 (s, 1H), 7.68 (d, J = 7.7 Hz, 2H), 7.46 (s, 2H), 7.37 (d, J = 6.9 Hz, 1H), 6.92 (t, J = 7.0 Hz, 1H), 3.99 (s, 6H), 3.94 (s, 3H). ^{13}C NMR (126 MHz, $CDCl_3$) δ 153.06, 139.51, 138.81, 130.32, 129.70, 126.23, 117.44, 109.21, 107.20, 61.07, 56.31, 21.47. HRMS $[C_{23}H_{20}F_3N_2O_3]^+$ calculated: 429.1426, observed: 429.1421. HPLC purity = 99.67% (Rt = 38.46 min)

Synthesis of 6-methyl-2-(p-tolyl)-8-(3,4,5-trimethoxyphenyl)imidazo[1,2-a]pyridine (4f). Compound **4f** was synthesized following the general procedure to prepare compounds **4a-4m**. A solution of 100 mg **3f** (0.28 mmol), 72 mg of 3,4,5- trimethoxyphenylboronic acid (0.34 mmol), 155 mg (1.12 mmol) of K_2CO_3, 47 mg of Pd (0) $[PPh_3]_4$ in dioxane was refluxed to obtain the crude product. An amount of 105 mg (96.4%, 0.27 mmol) of pure product was obtained as brown solid after purification (30% EtOAc/hexanes, Rf = 0.14). MP = 169.8 – 171.0 ˚C. ^{1}H NMR (500 MHz, $CDCl_3$) δ 8.03 – 7.64 (m, 4H), 7.60 – 7.37 (m, 2H), 7.28 (s, 1H), 7.20 – 6.94 (m, 2H), 4.19 – 3.64 (m, 9H), 2.38 (s, 6H). ^{13}C NMR (126 MHz, $CDCl_3$) δ 153.24, 138.52, 129.43, 128.82, 126.09, 122.52, 108.14, 106.52, 61.05, 56.38, 21.43, 18.36. HRMS $[C_{24}H_{25}N_2O_3]^+$ calculated: 389.1865, observed: 389.1860. HPLC purity = 99.78% (Rt = 30.03 min)

Synthesis of 2-(p-tolyl)-5-(3,4,5-trimethoxyphenyl)imidazo[1,2-a]pyridine (4g). Compound **4g** was synthesized following the general procedure to prepare compounds **4a-4m**. A

solution of 100 mg **3g** (0.35 mmol), 89 mg of 3,4,5-trimethoxyphenylboronic acid (0.42 mmol), 193 mg (1.4 mmol) of K_2CO_3, 47 mg of Pd (0) $[PPh_3]_4$ in dioxane was refluxed to obtain the crude product. An amount of 96 mg (74%, 0.26 mmol) of pure product was obtained as white solid after purification (30% EtOAc/hexanes, Rf = 0.35). MP = 183.5 – 185.5 ˚C. ^{1}H NMR (500 MHz, $CDCl_3$) δ 7.90 – 7.77 (m, 2H), 7.36 (t, J = 7.8 Hz, 1H), 7.12 (d, J = 7.9 Hz, 2H), 7.01 (d, J = 2.4 Hz, 2H), 6.98 – 6.92 (m, 1H), 6.48 (d, J = 7.5 Hz, 1H), 6.31 (d, J = 8.1 Hz, 1H), 3.87 (s, 3H), 3.74 (s, 6H), 2.37 (s, 3H). ^{13}C NMR (126 MHz, $CDCl_3$) δ 156.86, 153.15, 144.63, 137.96, 135.48, 133.24, 129.41, 128.82, 110.37, 108.55, 103.93, 60.93, 57.53, 55.81, 21.69. HRMS $[C_{23}H_{23}N_2O_3]^+$ calculated: 375.1709, observed: 375.1703. HPLC purity = 95.2% (Rt = 27.80 min)

Synthesis of 2-(p-tolyl)-8-(3,4,5-trimethoxyphenyl)imidazo[1,2-a]pyrazine (4h). Compound **4h** was synthesized following the general procedure to prepare compounds **4a-4m**. A solution of 100 mg **3h** (0.41 mmol), 104 mg of 3,4,5-trimethoxyphenylboronic acid (0.49 mmol), 227 mg (1.64 mmol) of K_2CO_3, 47 mg of Pd (0) $[PPh_3]_4$ in dioxane was refluxed to obtain the crude product. An amount of 98 mg (63.4%, 0.26 mmol) of pure product was obtained as brownish wax after purification (30% EtOAc/hexanes, Rf = 0.37). ^{1}H NMR (500 MHz, $CDCl_3$) δ 8.35 (d, J = 3.2 Hz, 2H), 8.10 – 7.65 (m, 5H), 7.32 – 7.23 (m, 2H), 4.49 – 3.42 (m, 9H), 2.42 (s, 3H). ^{13}C NMR (126 MHz, $CDCl_3$) δ 153.06, 139.51, 138.81, 130.32, 129.70, 126.23, 117.44, 109.21, 107.20, 61.07, 56.31, 21.47. HRMS $[C_{22}H_{22}N_3O_3]^+$ calculated: 376.1661, observed: 376.1656. HPLC purity = 97.2% (Rt = 37.91 min)

Synthesis of 8-(3,5-difluorophenyl)-2-(p-tolyl)imidazo[1,2-a]pyrazine (4i). Compound **4i** was synthesized following the general procedure to prepare compounds **4a-4m**. A solution of 100 mg **3h** (0.41 mmol), 77 mg of (3,5-difluorophenyl) boronic acid (0.49 mmol), 227 mg (1.64 mmol) of K2CO3, 47 mg of Pd (0) $[PPh_3]_4$ in dioxane was refluxed to obtain the crude

product. An amount of 102 mg (78%, 0.32 mmol) of pure product was obtained as yellowish solid after purification (30% EtOAc/hexanes, Rf = 0.44). MP = 170.9 – 172.1 ˚C. ^{1}H NMR (500 MHz, $CDCl_3$) δ 8.64 – 8.45 (m, 2H), 8.07 (dd, J = 4.4, 1.2 Hz, 1H), 8.00 – 7.77 (m, 4H), 7.38 – 7.26 (m, 2H), 7.03 – 6.85 (m, 1H), 2.42 (s, 3H). ^{13}C NMR (126 MHz, $CDCl_3$) δ 164.02, 162.06, 161.96, 147.81, 139.06, 129.98, 129.71, 129.02, 126.51, 118.35, 112.77, 112.55, 109.23, 105.56, 21.51. HRMS $[C_{19}H_{14}F_2N_3]^+$ calculated: 322.1156, observed: 322.1150. HPLC purity = 98.74% (Rt = 41.59 min)

Synthesis of 8-(3,5-difluoro-4-methoxyphenyl)-2-(p-tolyl)imidazo[1,2-a]pyrazine (4j). Compound **4j** was synthesized following the general procedure to prepare compounds **4a-4m**. A solution of 100 mg **3h** (0.41 mmol), 92 mg of (3,5-difluoro-4- methoxyphenyl) boronic acid (0.49 mmol), 227 mg (1.64 mmol) of K_2CO_3, 47 mg of Pd (0) $[PPh_3]_4$ in dioxane was refluxed to obtain the crude product. An amount of 102 mg (78%, 0.32 mmol) of pure product was obtained as white solid after purification (30% EtOAc/hexanes, Rf = 0.38). MP = 128.1 – 129 ˚C. ^{1}H NMR (500 MHz, $CDCl_3$) δ 8.81 – 8.37 (m, 2H), 8.19 – 7.71 (m, 5H), 7.34 – 7.26 (m, 2H), 4.11 (s, 3H), 2.42 (s, 3H). ^{13}C NMR (126 MHz, $CDCl_3$) δ 156.22, 156.17, 154.26, 147.72, 146.21, 139.21, 139.02, 130.00, 129.70, 126.47, 117.94, 113.91, 113.76, 113.70, 109.26, 61.89, 21.50. HRMS $[C_{20}H_{16}F_2N_3O]^+$ calculated: 352.1261, observed: 352.1256. HPLC purity = 97.86% (Rt = 42.25 min)

Synthesis of 8-(3,5-dichloro-4-methoxyphenyl)-2-(p-tolyl) imidazo[1,2-a] pyrazine (4k). Compound **4k** was synthesized following the general procedure to prepare compounds **4a-4m**. A solution of 100 mg **3h** (0.41 mmol), 108 mg of (3,5-dichloro-4- methoxyphenyl) boronic acid (0.49 mmol), 227 mg (1.64 mmol) of K_2CO_3, 47 mg of Pd (0) $[PPh_3]_4$ in dioxane was refluxed to obtain the crude product. An amount of 95 mg (61%, 0.25 mmol) of pure product was obtained

as brown solid after purification (30% EtOAc/hexanes, Rf = 0.41). MP = 152.8 – 153.9 ˚C. ^{1}H NMR (500 MHz, $CDCl_3$) δ 8.96 (d, J = 1.9 Hz, 2H), 8.20 – 7.75 (m, 5H), 7.34 – 7.27 (m, 2H), 4.00 (s, 3H), 2.43 (s, 3H). ^{13}C NMR (126 MHz, $CDCl_3$) δ 153.98, 147.98, 145.95, 139.12, 133.10, 130.32, 129.90, 129.75, 128.84, 126.49, 118.16, 109.44, 60.97, 21.52. HRMS $[C_{20}H_{16}Cl_2N_3O]^+$ calculated: 384.0670, observed: 384.0665. HPLC purity = 99.27% (Rt = 45.29 min)

Synthesis of 8-(3,5-dibromo-4-methoxyphenyl)-2-(p-tolyl) imidazo[1,2-a] pyrazine (4l). Compound **4l** was synthesized following the general procedure to prepare compounds **4a-4m**. A solution of 100 mg **3h** (0.41 mmol), 152 mg of (3,5-dibromo-4- methoxyphenyl) boronic acid (0.49 mmol), 227 mg (1.64 mmol) of K_2CO_3, 47 mg of Pd (0) $[PPh_3]_4$ in dioxane was refluxed to obtain the crude product. An amount of 85 mg (44%, 0.18 mmol) of pure product was obtained as yellowish brown solid after purification (30% EtOAc/hexanes, Rf = 0.41). MP = 187.3 – 193.5 ˚C. ^{1}H NMR (500 MHz, $CDCl_3$) δ 9.16 (s, 2H), 8.05 (dd, J = 4.4, 1.1 Hz, 1H), 7.98 (dd, J = 4.3, 1.1 Hz, 1H), 7.96 – 7.91 (m, 3H), 7.31 (s, 1H), 7.29 (s, 1H), 3.97 (d, J = 1.0 Hz, 3H), 2.42 (s, 3H). ^{13}C NMR (126 MHz, $CDCl_3$) δ 155.68, 147.76, 145.83, 139.04, 134.50, 134.02, 129.98, 129.74, 129.09, 126.46, 118.09, 109.26, 60.85, 21.51. HRMS $[C_{20}H_{16}Br_2N_3O]^+$ calculated: 471.9660, observed: 471.9658. HPLC purity = 98.07% (Rt = 35.77 min)

Synthesis of 8-(3,5-dichloro-4-fluorophenyl)-2-(p-tolyl) imidazo[1,2-a] pyrazine (4m). Compound **4m** was synthesized following the general procedure to prepare compounds **4a-4m**. A solution of 100 mg **3h** (0.41 mmol), 102 mg of (3,5-dichloro-4- fluorophenyl) boronic acid (0.49 mmol), 227 mg (1.64 mmol) of K_2CO_3, 47 mg of Pd (0) $[PPh_3]_4$ in dioxane was refluxed to obtain the crude product. An amount of 105 mg (68%, 0.28 mmol) of pure product was obtained as off-white solid after purification (30% EtOAc/hexanes, Rf = 0.44). MP = 224.2 – 225.4 ˚C. ^{1}H NMR (500 MHz, DMSO-D6) δ 9.07 (q, J = 7.9 Hz, 2H), 8.80 – 8.38 (m, 2H), 8.12 – 7.74 (m, 3H), 7.43

– 7.18 (m, 2H), 2.36 (s, 3H). ^{13}C NMR (126 MHz, $CDCl_3$) δ 147.77, 145.26, 139.04, 133.10, 130.31, 129.66, 128.90, 126.37, 122.28, 122.14, 118.19, 109.22, 21.42. HRMS $[C_{19}H_{13}Cl_2FN_3]^+$ calculated: 372.0471, observed: 372.0465. HPLC purity: 99.8% (Rt = 39.38 min)

1.D.3. Cell culture and cell viability screening

Kelly and CHP-134 cells were obtained from Sigma, and Be(2)C cells are in-house stocks. All neuroblastoma cells were cultured in RPMI-1640 with l-glutamine (Corning) supplemented with 10% fetal bovine serum and 1% Penicillin and Streptomycin. All cell lines are tested regularly for mycoplasma contamination (MP Biomedicals kit). For cell viability assays, 5,000 cells per cell line were plated in triplicate on a 96-well white plate with clear bottom using 0.05-0.25% DMSO or a nine-point serial dilution of compounds. Commercially available colchicine (MedChem Express) was included as a control. After three days, cell viability was measured using CellTiter-Glo (Promega), according to manufacturer's instructions. Graphpad Prism software was used to calculate the IC50 or GI50 values, with standard error using non-linear fit of the data ([inhibitor vs. normalized response]). A minimum of two independent experiments were performed for each cell line.

1.D.4. *In vitro* tubulin polymerization assay

In vitro tubulin polymerization was measured using the optical density tubulin polymerization kit (Cytoskeleton, Inc) following manufacturer's instructions. Briefly, 4 mg/mL frozen tubulin was diluted in a general tubulin buffer containing guanosine triphosphate and then added into wells of a prewarmed plate containing either paclitaxel, colchicine (MedChem Express), test compounds, or buffer only. Absorbance at 420 nm was read every 30 seconds for 45 minutes in a pre-warmed 37°C BMG Clariostar plate reader using plate shaking function. All

values obtained were normalized to the value at time zero to determine the amount of tubulin polymerization during the 45-minute timepoint. A minimum of two independent experiments were performed per compound.

1.D.5. Western blotting and antibodies

2.5 x 106 Kelly orCHP134 cells were plated onto five separate plates with media containing indicated compounds or matched DMSO as a control. After a 24-hour incubation period, cells were collected from each plate and placed in chilled lysis buffer (150 mM Tris, pH 8.0, 5 mM EDTA, 150 mM NaCl, 1% Triton X-100, with the Roche protease inhibitor cocktail and PMSF). The cells were sonicated at 25% power for 15 seconds and cellular debris was removed via a chilled centrifuge. For SDS-PAGE loading, protein concentration was determined by the BioRad Bradford assay. 15-30 ug of protein was resolved by SDS-PAGE and transferred to PVDF membranes. The membranes soaked in 5% block containing milk and TBS-T (50 mM Tris, pH 7.5, 0.1% Tween-20, 150 mM NaCl) for one hour. The antibodies Cyclin B1 (Cell Signaling, 4138), Phospho-histone Ser10 (Cell Signaling, D7N8E), and GAPDH-HRP (Cell Signaling, D16H11) were used for immunoblotting. Bands were visualized with BioRad Clarity ECL substrate and a BioRad ChemiDoc MP machine. Western blots are representative of three independent experiments performed.

1.D.6. Cell cycle analysis

1.5 x 106 – 2.5 x 106 of Kelly or CHP134 cells were plated onto three separate plates with media containing either indicated compounds or matched DMSO control. After a 24-hour incubation period, 1.0 x 106 cells were collected from each plate and fixed in cold 70% ethanol. The fixed cells were stored at -20°C until ready to stain. After thawing, the fixed cells were washed

with 1X phosphate buffered saline (PBS) and resuspended into a solution of propidium iodide (PI) stain (1X PBS + 10 μg/ml PI + 100 μg/ml RNAse A + 2 mM MgCl2). The fixed cells were allowed to stain overnight at 4°C. The stained cells were resuspended and filtered through a 35 μm nylon mesh cell strainer Falcon tube. After filtering, a minimum of 10,000 cells were counted with a Guava easyCyte Flow Cytometer instrument (Luminex). The number of independent experiments is indicated in the figure legend.

1.D.7. Immunofluorescence staining

Kelly or Be(2)C cells were plated onto poly-D-lysine (Gibco) treated coverslips in normal maintenance media. Cells were treated for 24 hours with indicated compounds or a DMSO only control. Cells were fixed using methanol-free 4% formaldehyde, permeabilized with a solution of 0.2% Triton X-100 and blocked with 5% goat serum and 3% bovine serum albumin. The primary antibody used for staining was Alpha Tubulin Rabbit PolyAb (Proteintech, 11224-1-AP) while the secondary antibody used was Alexa-488 Goat Anti-rabbit (Invitrogen, A11008). Slides were then mounted with Invitrogen ProLong Diamond Antifade Mounting media with DAPI (Invitrogen, P36966). Images were obtained using an OLYMPUS IX83 Research Inverted Microscope with the DAPI and Alexa 488 (GFP) settings using 60X magnification. Scale bar was added using ImageJ software.

1.D.8. Molecular modeling

The four most potent candidates (**4b, 4h, 4k,** and **4j**) were subjected to molecular docking at the colchicine binding site of tubulin (PDB: 6X1F) to assess their binding interactions with the colchicine binding site. The Discovery Studio Visualizer was used to determine the position coordinates from the PDB 6X1F (16.752348, -66.405087, and -42.326304). The PyRx/Autodock

Vina software was used to perform molecular docking. The receptor grid was generated by keeping the bound ligands (Y5M) in the crystal structure as the center of the grid box. It was made sure that all crucial amino acid residues are inside of the grid box. The size of the box was set to 24 X 24 X 24 Å. The MMFF94 forcefield was used for energy minimization of the candidates. Polar hydrogen bonds were added, and Gasteiger partial charges were assigned to the ligand atoms. Docking score was used to rank the candidates based on their binding affinities. Candidates with docking score – 8 kcal/mol or above were considered as hits identifying potential target. The docking procedure was validated by a control study. For this the bound ligand in the crystal structures 6X1F (Y5M) was re-docked to the pre-processed and prepared protein keeping the same grid box. The docking score for this docking was used as a standard value against which the scores for the candidates were compared. The control docking was performed using Autodock Vina. The molecular dynamics simulation for the complexes containing the top two tubulin inhibitors (**4h** and **4k**) bound to the colchicine binding site of tubulin was performed using YASARA Structure in three replicates. The MD simulation set up took into consideration the hydrogen bonding network optimization to maximize the solute stability, and a pKa prediction to precisely control the protonation states of protein residues at the selected pH of 7.4. 0.9% physiological concentration of NaCl ions were supplied, along with an excess of either Na or Cl to neutralize the cell. Energy-minimization was carried out to eliminate bumps and adjust the covalent geometry of the structure in YASARA. Following a brief steepest descent minimization to remove conformational stress, the process continued with simulated annealing (timestep 2 fs, atom velocities scaled down by 0.9 every 10 steps) until convergence was reached that is the energy increased by less than 0.05 kJ/mol per atom during 200 steps. The simulation was accomplished using the AMBER14 force field for the solute for 100 nanoseconds after steepest descent and

simulated annealing minimizations were applied to get rid of clashes. The cut-off for Van der Waals forces (the default used by AMBER) was set to 8 Å. There was no cut-off applied to electrostatic forces.

1.D.9. *In vitro* microsomal stability

In vitro microsomal stability of top three compounds, **4h**, **4j**, and **4k**, as well as colchicine were performed against the human liver microsome at the Eurofins Panlab, Inc. at 15 Research Park Dr., St Charles, MO 63304, USA. Safety Statement. No unexpected or unusually high safety hazards were encountered.

REFERENCES

(1) Honore, S.; Pasquier, E.; Braguer, D. Understanding microtubule dynamics for improved cancer therapy. *Cell. Mol. Life Sci.* **2005**, *62* (24), 3039-3056, DOI: 10.1007/s00018-005-5330-x.

(2) Gaspari, R.; Prota, A. E.; Bargsten, K.; Cavalli, A.; Steinmetz, M. O. Structural Basis of cis- and trans-Combretastatin Binding to Tubulin. *Chem* **2017**, *2* (1), 102-113, DOI: 10.1016/j.chempr.2016.12.005.

(3) Arnst, K. E.; Banerjee, S.; Chen, H.; Deng, S.; Hwang, D.-J.; Li, W.; Miller, D. D. Current advances of tubulin inhibitors as dual acting small molecules for cancer therapy. *Med. Res. Rev.* **2019**, *39* (4), 1398-1426, DOI: 10.1002/med.21568.

(4) Arnst, K. E.; Banerjee, S.; Wang, Y.; Chen, H.; Li, Y.; Yang, L.; Li, W.; Miller, D. D.; Li, W. X-ray Crystal Structure Guided Discovery and Antitumor Efficacy of Dihydroquinoxalinone as Potent Tubulin Polymerization Inhibitors. *ACS Chem. Biol.* **2019**, *14* (12), 2810-2821, DOI: 10.1021/acschembio.9b00696.

(5) Cui, M.-T.; Jiang, L.; Goto, M.; Hsu, P.-L.; Li, L.; Zhang, Q.; Wei, L.; Yuan, S.-J.; Hamel, E.; Morris-Natschke, S. L.; Lee, K. H.; Xie, L. In Vivo and Mechanistic Studies on Antitumor Lead 7-Methoxy-4-(2-methylquinazolin-4-yl)-3,4-dihydroquinoxalin-2(1H)-one and Its Modification as a Novel Class of Tubulin-Binding Tumor-Vascular Disrupting Agents. *J. Med. Chem.* **2017**, *60* (13), 5586-5598, DOI: 10.1021/acs.jmedchem.7b00273.

(6) Kaur, R.; Kaur, G.; Gill, R. K.; Soni, R.; Bariwal, J. Recent developments in tubulin polymerization inhibitors: An overview. *Eur. J. Med. Chem.* **2014**, *87*, 89-124, DOI: 10.1016/j.ejmech.2014.09.051.

(7) Haider, K.; Rahaman, S.; Yar, M. S.; Kamal, A. Tubulin inhibitors as novel anticancer agents: an overview on patents (2013-2018). *Expert Opin. Ther. Pat.* **2019**, *29* (8), 623-641. DOI: 10.1080/13543776.2019.1648433, DOI: 10.1080/13543776.2019.1648433.

(8) Deng, S.; Banerjee, S.; Chen, H.; Pochampally, S.; Wang, Y.; Yun, M.-K.; White, S. W.; Parmar, K.; Meibohm, B.; Hartman, K. L.; Zhongzhi, W.; Miller, D. D.; Li, W. SB226, an inhibitor of tubulin polymerization, inhibits paclitaxel-resistant melanoma growth and spontaneous metastasis. *Cancer Lett.* **2023**, *555*, 216046, DOI: 10.1016/j.canlet.2022.216046.

(9) Banerjee, S.; Arnst, K. E.; Wang, Y.; Kumar, G.; Deng, S.; Yang, L.; Li, G.-b.; Yang, J.; White, S. W.; Li, W.; Miller, D. D. Heterocyclic-Fused Pyrimidines as Novel Tubulin Polymerization Inhibitors Targeting the Colchicine Binding Site: Structural Basis and Antitumor Efficacy. *J. Med. Chem.* **2018**, *61* (4), 1704-1718, DOI: 10.1021/acs.jmedchem.7b01858.

(10) Peng, X.; Ren, Y.; Pan, W.; Liu, J.; Chen, J. Discovery of Novel Acridane-Based Tubulin Polymerization Inhibitors with Anticancer and Potential Immunomodulatory Effects. *J. Med. Chem.* **2023**, *66* (1), 627-640, DOI: 10.1021/acs.jmedchem.2c01566.

(11) Leng, J.; Zhao, Y.; Sheng, P.; Xia, Y.; Chen, T.; Zhao, S.; Xie, S.; Yan, X.; Wang, X.; Yin, Y.; Kong, L. Discovery of Novel N-Heterocyclic-Fused Deoxypodophyllotoxin Analogues as Tubulin Polymerization Inhibitors Targeting the Colchicine-Binding Site for Cancer Treatment. *J. Med. Chem.* **2022**, *65* (24), 16774-16800, DOI: 10.1021/acs.jmedchem.2c01595.

(12) Banerjee, S.; Hwang, D. J.; Li, W.; Miller, D. D. Current Advances of Tubulin Inhibitors in Nanoparticle Drug Delivery and Vascular Disruption/Angiogenesis. *Molecules* **2016**, *21* (11), DOI: 10.3390/molecules21111468.

(13) Fanale, D.; Bronte, G.; Passiglia, F.; Calò, V.; Castiglia, M.; Di Piazza, F.; Barraco, N.; Cangemi, A.; Catarella, M. T.; Insalaco, L.; Listi, A.; Maragliano, R.; Massihnia, D.; Perez, A.;

Toia, F.; Cicero, G.; Bazan, V. Stabilizing versus Destabilizing the Microtubules: A Double-Edge Sword for an Effective Cancer Treatment Option? *Anal. Cell. Pathol.* **2015**, *2015*, 690916, DOI: 10.1155/2015/690916.

(14) Wang, Z.; Chen, J.; Wang, J.; Ahn, S.; Li, C.-M.; Lu, Y.; Loveless, V. S.; Dalton, J. T.; Miller, D. D.; Li, W. Novel Tubulin Polymerization Inhibitors Overcome Multidrug Resistance and Reduce Melanoma Lung Metastasis. *Pharm. Res.* **2012**, *29* (11), 3040-3052, DOI: 10.1007/s11095-012-0726-4.

(15) Wang, J.; Chen, J.; Miller, D. D.; Li, W. Synergistic Combination of Novel Tubulin Inhibitor ABI-274 and Vemurafenib Overcomes Vemurafenib Acquired Resistance in BRAFV600E Melanoma. *Mol. Cancer Ther.* **2014**, *13* (1), 16-26, DOI: 10.1158/1535-7163.MCT-13-0212.

(16) Giacomini, K. M.; Huang, S.-M.; Tweedie, D. J.; Benet, L. Z.; Brouwer, K. L. R.; Chu, X.; Dahlin, A.; Evers, R.; Fischer, V.; Hillgren, K. M.; Hoffmaster, K. A.; Ishikawa, T.; Keppler, D.; Kim, R. B.; Lee, C. A.; Niemi, M.; Polli, J. W.; Sugiyama, Y.; Swaan, P. W.; Ware, J. A.; Wright, S. H.; Yee, S. W.; Zamek-Gliszczynski, M. J; .Zhang, L. Membrane transporters in drug development. *Nat. Rev. Drug Discov.* **2010**, *9* (3), 215-236, DOI: 10.1038/nrd3028.

(17) Kavallaris, M. Microtubules and resistance to tubulin-binding agents. *Nat. Rev. Cancer* **2010**, *10* (3), 194-204, DOI: 10.1038/nrc2803.

(18) Zhang, Y.; Yang, S.-H.; Guo, X.-L. New insights into Vinca alkaloids resistance mechanism and circumvention in lung cancer. *Biomed. Pharmacother.* **2017**, *96*, 659-666, DOI: 10.1016/j.biopha.2017.10.041.

(19) Ganguly, A.; Cabral, F. New insights into mechanisms of resistance to microtubule inhibitors. *Biochim. Biophys. Acta* **2011**, *1816* (2), 164-171, DOI: 10.1016/j.bbcan.2011.06.001.

(20) Banerjee, S.; Mahmud, F.; Deng, S.; Ma, L.; Yun, M.-K.; Fakayode, S. O.; Arnst, K. E.; Yang, L.; Chen, H.; Wu, Z.; Lukka, P. B.; Parmer, K.; Meibohm, B.; White, S. W.; Wang, Y.; Li, W.; Miller, D. D. X-ray Crystallography-Guided Design, Antitumor Efficacy, and QSAR Analysis of Metabolically Stable Cyclopenta-Pyrimidinyl Dihydroquinoxalinone as a Potent Tubulin Polymerization Inhibitor. *J. Med. Chem.* **2021**, *64* (17), 13072-13095, DOI: 10.1021/acs.jmedchem.1c01202.

(21) McLoughlin, E. C.; O'Boyle, N. M. Colchicine-Binding Site Inhibitors from Chemistry to Clinic: A Review. *Pharmaceuticals*, **2020**; *13* (1), 8, DOI: 10.3390/ph13010008.

(22) Duan, Y.; Liu, W.; Tian, L.; Mao, Y.; Song, C. Targeting Tubulin-colchicine Site for Cancer Therapy: Inhibitors, Antibody- Drug Conjugates and Degradation Agents. *Curr. Top. Med. Chem.* **2019**, *19* (15), 1289-1304, DOI: 10.2174/1568026619666190618130008.

(23) Song, J.; Wang, S.-H.; Song, C.-H.; Zhang, W.-X.; Zhu, J.-X.; Tian, X.-Y.; Fu, X.-J.; Xu, Y.; Jin, C.-Y.; Zhang, S.-Y. Discovery of N-benzylarylamide derivatives as novel tubulin polymerization inhibitors capable of activating the Hippo pathway. *Eur. J. Med. Chem.* **2022**, *240*, 114583, DOI: 10.1016/j.ejmech.2022.114583.

(24) Mundra, V.; Lu, Y.; Danquah, M.; Li, W.; Miller, D. D.; Mahato, R. I. Formulation and Characterization of Polyester/Polycarbonate Nanoparticles for Delivery of a Novel Microtubule Destabilizing Agent. *Pharm. Res.* **2012**, *29* (11), 3064-3074, DOI: 10.1007/s11095-012-0881-7.

(25) Shuai, W.; Wang, G.; Zhang, Y.; Bu, F.; Zhang, S.; Miller, D. D.; Li, W.; Ouyang, L.; Wang, Y. Recent Progress on Tubulin Inhibitors with Dual Targeting Capabilities for Cancer Therapy. *J. Med. Chem.* **2021**, *64* (12), 7963-7990, DOI: 10.1021/acs.jmedchem.1c00100.

(26) Lu, Y.; Chen, J.; Wang, J.; Li, C.-M.; Ahn, S.; Barrett, C. M.; Dalton, J. T.; Li, W.; Miller, D. D. Design, Synthesis, and Biological Evaluation of Stable Colchicine Binding Site Tubulin

Inhibitors as Potential Anticancer Agents. *J. Med. Chem.* **2014**, *57* (17), 7355-7366, DOI: 10.1021/jm500764v.

(27) Li, L.; Quan, D.; Chen, J.; Ding, J.; Zhao, J.; Lv, L.; Chen, J. Design, synthesis, and biological evaluation of 1-substituted -2-aryl imidazoles targeting tubulin polymerization as potential anticancer agents. *Eur. J. Med. Chem.* **2019**, *184*, 111732, DOI: 10.1016/j.ejmech.2019.111732.

(28) Chen, J.; Ahn, S.; Wang, J.; Lu, Y.; Dalton, J. T.; Miller, D. D.; Li, W. Discovery of Novel 2-Aryl-4-benzoyl-imidazole (ABI-III) Analogues Targeting Tubulin Polymerization As Antiproliferative Agents. *J. Med. Chem.* **2012**, *55* (16), 7285-7289, DOI: 10.1021/jm300564b.

(29) Lu, Y.; Li, C.-M.; Wang, Z.; Chen, J.; Mohler, M. L.; Li, W.; Dalton, J. T.; Miller, D. D. Design, Synthesis, and SAR Studies of 4-Substituted Methoxylbenzoyl-aryl-thiazoles Analogues as Potent and Orally Bioavailable Anticancer Agents. *J. Med. Chem.* **2011**, *54* (13), 4678-4693, DOI: 10.1021/jm2003427.

(30) Hwang, D.-J.; Wang, J.; Li, W.; Miller, D. D. Structural Optimization of Indole Derivatives Acting at Colchicine Binding Site as Potential Anticancer Agents. *ACS Med. Chem. Lett.* **2015**, *6* (9), 993-997, DOI: 10.1021/acsmedchemlett.5b00208.

(31) Ren, Y.; Wang, Y.; Li, G.; Zhang, Z.; Ma, L.; Cheng, B.; Chen, J. Discovery of Novel Benzimidazole and Indazole Analogues as Tubulin Polymerization Inhibitors with Potent Anticancer Activities. *J. Med. Chem.* **2021**, *64* (8), 4498-4515, DOI: 10.1021/acs.jmedchem.0c01837.

(32) Deep, A.; Bhatia, R. K.; Kaur, R.; Kumar, S.; Jain, U. K.; Singh, H.; Batra, S.; Kaushik, D.; Deb, P. K. Imidazo[1,2-a]pyridine Scaffold as Prospective Therapeutic Agents. *Curr. Top. Med. Chem.* **2017**, *17* (2), 238-250, DOI: 10.2174/1568026616666160530153233.

(33) Costa, R. A.; Seuánez, H. N. Investigation of major genetic alterations in neuroblastoma. *Mol. Biol. Rep.* **2018**, *45* (3), 287-295. DOI: 10.1007/s11033-018-4161-4.

(34) Swift, C. C.; Eklund, M. J.; Kraveka, J. M.; Alazraki, A. L. Updates in Diagnosis, Management, and Treatment of Neuroblastoma. *Radiographics* **2018**, *38* (2), 566-580, DOI: 10.1148/rg.2018170132.

(35) Don, S.; Verrills, N. M.; Liaw, T. Y.; Liu, M. L.; Norris, M. D.; Haber, M.; Kavallaris, M. Neuronal-associated microtubule proteins class III beta-tubulin and MAP2c in neuroblastoma: role in resistance to microtubule-targeted drugs. *Mol. Cancer Ther.* **2004**, *3* (9), 1137-1146, DOI: 10.1158/1535-7163.1137.3.9.

(36) Kotchetkov, R.; Cinatl, J.; Blaheta, R.; Vogel, J.-U.; Karaskova, J.; Squire, J.; Hernáiz Driever, P.; Klingebiel, T.; Cinatl Jr, J. Development of resistance to vincristine and doxorubicin in neuroblastoma alters malignant properties and induces additional karyotype changes: A preclinical model. *Int. J. Cancer* **2003**, *104* (1), 36-43, DOI: 10.1002/ijc.10917.

(37) Meany, H. J.; Sackett, D. L.; Maris, J. M.; Ward, Y.; Krivoshik, A.; Cohn, S. L.; Steinberg, S. M.; Balis, F. M.; Fox, E. Clinical outcome in children with recurrent neuroblastoma treated with ABT-751 and effect of ABT-751 on proliferation of neuroblastoma cell lines and on tubulin polymerization in vitro. *Pediatr. Blood Cancer* **2010**, *54* (1), 47-54, DOI: 10.1002/pbc.22267.

(38) Frommann, K.; Appl, B.; Hundsdoerfer, P.; Reinshagen, K.; Eschenburg, G. Vincristine resistance in relapsed neuroblastoma can be efficiently overcome by Smac mimetic LCL161 treatment. *J. Pediatr. Surg.* **2018**, *53* (10), 2059-2064, DOI: 10.1016/j.jpedsurg.2018.01.012.

(39) Park, J. R.; Bagatell, R.; London, W. B.; Maris, J. M.; Cohn, S. L.; Mattay, K. K.; Hogarty, M. Children's Oncology Group's 2013 blueprint for research: neuroblastoma. *Pediatr. Blood Cancer* **2013**, *60* (6), 985-993, DOI: 10.1002/pbc.24433.

(40) Aho, E. R.; Weissmiller, A. M.; Fesik, S. W.; Tansey, W. P. Targeting WDR5: A WINning Anti-Cancer Strategy? *Epigenet. Insights* **2019**, *12*, 2516865719865282, DOI: 10.1177/2516865719865282.

(41) Bryan, A. F.; Wang, J.; Howard, G. C.; Guarnaccia, A. D.; Woodley, C. M.; Aho, E. R.; Rellinger, E. J.; Matlock, B. K.; Flaherty, D. K.; Lorey, S. L.; Chung, D. H; Fesik, S. W.; Liu, Qi.; Weissmiller, A. M.; Tansey, W. P. WDR5 is a conserved regulator of protein synthesis gene expression. *Nucleic Acids Res.* **2020**, *48*, 2924, DOI: 10.1093/nar/gkaa051.

(42) Gong, D.; Ferrell, J. E., Jr. The roles of cyclin A2, B1, and B2 in early and late mitotic events. *Mol. Biol. Cell* **2010**, *21* (18), 3149-3161, DOI: 10.1091/mbc.e10-05-0393.

(43) Gurley, L. R.; D'Anna, J. A.; Barham, S. S.; Deaven, L. L.; Tobey, R. A. Histone phosphorylation and chromatin structure during mitosis in Chinese hamster cells. *Eur. J. Biochem.* **1978**, *84* (1), 1-15, DOI: 10.1111/j.1432-1033.1978.tb12135.x.

(44) Taubenberger, A. V.; Baum, B.; Matthews, H. K. The Mechanics of Mitotic Cell Rounding. *Front. Cell Dev. Biol.* **2020**, *8*, 687, DOI: 10.3389/fcell.2020.00687.

(45) Beltran, H. The N-myc Oncogene: Maximizing its Targets, Regulation, and Therapeutic Potential. *Mol. Cancer Res.* **2014**, *12* (6), 815-822, DOI: 10.1158/1541-7786.MCR-13-0536.

CHAPTER II

Synthesis, and Mechanistic Evaluation of Pyrazolo[5,1-b]quinazolin-8(4H)-one Derivatives as Potential Autotaxin Inhibitors

2.A. Introduction

Autotaxin (ATX), also known as ectonucleotide pyrophosphatase/phosphodiesterase 2 (ENPP2), is an important secreted enzyme that has attracted growing interest in cancer research.[1,2] It works by converting a common lipid molecule in the body, lysophosphatidylcholine (LPC), into lysophosphatidic acid (LPA). LPA is a small signaling molecule (also called a bioactive lipid) that plays a vital role in several normal cellular processes such as cell growth, survival, movement (migration), and the formation of new blood vessels (angiogenesis) (**Figure 8)**.[3–5] However, when the ATX-LPA signaling pathway becomes overactive, it can contribute to the development and spread of cancer.

LPA exerts its effects by binding to specific G protein-coupled receptors on the surface of cells, called LPAR1 to LPAR6.[6] Once LPA binds to these receptors, it activates several signaling pathways inside the cell, including the PI3K/Akt, RhoA, and MAPK/ERK pathways.[6]

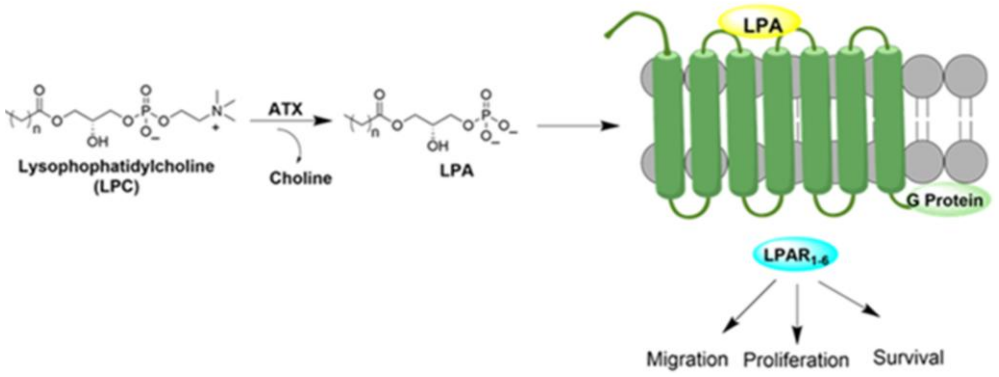

Figure 8. ATX catalyzes the conversion of LPC from LPA and subsequently activates different LPARs producing various cellular responses.

These pathways are well known for promoting cancer-related behaviors, such as increased cell division, resistance to cell death, and the ability of cancer cells to invade surrounding tissues. One of the most concerning aspects of the ATX-LPA signaling axis is its role in cancer therapy resistance. Many studies have shown that high levels of ATX and LPA in the tumor environment can protect cancer cells from the effects of chemotherapy and radiation therapy.[7,8] This makes tumors harder to treat and increases the chance of relapse. As a result, targeting ATX has become a promising strategy in the development of new cancer therapies, especially those aimed at preventing or reversing resistance to existing treatments.

In recent years, researchers have focused on developing small-molecule inhibitors that can block the activity of ATX and reduce the production of LPA.[9–12] One promising strategy involves the design of compounds containing fused heterocyclic structures, which are chemical frameworks formed by the fusion of multiple ring systems.[13] These scaffolds often offer enhanced biological activity and favorable drug-like properties. Among them, pyrazolo[5,1-b]quinazolin-8(4H)-one has emerged as a structurally attractive yet underexplored scaffold for ATX inhibition. This study draws inspiration from our laboratory's recently published work, in which two novel ATX inhibitors were discovered through virtual screening approaches.[13,14] These compounds were subsequently validated *in vitro* and showed strong synergistic anti-cancer effects when combined with Paclitaxel in breast cancer and melanoma cell lines. Motivated by these findings, the current research aims to expand the chemical diversity of ATX inhibitors by synthesizing and evaluating a new series of pyrazolo[5,1-b]quinazolin-8(4H)-one derivatives to further explore their potential as anti-cancer agents.

In the present study, a series of 21 novel pyrazolo[5,1-b]quinazolin-8(4H)-one derivatives were designed and synthesized in the laboratory. These compounds were tested using a

biochemical assay to evaluate their ability to inhibit ATX. The purpose of this work was to identify new chemical structures that can effectively block the ATX-LPA pathway and potentially reduce cancer cell survival and drug resistance. In future studies, these compounds will be further tested in cancer cell lines to determine their effectiveness as single agents or in combination with established chemotherapy drugs such as Paclitaxel. This may provide valuable insights into their potential as novel anti-cancer therapies that work by targeting the ATX-LPA signaling axis.

2.B. Results and Discussions

In the initial phase of this study, a series of 13 novel tricyclic pyrazolo[5,1-b]quinazolin-8(4H)-one analogues were synthesized to evaluate their potential as ATX inhibitors. These compounds featured fused A, B, and C ring systems, with variations at the R_1, R_2, R_3 and R_4 positions (Scheme 4), various substituents were introduced. The synthetic strategy employed a three-component one-pot condensation reaction, using commercially available pyrazol-amines, dimedone derivatives, and benzaldehyde derivatives. The reaction was carried out under reflux in ethanol at 80 °C for 72 hours, resulting in the desired pyrazolo[5,1-b]quinazolin-8(4H)-one derivatives with moderate to good yields. The products were purified using standard recrystallization and chromatographic techniques. Structural confirmation of the synthesized compounds was achieved through spectral characterization, including ^{1}H NMR and ^{13}C NMR. The success of the synthetic route highlights the efficiency and versatility of this multicomponent reaction in generating structurally diverse tricyclic scaffolds.

The synthesized compounds were screened for their ability to inhibit human recombinant ATX (hATX) enzyme using the fluorogenic substrate FS-3-based enzyme inhibition assay, which

quantitatively measures ATX enzymatic activity. The known ATX inhibitor BMP-22 was employed as a positive control in this assay to ensure experimental validity.

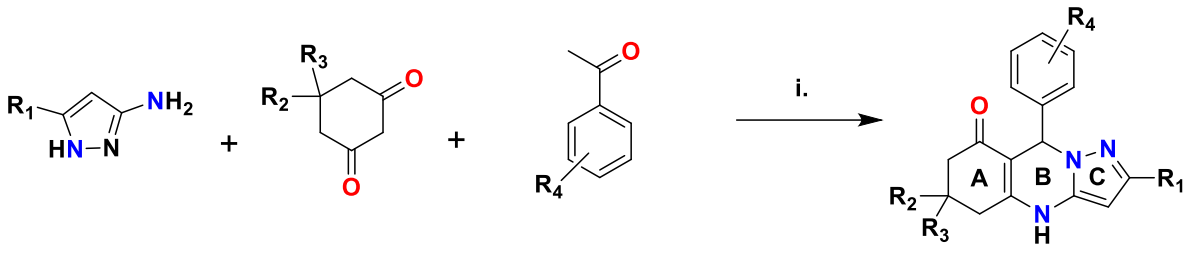

i. EtOH, 80°C, 72 hrs.

TC1a: $R_1 = R_2 = CH_3$, $R_3 = H$, $R_4 = 3,5\text{-F}$

TC1b: $R_1 = H$, $R_2 = CH_3$, $R_3 = H$, $R_4 = 3,5\text{-F}$

TC1c: $R_1 = R_2 = CH_3$, $R_3 = H$, $R_4 = 3,4,5\text{-OMe}$

TC1d: $R_1 = H$, $R_2 = CH_3$, $R_3 = H$, $R_4 = 3,4,5\text{-OMe}$

TC1e: $R_1 = H$, $R_2 = CH_3$, $R_3 = H$, $R_4 = 3\text{-OMe, 4-F}$

TC1f: $R_1 = H$, $R_2 = CH_3$, $R_3 = H$, $R_4 = 3,5\text{-OMe}$

TC1g: $R_1 = H$, $R_2 = CH_3$, $R_3 = H$, $R_4 = 3,4\text{-OMe}$

TC1h: $R_1 = H$, $R_2 = CH_3$, $R_3 = H$, $R_4 = 3,4\text{-F}$

TC1i: $R_1 = H$, $R_2 = CH_3$, $R_3 = H$, $R_4 = 2\text{-F, 5-OMe}$

TC1j: $R_1 = H$, $R_2 = CH_3$, $R_3 = H$, $R_4 = 2\text{-F, 3-OMe}$

TC1k: $R_1 = H$, $R_2 = CH_3$, $R_3 = H$, $R_4 = 4\text{-OMe}$

TC1l: $R_1 = R_2 = CH_3$, $R_3 = H$, $R_4 = 3\text{-OMe, 4-F}$

TC1m: $R_1 = R_2 = CH_3$, $R_3 = H$, $R_4 = 3,5\text{-OMe}$

TC2a: $R_1 = 4\text{-methylphenyl}$, $R_2 = CH_3$, $R_3 = H$, $R_4 = 3\text{-Br, 4,5-OMe}$

TC2b: $R_1 = 4\text{-methylphenyl}$, $R_2 = CH_3$, $R_3 = CH_3$, $R_4 = 3\text{-Br, 4,5-OMe}$

TC2c: $R_1 = 4\text{-methylphenyl}$, $R_2 = CH_3$, $R_3 = CH_3$, $R_4 = 3,4,5\text{-OMe}$

TC2d: $R_1 = 4\text{-methylphenyl}$, $R_2 = H$, $R_3 = H$, $R_4 = 3\text{-Br, 4,5-OMe}$

TC2e: $R_1 = 4\text{-methylphenyl}$, $R_2 = H$, $R_3 = H$, $R_4 = 3,4,5\text{-OMe}$

TC2f: $R_1 = 4\text{-methylphenyl}$, $R_2 = CH_3$, $R_3 = H$, $R_4 = 3,4,5\text{-OMe}$

TC2g: $R_1 = 4\text{-methylphenyl}$, $R_2 = CH_3$, $R_3 = H$, $R_4 = 3,4\text{-F}$

TC2h: $R_1 = 4\text{-methylphenyl}$, $R_2 = CH_3$, $R_3 = H$, $R_4 = 3,4,5\text{-F}$

Scheme 4. Synthesis of tricyclic pyrazolo[5,1-b]quinazolin-8(4H)-one analogues.

In the initial screening campaign, all 13 compounds were tested at a single concentration of 10 µM. Unfortunately, none of the compounds exhibited greater than 20% inhibition of ATX activity at this dose **(**Figure 9), suggesting that substitutions at the R_1 position limited to hydrogen or methyl were insufficient for achieving significant enzyme binding or inhibition. To improve the inhibitory activity, structural modification was performed at the R_1 position by introducing a 4-methylphenyl substituent, a hydrophobic and sterically bulky moiety that was hypothesized to enhance interactions within the ATX active site. This led to the synthesis of an additional eight analogues, using the same general synthetic protocol. This structural modification yielded promising results: two of the newly synthesized compounds demonstrated greater than 50%

inhibition of ATX activity at the 10 µM screening concentration (Figure 10). These hits, designated TC2c and TC2f, were selected for further evaluation using a dose–response assay ranging from 10 µM to 3 nM to determine their half-maximal inhibitory concentrations (IC_{50} values).

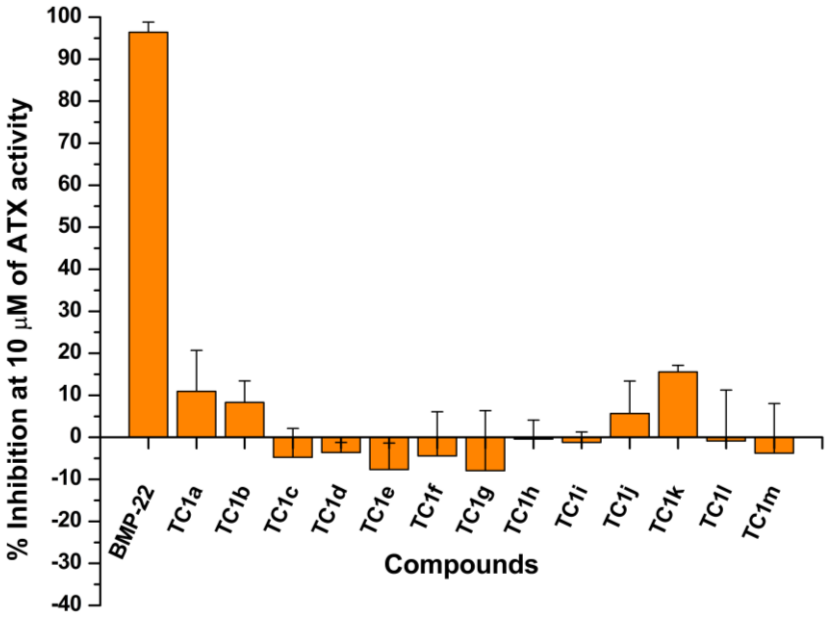

Figure 9. Percent inhibition of the initially synthesized 13 pyrazolo[5,1-b]quinazolin-8(4H)-one derivatives at 10 µM concentration against hATX. Data represent the mean ± standard deviation (SD). BMP-22 was included as a validated positive control.

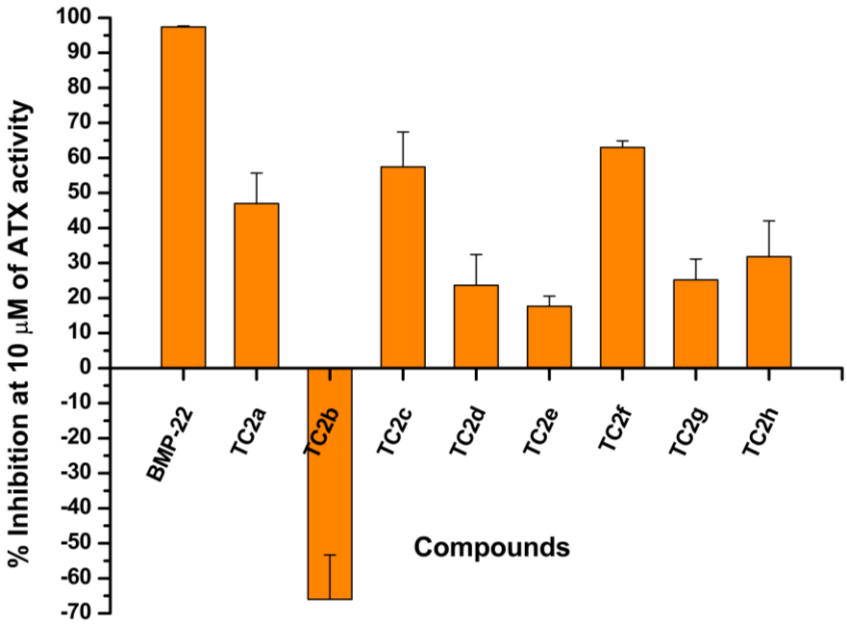

Figure 10. Percent inhibition of the 8 pyrazolo[5,1-b]quinazolin-8(4H)-one derivatives synthesized in the second phase at 10 µM concentration against hATX. Data represent the mean ± standard deviation (SD). BMP-22 was included as a validated positive control.

The dose–response experiments revealed that compound TC2c exhibited an IC_{50} of 2.0 ± 0.3 µM, while TC2f showed slightly better potency with an IC_{50} of 1.8 ± 0.2 µM. These values demonstrate a substantial improvement in inhibitory activity compared to the initial library and highlight the importance of hydrophobic aryl substitution at R_1 for enhancing ATX binding affinity. The results indicate that modifications at the R_1 position significantly influence the biological activity of pyrazolo[5,1-b]quinazolin-8(4H)-one derivatives. While simple hydrogen and methyl groups were not sufficient to achieve meaningful ATX inhibition, the incorporation of a 4-methylphenyl ring introduced favorable interactions that enhanced inhibitory potency.

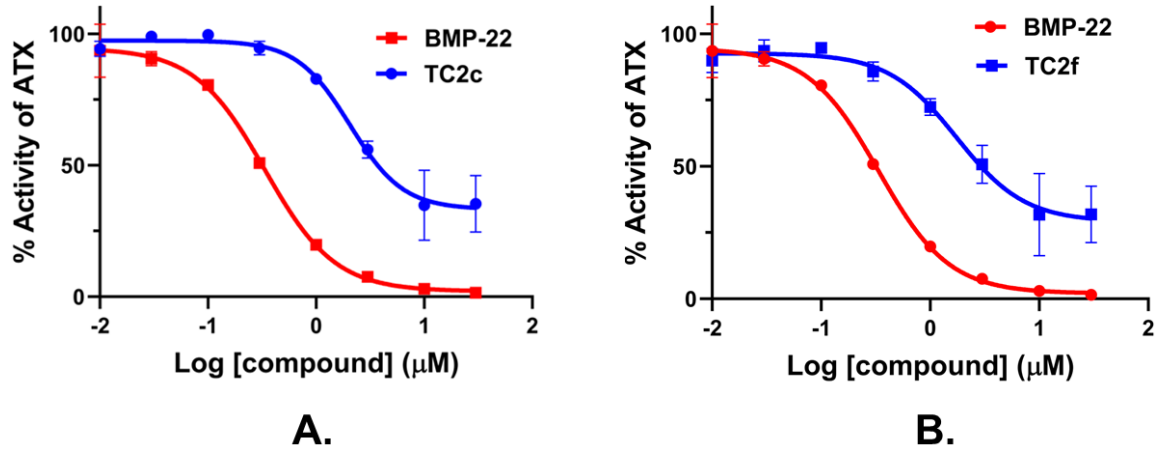

Figure 11. Representative dose–response curves from the FS-3-based Autotaxin (ATX) enzyme inhibition assay. (A) Inhibitory activity of compound TC2c compared with the validated ATX inhibitor BMP-22. **(B)** Inhibitory activity of compound TC2f alongside BMP-22. Assays were performed in biological duplicates (n = 2). TC2c exhibited an average IC_{50} of 2.0 ± 0.3 µM, while TC2f showed an average IC_{50} of 1.8 ± 0.2 µM. The reference inhibitor BMP-22 demonstrated an average IC_{50} of 0.4 ± 0.1 µM.

2.C. Conclusion

This study reports the successful design, synthesis, and preliminary biological evaluation of 21 novel pyrazolo[5,1-b]quinazolin-8(4H)-one derivatives as potential ATX inhibitors. The initial library of 13 compounds, featuring hydrogen or methyl groups at the R_1 position, showed limited ATX inhibition, with less than 20% activity at 10 µM. Guided by structure–activity

relationship insights, strategic modification with a 4-methylphenyl substituent at R_1 led to the synthesis of an additional eight analogues, two of which (TC2c and TC2f) demonstrated significantly enhanced ATX inhibitory activity, with IC_{50} values of $2.0 \pm 0.25\ \mu M$ and $1.8 \pm 0.15\ \mu M$, respectively. These results underscore the importance of hydrophobic aryl substitutions in optimizing binding interactions within the ATX active site and validate the pyrazolo[5,1-b]quinazolin-8(4H)-one scaffold as a promising chemotype for further development. The synthetic approach proved efficient and reproducible, enabling rapid generation of structurally diverse analogues with drug-like features. Importantly, this work builds upon our lab's recent discovery of novel ATX inhibitors with synergistic anti-cancer effects in breast and melanoma cell lines, further supporting the therapeutic relevance of ATX targeting in oncology. The newly identified compounds, TC2c and TC2f, will now serve as leading candidates for *in vitro* cell-based studies, including evaluation of their efficacy as single agents and in combination with chemotherapeutics such as Paclitaxel, to explore their potential to overcome cancer therapy resistance.

2.D. Experimental protocols

2.D.1. Chemistry- general protocols

All non-aqueous reactions were carried out in oven-dried glassware under an inert atmosphere of dry nitrogen to prevent moisture-sensitive side reactions. Unless otherwise stated, all reagents and solvents were obtained from commercial suppliers, including Sigma-Aldrich (St. Louis, MO), Alfa Aesar (Ward Hill, MA), Combi-Blocks (San Diego, CA), and Ark Pharm (Libertyville, IL), and were used as received without further purification. Reaction progress was monitored by analytical thin-layer chromatography (TLC) using silica gel GHLF 10 × 20 cm TLC

plates (Analtech, Newark, DE). Visualization was achieved by quenching of fluorescence under UV light (254 nm). Final compounds were purified using flash column chromatography on a Teledyne CombiFlash system, employing gradient elution as required. ^{1}H and ^{13}C NMR spectra were recorded on a JEOL 500 MHz NMR spectrometer. Chemical shifts (δ) are reported in parts per million (ppm) and are referenced to the residual solvent peaks: $CDCl_3$ (δ = 7.26 ppm for ^1H, 77.23 ppm for ^{13}C) and DMSO-d_6 (δ = 2.50 ppm for ^{1}H, 39.51 ppm for ^{13}C). Spectral data were used to confirm the chemical identity and purity of all final compounds.

2.D.2. Chemical synthesis

General procedure for the synthesis of tricyclic pyrazolo[5,1-b]quinazolin-8(4H)-one compounds

A mixture containing 5-methyl-1H-pyrazol-3-amine (1.0 equiv) or 1H-pyrazol-3-amine (1.0 equiv) or 5-amino-3-(4-methylphenyl)-1H-pyrazole (1.0 equiv), along with a cyclic 1,3-diketone—either 1,3-cyclohexanedione, 5-methylcyclohexane-1,3-dione, or 5,5-dimethylcyclohexane-1,3-dione (1.0 equiv)—and a suitable benzaldehyde derivative (1.0 equiv), was dissolved in anhydrous ethanol (absolute, 20 mL) in a three-neck round-bottom flask under a dry argon atmosphere. The reaction mixture was stirred and heated under reflux at 80 °C for 72 hours. After completion, the reaction was allowed to cool to room temperature and left to stand overnight. The solvent was removed under reduced pressure using a rotary evaporator, yielding a crude solid product. The resulting crude material was purified by flash column chromatography using a 2:23 ethanol: dichloromethane (EtOH:DCM) solvent system to afford the desired pyrazolo[5,1-b]quinazolin-8(4H)-one derivatives in pure form. The products were characterized by NMR spectroscopy and were used for subsequent biological evaluation.

Synthesis of TC1a:

TC1a was synthesized following the general procedure. An amount of 137 mg of 5-methyl-1H-pyrazol-3-amine (1.41 mmol), 178 mg of 5-methylcyclohexane-1,3-dione (1.25 mmol), and 200 mg of 3,5-difluorobenzaldehyde (1.41 mmol) in 20 mL of absolute ethanol yielded a purified product (1.42 mmol, 10.1%) as a white solid after purification (8% EtOH / 92% DCM, R_f = 0.77). MP = 207.7°C (Decomposition occurred) ^{1}H NMR (500 MHz, DMSO-D_6) δ 10.47 (s, 1H), 7.05 (tt, J = 9.2, 2.4 Hz, 1H), 6.75 (dd, J = 8.0, 2.3 Hz, 2H), 6.08 (s, 1H), 5.58 (d, J = 2.5 Hz, 1H), 2.50 (q, J = 2.2 Hz, 7H), 2.34 – 2.17 (m, 2H), 2.04 (d, J = 2.9 Hz, 4H), 0.98 (d, J = 6.4 Hz, 3H). ^{13}C NMR (76 MHz, DMSO-D_6) δ 193.14, 151.39, 148.76, 147.92, 137.76, 110.55, 110.21, 104.55, 103.19, 88.76, 57.05, 44.74, 34.55, 28.99, 20.92, 14.29.

Synthesis of TC1b:

TC1b was synthesized following the general procedure. An amount of 117 mg of 1H-pyrazol-3-amine (1.41 mmol), 126 mg of 5-methylcyclohexane-1,3-dione (1.41 mmol), and 200 mg of 3,5-difluorobenzaldehyde (1.41 mmol) in 20 mL of absolute ethanol yielded a purified product (0.214 mmol, 15.7%) as a brown-white solid after purification (8% EtOH / 92% DCM, R_f = 0.74). MP = 234.2 – 236.4°C. ^{1}H NMR (500 MHz, DMSO-D_6) δ 10.53 (s, 1H), 7.31 (s, 1H), 7.08 – 6.90 (m, 1H), 6.73 (t, J = 4.1 Hz, 2H), 6.16 (s, 1H), 5.72 (d, J = 2.1 Hz, 1H), 2.62 – 2.37 (m, 6H), 2.31 – 2.15 (m, 2H), 2.07 – 1.95 (m, 1H), 1.04 – 0.88 (m, 3H). ^{13}C NMR (126 MHz, DMSO-D_6) δ 193.21, 163.51, 161.55, 151.58, 147.65, 140.44, 137.35, 110.28, 104.33, 103.26, 57.31, 44.74, 34.58, 29.01, 20.95.

Synthesis of TC1c:

TC1c was synthesized following the general procedure. An amount of 124 mg of 5-methyl-1H-pyrazol-3-amine (1.27 mmol), 160 mg of 5-methylcyclohexane-1,3-dione (1.27 mmol), and 250

mg of 3,4,5-trimethoxybenzaldehyde (1.27 mmol) in 20 mL of absolute ethanol yielded a purified product (0.0568 mmol, 4.5%) as a white solid after purification (8% EtOH / 92% DCM, R_f = 0.69). MP = 190.2 – 190.8°C. ^{1}H NMR (301 MHz, DMSO-*D*6) δ 10.29 (s, 1H), 6.34 (d, *J* = 3.8 Hz, 2H), 5.96 (s, 1H), 5.52 (s, 1H), 3.64 (dt, *J* = 7.4, 3.2 Hz, 5H), 3.56 (dt, *J* = 7.2, 3.0 Hz, 4H), 2.59 (d, *J* = 16.6 Hz, 1H), 2.30 (d, *J* = 18.2 Hz, 3H), 2.01 (dd, *J* = 5.4, 2.6 Hz, 4H), 0.99 (d, *J* = 6.5 Hz, 3H).^{13}C NMR (76 MHz, DMSO-D_6) δ 193.00, 152.99, 150.68, 148.11, 139.36, 137.75, 137.08, 105.58, 104.65, 88.43, 60.38, 57.68, 56.27, 44.73, 34.47, 28.81, 20.77, 14.34.

Synthesis of TC1d:

TC1d was synthesized following the general procedure. An amount of 106 mg of 1H-pyrazol-3-amine (1.27 mmol), 160 mg of 5-methylcyclohexane-1,3-dione (1.27 mmol), and 250 mg of 3,4,5-trimethoxybenzaldehyde (1.27 mmol) in 20 mL of absolute ethanol yielded a purified product (0.496 mmol, 38.89%) as a brownish-white solid after purification (8% EtOH / 92% DCM, R_f = 0.69). MP = 212.2 – 215.8°C. ^{1}H NMR (500 MHz $CDCl_3$) δ 7.44 (d, *J* = 38.4 Hz, 2H), 6.47 – 6.20 (m, 3H), 5.67 (s, 1H), 3.98 – 3.49 (m, 9H), 2.43 (dd, *J* = 47.0, 17.2 Hz, 4H), 2.10 (s, 1H), 1.12 – 0.91 (m, 3H). ^{13}C NMR (126 MHz, $CDCl_3$) δ 193.96, 153.13, 148.53, 140.13, 137.98, 137.30, 136.80, 107.77, 104.07, 88.51, 60.74, 58.25, 56.08, 44.83, 35.57, 29.11, 20.78.

Synthesis of TC1e:

TC1e was synthesized following the general procedure. An amount of 108 mg of 1H-pyrazol-3-amine (1.30 mmol), 164 mg of 5-methylcyclohexane-1,3-dione (1.30 mmol), and 200 mg of 4-fluoro-3-methoxybenzaldehyde (1.30 mmol) in 20 mL of absolute ethanol yielded a purified product (0.392 mmol, 30.21%) as a white solid after purification (8% EtOH / 92% DCM, R_f = 0.69). MP = 233.2 – 234.6°C. ^{1}H NMR (301 MHz, $CDCl_3$) δ 7.41 (d, *J* = 14.0 Hz, 2H), 7.15 –

6.77 (m, 2H), 6.58 (s, 1H), 6.38 (s, 1H), 5.66 (s, 1H), 4.00 – 3.66 (m, 3H), 2.61 – 1.97 (m, 5H), 1.06 (d, J = 5.1 Hz, 3H). ^{13}C NMR (126 MHz, DMSO-D_6) δ 193.08, 152.09, 150.96, 150.16, 146.91, 140.01, 137.31, 119.10, 115.99, 115.85, 113.20, 105.25, 88.77, 57.59, 56.41, 44.77, 34.54, 28.91, 20.87.

Synthesis of TC1f:

TC1f was synthesized following the general procedure. An amount of 100 mg of 1H-pyrazol-3-amine (1.20 mmol), 152 mg of 5-methylcyclohexane-1,3-dione (1.20 mmol), and 200 mg of 3,5-dimethoxybenzaldehyde (1.20 mmol) in 20 mL of absolute ethanol yielded a purified product (0.229 mmol, 19.02%) as a brown-white solid after purification (8% EtOH / 92% DCM, R_f = 0.74). MP = 226.0 – 227.5°C. ^{1}H NMR (301 MHz, $CDCl_3$) δ 7.71 (s, 1H), 7.37 (s, 1H), 6.42 – 6.30 (m, 3H), 6.27 (s, 1H), 5.61 (s, 1H), 3.75 – 3.66 (m, 6H), 2.42 (d, J = 36.3 Hz, 4H), 2.09 (dd, J = 16.1, 9.3 Hz, 1H), 1.09 – 0.98 (m, 3H). ^{13}C NMR (126 MHz, DMSO-D_6) δ 193.03, 160.64, 150.93, 145.64, 139.90, 137.47, 105.60, 105.41, 98.77, 88.73, 57.76, 55.56, 44.75, 34.50, 28.91, 20.83.

Synthesis of TC1g:

TC1g was synthesized following the general procedure. An amount of 100 mg of 1H-pyrazol-3-amine (1.20 mmol), 152 mg of 5-methylcyclohexane-1,3-dione (1.20 mmol), and 200 mg of 3,4-dimethoxybenzaldehyde (1.20 mmol) in 20 mL of absolute ethanol yielded a purified product (0.0236 mmol, 1.96%) as a brown-white solid after purification (8% EtOH / 92% DCM, R_f = 0.71). MP = 256.5 – 257.8°C. ^{1}H NMR (500 MHz, $CDCl_3$) δ 7.35 (d, J = 29.2 Hz, 2H), 6.86 (s, 1H), 6.77 – 6.56 (m, 2H), 6.37 (d, J = 3.6 Hz, 1H), 5.65 (s, 1H), 3.79 (dd, J = 15.7, 3.8 Hz, 6H), 2.57 – 2.28 (m, 4H), 2.15 – 2.00 (m, 1H), 1.18 – 0.93 (m, 3H). ^{13}C NMR (126 MHz, DMSO-D_6)

δ 193.02, 150.68, 148.67, 148.47, 139.74, 137.32, 136.10, 119.14, 111.99, 111.47, 105.67, 88.61, 57.60, 56.02, 55.94, 44.79, 34.52, 28.87, 20.85.

Synthesis of TC1h:

TC1h was synthesized following the general procedure. An amount of 108 mg of 1H-pyrazol-3-amine (1.41 mmol), 164 mg of 5-methylcyclohexane-1,3-dione (1.41 mmol), and 200 mg of 3,4-difluorobenzaldehyde (1.41 mmol) in 20 mL of absolute ethanol yielded a purified product (0.169 mmol, 12.01%) as a yellow-white solid after purification (8% EtOH / 92% DCM, R_f = 0.74). MP = 221.9 – 223.2°C. ^{1}H NMR (500 MHz, $CDCl_3$) δ 7.39 (s, 1H), 7.17 (s, 1H), 7.05 – 6.89 (m, 3H), 6.37 (s, 1H), 5.68 (d, *J* = 2.0 Hz, 1H), 2.57 – 2.33 (m, 4H), 2.10 (dd, *J* = 16.4, 10.1 Hz, 1H), 1.08 (d, *J* = 6.5 Hz, 3H). ^{13}C NMR (126 MHz, DMSO-D_6) δ 193.18, 151.32, 141.02, 140.29, 137.27, 123.95, 117.65, 116.34, 104.71, 100.00, 88.93, 57.18, 44.78, 34.59, 29.00, 20.97.

Synthesis of TC1i:

TC1i was synthesized following the general procedure. An amount of 108 mg of 1H-pyrazol-3-amine (1.30 mmol), 164 mg of 5-methylcyclohexane-1,3-dione (1.30 mmol), and 200 mg of 2-fluoro-5-methoxybenzaldehyde (1.30 mmol) in 20 mL of absolute ethanol yielded a purified product (0.210 mmol, 16.2%) as a brown-white solid after purification (8% EtOH / 92% DCM, R_f = 0.77). MP = 257.6 – 258.8°C. ^{1}H NMR (500 MHz, DMSO-D_6) δ 10.44 (s, 1H), 7.23 (d, *J* = 1.9 Hz, 1H), 6.99 – 6.89 (m, 1H), 6.74 (dt, *J* = 9.0, 3.6 Hz, 1H), 6.60 (dd, *J* = 6.0, 3.1 Hz, 1H), 6.26 (s, 1H), 5.64 (d, *J* = 1.9 Hz, 1H), 3.62 (d, *J* = 1.8 Hz, 3H), 2.60 (dd, *J* = 16.2, 4.5 Hz, 1H), 2.35 – 2.15 (m, 2H), 2.05 – 1.88 (m, 1H), 0.97 (s, 3H). ^{13}C NMR (126 MHz, DMSO-D_6) δ 192.87, 155.61, 153.77, 151.20, 140.05, 137.15, 131.02, 116.30, 115.08, 113.71, 104.12, 88.60, 55.95, 52.94, 44.68, 34.53, 28.78, 20.76.

Synthesis of TC1j:

TC1j was synthesized following the general procedure. An amount of 162 mg of 1H-pyrazol-3-amine (1.95 mmol), 246 mg of 5-methylcyclohexane-1,3-dione (1.95 mmol), and 300 mg of 2-fluoro-3-methoxybenzaldehyde (1.95 mmol) in 20 mL of absolute ethanol yielded a purified product (0.210 mmol, 16.2%) as a yellow-white solid after purification (8% EtOH / 92% DCM, R_f = 0.83). MP = 246.5 – 247.9°C. ^{1}H NMR (500 MHz, $CDCl_3$) δ 7.66 (s, 1H), 7.33 (t, *J* = 1.7 Hz, 1H), 7.09 – 7.00 (m, 1H), 6.97 (t, *J* = 7.9 Hz, 1H), 6.79 (t, *J* = 7.9 Hz, 1H), 6.48 (s, 1H), 5.52 (t, *J* = 1.7 Hz, 1H), 3.77 (q, *J* = 1.3 Hz, 3H), 3.72 (d, *J* = 8.0 Hz, 2H), 2.57 – 2.22 (m, 4H), 2.07 (dd, *J* = 16.3, 9.7 Hz, 1H), 1.07 (dd, *J* = 6.4, 1.3 Hz, 3H). ^{13}C NMR (126 MHz, DMSO-D_6) δ 192.89, 151.14, 140.03, 137.13, 131.07, 124.24, 120.25, 112.89, 104.29, 100.01, 88.58, 56.56, 52.32, 44.72, 34.55, 28.81, 20.83, 19.10.

Synthesis of TC1k:

TC1k was synthesized following the general procedure. An amount of 183 mg of 1H-pyrazol-3-amine (2.20 mmol), 278 mg of 5-methylcyclohexane-1,3-dione (2.20 mmol), and 300 mg of 4-methoxybenzaldehyde (2.20 mmol) in 20 mL of absolute ethanol yielded a purified product (0.563 mmol, 25.57%) as a brown-white solid after purification (8% EtOH / 92% DCM, R_f = 0.77). MP = 211.1 – 212.5°C. ^{1}H NMR (500 MHz, $CDCl_3$) δ 7.54 (s, 1H), 7.36 (d, *J* = 2.0 Hz, 1H), 7.17 – 7.08 (m, 2H), 6.78 – 6.68 (m, 2H), 6.36 (s, 1H), 5.61 (d, *J* = 2.0 Hz, 1H), 3.70 (s, 3H), 2.55 – 2.28 (m, 4H), 2.08 (dd, *J* = 16.1, 10.2 Hz, 1H), 1.05 (d, *J* = 6.1 Hz, 3H). ^{13}C NMR (126 MHz, DMSO-D_6) δ 192.98, 158.84, 150.63, 139.75, 137.30, 135.73, 128.32, 113.83, 105.75, 88.60, 57.44, 55.54, 44.84, 34.55, 28.96, 20.93.

Synthesis of TC1l:

TC1l was synthesized following the general procedure. An amount of 189 mg of 5-methyl-1H-

pyrazol-3-amine (1.95 mmol), 246 mg of 5-methylcyclohexane-1,3-dione (1.95 mmol), and 300 mg of 4-fluoro-3-methoxybenzaldehyde (1.95 mmol) in 20 mL of absolute ethanol yielded a purified product (0.149 mmol, 7.63%) as a yellow-white solid after purification (8% EtOH / 92% DCM, R_f = 0.77). MP = 200.1 – 200.8°C. ^{1}H NMR (500 MHz, $CDCl_3$) δ 7.53 (s, 1H), 7.00 (dd, *J* = 8.1, 2.2 Hz, 1H), 6.93 – 6.80 (m, 1H), 6.53 (ddt, *J* = 9.0, 4.6, 2.2 Hz, 1H), 6.28 (d, *J* = 3.5 Hz, 1H), 5.44 (d, *J* = 4.5 Hz, 1H), 3.81 (d, *J* = 4.8 Hz, 3H), 2.52 – 2.24 (m, 4H), 2.21 – 2.10 (m, 3H), 2.09 – 1.99 (m, 1H), 1.04 (d, *J* = 5.9 Hz, 3H). ^{13}C NMR (126 MHz, DMSO-D_6) δ 193.00, 152.04, 150.73, 150.11, 148.27, 146.87, 140.44, 137.75, 119.20, 115.99, 113.20, 105.51, 88.47, 57.29, 56.41, 44.76, 34.51, 28.89, 20.84, 14.30.

Synthesis of TC1m:

TC1m was synthesized following the general procedure. An amount of 175 mg of 5-Methyl-1H-Pyrazol-3-Amine (1.81 mmol), 228 mg of 5-Methylcyclohexane-1,3-dione (1.81 mmol), and 300 mg of 3,5-dimethoxybenzaldehyde (1.81 mmol) in 20 mL of absolute Ethanol yielded a purified product (0.216 mmol, 11.94%) as a yellow-white solid after purification (8% EtOH / 92% DCM, R_f = 0.77). MP = 242.9 – 245.7°C. ^{1}H NMR (500 MHz, $CDCl_3$) δ 7.84 (s, 1H), 6.47 – 6.12 (m, 4H), 5.40 (dd, *J* = 6.1, 2.9 Hz, 1H), 3.75 – 3.60 (m, 6H), 2.37 – 1.91 (m, 7H), 1.09 – 0.84 (m, 3H). ^{13}C NMR (126 MHz, DMSO-D_6) δ 192.92, 160.60, 150.68, 148.13, 145.93, 137.89, 105.68, 98.61, 88.42, 57.48, 56.56, 55.55, 44.76, 34.48, 28.90, 20.82, 19.10, 14.32.

Synthesis of TC2a:

TC2a was synthesized following the general procedure. An amount of 212 mg of 5-Amino-3-(4-methylphenyl)pyrazole (1.22 mmol), 154 mg of 5-Methylcyclohexane-1,3-dione (1.22 mmol), and 300 mg of 3-Bromo-4,5-Dimethoxybenzaldehyde (1.22 mmol) in 20 mL of absolute Ethanol yielded a purified product (0.279 mmol, 22.71%) as a white solid after purification (8% EtOH /

92% DCM, R_f = 0.74). MP = 260+°C. ^{1}H NMR (500 MHz, DMSO-D_6) δ 12.48 (s, 1H), 9.95 (d, *J* = 19.0 Hz, 1H), 7.42 (d, *J* = 5.6 Hz, 2H), 7.22 (d, *J* = 7.2 Hz, 2H), 6.80 – 6.68 (m, 1H), 6.58 (d, *J* = 1.9 Hz, 1H), 5.31 (d, *J* = 20.5 Hz, 1H), 3.52 (ddd, *J* = 22.5, 5.7, 2.4 Hz, 6H), 2.58 (d, *J* = 16.8 Hz, 1H), 2.41 (s, 1H), 2.28 (s, 4H), 2.18 (s, 1H), 1.99 (s, 1H), 0.96 (d, *J* = 7.7 Hz, 3H). ^{13}C NMR (126 MHz, DMSO-D_6) δ 193.57, 154.32, 152.85, 147.91, 145.72, 143.67, 138.35, 138.12, 129.87, 127.28, 126.93, 122.62, 116.53, 112.28, 107.66, 102.81, 60.37, 45.34, 35.71, 35.44, 29.05, 21.31, 20.93.

Synthesis of TC2b:

TC2b was synthesized following the general procedure. An amount of 177 mg of 5-Amino-3-(4-methylphenyl)pyrazole (1.02 mmol), 143 mg of 5,5-Dimethylcyclohexane-1,3-dione (1.02 mmol), and 250 mg of 3-Bromo-4,5-dimethoxybenzaldehyde (1.02 mmol) in 20 mL of absolute Ethanol yielded a purified product (0.155 mmol, 15.18%) as a white solid after purification (8% EtOH / 92% DCM, R_f = 0.77). MP = 176.1 – 177.5°C. ^{1}H NMR (500 MHz, DMSO-D_6) δ 12.37 (s, 1H), 9.94 (s, 1H), 7.44 (d, *J* = 8.0 Hz, 2H), 7.23 (d, *J* = 8.2 Hz, 2H), 6.69 (d, *J* = 54.0 Hz, 2H), 5.30 (s, 1H), 3.61 – 3.43 (m, 6H), 2.35 – 1.85 (m, 6H), 1.05 – 0.94 (m, 3H), 0.92 (d, *J* = 6.2 Hz, 3H). ^{13}C NMR (126 MHz, DMSO-D_6) δ 193.49, 153.39, 152.90, 147.96, 145.68, 143.68, 138.36, 138.11, 129.86, 126.91, 125.99, 122.74, 116.48, 112.20, 107.15, 102.96, 60.38, 56.11, 50.86, 41.37, 35.35, 32.52, 29.50, 27.10, 21.31.

Synthesis of TC2c:

TC2c was synthesized following the general procedure. An amount of 221 mg of 5-Amino-3-(4-methylphenyl)pyrazole (1.27 mmol), 179 mg of 5,5-Dimethylcyclohexane-1,3-dione (1.27 mmol), and 250 mg of 3,4,5-Trimethoxybenzaldehyde (1.27 mmol) in 20 mL of absolute Ethanol yielded a purified product (0.995 mmol, 78.05%) as a white solid after purification (8% EtOH /

92% DCM, R_f = 0.74). MP = 202.7 – 206.8°C. ^{1}H NMR (500 MHz, DMSO-D_6) δ 12.41 (s, 1H), 9.85 (s, 1H), 7.45 (d, J = 8.2 Hz, 3H), 7.24 (d, J = 7.8 Hz, 3H), 6.25 (d, J = 2.4 Hz, 3H), 5.28 (d, J = 2.2 Hz, 2H), 4.33 (t, J = 5.1 Hz, 1H), 2.28 (d, J = 2.3 Hz, 4H), 2.17 (d, J = 16.0 Hz, 2H), 1.99 (d, J = 16.0 Hz, 2H), 1.01 (s, 5H), 0.96 (d, J = 2.4 Hz, 4H). ^{1}H NMR (500 MHz, DMSO-D_6) δ 12.41 (s, 1H), 9.85 (s, 1H), 7.45 (d, J = 8.2 Hz, 3H), 7.24 (d, J = 7.8 Hz, 3H), 6.25 (d, J = 2.4 Hz, 3H), 5.28 (d, J = 2.2 Hz, 2H), 4.33 (t, J = 5.1 Hz, 1H), 2.28 (d, J = 2.3 Hz, 4H), 2.17 (d, J = 16.0 Hz, 2H), 1.99 (d, J = 16.0 Hz, 2H), 1.01 (s, 5H), 0.96 (d, J = 2.4 Hz, 4H).

Synthesis of TC2d:

TC2d was synthesized following the general procedure. An amount of 177 mg of 5-Amino-3-(4-methylphenyl)pyrazole (1.02 mmol), 114 mg of 1,3-Cyclohexanedione (1.02 mmol), and 250 mg of 3-Bromo-4,5-Dimethoxybenzaldehyde (1.02 mmol) in 20 mL of absolute yielded a purified product (0.109 mmol, 10.67%) as a brown solid after purification (8% EtOH / 92% DCM, R_f = 0.80). MP = 159.7 – 161.2°C. ^{1}H NMR (301 MHz, DMSO-D_6) δ 10.59 (s, 1H), 7.59 (dd, J = 8.1, 2.0 Hz, 2H), 7.14 (dd, J = 7.3, 1.2 Hz, 2H), 6.90 (d, J = 2.0 Hz, 1H), 6.76 (d, J = 1.8 Hz, 1H), 6.17 – 6.10 (m, 2H), 3.74 (d, J = 1.7 Hz, 3H), 3.67 – 3.59 (m, 3H), 2.64 (q, J = 13.1 Hz, 2H), 2.26 (s, 4H), 1.90 (dd, J = 41.0, 24.5 Hz, 3H). ^{13}C NMR (126 MHz, DMSO-D_6) δ 193.44, 153.53, 152.17, 150.96, 145.24, 140.82, 138.58, 137.60, 130.74, 129.62, 125.59, 122.27, 116.84, 111.88, 105.69, 85.86, 60.45, 57.13, 56.51, 36.82, 27.01, 21.35.

Synthesis of TC2e:

TC2e was synthesized following the general procedure. An amount of 132 mg of 5-Amino-3-(4-methylphenyl)pyrazole (0.765 mmol), 86 mg of 1,3-Cyclohexanedione (0.765 mmol), and 150 mg of 3,4,5-Trimethoxybenzaldehyde (0.765 mmol) in 20 mL of absolute yielded a purified product (0.137 mmol, 17.97%) as a light-brown solid after purification (8% EtOH / 92% DCM,

R_f = 0.80). MP = 260+°C. ^{1}H NMR (500 MHz, DMSO-D_6) δ 10.51 (s, 1H), 7.59 (s, 2H), 7.14 (s, 2H), 6.42 (d, *J* = 4.7 Hz, 2H), 6.12 (dt, *J* = 15.0, 4.5 Hz, 2H), 3.68 – 3.60 (m, 6H), 3.60 – 3.50 (m, 3H), 2.64 (q, *J* = 14.8 Hz, 2H), 2.26 (s, 5H), 1.91 (d, *J* = 42.9 Hz, 2H). ^{13}C NMR (126 MHz, DMSO-D_6) δ 193.39, 153.07, 152.01, 150.68, 138.91, 138.62, 137.47, 137.23, 130.90, 129.60, 125.55, 106.06, 104.60, 85.67, 60.38, 57.62, 56.31, 36.90, 27.03, 21.40, 21.35.

Synthesis of TC2f:

TC2f was synthesized following the general procedure. An amount of 132 mg of 5-Amino-3-(4-methylphenyl)pyrazole (0.765 mmol), 96 mg of 5-Methylcyclohexan-1,3-dione (0.765 mmol), and 150 mg of 3,4,5-Trimethoxybenzaldehyde (0.765 mmol) in 20 mL of absolute Ethanol yielded a purified product (0.346 mmol, 45.26%) as an off-white solid after purification (8% EtOH / 92% DCM, R_f = 0.74). MP = 260+°C. ^{1}H NMR (500 MHz, DMSO-D_6) δ 12.39 (s, 1H), 9.86 (d, *J* = 20.5 Hz, 1H), 7.44 (d, *J* = 8.1 Hz, 2H), 7.24 (d, *J* = 8.1 Hz, 2H), 6.23 (d, *J* = 6.4 Hz, 2H), 5.31 (d, *J* = 23.7 Hz, 1H), 3.45 (dd, *J* = 13.1, 2.2 Hz, 9H), 2.61 (dd, *J* = 16.1, 4.3 Hz, 1H), 2.28 (s, 6H), 1.98 (dd, *J* = 15.9, 9.2 Hz, 1H), 1.00 – 0.96 (m, 3H). ^{13}C NMR (126 MHz, DMSO-D_6) δ 193.55, 154.18, 152.63, 147.95, 143.99, 138.27, 138.01, 135.68, 129.81, 127.64, 127.12, 107.89, 104.57, 103.46, 60.31, 55.88, 45.33, 35.69, 35.61, 28.88, 21.30, 20.93.

Synthesis of TC2g:

TC2g was synthesized following the general procedure. An amount of 183 mg of 5-Amino-3-(4-methylphenyl)pyrazole (1.06 mmol), 133 mg of 5-Methylcyclohexan-1,3-dione (1.06 mmol), and 150 mg of 3,4-Difluorobenzaldehyde (1.06 mmol) in 20 mL of absolute Ethanol yielded a purified product (0.225 mmol, 21.33%) as a light-brown solid after purification (8% EtOH / 92% DCM, R_f = 0.86). MP = 217.8 – 219.1°C. ^{1}H NMR (500 MHz, DMSO-D_6) δ 10.59 (s, 1H), 7.57 (d, *J* = 8.1 Hz, 2H), 7.34 – 7.06 (m, 4H), 6.95 (s, 1H), 6.20 – 6.05 (m, 2H), 2.60 (d, *J* = 16.4 Hz,

1H), 2.33 – 2.15 (m, 5H), 2.01 (dd, *J* = 15.7, 9.7 Hz, 1H), 0.97 (d, *J* = 8.6 Hz, 4H). ^{13}C NMR (126 MHz, DMSO-D_6) δ 193.17, 151.18, 151.05, 138.55, 137.65, 130.70, 129.61, 125.64, 123.99, 117.63, 116.31, 85.93, 57.30, 44.79, 34.59, 28.98, 21.40, 21.00.

Synthesis of TC2h:

TC2h was synthesized following the general procedure. An amount of 162 mg of 5-Amino-3-(4-methylphenyl)pyrazole (0.765 mmol), 118 mg of 5-Methylcyclohexan-1,3-dione (0.937 mmol), and 150 mg of 3,4,5-Trifluorobenzaldehyde (0.937 mmol) in 20 mL of absolute Ethanol yielded a purified product (0.184 mmol, 19.61%) as a light yellow solid after purification (8% EtOH / 92% DCM, R_f = 0.86). MP = 200.4 – 203.2°C. ^{1}H NMR (301 MHz, DMSO-D_6) δ 10.65 (s, 1H), 7.58 (d, *J* = 8.0 Hz, 2H), 7.20 – 7.00 (m, 4H), 6.15 (d, *J* = 8.9 Hz, 2H), 2.55 (d, *J* = 8.3 Hz, 2H), 2.26 (s, 5H), 0.98 (d, *J* = 6.1 Hz, 4H). ^{13}C NMR (126 MHz, DMSO-D_6) δ 193.27, 151.67, 151.23, 138.44, 137.73, 129.62, 125.67, 112.05, 111.92, 86.11, 57.28, 44.84, 34.65, 29.07, 21.40, 21.10.

2.D.3. Autotaxin enzyme inhibition assay

Stock solutions (25 mM) of the test compounds were prepared in dimethyl sulfoxide (DMSO) and stored at −20 °C. For biological assays, working solutions were freshly diluted in either assay buffer or DMSO, depending on the experimental protocol. Human recombinant ATX (hATX) protein was acquired from Dr. Tigyi's lab at the University of Tennessee Health Science Center, Memphis, TN. The ATX inhibitory activity of the compounds was evaluated using the FS-3-based fluorometric assay. FS-3 is a synthetic lipid (LPC) analog (purchased from Echelon Biosciences, Salt Lake City, UT, USA) that fluoresces upon cleavage by active ATX. Each reaction well in a black 96-well microplate received 60 µL of ATX assay buffer (50 mM Tris, pH 8.0, supplemented with 10 µM BSA, 140 mM NaCl, 5 mM KCl, 1 mM $CaCl_2$, and 1 mM $MgCl_2$). Purified ATX was then added to reach a final concentration of 10 nM per well. Test compounds were introduced into the wells in technical triplicate; single-point screening was conducted at a final concentration of 10 µM, while dose–response studies utilized eight serial dilutions ranging from 10 µM to 3 nM. Following compound addition, FS-3 was added to each well to achieve a final concentration of 1 µM. The reaction was monitored for 2 hours using a CLARIOstar Plus microplate reader (BMG Labtech, Germany), with fluorescence measurements collected every 2 minutes at an excitation wavelength of 485 nm and emission at 528 nm. Percent inhibition was calculated relative to control wells treated with DMSO alone. IC_{50} values were derived using non-linear regression analysis in GraphPad Prism (v10.3.0). Each dose–response experiment was performed in duplicate, and results are reported as mean ± standard deviation (SD).

REFERENCES

(1) Leblanc, R.; Peyruchaud, O. New Insights into the Autotaxin/LPA Axis in Cancer Development and Metastasis. *Exp. Cell. Res.* **2015**, *333* (2), 183–189. DOI: 10.1016/j.yexcr.2014.11.010.

(2) Tigyi, G.; Dacheux, M. A.; Lin, K.-H.; Yue, J.; Norman, D.; Benyó, Z.; Lee, S. C. Anti-Cancer Strategies Targeting the Autotaxin-Lysophosphatidic Acid Receptor Axis: Is There a Path Forward? *Cancer Metastasis Rev.* **2021**, *40* (1), 3–5. DOI: 10.1007/s10555-021-09955-5.

(3) Quan, M.; Cui, J.; Feng, X.; Huang, Q. The Critical Role and Potential Target of the Autotaxin/Lysophosphatidate Axis in Pancreatic Cancer. *Tumor Biology* **2017**, *39* (3), 101042831769454. DOI: 10.1177/1010428317694544.

(4) Drosouni, A.; Panagopoulou, M.; Aidinis, V.; Chatzaki, E. Autotaxin in Breast Cancer: Role, Epigenetic Regulation and Clinical Implications. *Cancers (Basel)* **2022**, *14* (21), 5437. DOI: 10.3390/cancers14215437.

(5) Benesch, M. G. K.; Tang, X.; Brindley, D. N. Autotaxin and Breast Cancer: Towards Overcoming Treatment Barriers and Sequelae. *Cancers (Basel)* **2020**, *12* (2), 374. DOI: 10.3390/cancers12020374.

(6) Perrakis, A.; Moolenaar, W. H. Autotaxin: Structure-Function and Signaling. *J. Lipid Res.* **2014**, *55* (6), 1010–1018. DOI: 10.1194/jlr.R046391.

(7) Brindley, D. N.; Lin, F.-T.; Tigyi, G. J. Role of the Autotaxin–Lysophosphatidate Axis in Cancer Resistance to Chemotherapy and Radiotherapy. *Biochimica et Biophysica Acta (BBA) - Molecular and Cell Biology of Lipids* **2013**, *1831* (1), 74–85. DOI: 10.1016/j.bbalip.2012.08.015.

(8) Samadi, N.; Bekele, R.; Capatos, D.; Venkatraman, G.; Sariahmetoglu, M.; Brindley, D. N. Regulation of Lysophosphatidate Signaling by Autotaxin and Lipid Phosphate Phosphatases with Respect to Tumor Progression, Angiogenesis, Metastasis and Chemo-Resistance. *Biochimie* **2011**, *93* (1), 61–70. DOI: 10.1016/j.biochi.2010.08.002.

(9) Banerjee, S.; Norman, D. D.; Lee, S. C.; Parrill, A. L.; Pham, T. C. T.; Baker, D. L.; Tigyi, G. J.; Miller, D. D. Highly Potent Non-Carboxylic Acid Autotaxin Inhibitors Reduce Melanoma Metastasis and Chemotherapeutic Resistance of Breast Cancer Stem Cells. *J. Med. Chem.* **2017**, *60* (4), 1309–1324. DOI: 10.1021/acs.jmedchem.6b01270.

(10) Banerjee, S.; Lee, S.; Norman, D. D.; Tigyi, G. J. Designing Dual Inhibitors of Autotaxin-LPAR GPCR Axis. *Molecules* **2022**, *27* (17), 5487. DOI: 10.3390/molecules27175487.

(11) Centonze, M.; Di Conza, G.; Lahn, M.; Fabregat, I.; Dituri, F.; Gigante, I.; Serino, G.; Scialpi, R.; Carrieri, L.; Negro, R.; Pizzuto, E.; Giannelli, G. Autotaxin Inhibitor IOA-289 Reduces Gastrointestinal Cancer Progression in Preclinical Models. *J. Exp. Clin. Cancer Res.* **2023**, *42* (1), 197. DOI: 10.1186/s13046-023-02780-4.

(12) Castagna, D.; Budd, D. C.; Macdonald, S. J. F.; Jamieson, C.; Watson, A. J. B. Development of Autotaxin Inhibitors: An Overview of the Patent and Primary Literature. *J. Med. Chem.* **2016**, *59* (12), 5604–5621. DOI: 10.1021/acs.jmedchem.5b01599.

(13) Rai, P.; Clark, C. J.; Kardam, V.; Womack, C. B.; Thammathong, J.; Norman, D. D.; Tigyi, G. J.; Bicker, K.; Weissmiller, A. M.; Dubey, K. D.; Banerjee, S. Structure-Based Discovery of MolPort-137: A Novel Autotaxin Inhibitor That Improves Paclitaxel Efficacy. *Int. J. Mol. Sci.* **2025**, *26* (2), 597. DOI: 10.3390/ijms26020597.

(14) Rai, P.; Clark, C. J.; Womack, C. B.; Dearing, C.; Thammathong, J.; Norman, D. D.; Tigyi, G. J.; Sen, S.; Bicker, K.; Weissmiller, A. M.; Banerjee, S. Novel Autotaxin Inhibitor ATX-1d Significantly Enhances Potency of Paclitaxel—An In Silico and In Vitro Study. *Molecules* **2024**, *29* (18), 4285. DOI: 10.3390/molecules29184285.

APPENDIX

Chapter I - ^{1}H and ^{13}C NMRs, HRMS spectra and HPLC traces for top five potent compounds

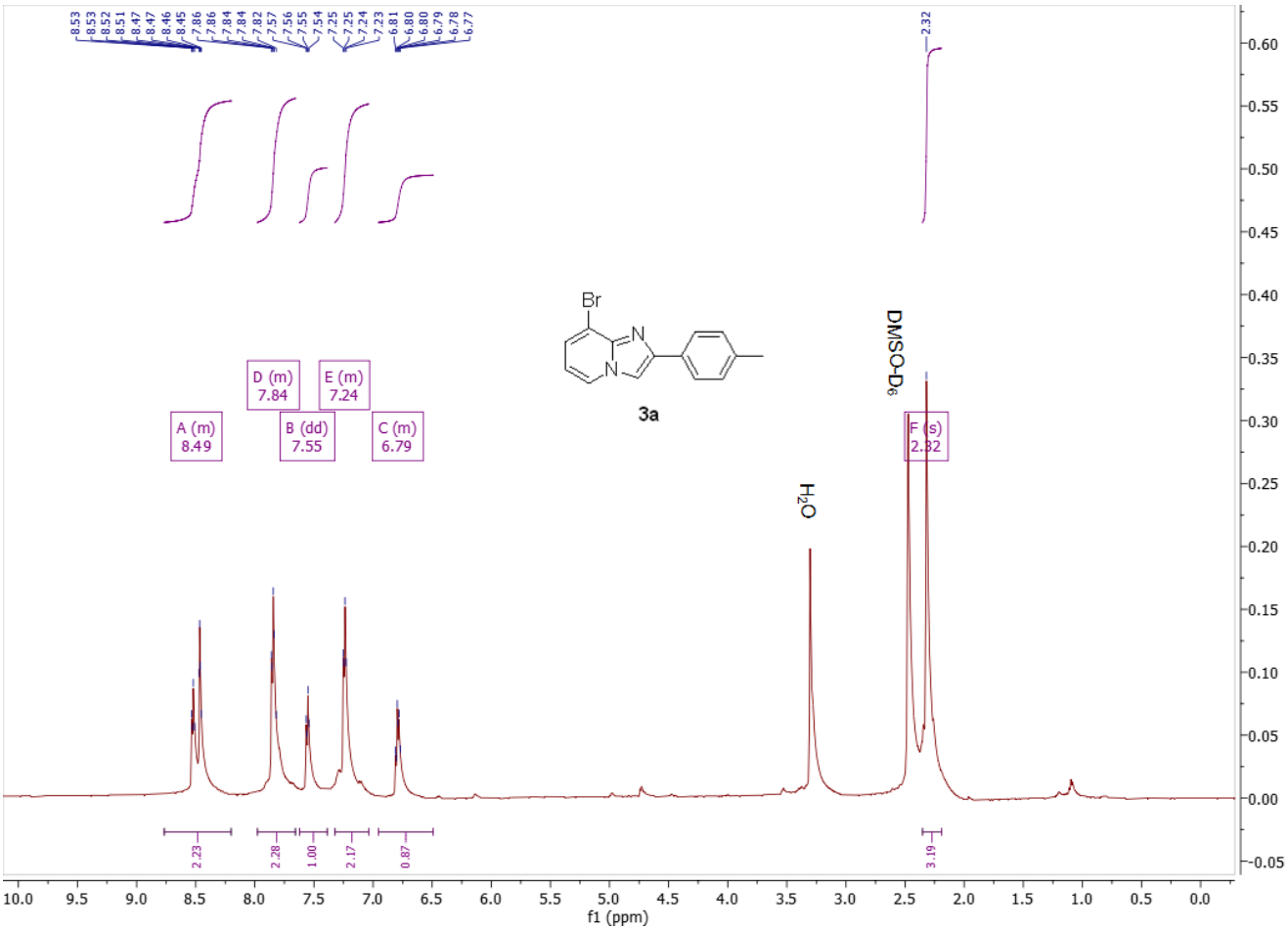

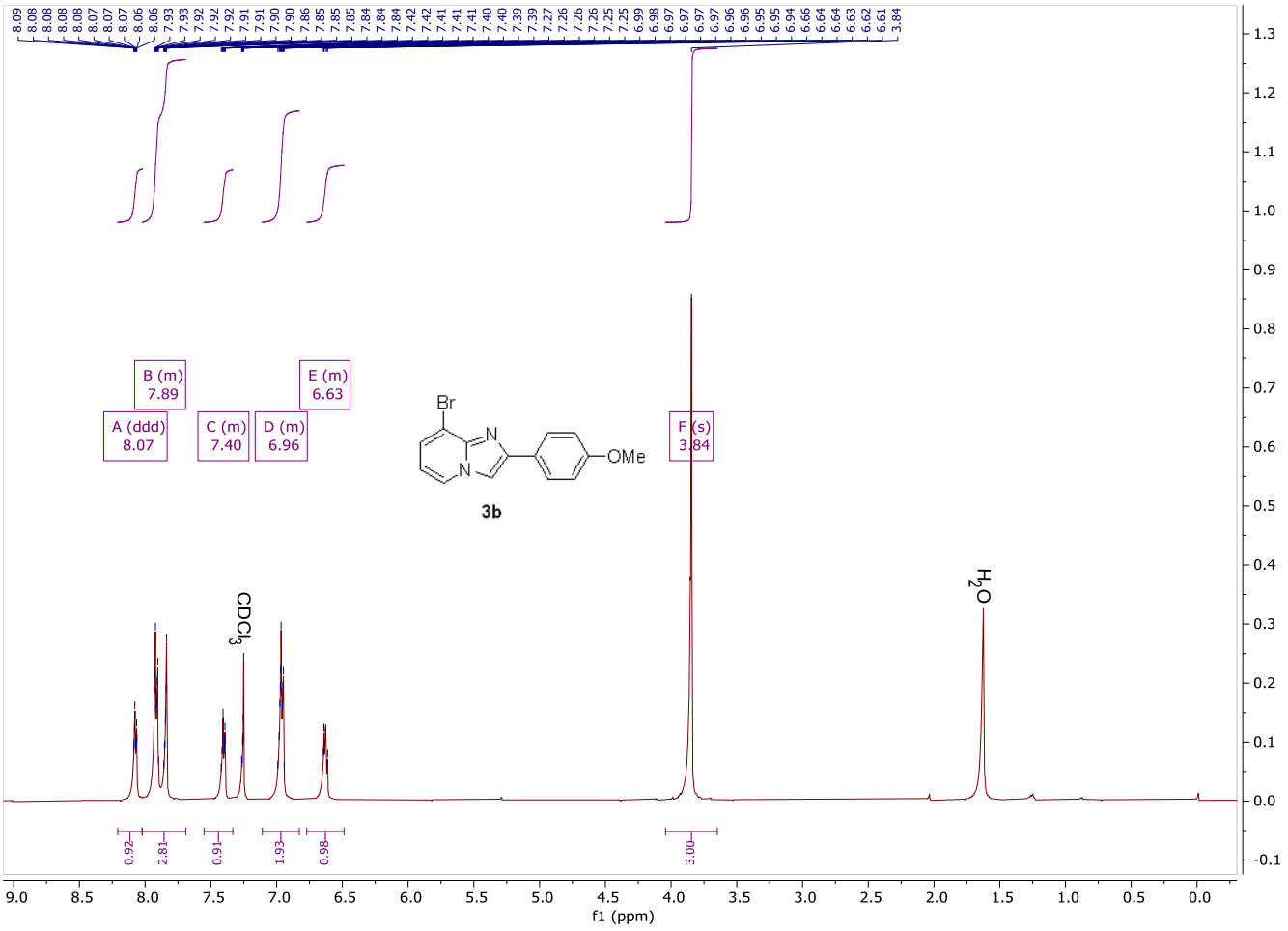
B (m)
7.89
E (m)
6.63
A (ddd)
8.07
C (m)
7.40
D (m)
6.96
F (s)
3.84
Br
N
N
OMe
3b
CDCl3
H2O
0.92
2.81
0.91
1.93
0.98
3.00
f1 (ppm)

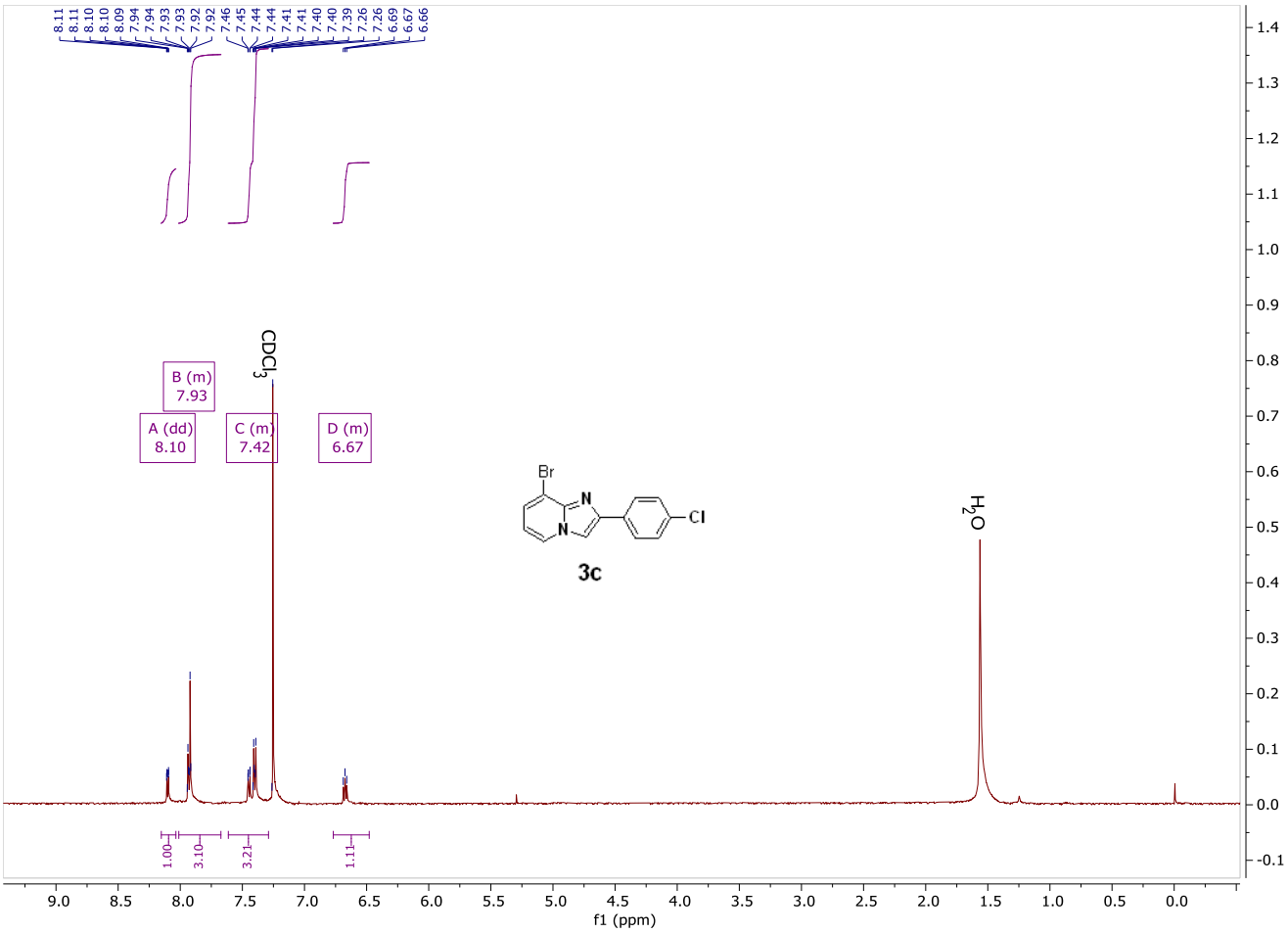
8.11
8.11
8.10
8.10
8.09
7.94
7.94
7.93
7.93
7.92
7.92
7.46
7.45
7.44
7.44
7.41
7.41
7.40
7.40
7.39
7.26
7.26
6.69
6.67
6.66
B (m)
7.93
A (dd)
8.10
C (m)
7.42
D (m)
6.67
CDCl3
Br
N
N
Cl
3c
H2O
1.00
3.10
3.21
1.11
f1 (ppm)

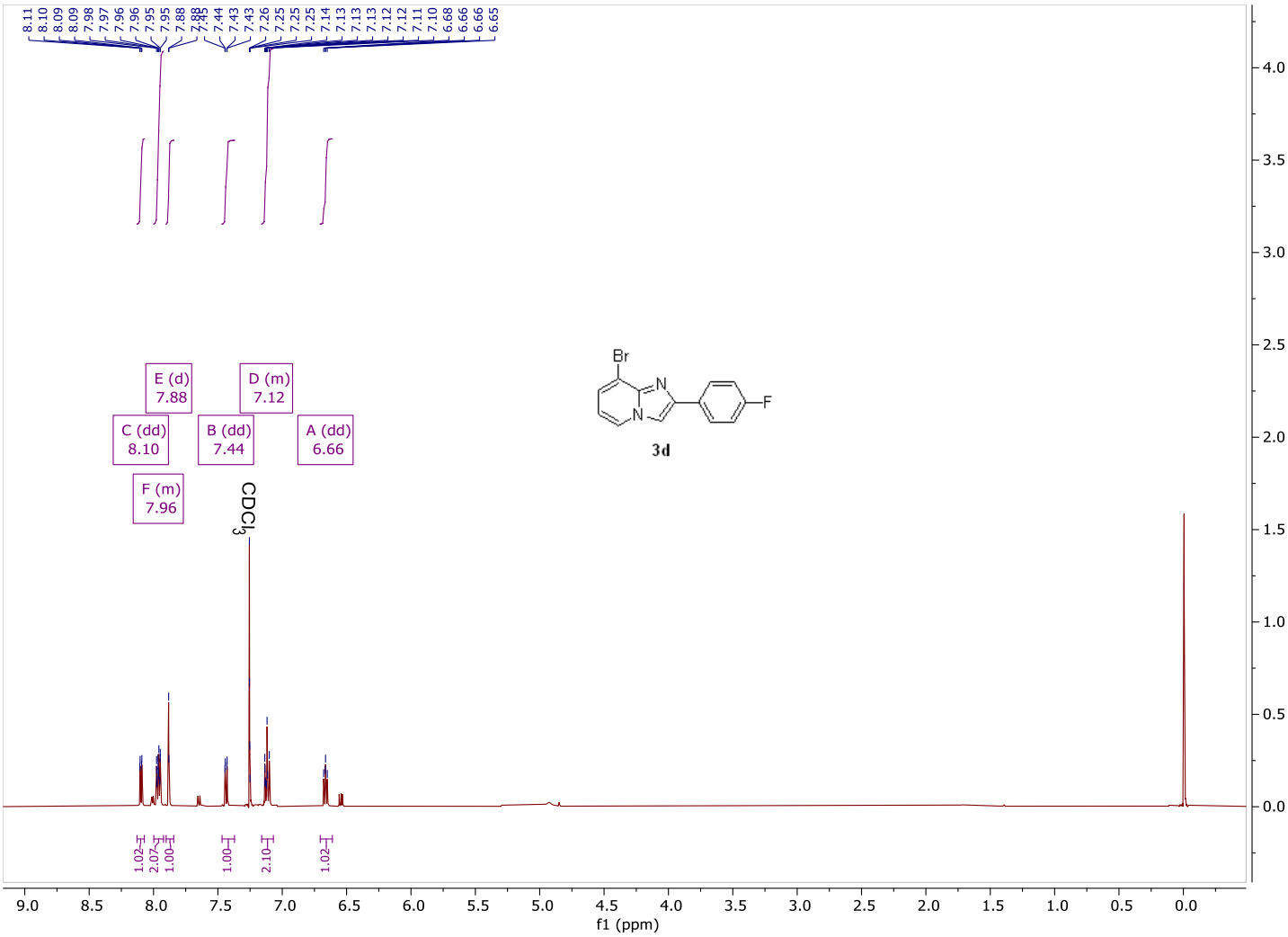
8.11
8.10
8.09
8.09
7.98
7.97
7.96
7.96
7.95
7.95
7.88
7.44
7.43
7.43
7.26
7.25
7.25
7.25
7.14
7.13
7.13
7.13
7.12
7.12
7.11
7.10
6.68
6.66
6.66
6.65
E (d)
7.88
D (m)
7.12
C (dd)
8.10
B (dd)
7.44
A (dd)
6.66
F (m)
7.96
CDCl3
Br
N
N
F
3d
1.02
2.07
1.00
1.00
2.10
1.02
9.0
8.5
8.0
7.5
7.0
6.5
6.0
5.5
5.0
4.5
4.0
3.5
3.0
2.5
2.0
1.5
1.0
0.5
0.0
f1 (ppm)
4.0
3.5
3.0
2.5
2.0
1.5
1.0
0.5
0.0

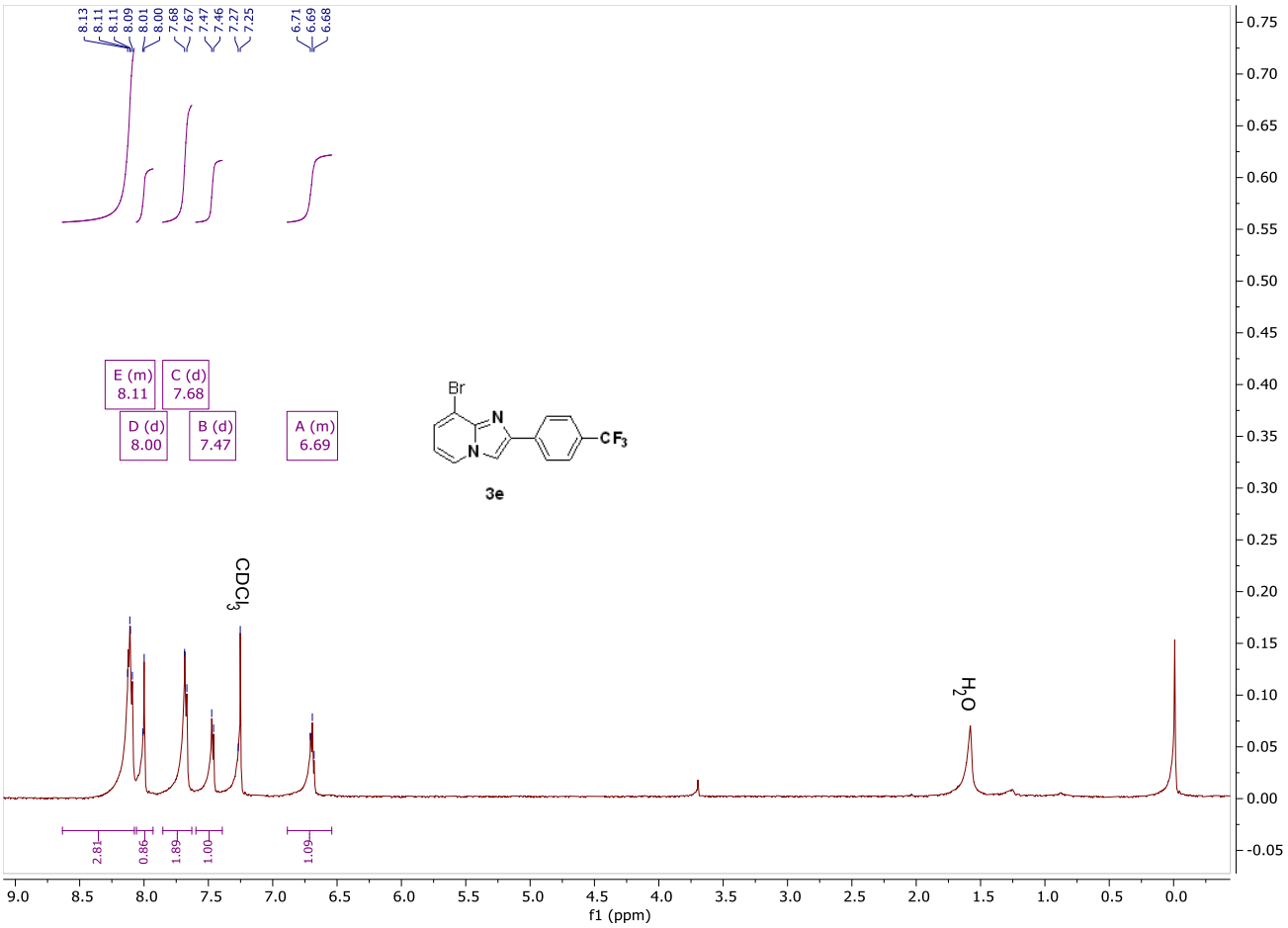
8.13
8.11
8.11
8.09
8.01
8.00
7.68
7.67
7.47
7.46
7.27
7.25
6.71
6.69
6.68
E (m) 8.11
C (d) 7.68
D (d) 8.00
B (d) 7.47
A (m) 6.69
Br
N
N
CF3
3e
CDCl3
H2O
2.81
0.86
1.89
1.00
1.09
f1 (ppm)

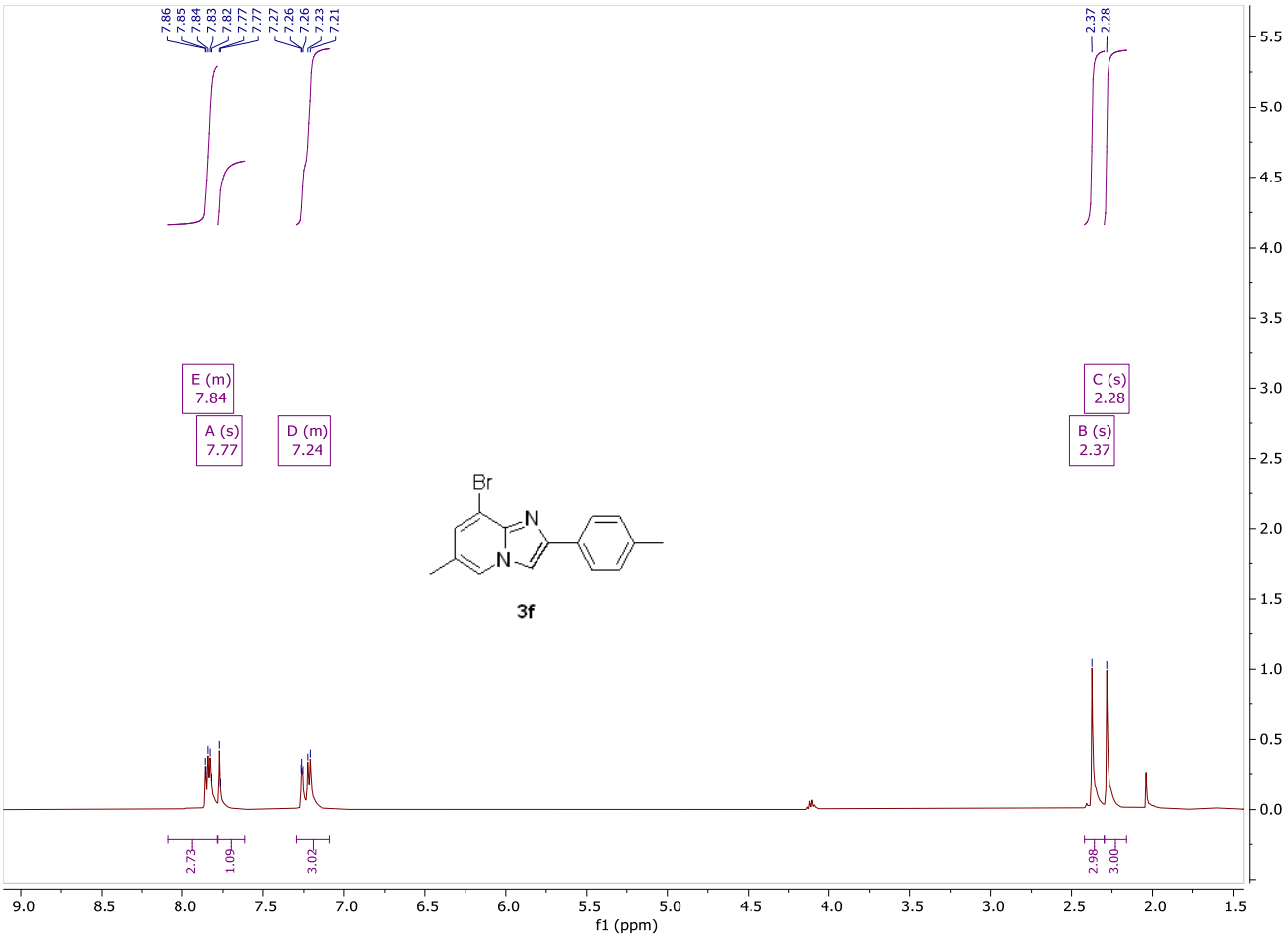
7.86
7.85
7.84
7.83
7.82
7.77
7.77
7.27
7.26
7.26
7.23
7.21
2.37
2.28
E (m)
7.84
A (s)
7.77
D (m)
7.24
C (s)
2.28
B (s)
2.37
Br
N
N
3f
2.73
1.09
3.02
2.98
3.00
f1 (ppm)

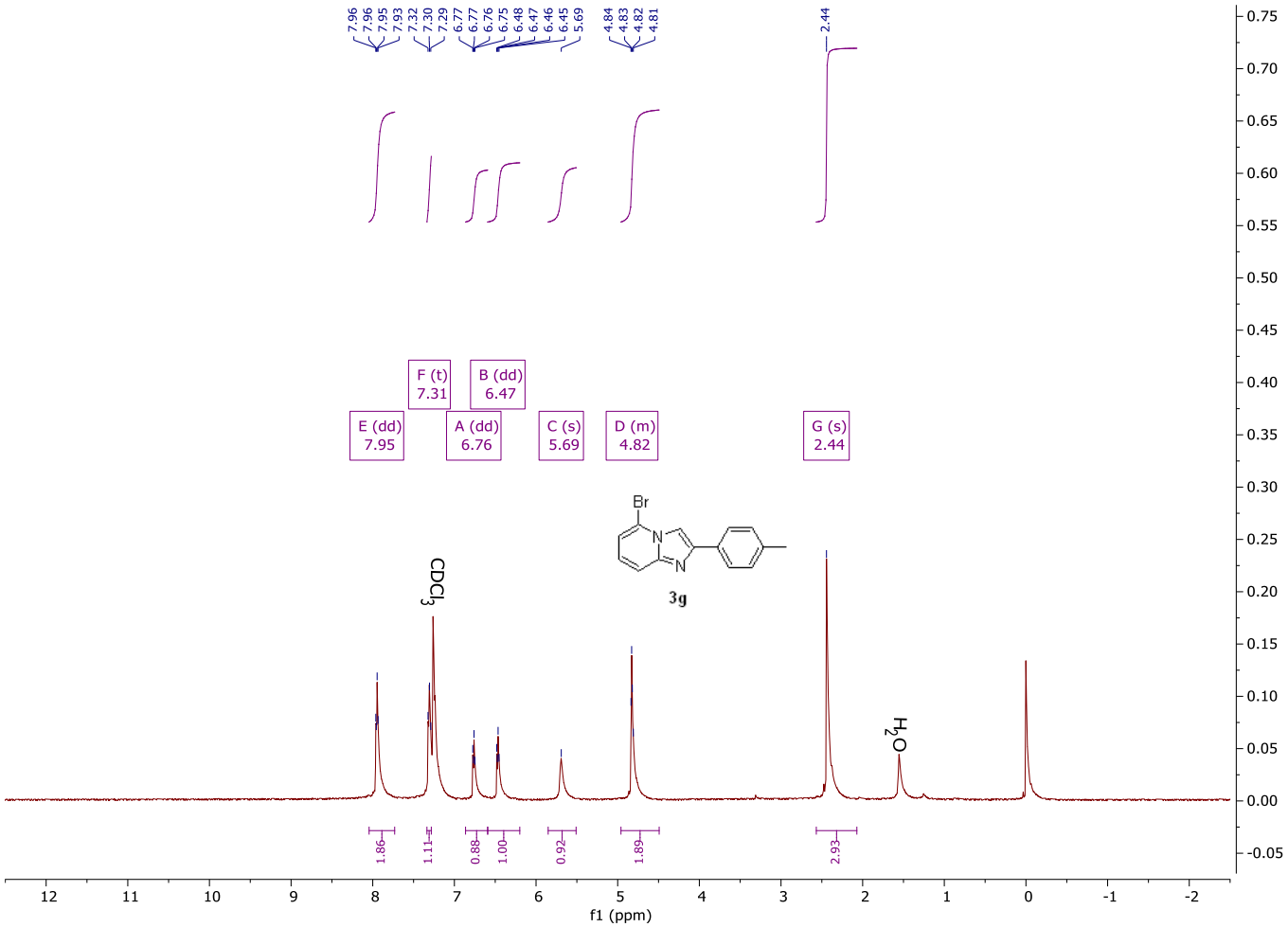
7.96
7.96
7.95
7.93
7.32
7.30
7.29
6.77
6.77
6.76
6.75
6.48
6.47
6.46
6.45
5.69
4.84
4.83
4.82
4.81
2.44
F (t)
7.31
B (dd)
6.47
E (dd)
7.95
A (dd)
6.76
C (s)
5.69
D (m)
4.82
G (s)
2.44
Br
N
N
3g
CDCl3
H2O
1.86
1.11
0.88
1.00
0.92
1.89
2.93
f1 (ppm)

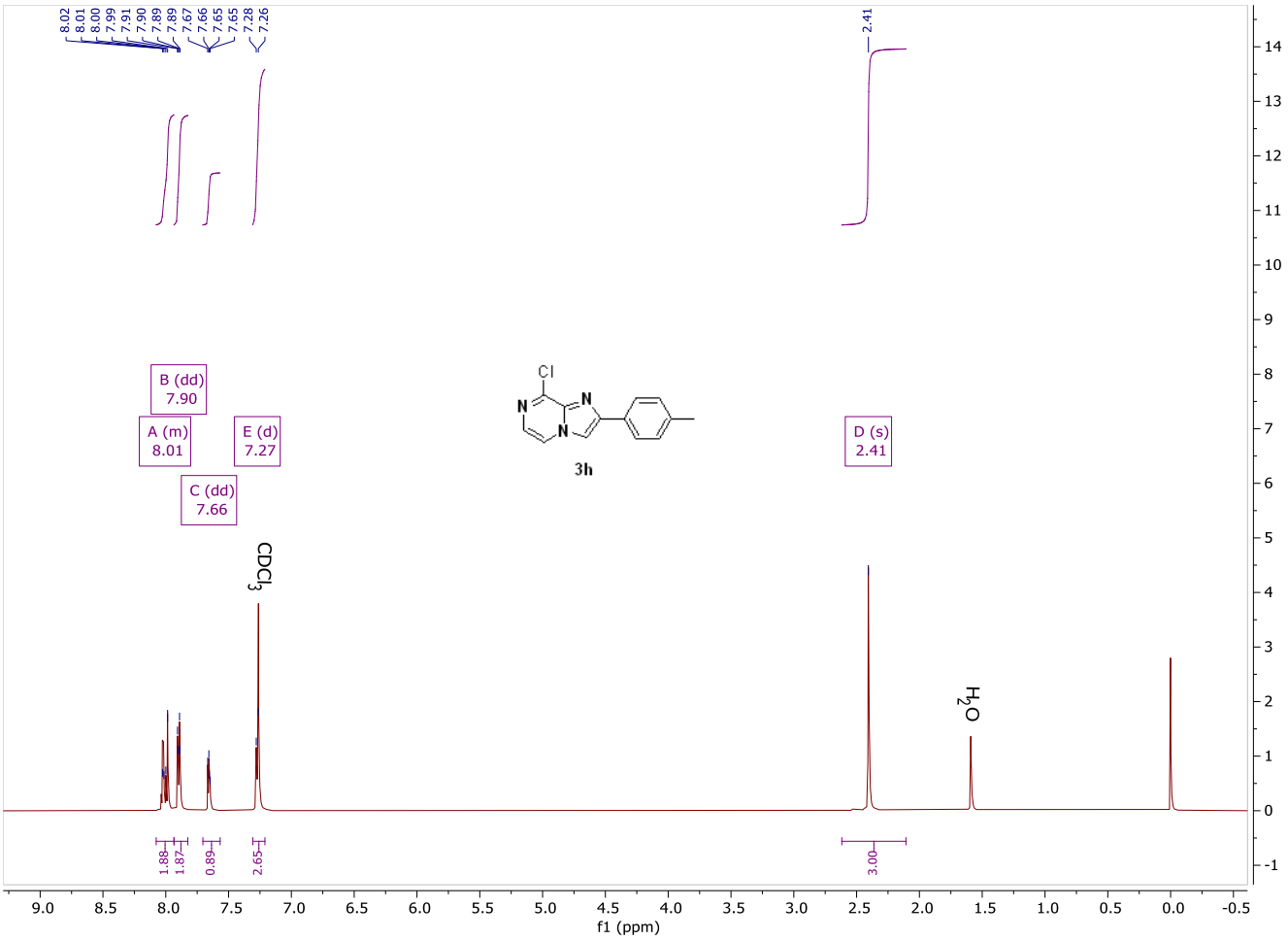
8.02
8.01
8.00
7.99
7.91
7.90
7.89
7.89
7.67
7.66
7.65
7.65
7.28
7.26
2.41
B (dd)
7.90
A (m)
8.01
E (d)
7.27
C (dd)
7.66
D (s)
2.41
Cl
N
N
N
3h
CDCl3
H2O
1.88
1.87
0.89
2.65
3.00
f1 (ppm)

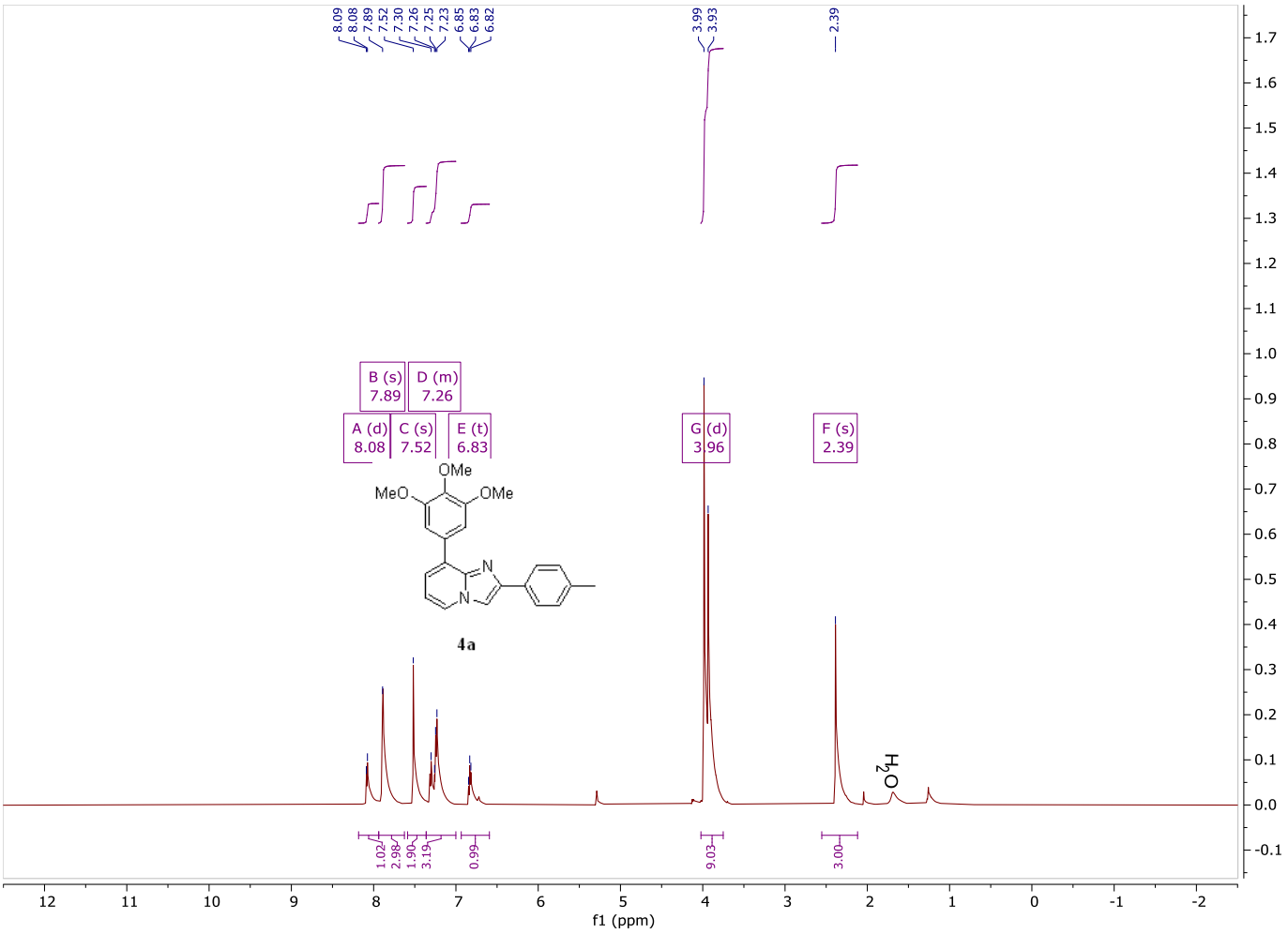
8.09
8.08
7.89
7.52
7.30
7.26
7.25
7.23
6.85
6.83
6.82
3.99
3.93
2.39
B (s) 7.89
D (m) 7.26
A (d) 8.08
C (s) 7.52
E (t) 6.83
G (d) 3.96
F (s) 2.39
OMe
MeO
OMe
N
N
4a
H2O
1.02
2.98
1.90
3.19
0.99
9.03
3.00
f1 (ppm)

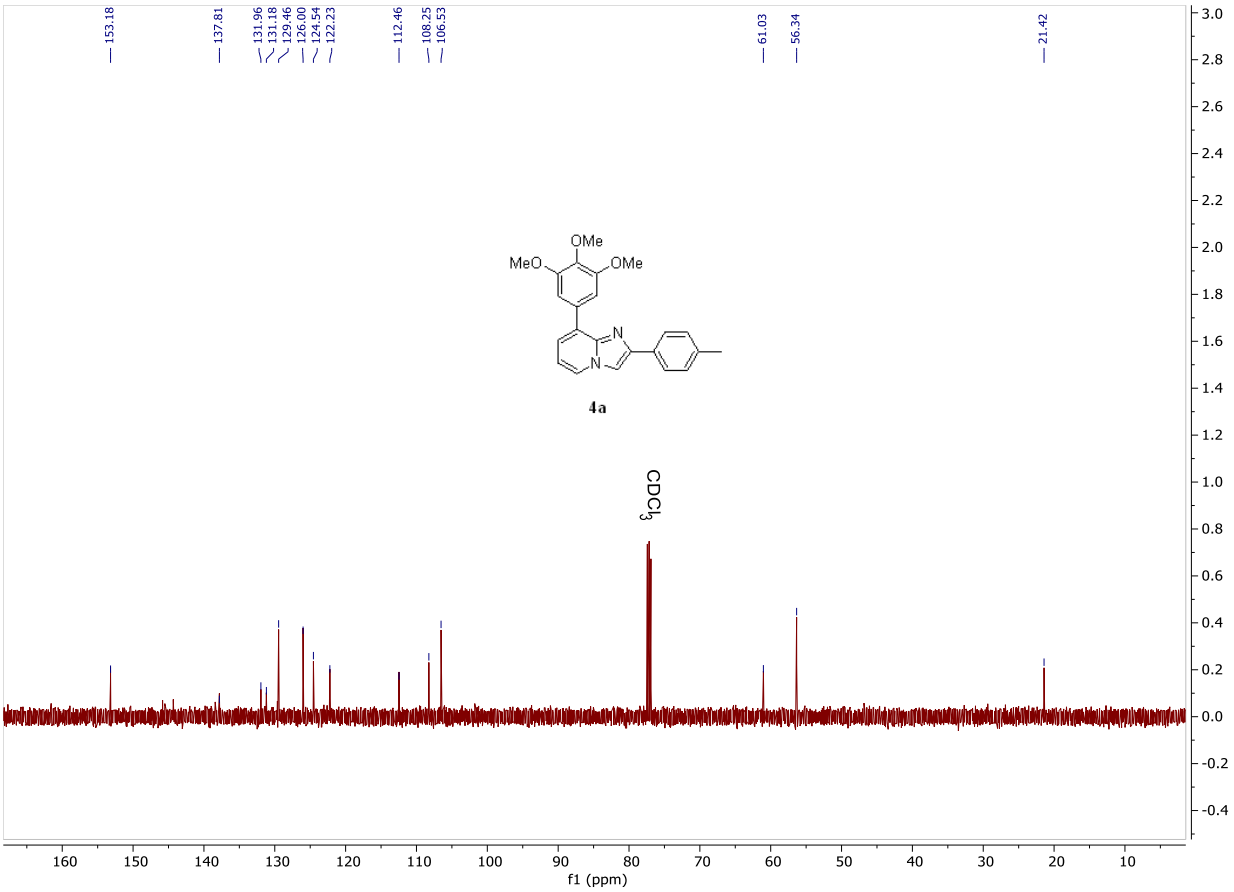
153.18
137.81
131.96
131.18
129.46
126.00
124.54
122.23
112.46
108.25
106.53
61.03
56.34
21.42
OMe
MeO
OMe
N
N
4a
CDCl3
f1 (ppm)

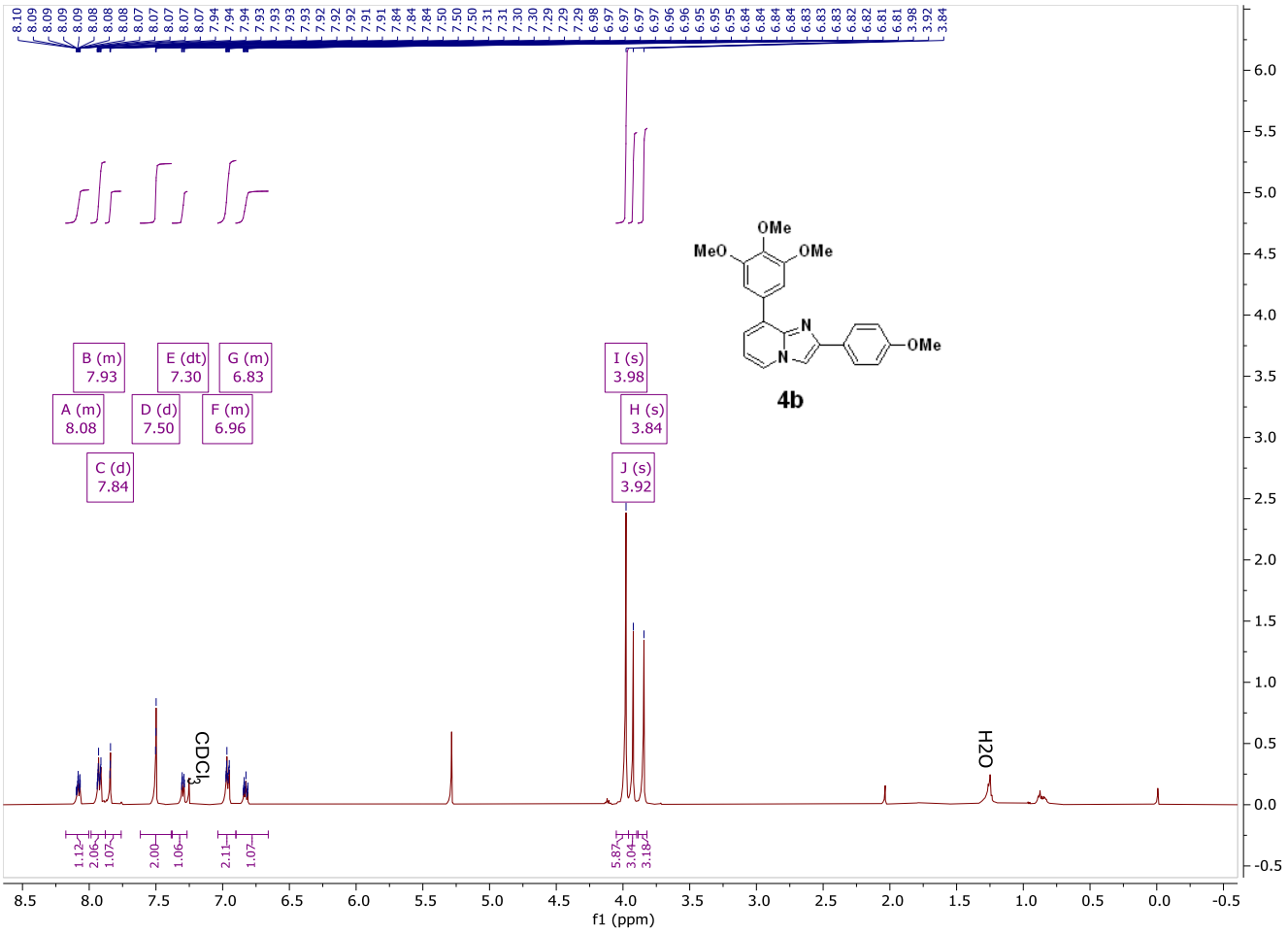
OMe
MeO
OMe
N
N
OMe
4b
B (m) 7.93
A (m) 8.08
C (d) 7.84
E (dt) 7.30
D (d) 7.50
G (m) 6.83
F (m) 6.96
I (s) 3.98
H (s) 3.84
J (s) 3.92
CDCl3
H2O
1.12
2.06
1.07
2.00
1.06
2.11
1.07
5.87
3.04
3.18
f1 (ppm)

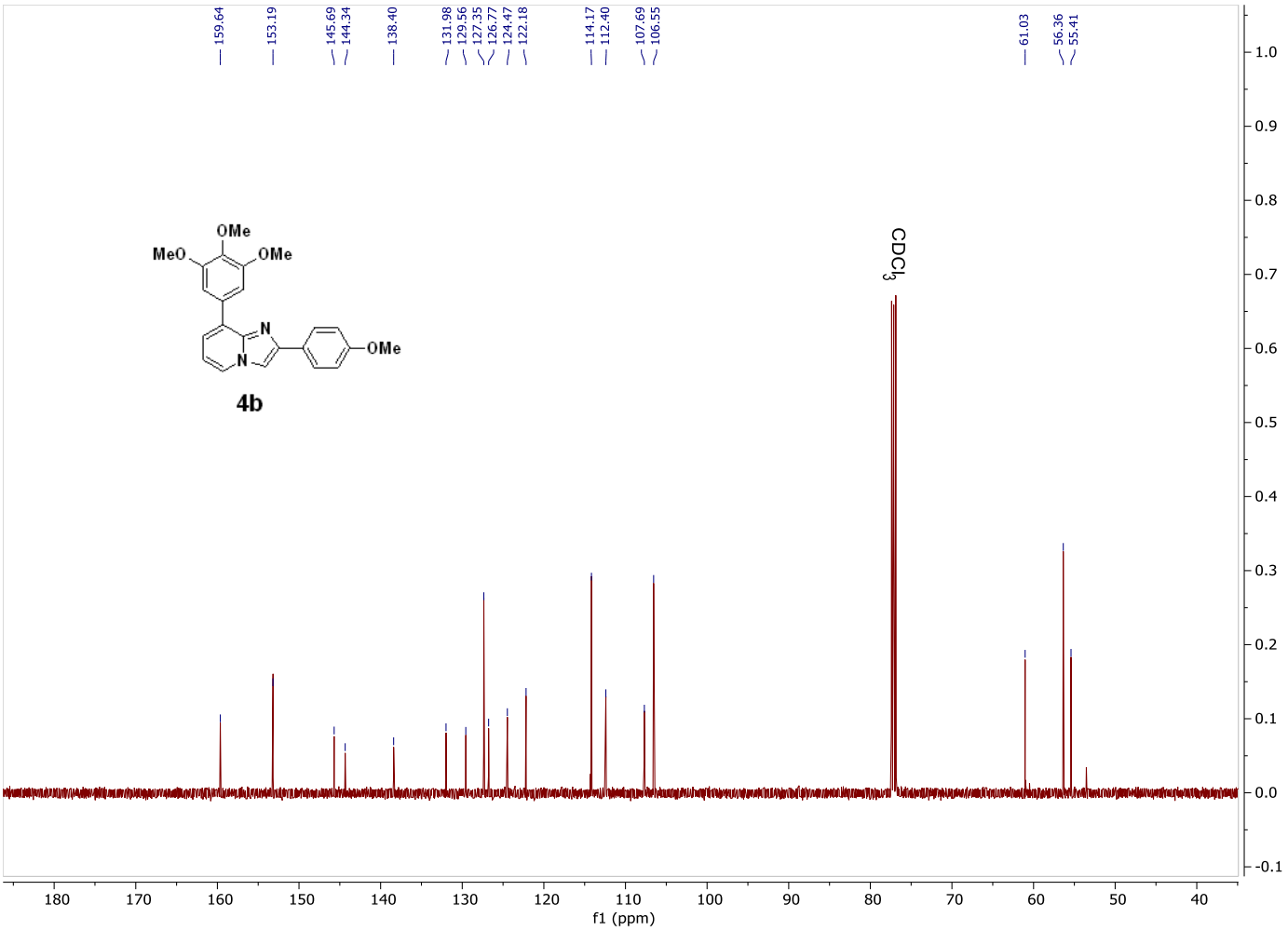
159.64
153.19
145.69
144.34
138.40
131.98
129.56
127.35
126.77
124.47
122.18
114.17
112.40
107.69
106.55
61.03
56.36
55.41
CDCl3
OMe
MeO
OMe
N
N
OMe
4b
f1 (ppm)

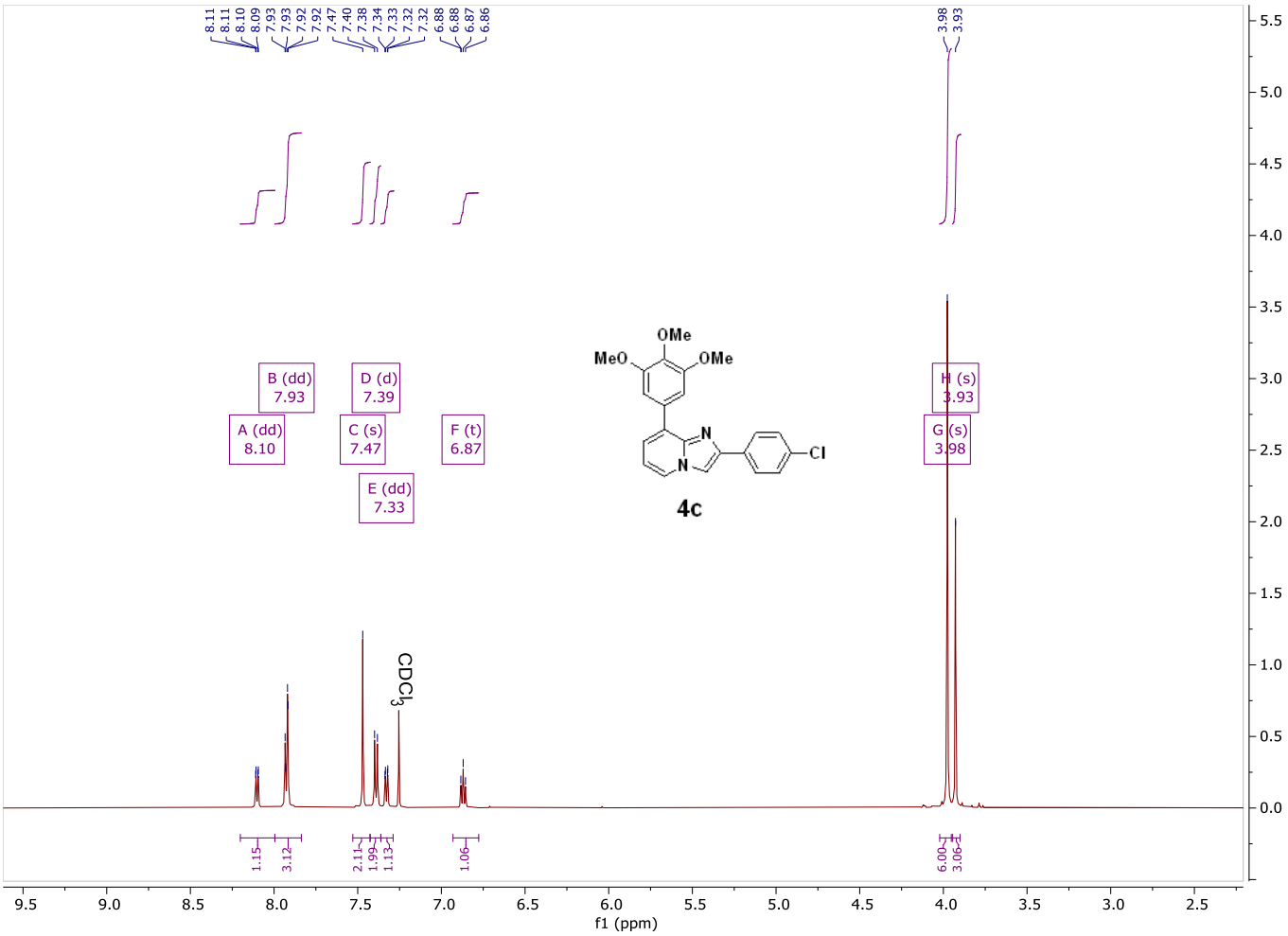
8.11
8.11
8.10
8.09
7.93
7.93
7.92
7.92
7.47
7.40
7.38
7.34
7.33
7.32
7.32
6.88
6.88
6.87
6.86
3.98
3.93
B (dd)
7.93
A (dd)
8.10
D (d)
7.39
C (s)
7.47
E (dd)
7.33
F (t)
6.87
H (s)
3.93
G (s)
3.98
OMe
MeO
OMe
N
N
Cl
4c
CDCl3
1.15
3.12
2.11
1.99
1.13
1.06
6.00
3.06
9.5
9.0
8.5
8.0
7.5
7.0
6.5
6.0
5.5
5.0
4.5
4.0
3.5
3.0
2.5
f1 (ppm)
5.5
5.0
4.5
4.0
3.5
3.0
2.5
2.0
1.5
1.0
0.5
0.0

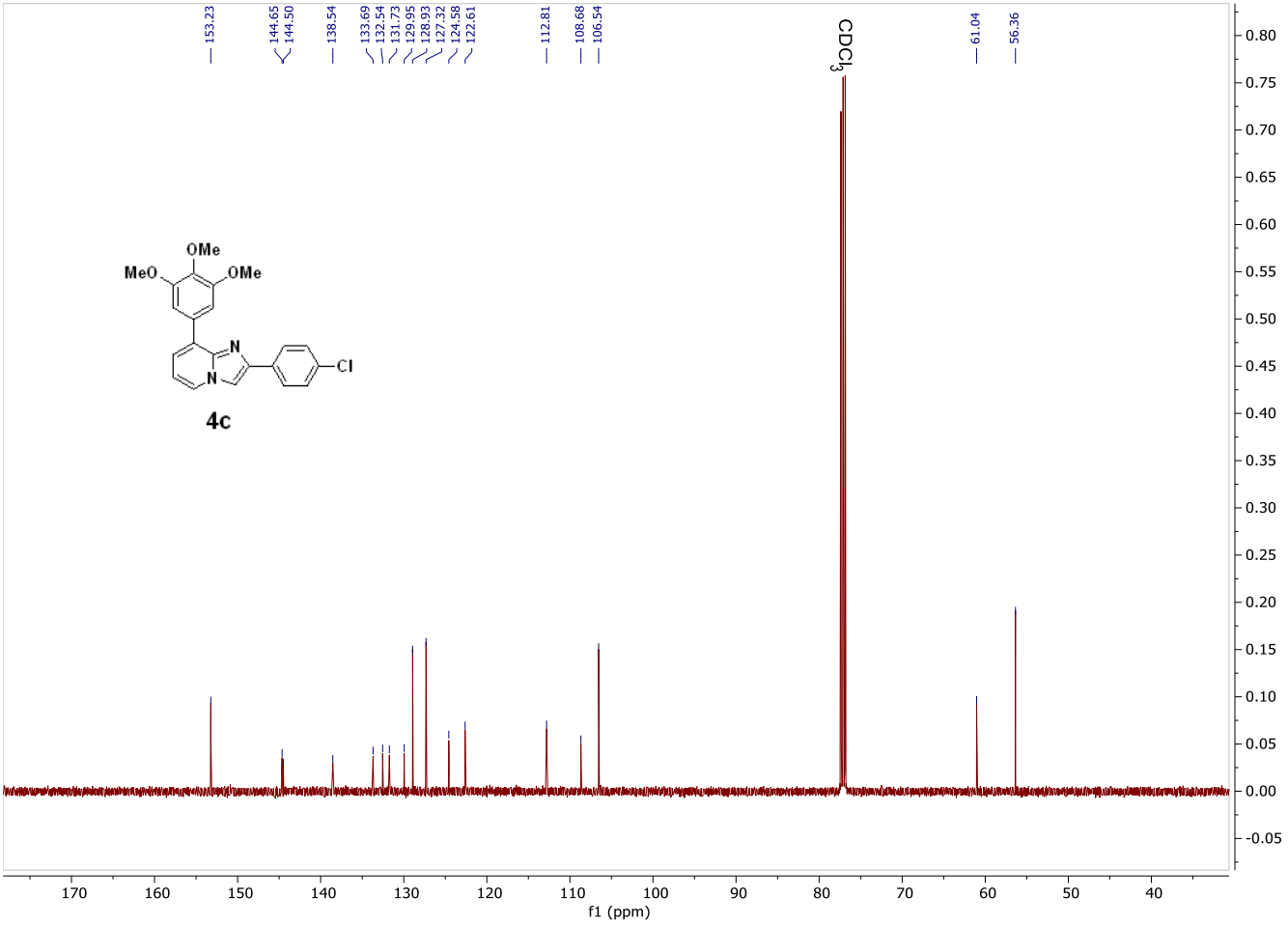
153.23
144.65
144.50
138.54
133.69
132.54
131.73
129.95
128.93
127.32
124.58
122.61
112.81
108.68
106.54
CDCl3
61.04
56.36
OMe
MeO
OMe
N
N
Cl
4c
f1 (ppm)

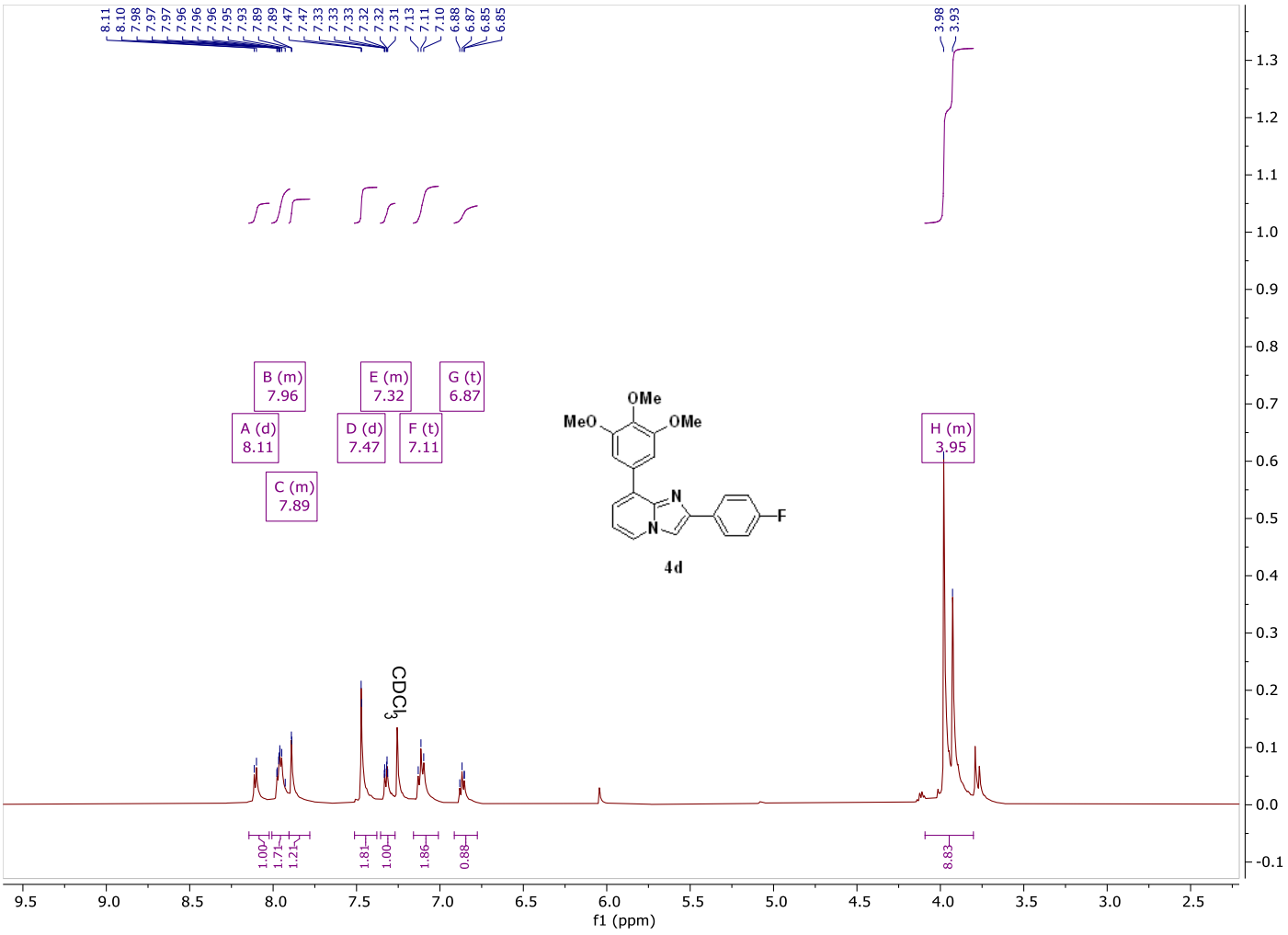
8.11
8.10
7.98
7.97
7.97
7.96
7.96
7.96
7.95
7.93
7.89
7.89
7.47
7.47
7.33
7.33
7.33
7.32
7.32
7.31
7.13
7.11
7.10
6.88
6.87
6.85
6.85
3.98
3.93
B (m)
7.96
A (d)
8.11
C (m)
7.89
E (m)
7.32
D (d)
7.47
F (t)
7.11
G (t)
6.87
H (m)
3.95
OMe
MeO
OMe
N
N
F
4d
CDCl3
1.00
1.71
1.21
1.81
1.00
1.86
0.88
8.83
f1 (ppm)

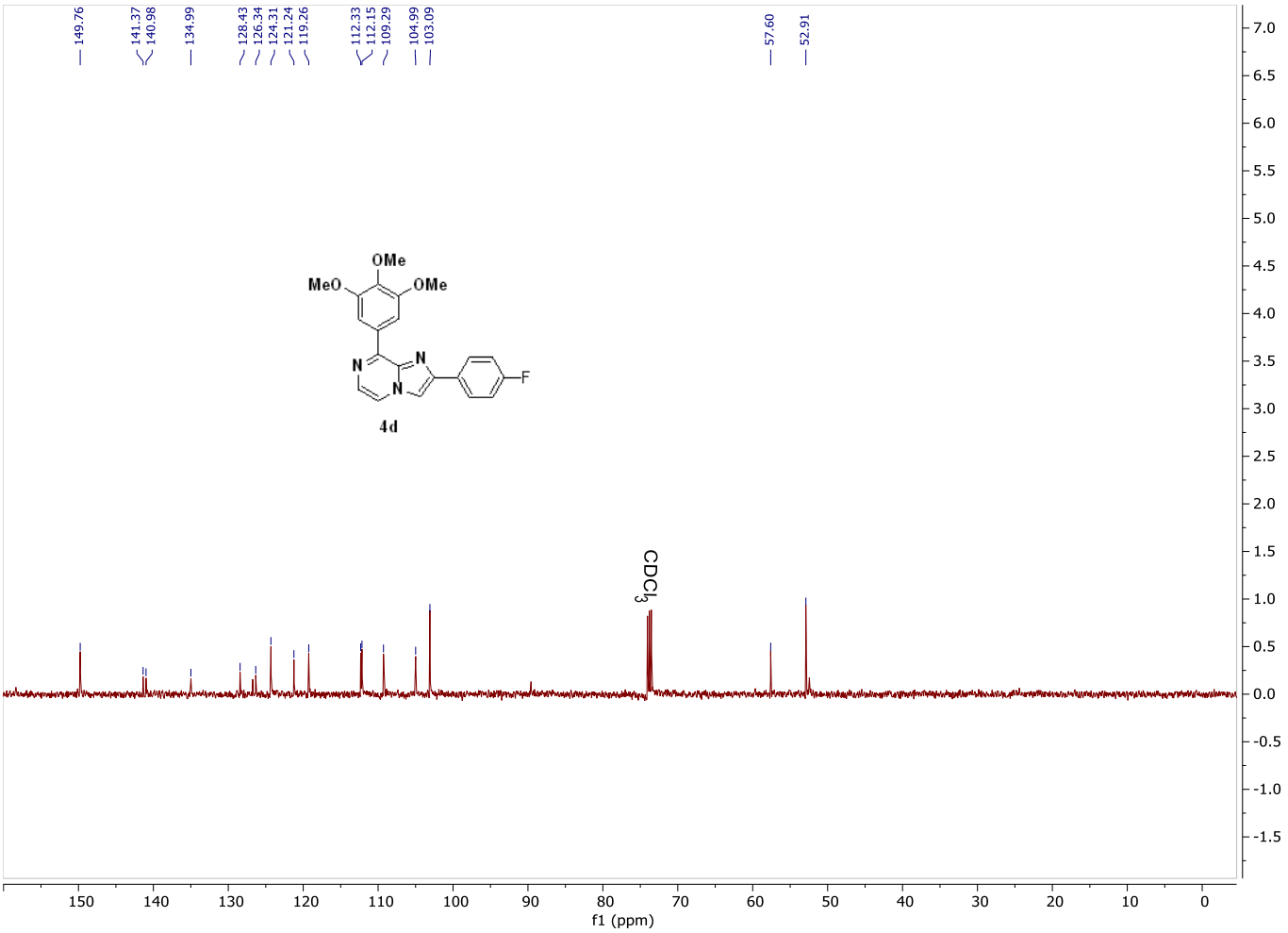
149.76
141.37
140.98
134.99
128.43
126.34
124.31
121.24
119.26
112.33
112.15
109.29
104.99
103.09
57.60
52.91
OMe
MeO
OMe
N
N
N
F
4d
CDCl3
7.0
6.5
6.0
5.5
5.0
4.5
4.0
3.5
3.0
2.5
2.0
1.5
1.0
0.5
0.0
-0.5
-1.0
-1.5
150
140
130
120
110
100
90
80
70
60
50
40
30
20
10
0
f1 (ppm)

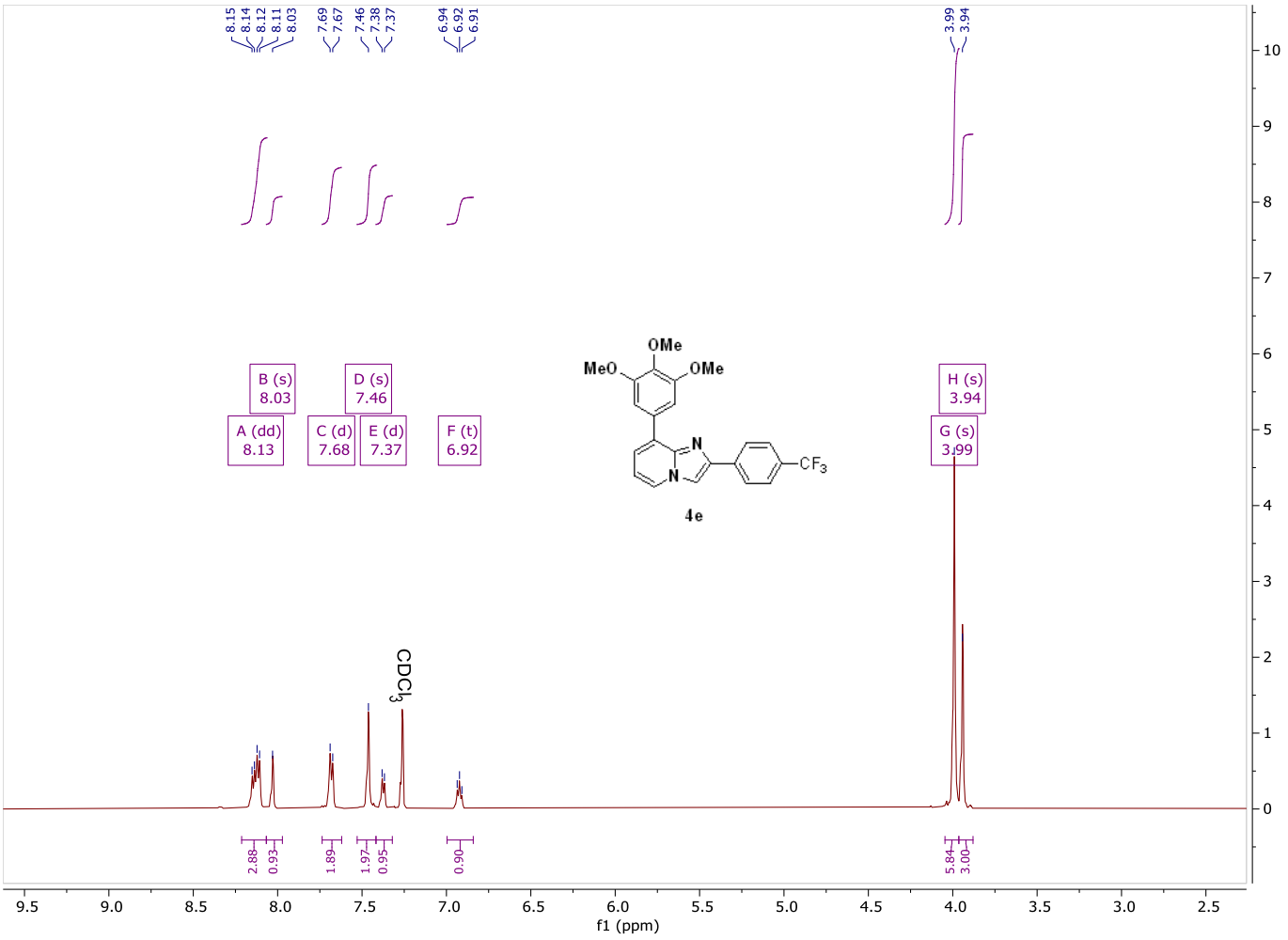
8.15
8.14
8.12
8.11
8.03
7.69
7.67
7.46
7.38
7.37
6.94
6.92
6.91
3.99
3.94
B (s)
8.03
D (s)
7.46
H (s)
3.94
A (dd)
8.13
C (d)
7.68
E (d)
7.37
F (t)
6.92
G (s)
3.99
OMe
MeO
OMe
N
N
CF3
4e
CDCl3
2.88
0.93
1.89
1.97
0.95
0.90
5.84
3.00
f1 (ppm)

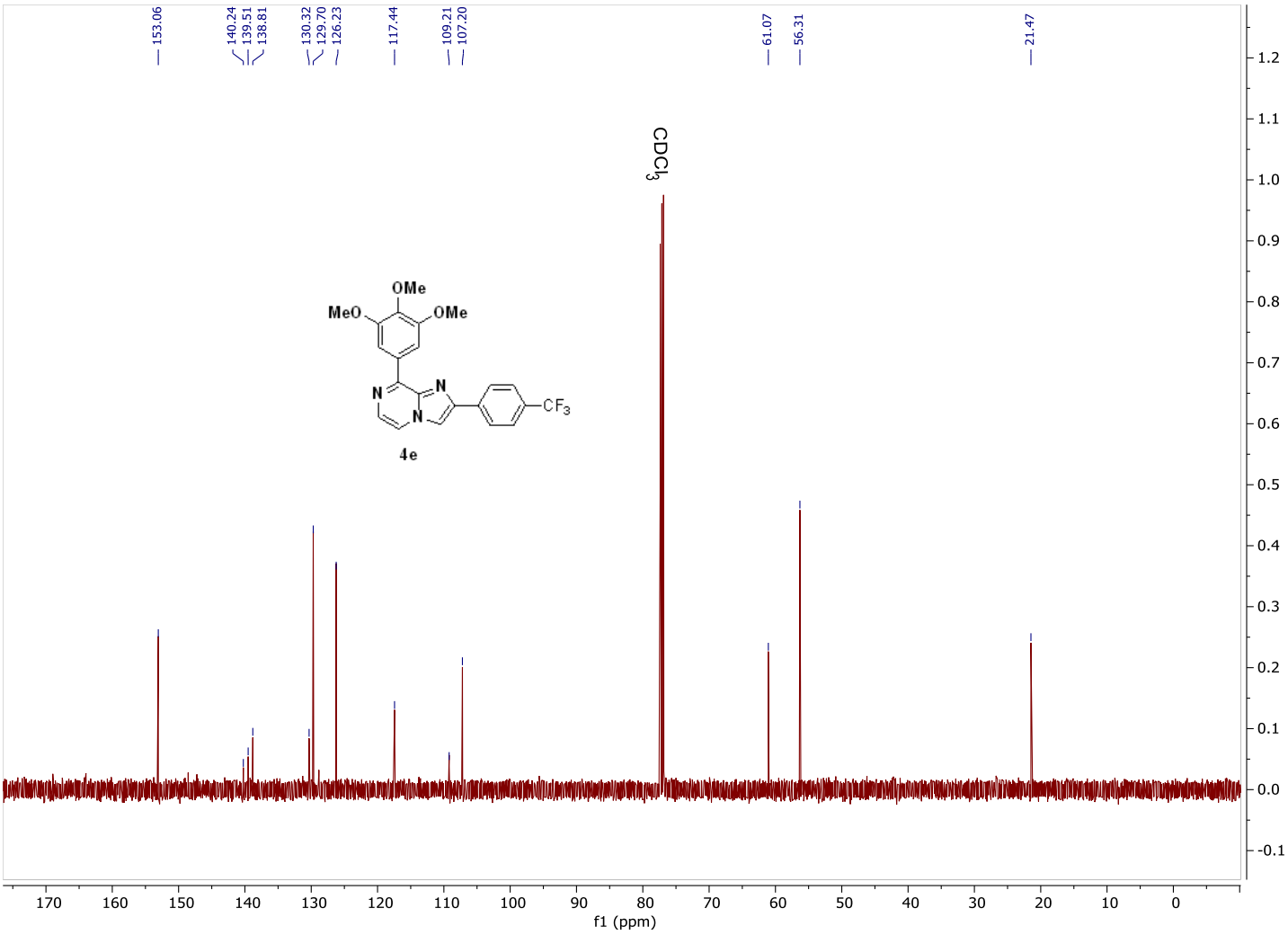
153.06
140.24
139.51
138.81
130.32
129.70
126.23
117.44
109.21
107.20
61.07
56.31
21.47
CDCl3
OMe
MeO
OMe
N
N
N
CF3
4e
f1 (ppm)

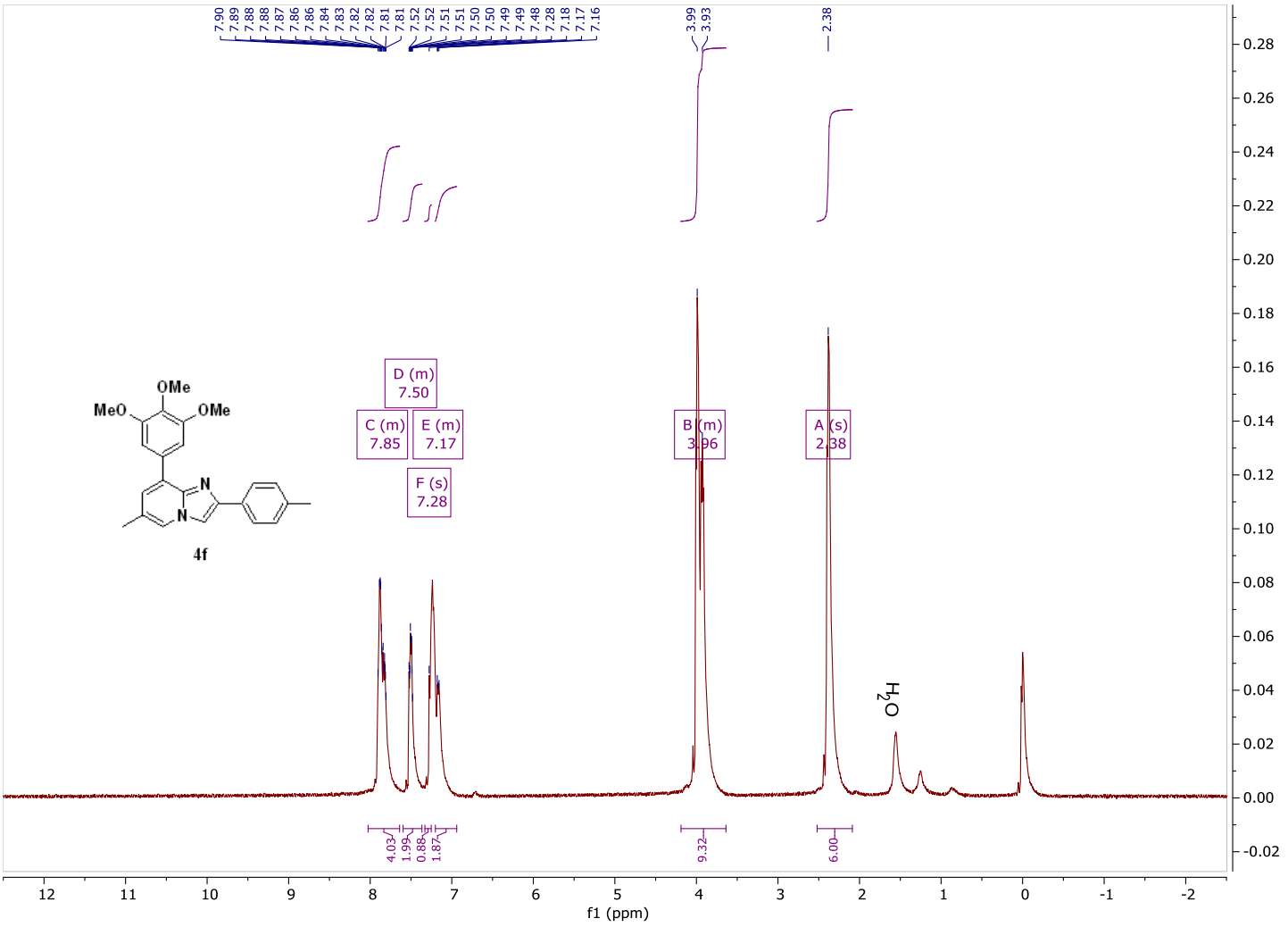
7.90
7.89
7.88
7.88
7.87
7.86
7.86
7.84
7.83
7.82
7.82
7.81
7.81
7.52
7.52
7.51
7.51
7.50
7.50
7.49
7.49
7.48
7.28
7.18
7.17
7.16
3.99
3.93
2.38
OMe
MeO
OMe
N
N
4f
D (m)
7.50
C (m)
7.85
E (m)
7.17
F (s)
7.28
B (m)
3.96
A (s)
2.38
H2O
4.03
1.99
0.88
1.87
9.32
6.00
f1 (ppm)

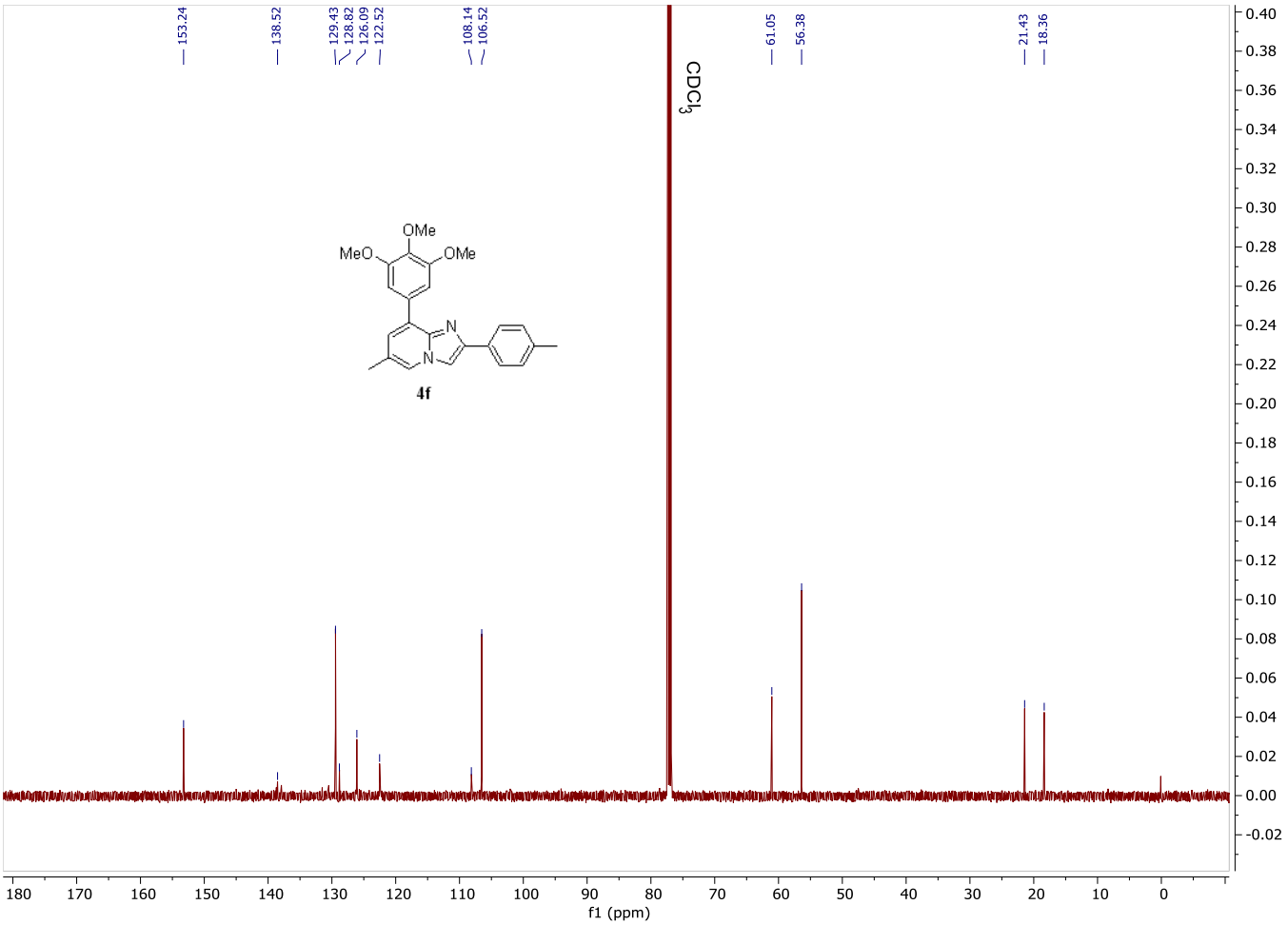
153.24
138.52
129.43
128.82
126.09
122.52
108.14
106.52
CDCl3
61.05
56.38
21.43
18.36
OMe
MeO
OMe
N
N
4f
f1 (ppm)

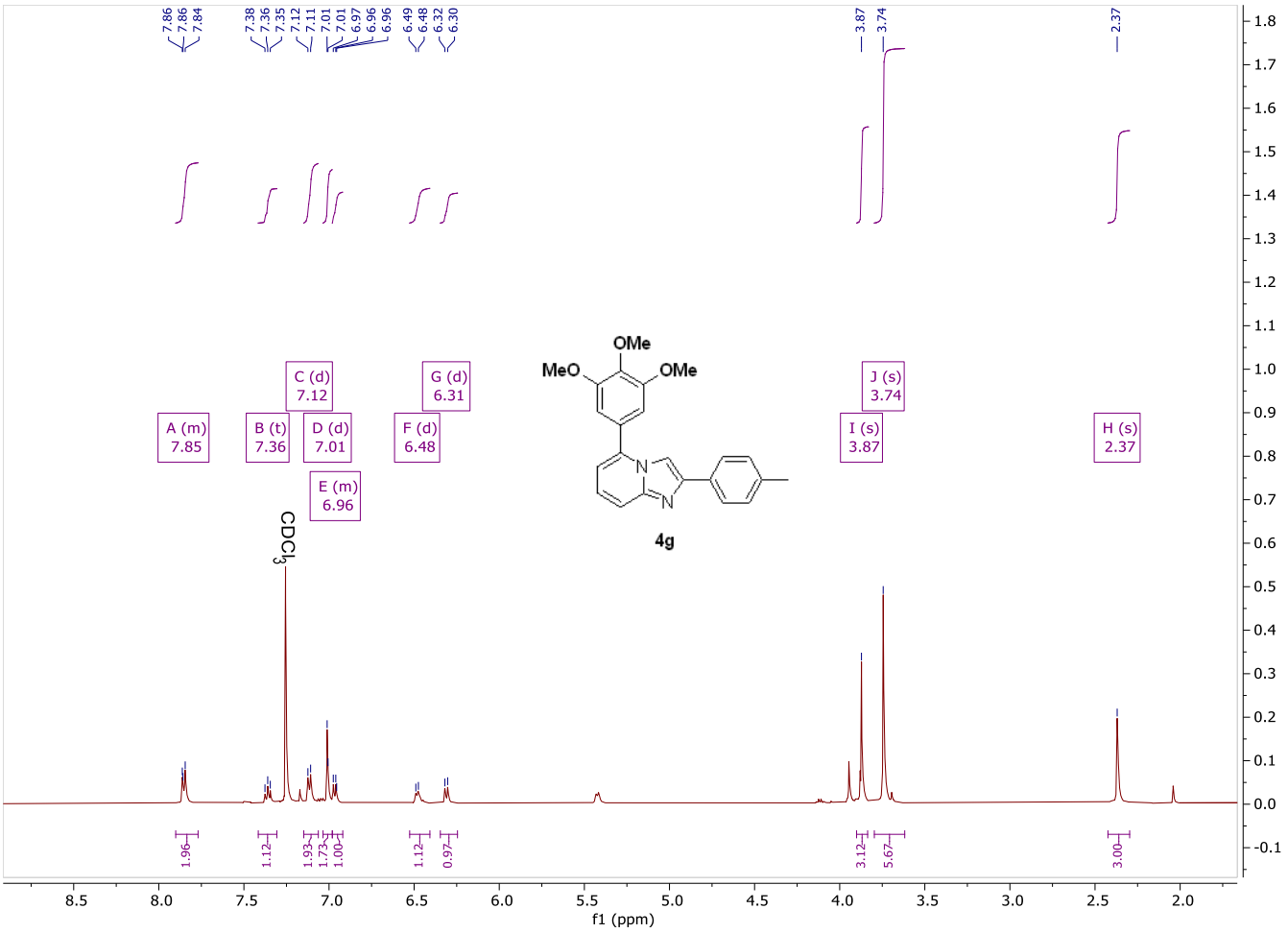
7.86
7.86
7.84
7.38
7.36
7.35
7.12
7.11
7.01
7.01
6.97
6.96
6.96
6.49
6.48
6.32
6.30
3.87
3.74
2.37
A (m)
7.85
B (t)
7.36
C (d)
7.12
D (d)
7.01
E (m)
6.96
F (d)
6.48
G (d)
6.31
I (s)
3.87
J (s)
3.74
H (s)
2.37
OMe
MeO
OMe
N
N
4g
CDCl3
1.96
1.12
1.93
1.73
1.00
1.12
0.97
3.12
5.67
3.00
f1 (ppm)

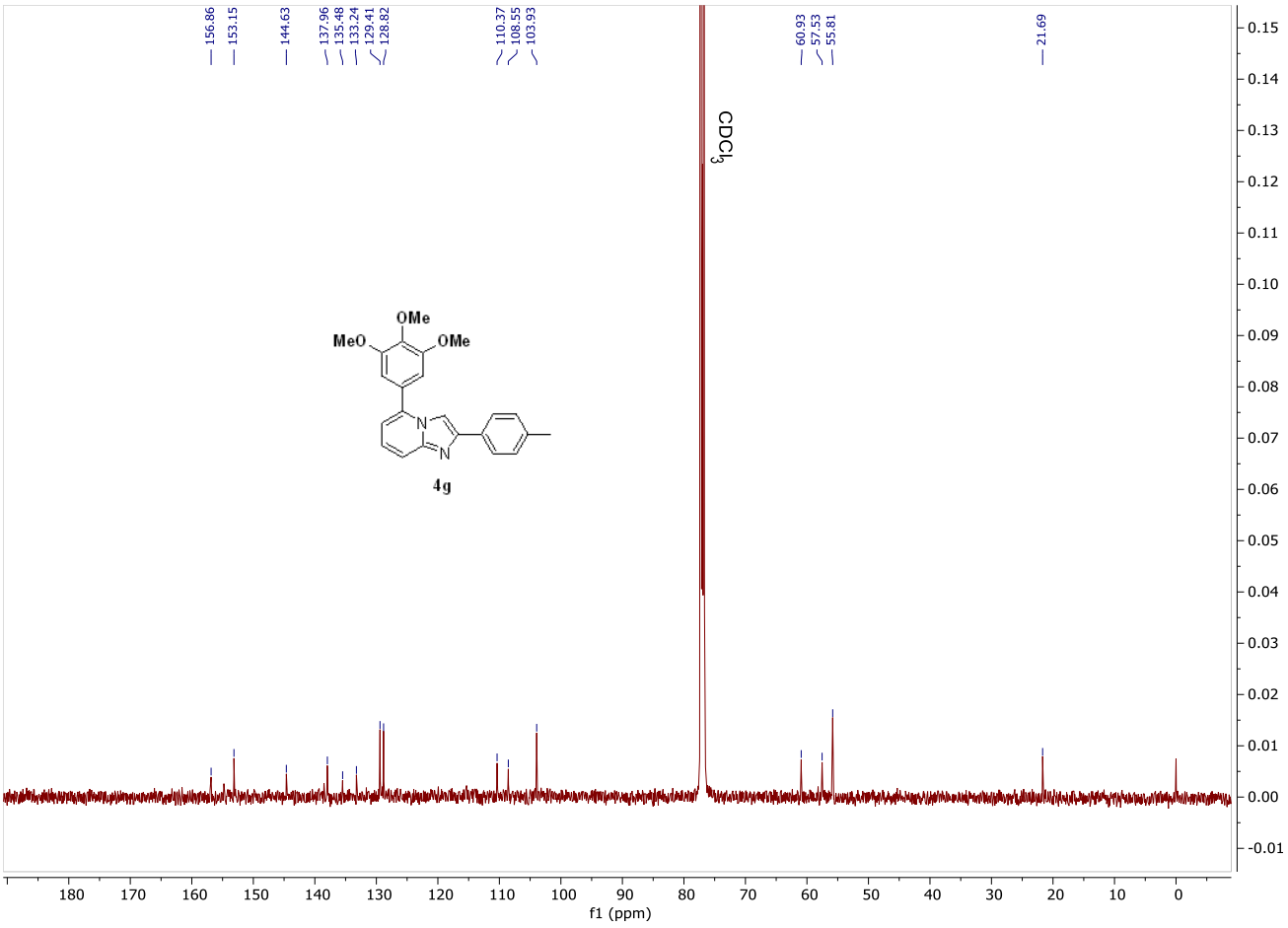
156.86
153.15
144.63
137.96
135.48
133.24
129.41
128.82
110.37
108.55
103.93
CDCl3
60.93
57.53
55.81
21.69
OMe
MeO
OMe
N
N
4g
f1 (ppm)

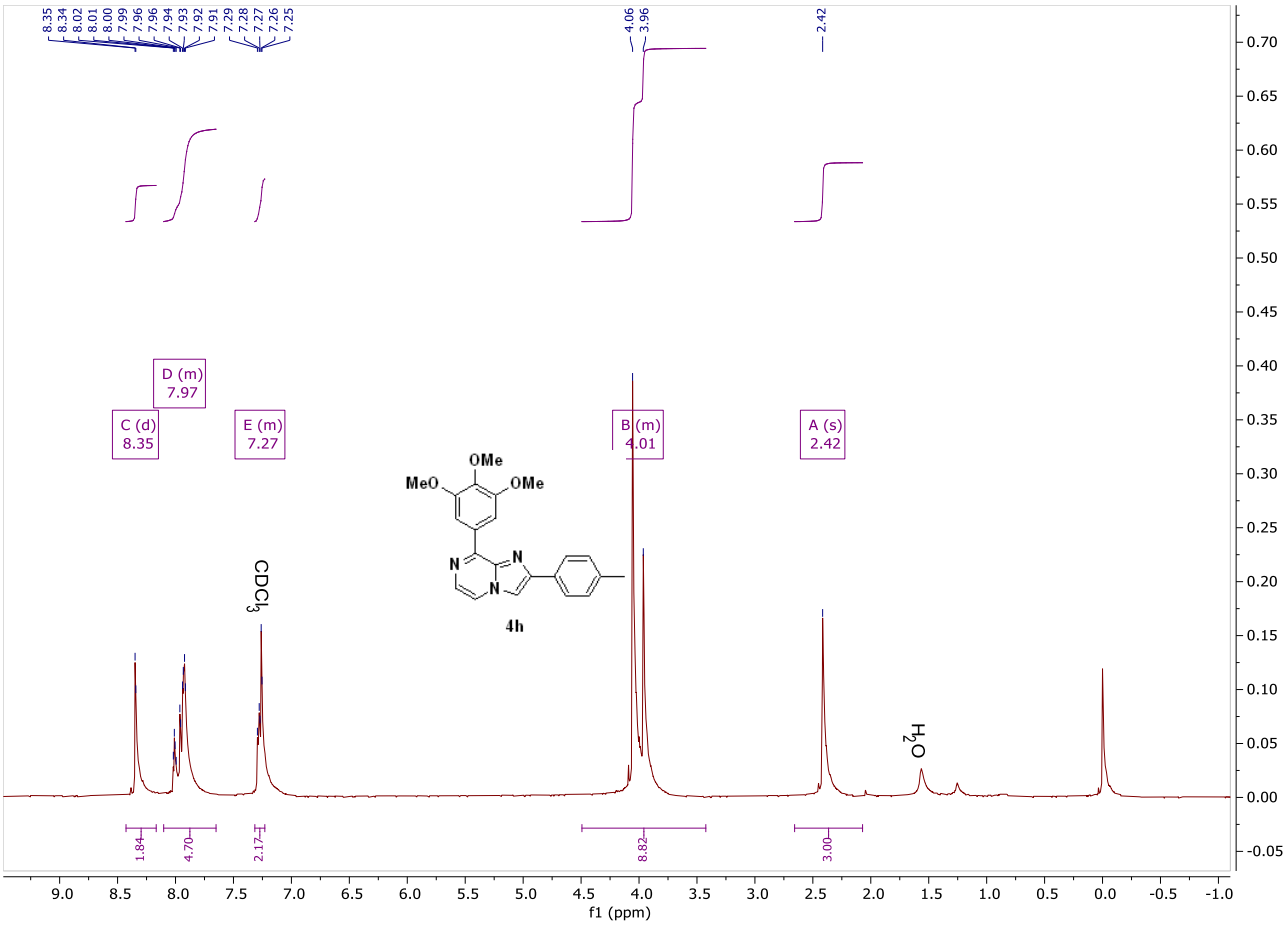
8.35
8.34
8.02
8.01
8.00
7.99
7.96
7.96
7.94
7.93
7.92
7.91
7.29
7.28
7.27
7.26
7.25
4.06
3.96
2.42
D (m)
7.97
C (d)
8.35
E (m)
7.27
B (m)
4.01
A (s)
2.42
OMe
MeO
OMe
N
N
N
4h
CDCl3
H2O
1.84
4.70
2.17
8.82
3.00
f1 (ppm)

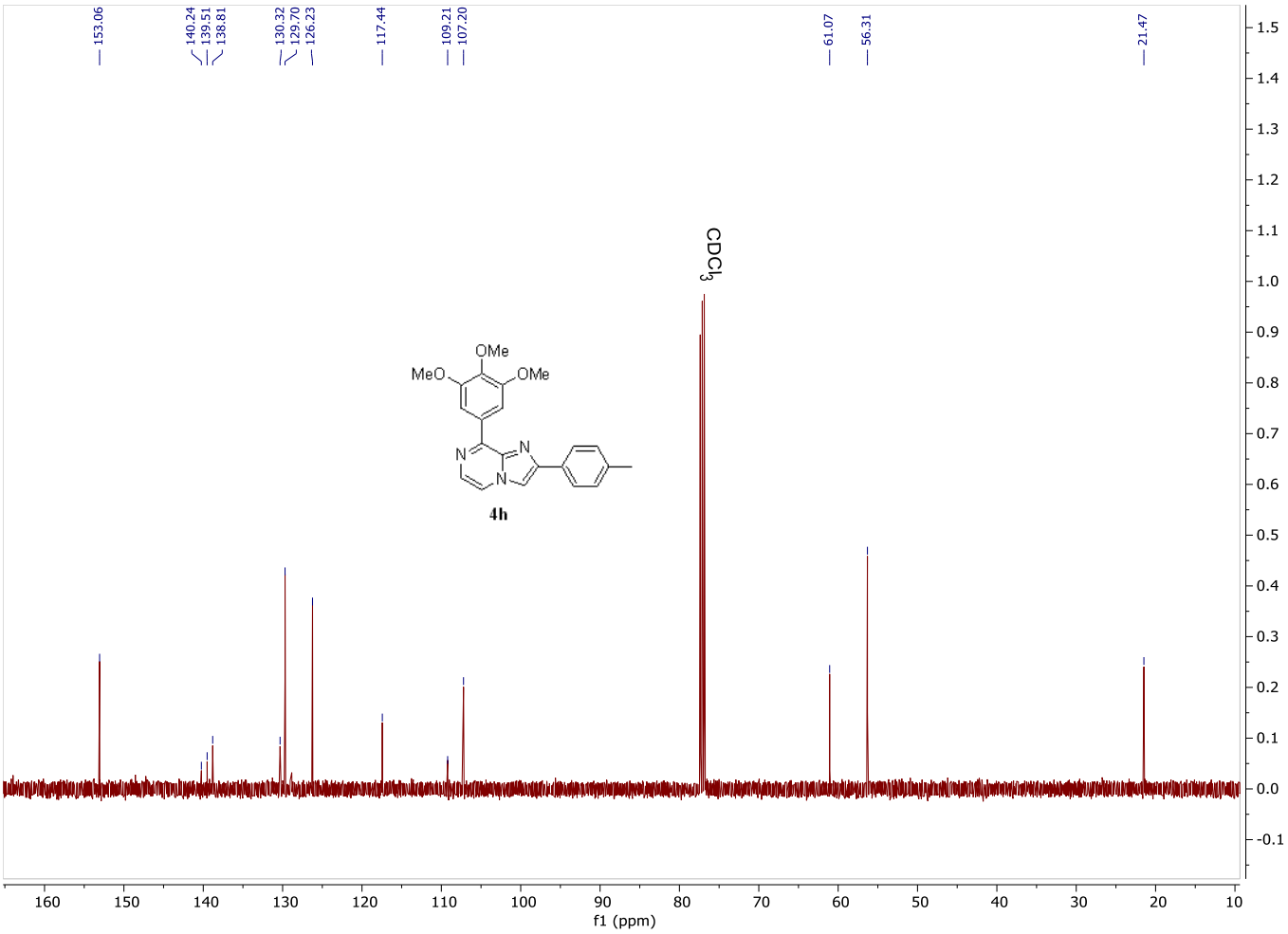
153.06
140.24
139.51
138.81
130.32
129.70
126.23
117.44
109.21
107.20
61.07
56.31
21.47
CDCl3
OMe
MeO
OMe
N
N
N
4h
f1 (ppm)

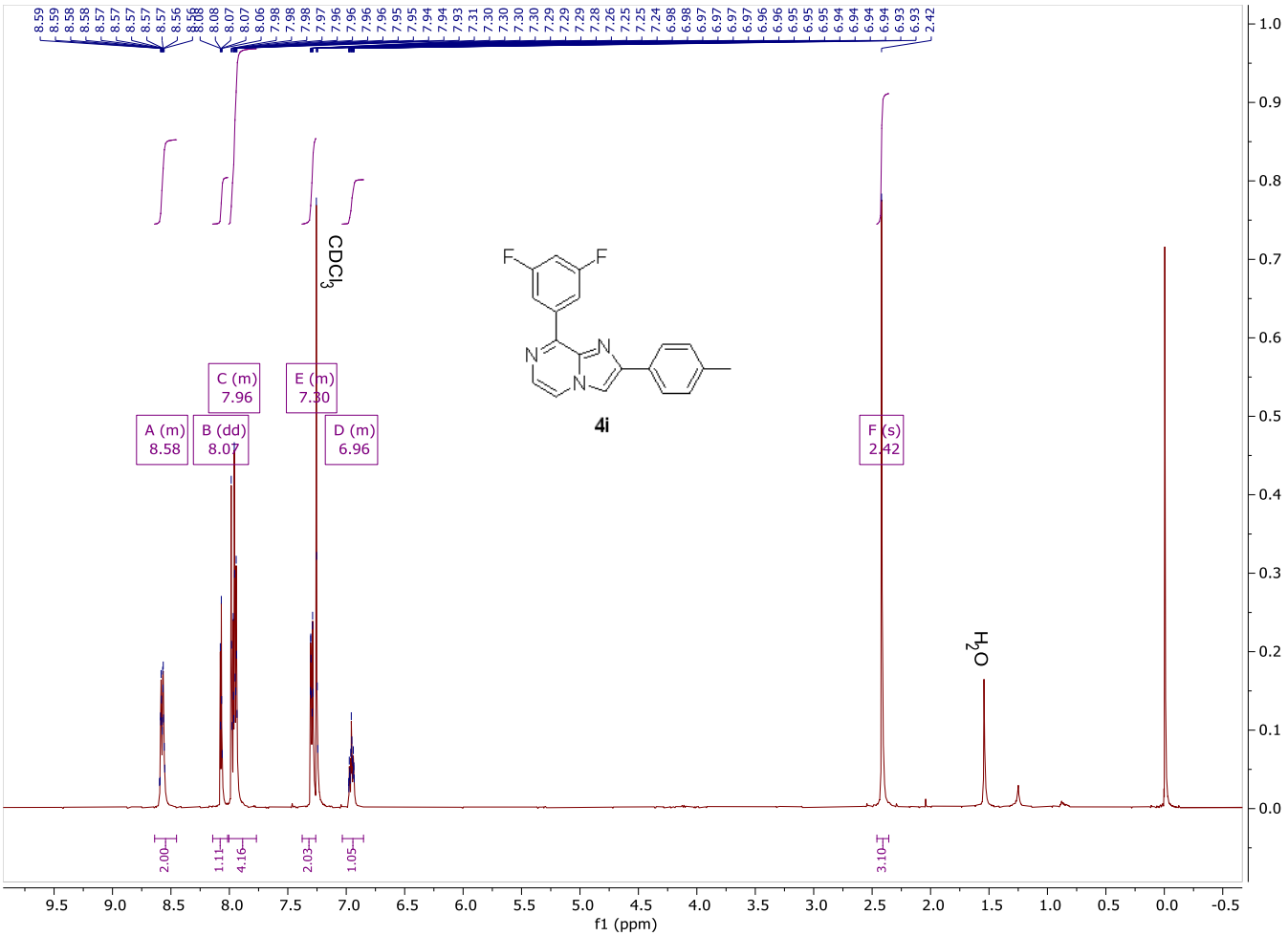
CDCl3
H2O
A (m) 8.58
B (dd) 8.07
C (m) 7.96
D (m) 6.96
E (m) 7.30
F (s) 2.42
4i
2.00
1.11
4.16
2.03
1.05
3.10
f1 (ppm)

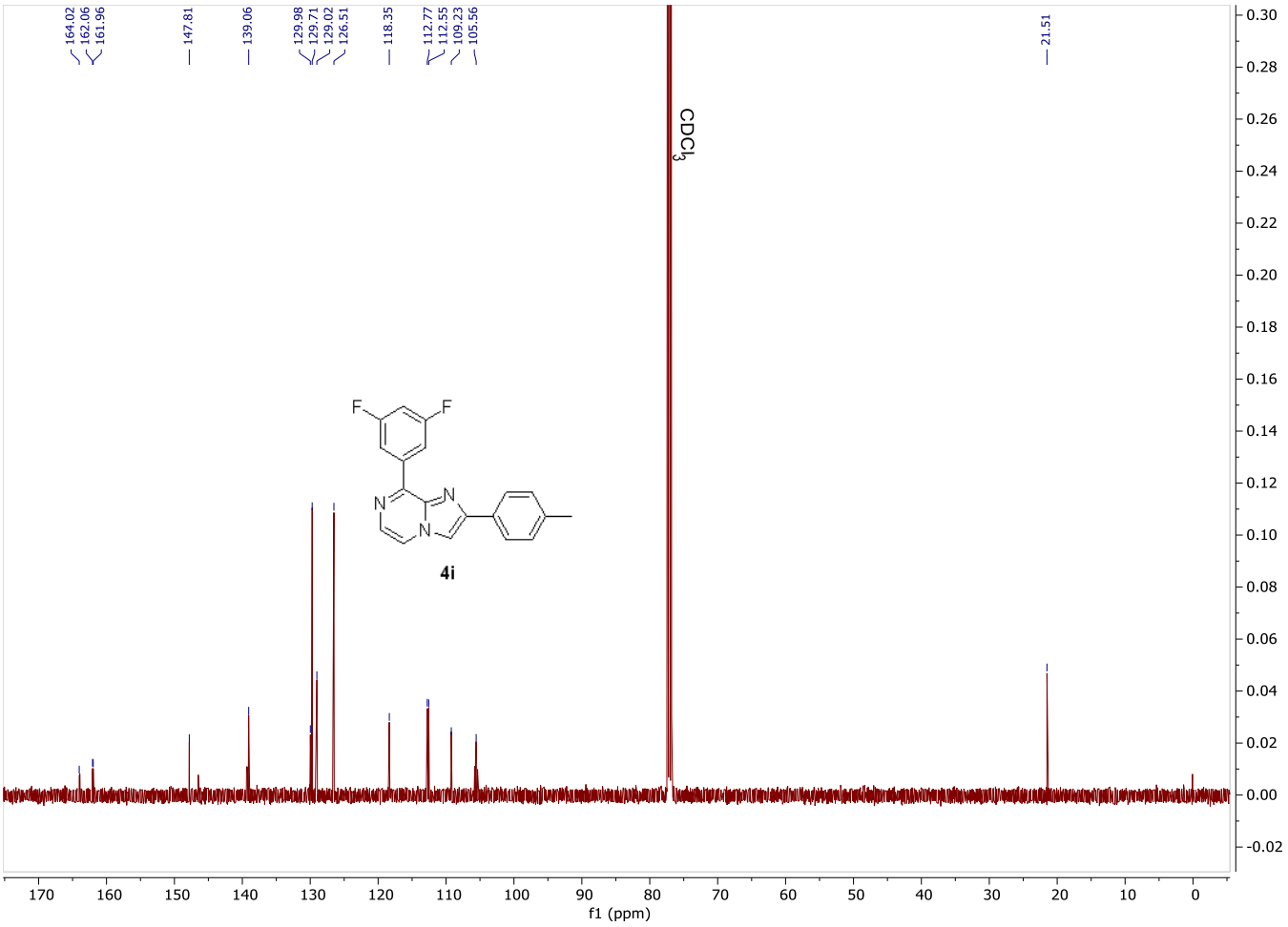
164.02
162.06
161.96
147.81
139.06
129.98
129.71
129.02
126.51
118.35
112.77
112.55
109.23
105.56
21.51
CDCl3
F
F
N
N
N
4i
f1 (ppm)

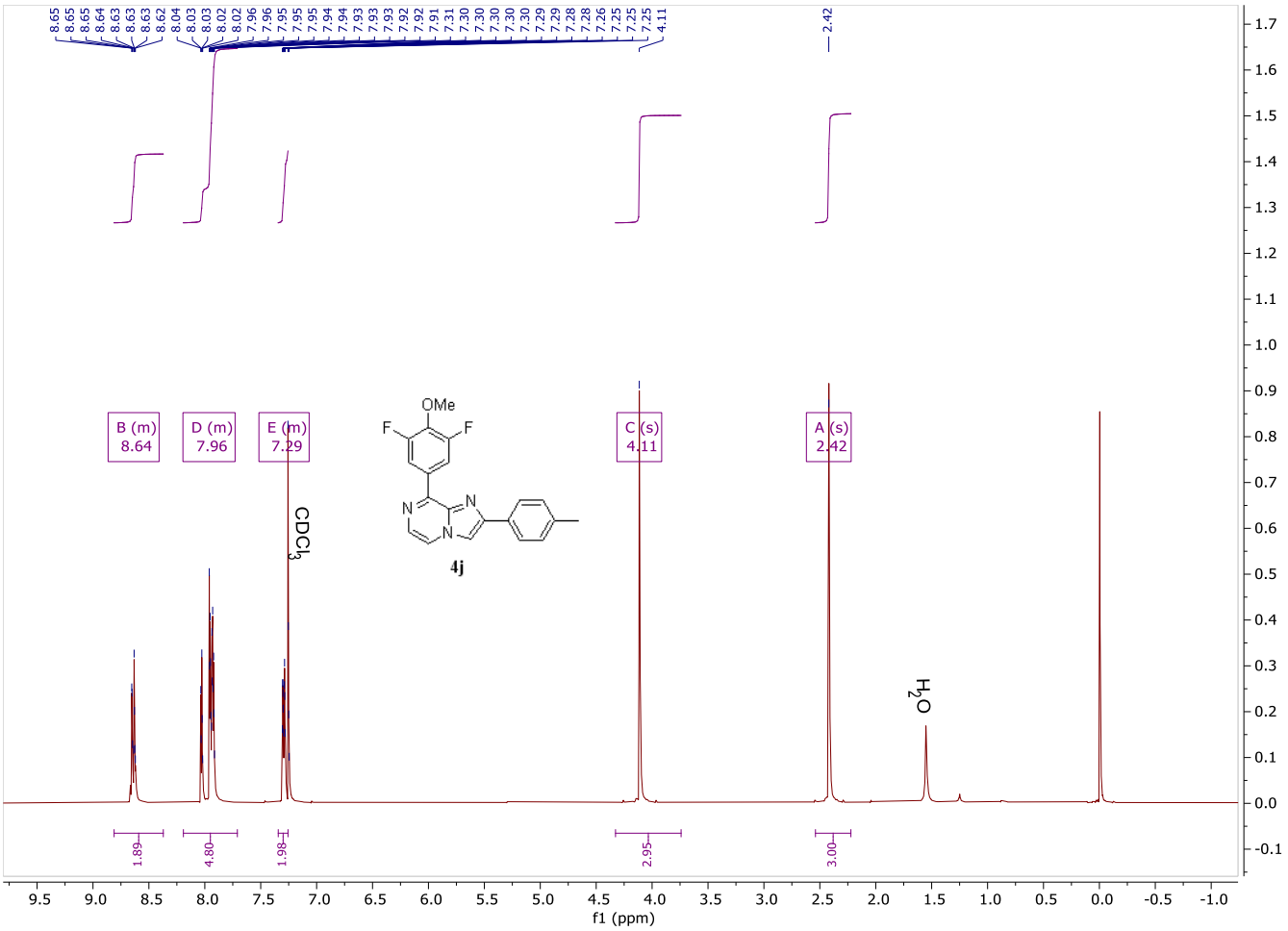
B (m)
8.64
D (m)
7.96
E (m)
7.29
C (s)
4.11
A (s)
2.42
CDCl3
H2O
OMe
F
F
N
N
4j
1.89
4.80
1.98
2.95
3.00
f1 (ppm)

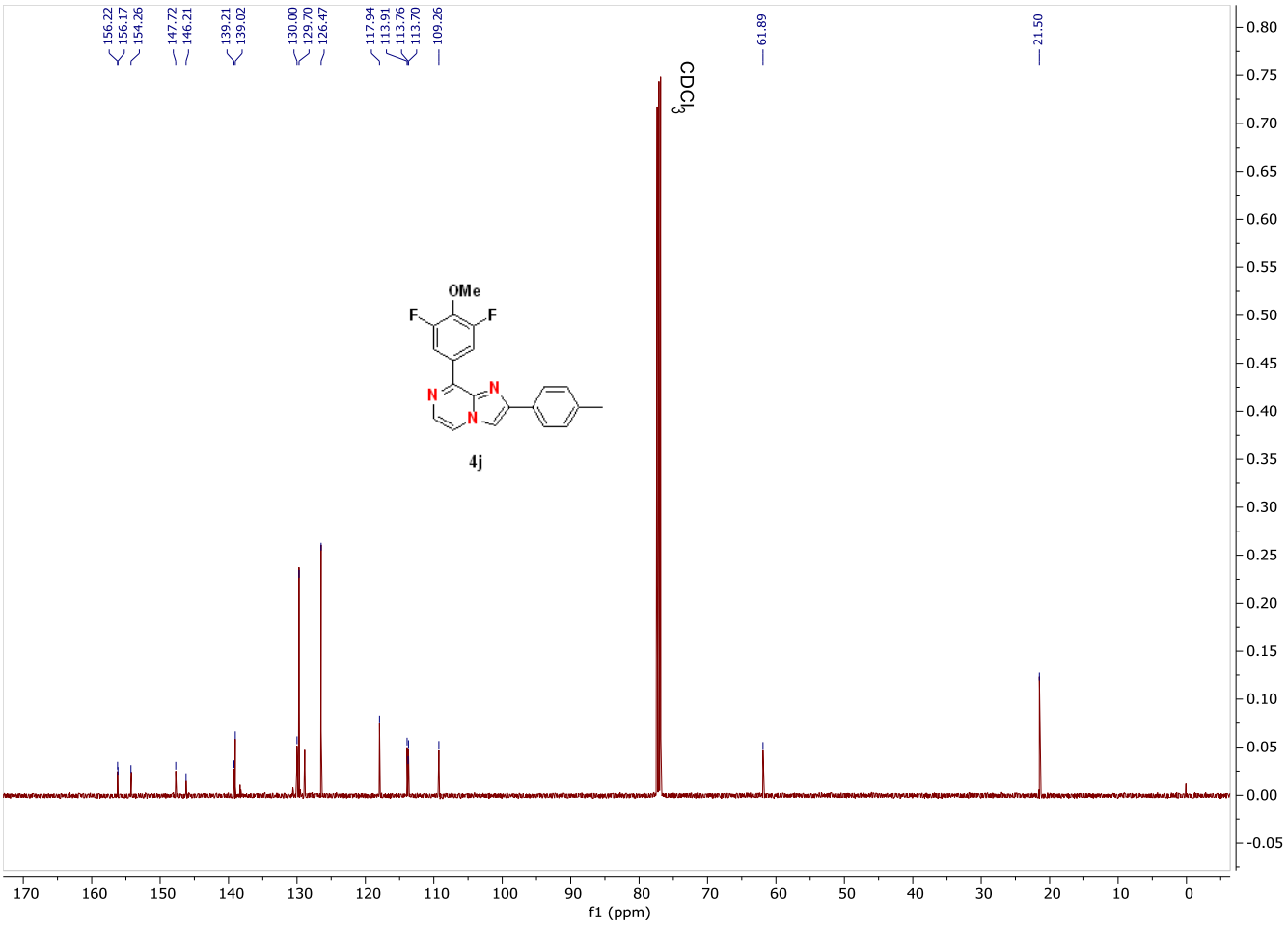
156.22
156.17
154.26
147.72
146.21
139.21
139.02
130.00
129.70
126.47
117.94
113.91
113.76
113.70
109.26
61.89
21.50
CDCl3
OMe
F
F
N
N
N
4j
f1 (ppm)

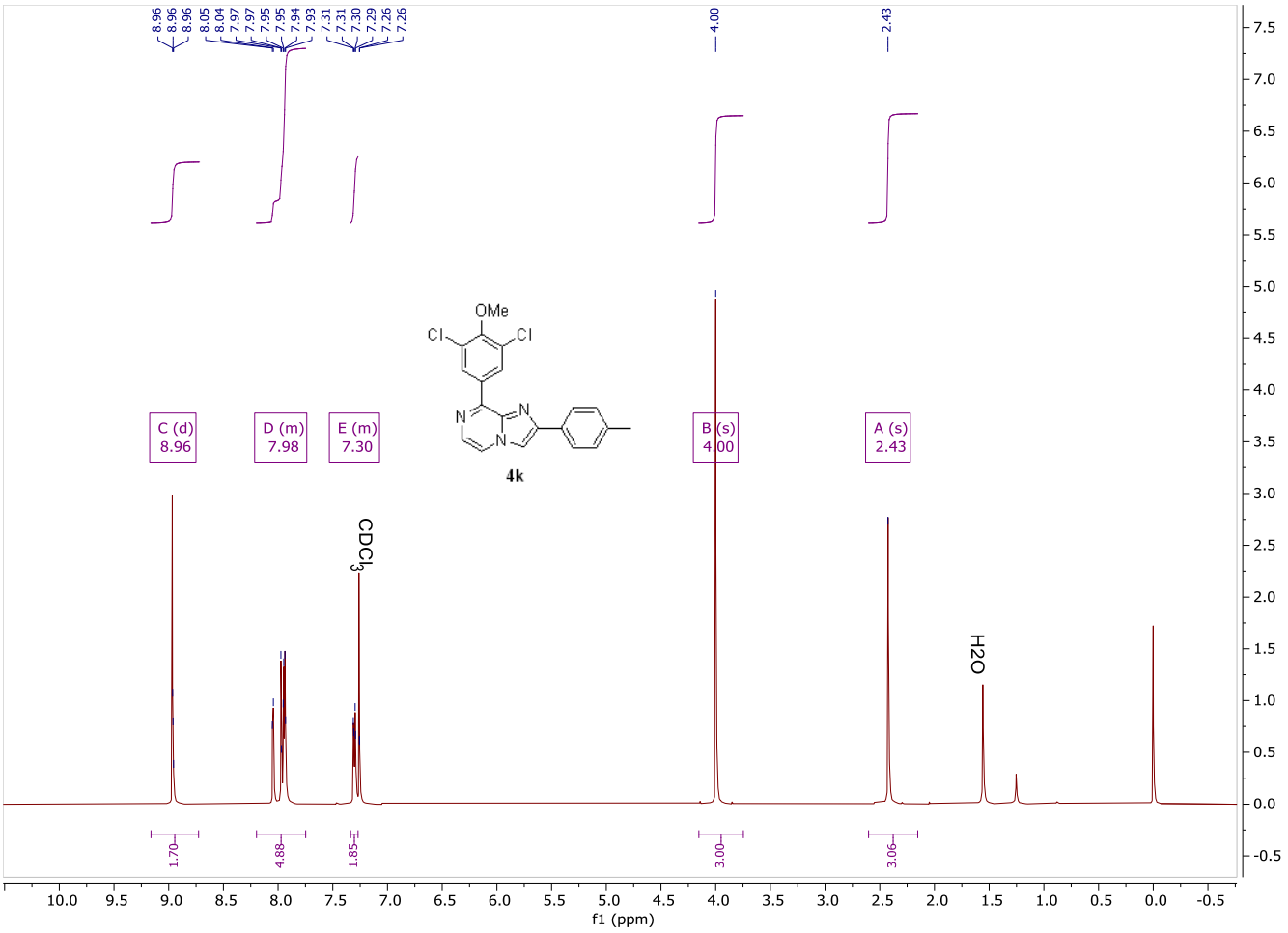
8.96
8.96
8.96
8.05
8.04
7.97
7.97
7.95
7.95
7.94
7.93
7.31
7.31
7.30
7.29
7.26
7.26
4.00
2.43
OMe
Cl
Cl
N
N
N
4k
C (d)
8.96
D (m)
7.98
E (m)
7.30
B (s)
4.00
A (s)
2.43
CDCl3
H2O
1.70
4.88
1.85
3.00
3.06
f1 (ppm)

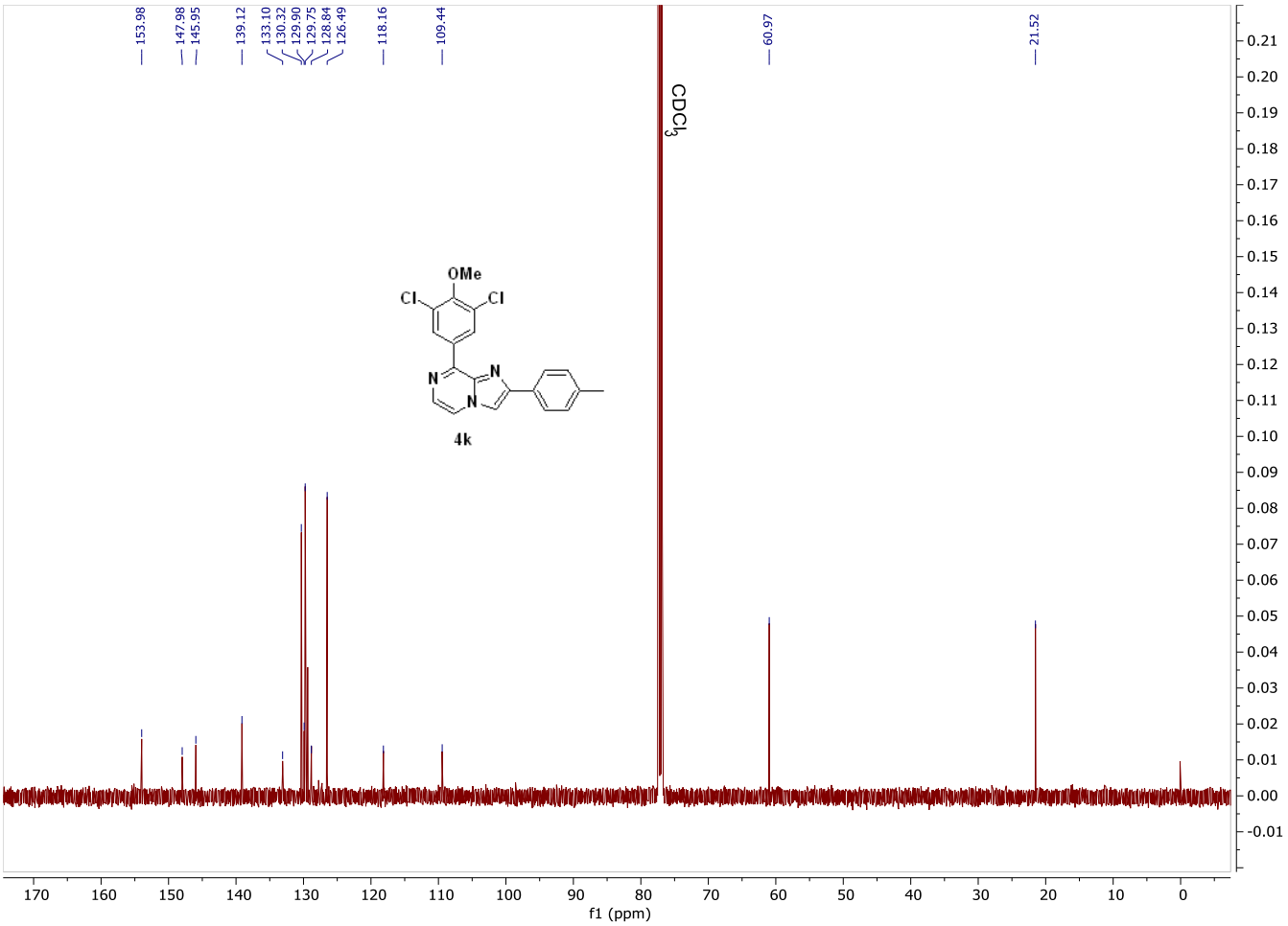
153.98
147.98
145.95
139.12
133.10
130.32
129.90
129.75
128.84
126.49
118.16
109.44
CDCl3
60.97
21.52
OMe
Cl
Cl
N
N
N
4k
f1 (ppm)

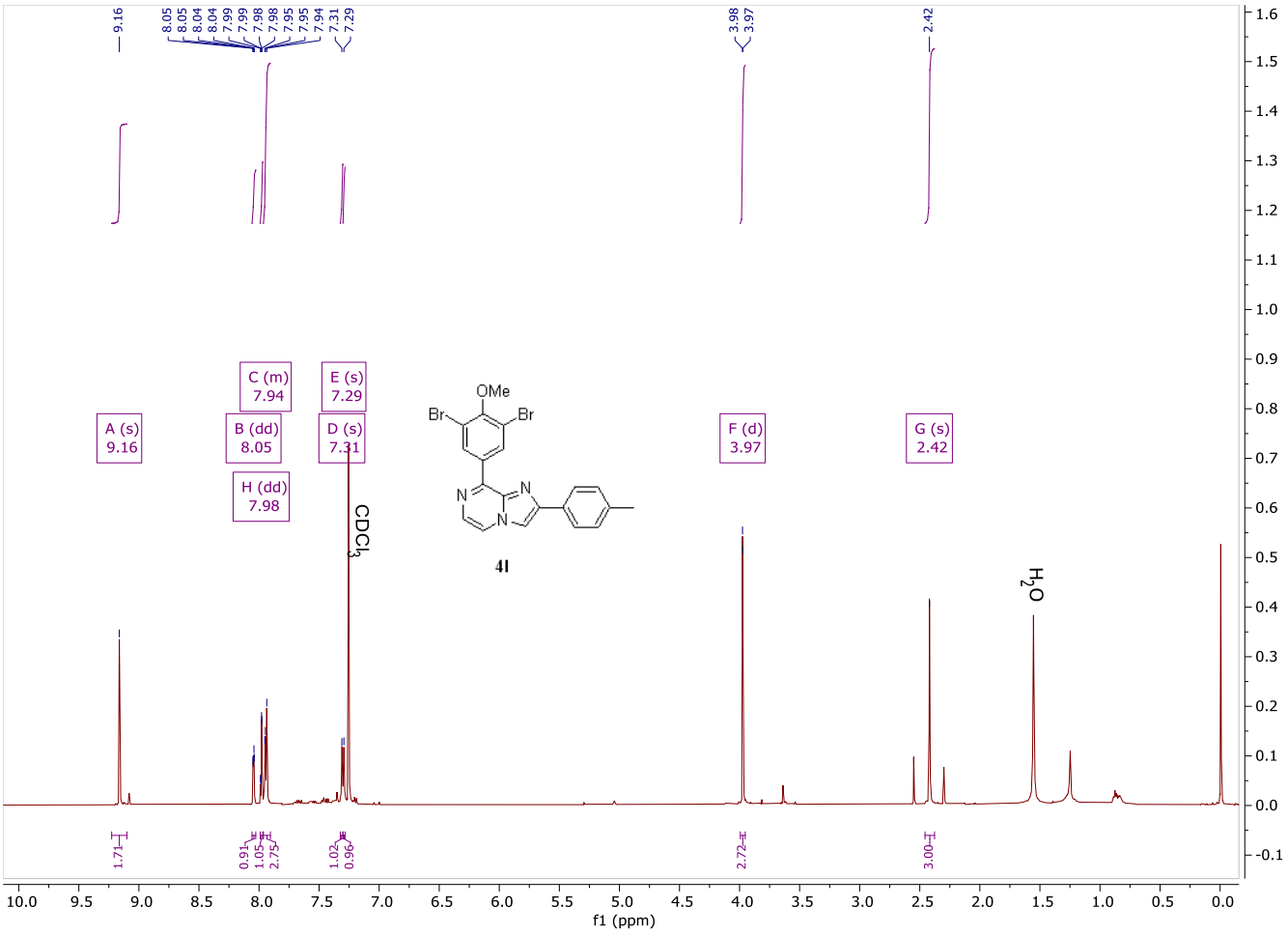
9.16
8.05
8.05
8.04
8.04
7.99
7.99
7.98
7.98
7.95
7.95
7.94
7.31
7.29
3.98
3.97
2.42
A (s)
9.16
B (dd)
8.05
H (dd)
7.98
C (m)
7.94
E (s)
7.29
D (s)
7.31
F (d)
3.97
G (s)
2.42
CDCl3
H2O
OMe
Br
Br
N
N
N
4l
1.71
0.91
1.05
2.75
1.02
0.96
2.72
3.00
f1 (ppm)

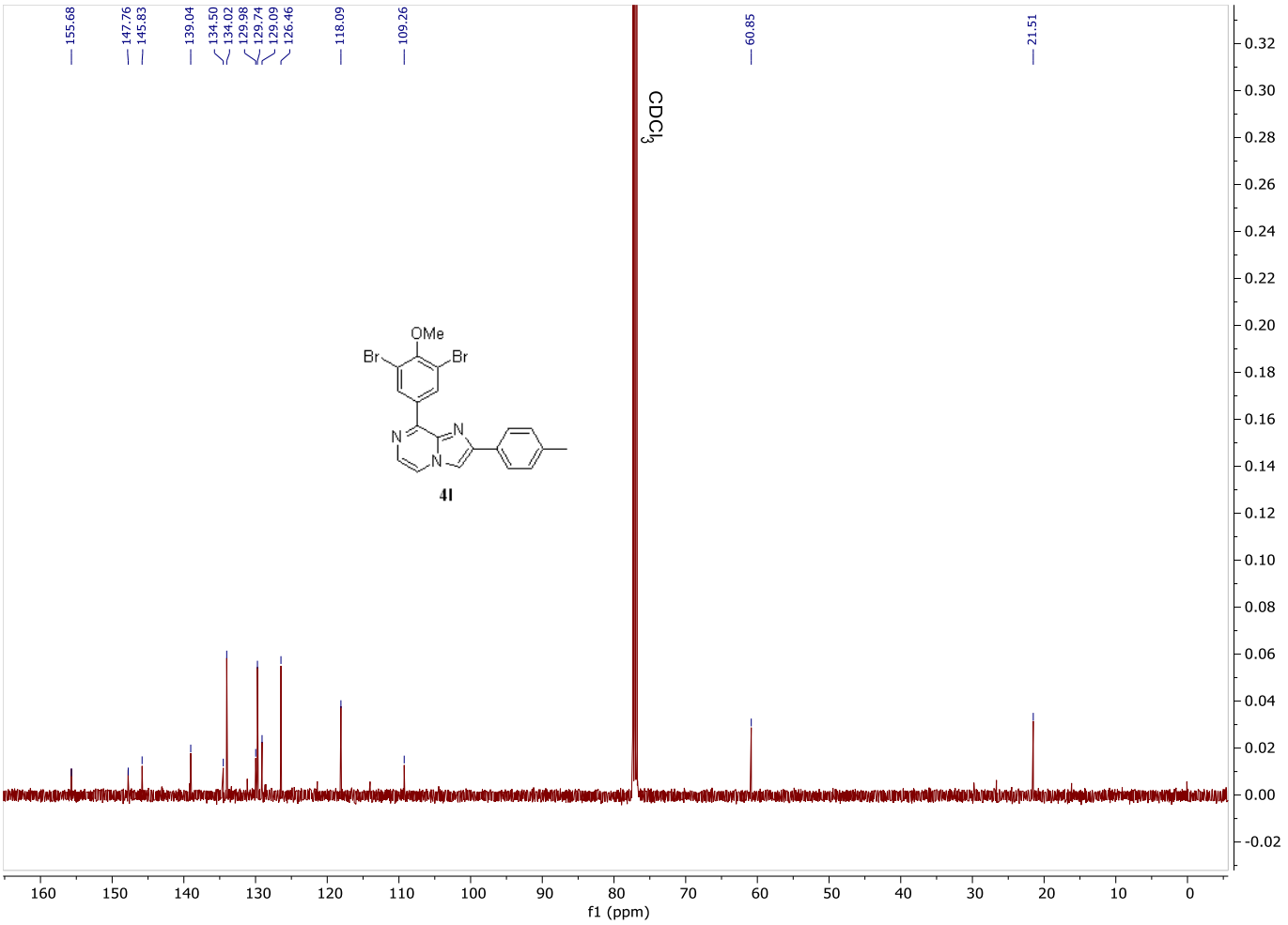
155.68
147.76
145.83
139.04
134.50
134.02
129.98
129.74
129.09
126.46
118.09
109.26
CDCl3
60.85
21.51
OMe
Br
Br
N
N
N
4l
f1 (ppm)

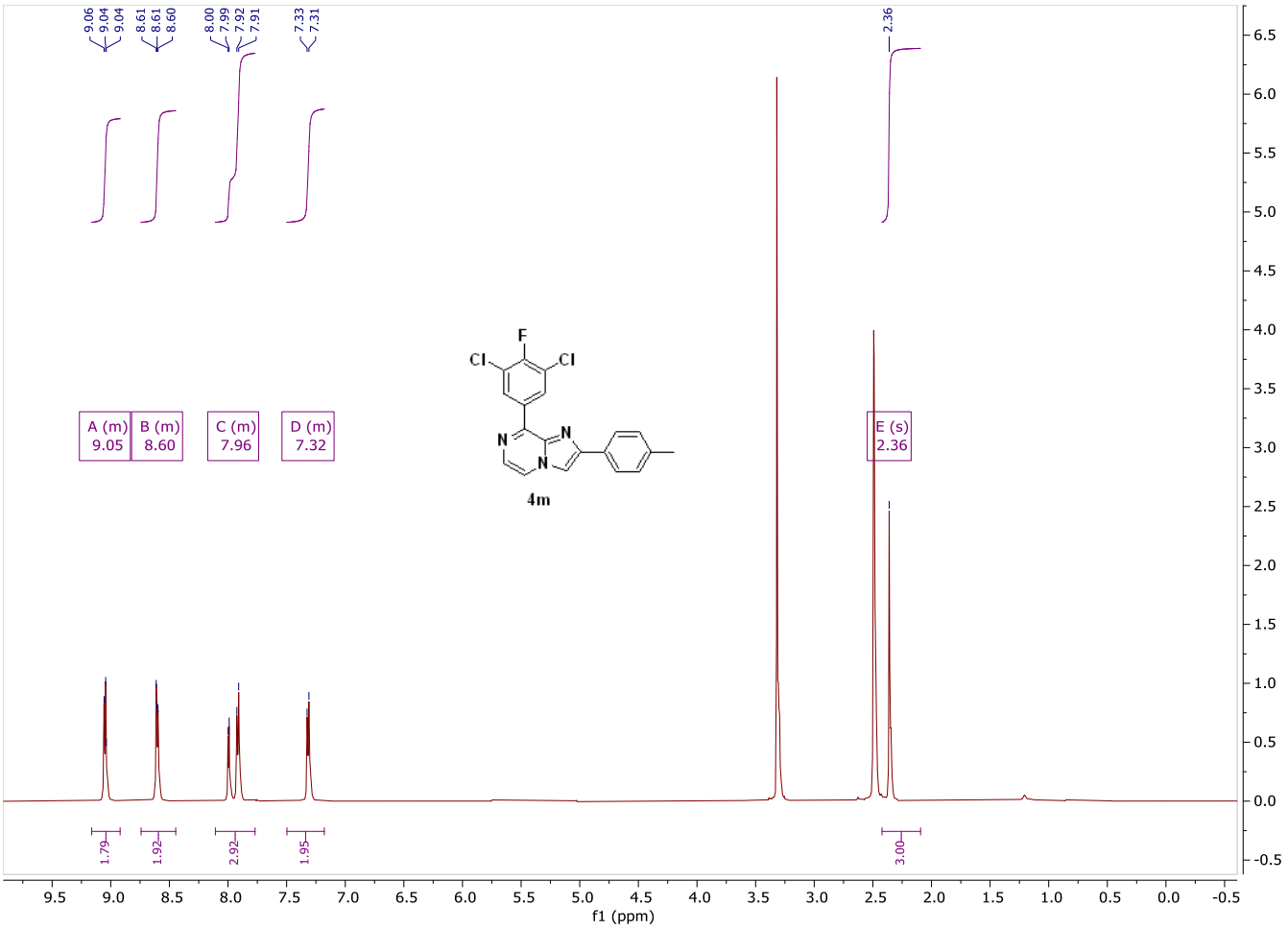
9.06
9.04
9.04
8.61
8.61
8.60
8.00
7.99
7.92
7.91
7.33
7.31
2.36
A (m)
9.05
B (m)
8.60
C (m)
7.96
D (m)
7.32
E (s)
2.36
F
Cl
Cl
N
N
N
4m
1.79
1.92
2.92
1.95
3.00
f1 (ppm)

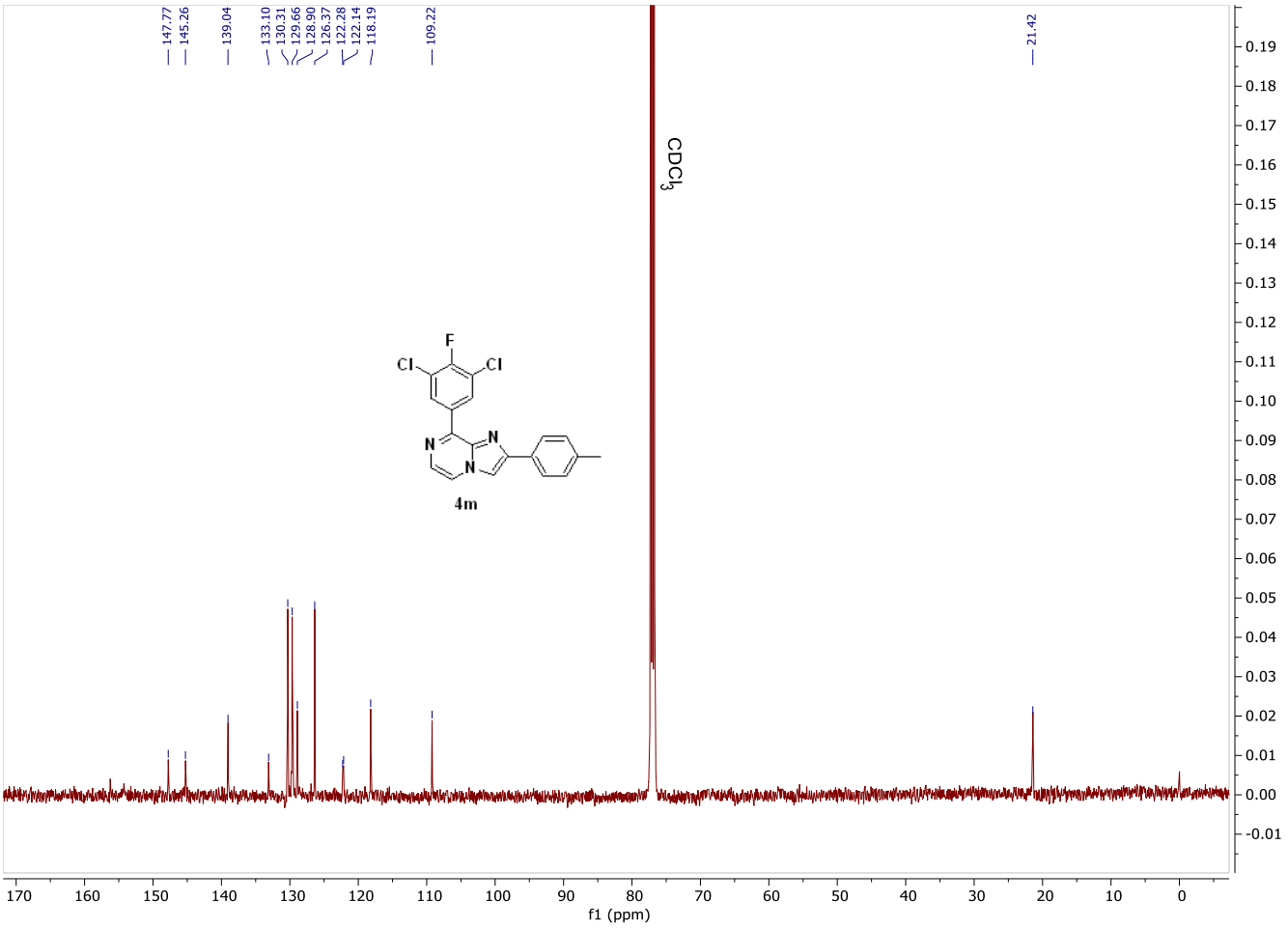
147.77
145.26
139.04
133.10
130.31
129.66
128.90
126.37
122.28
122.14
118.19
109.22
21.42
CDCl3
F
Cl
Cl
N
N
N
4m
0.19
0.18
0.17
0.16
0.15
0.14
0.13
0.12
0.11
0.10
0.09
0.08
0.07
0.06
0.05
0.04
0.03
0.02
0.01
0.00
-0.01
170
160
150
140
130
120
110
100
90
80
70
60
50
40
30
20
10
0
f1 (ppm)

Mass Spectrometry & Proteomics Facility

Mass Spectrum SmartFormula Report

Analysis Info

Analysis Name	D:\Data\Nonka\Aug,23\SW_080423 - 13s\4A_GA1_01_40355.d	Acquisition Date	8/4/2023 2:29:00 PM
Method	tune_low_lc_pos_bb_6jun.m	Operator	BDAL@DE
Sample Name	4A	Instrument / Ser#	micrOTOF-Q 228888.10195
Comment			

Acquisition Parameter

Source Type	ESI	Ion Polarity	Positive	Set Nebulizer	4.0 Bar
Focus	Not active	Set Capillary	2800 V	Set Dry Heater	180 °C
Scan Begin	50 m/z	Set End Plate Offset	-500 V	Set Dry Gas	7.0 l/min
Scan End	3000 m/z	Set Collision Cell RF	150.0 Vpp	Set Divert Valve	Source

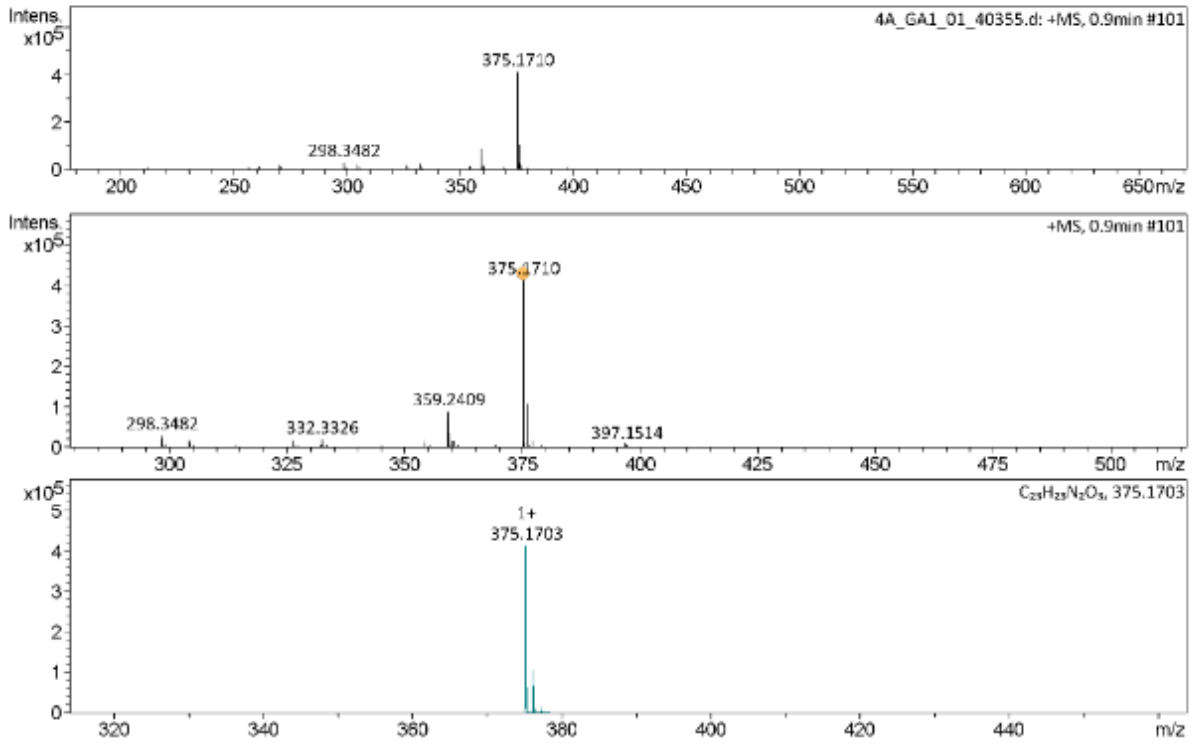

Meas. m/z	#	Ion Formula	m/z	err [ppm]	mSigma	# mSigma	Score	rdb	e⁻ Conf	N-Rule
375.1710	1	C23H23N2O3	375.1703	-1.9	0.7	3	97.43	13.5	even	ok

This material is based upon work supported by the National Science Foundation under CHE-0741793

Mass Spectrometry & Proteomics Facility

Mass Spectrum SmartFormula Report

Analysis Info

Analysis Name	D:\Data\Nonka\Aug,23\SW_080423 - 13s\4B_GA2_01_40356.d	Acquisition Date	8/4/2023 2:31:24 PM
Method	tune_low_lc_pos_bb_6jun.m	Operator	BDAL@DE
Sample Name	4B	Instrument / Ser#	micrOTOF-Q 228888.10195
Comment			

Acquisition Parameter

Source Type	ESI	Ion Polarity	Positive	Set Nebulizer	4.0 Bar
Focus	Not active	Set Capillary	2800 V	Set Dry Heater	180 °C
Scan Begin	50 m/z	Set End Plate Offset	-500 V	Set Dry Gas	7.0 l/min
Scan End	3000 m/z	Set Collision Cell RF	150.0 Vpp	Set Divert Valve	Source

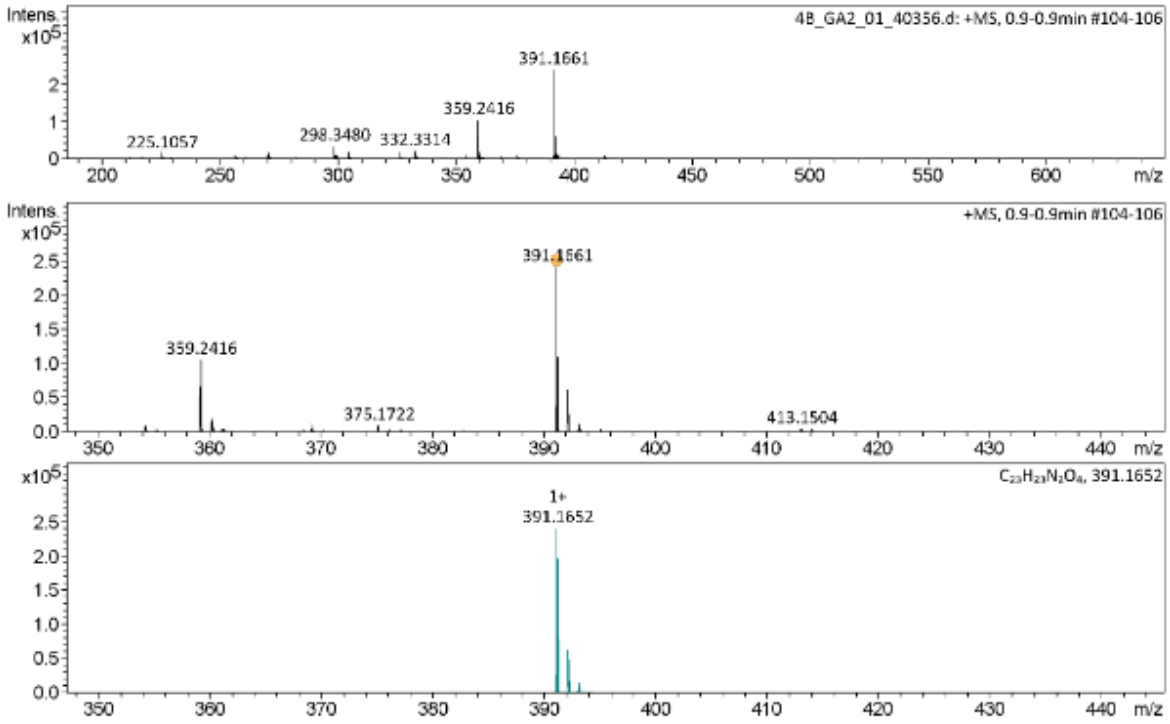

Meas. m/z	#	Ion Formula	m/z	err [ppm]	mSigma	# mSigma	Score	rdb	e⁻ Conf	N-Rule
391.1661	1	C23H23N2O4	391.1652	-2.2	2.5	1	100.00	13.5	even	ok

This material is based upon work supported by the National Science Foundation under CHE-0741793

Mass Spectrometry & Proteomics Facility

Mass Spectrum SmartFormula Report

Analysis Info

Analysis Name	D:\Data\Nonka\Aug,23\SW_080423 - 13s\4C_GA3_01_40358.d	Acquisition Date	8/4/2023 2:36:18 PM
Method	tune_low_lc_pos_bb_6jun.m	Operator	BDAL@DE
Sample Name	4C	Instrument / Ser#	micrOTOF-Q 228888.10195
Comment			

Acquisition Parameter

Source Type	ESI	Ion Polarity	Positive	Set Nebulizer	4.0 Bar
Focus	Not active	Set Capillary	2800 V	Set Dry Heater	180 °C
Scan Begin	50 m/z	Set End Plate Offset	-500 V	Set Dry Gas	7.0 l/min
Scan End	3000 m/z	Set Collision Cell RF	150.0 Vpp	Set Divert Valve	Source

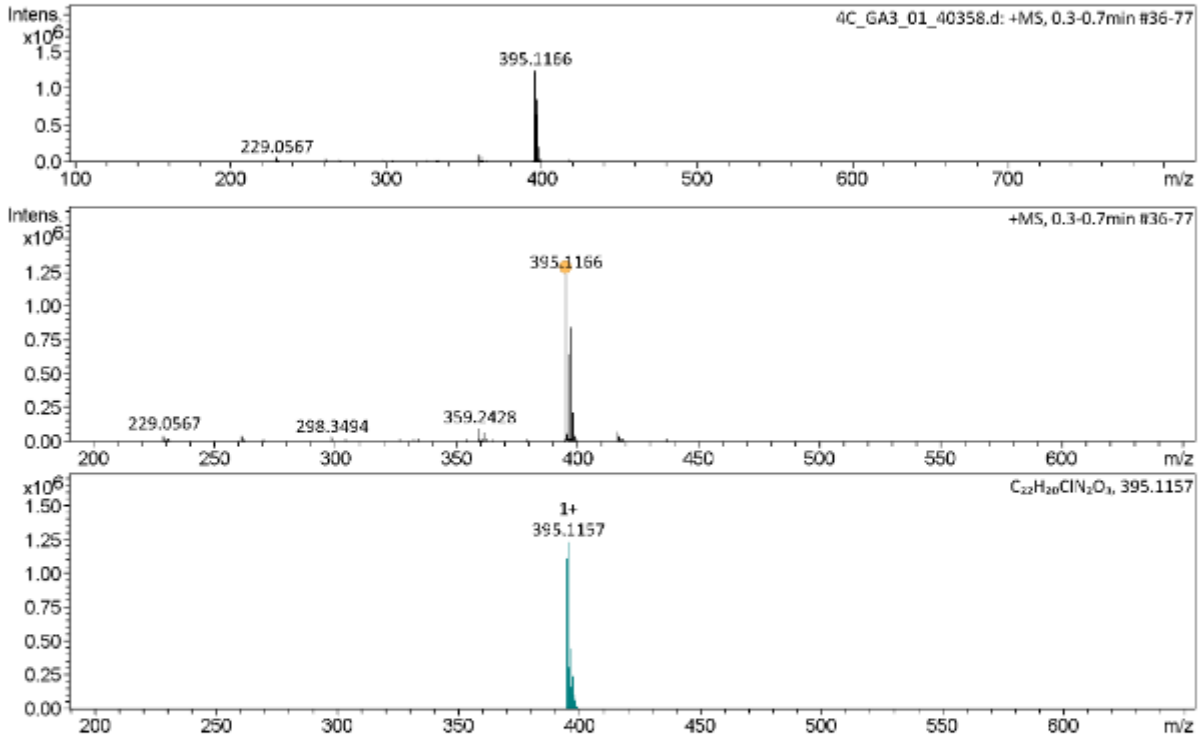

Meas. m/z	#	Ion Formula	m/z	err [ppm]	mSigma	# mSigma	Score	rdb	e⁻ Conf	N-Rule
395.1166	1	C22H20ClN2O3	395.1157	-2.2	195.5	1	100.00	13.5	even	ok

This material is based upon work supported by the National Science Foundation under CHE-0741793

Mass Spectrometry & Proteomics Facility

Mass Spectrum SmartFormula Report

Analysis Info

Analysis Name	D:\Data\Nonka\Aug,23\SW_080423 - 13s\4D_GA4_01_40359.d	Acquisition Date	8/4/2023 2:38:44 PM
Method	tune_low_lc_pos_bb_6jun.m	Operator	BDAL@DE
Sample Name	4D	Instrument / Ser#	micrOTOF-Q 228888.10195
Comment			

Acquisition Parameter

Source Type	ESI	Ion Polarity	Positive	Set Nebulizer	4.0 Bar
Focus	Not active	Set Capillary	2800 V	Set Dry Heater	180 °C
Scan Begin	50 m/z	Set End Plate Offset	-500 V	Set Dry Gas	7.0 l/min
Scan End	3000 m/z	Set Collision Cell RF	150.0 Vpp	Set Divert Valve	Source

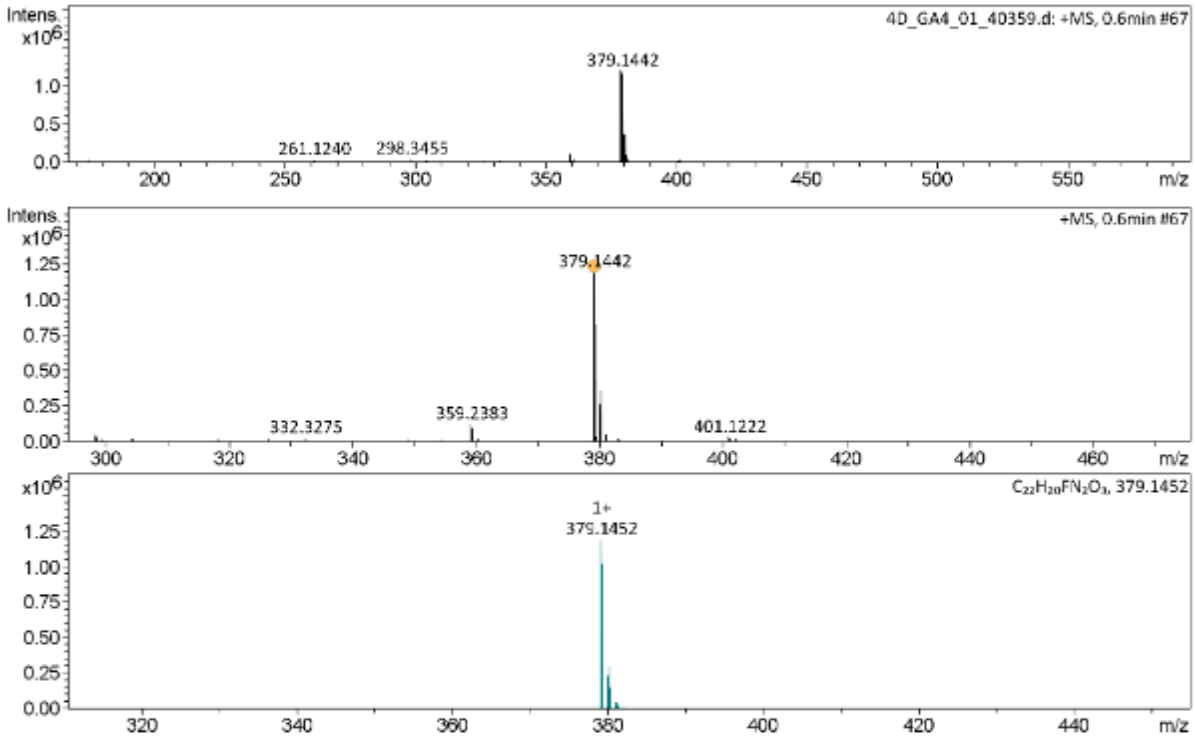

Meas. m/z	#	Ion Formula	m/z	err [ppm]	mSigma	# mSigma	Score	rdb	e¯ Conf	N-Rule
379.1442	1	C22H20FN2O3	379.1452	2.8	32.1	2	100.00	13.5	even	ok

This material is based upon work supported by the National Science Foundation under CHE-0741793

Mass Spectrometry & Proteomics Facility

Mass Spectrum SmartFormula Report

Analysis Info

Analysis Name	D:\Data\Nonka\Aug,23\SW_080423 - 13s\4E_GA5_01_40361.d	Acquisition Date	8/4/2023 2:43:50 PM
Method	tune_low_lc_pos_bb_6jun.m	Operator	BDAL@DE
Sample Name	4E	Instrument / Ser#	micrOTOF-Q 228888.10195
Comment			

Acquisition Parameter

Source Type	ESI	Ion Polarity	Positive	Set Nebulizer	4.0 Bar
Focus	Not active	Set Capillary	2800 V	Set Dry Heater	180 °C
Scan Begin	50 m/z	Set End Plate Offset	-500 V	Set Dry Gas	7.0 l/min
Scan End	3000 m/z	Set Collision Cell RF	150.0 Vpp	Set Divert Valve	Source

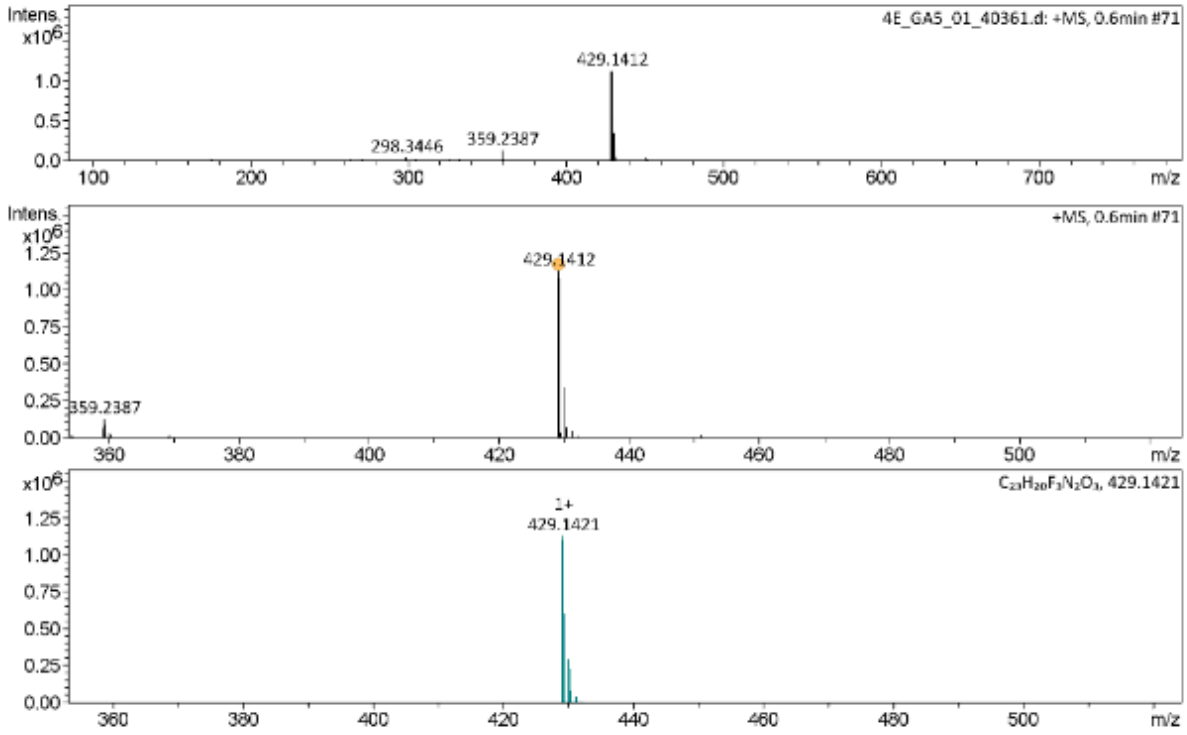

Meas. m/z	#	Ion Formula	m/z	err [ppm]	mSigma	# mSigma	Score	rdb	e⁻ Conf	N-Rule
429.1412	1	C23H20F3N2O3	429.1421	2.0	26.1	2	100.00	13.5	even	ok

This material is based upon work supported by the National Science Foundation under CHE-0741793

Mass Spectrometry & Proteomics Facility

Mass Spectrum SmartFormula Report

Analysis Info

Analysis Name	D:\Data\Nonka\Aug,23\SW_080423 - 13s\4F_GA6_01_40362.d	Acquisition Date	8/4/2023 2:46:15 PM
Method	tune_low_lc_pos_bb_6jun.m	Operator	BDAL@DE
Sample Name	4F	Instrument / Ser#	micrOTOF-Q 228888.10195
Comment			

Acquisition Parameter

Source Type	ESI	Ion Polarity	Positive	Set Nebulizer	4.0 Bar
Focus	Not active	Set Capillary	2800 V	Set Dry Heater	180 °C
Scan Begin	50 m/z	Set End Plate Offset	-500 V	Set Dry Gas	7.0 l/min
Scan End	3000 m/z	Set Collision Cell RF	150.0 Vpp	Set Divert Valve	Source

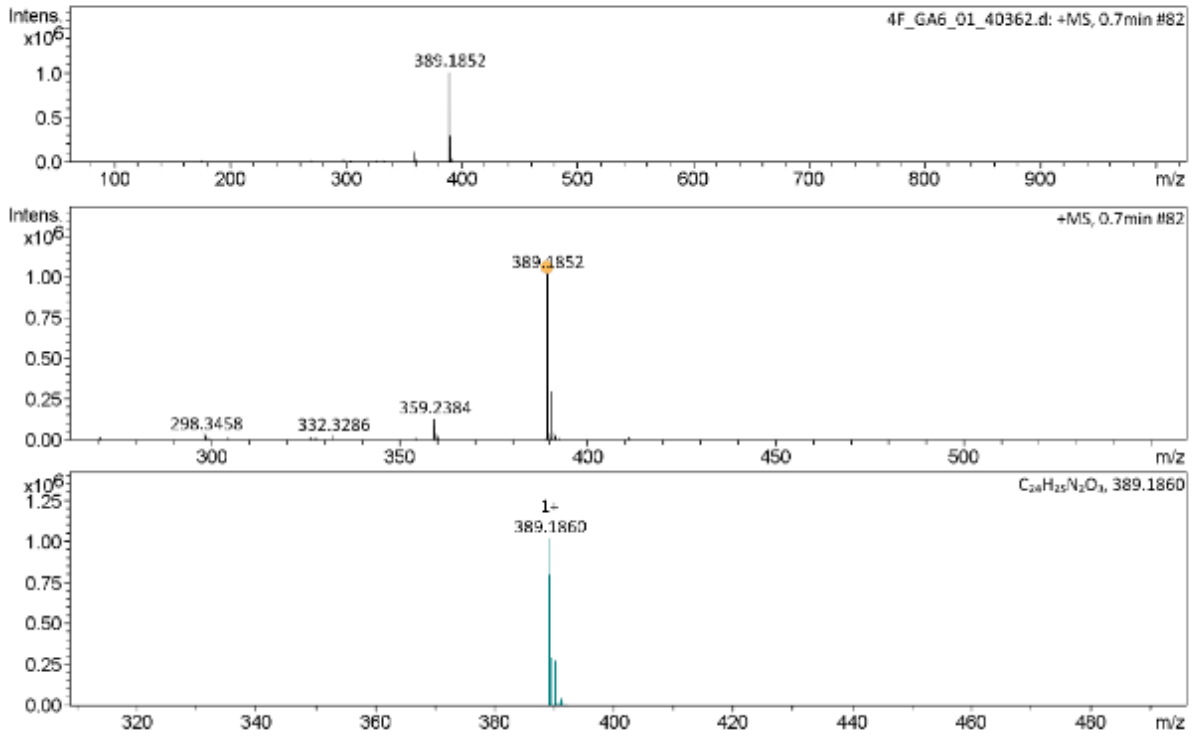

Meas. m/z	#	Ion Formula	m/z	err [ppm]	mSigma	# mSigma	Score	rdb	e⁻ Conf	N-Rule
389.1852	1	C24H25N2O3	389.1860	2.0	10.7	3	100.00	13.5	even	ok

This material is based upon work supported by the National Science Foundation under CHE-0741793

Mass Spectrometry & Proteomics Facility

Analysis Info

Analysis Name	D:\Data\Nonka\Aug,23\SW_080423 - 13s\4G_GA7_01_40364.d	Acquisition Date	8/4/2023 2:51:13 PM
Method	tune_low_lc_pos_bb_6jun.m	Operator	BDAL@DE
Sample Name	4G	Instrument	micrOTOF-Q 228888.10195
Comment			

Acquisition Parameter

Source Type	ESI	Ion Polarity	Positive	Set Nebulizer	4.0 Bar
Focus	Not active	Set Capillary	2800 V	Set Dry Heater	180 °C
Scan Begin	50 m/z	Set End Plate Offset	-500 V	Set Dry Gas	7.0 l/min
Scan End	3000 m/z	Set Collision Cell RF	150.0 Vpp	Set Divert Valve	Source

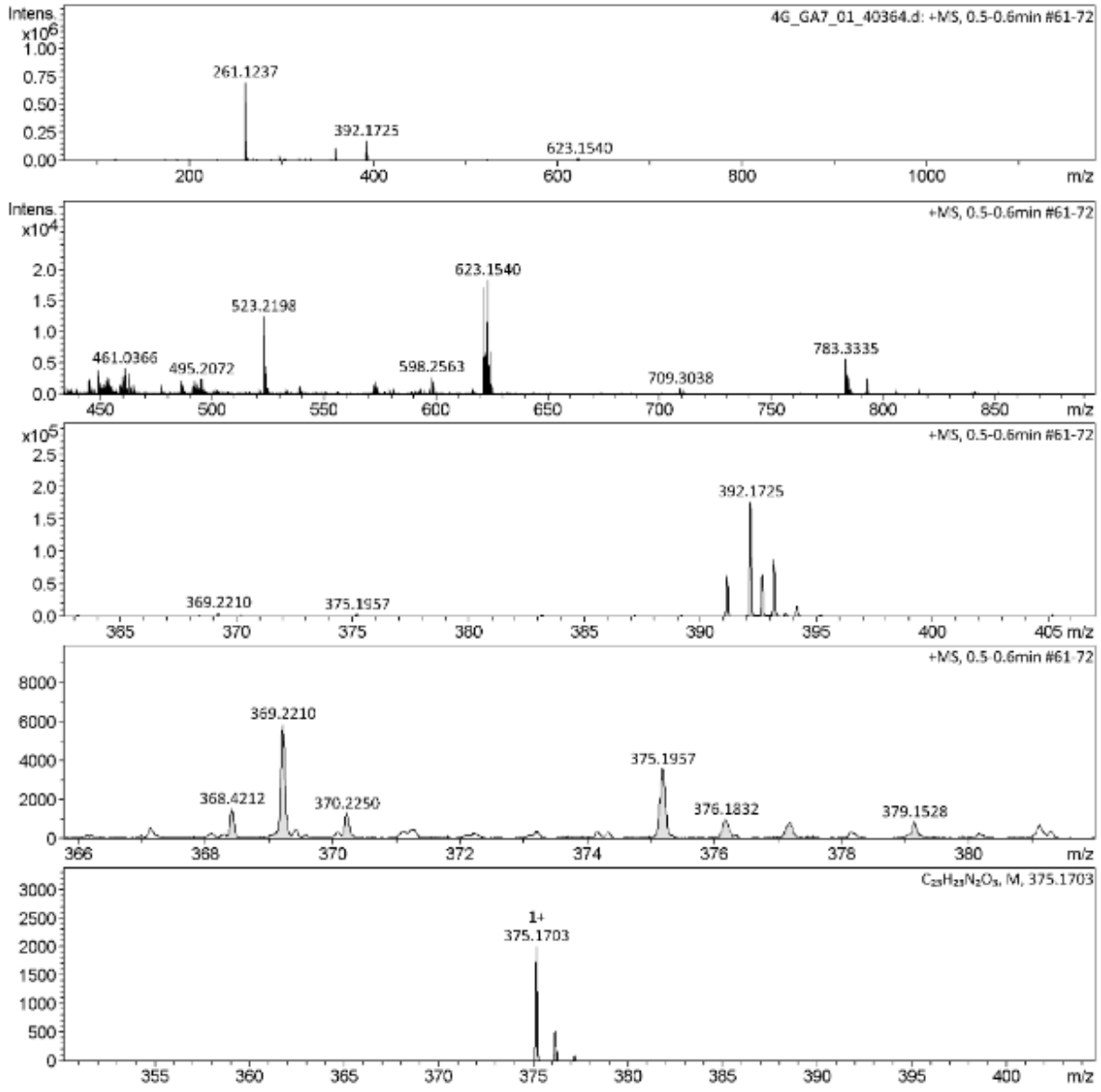

Mass Spectrometry & Proteomics Facility

Mass Spectrum SmartFormula Report

Analysis Info

Analysis Name	D:\Data\Nonka\Aug,23\SW_080423 - 13s\4H_GA8_01_40365.d	Acquisition Date	8/4/2023 2:53:39 PM
Method	tune_low_lc_pos_bb_6jun.m	Operator	BDAL@DE
Sample Name	4H	Instrument / Ser#	micrOTOF-Q 228888.10195
Comment			

Acquisition Parameter

Source Type	ESI	Ion Polarity	Positive	Set Nebulizer	4.0 Bar
Focus	Not active	Set Capillary	2800 V	Set Dry Heater	180 °C
Scan Begin	50 m/z	Set End Plate Offset	-500 V	Set Dry Gas	7.0 l/min
Scan End	3000 m/z	Set Collision Cell RF	150.0 Vpp	Set Divert Valve	Source

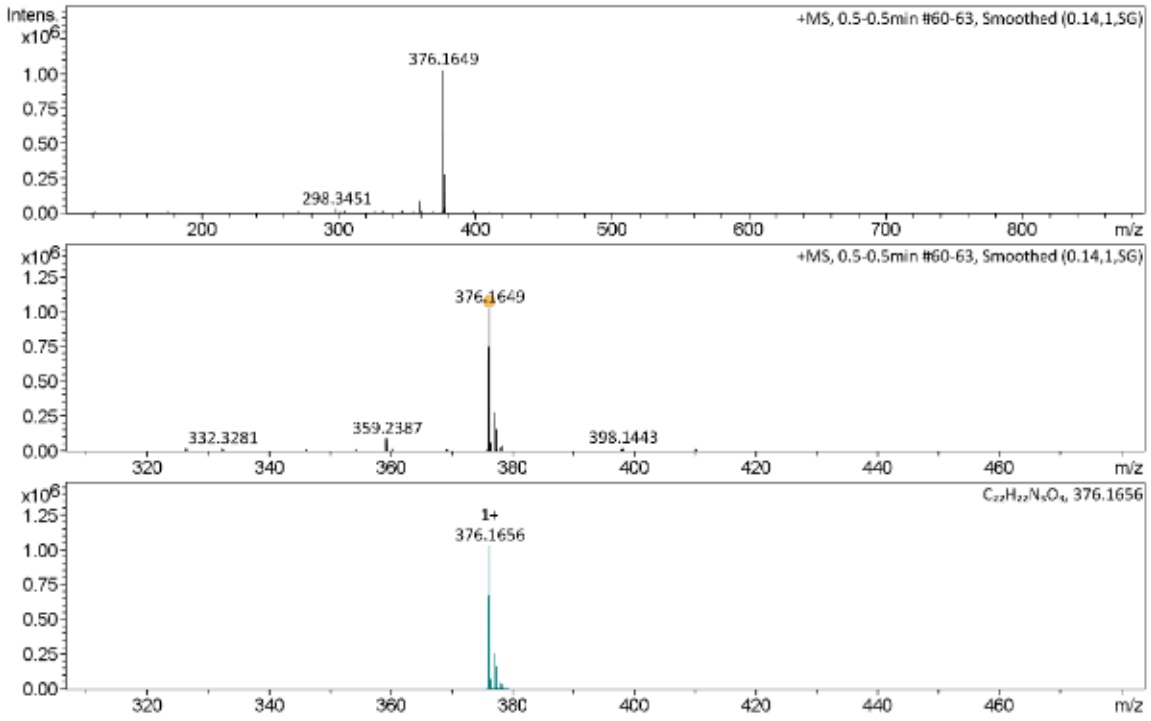

Meas. m/z	#	Ion Formula	m/z	err [ppm]	mSigma	# mSigma	Score	rdb	e⁻ Conf	N-Rule
376.1649	1	C22H22N3O3	376.1656	1.7	10.4	2	100.00	13.5	even	ok

This material is based upon work supported by the National Science Foundation under CHE-0741793

Mass Spectrometry & Proteomics Facility

Mass Spectrum SmartFormula Report

Analysis Info

Analysis Name	D:\Data\Nonka\Aug,23\SW_080423 - 13s\4I_GB1_01_40367.d	Acquisition Date	8/4/2023 2:58:35 PM
Method	tune_low_lc_pos_bb_6jun.m	Operator	BDAL@DE
Sample Name	4I	Instrument / Ser#	micrOTOF-Q 228888.10195
Comment			

Acquisition Parameter

Source Type	ESI	Ion Polarity	Positive	Set Nebulizer	4.0 Bar
Focus	Not active	Set Capillary	2800 V	Set Dry Heater	180 °C
Scan Begin	50 m/z	Set End Plate Offset	-500 V	Set Dry Gas	7.0 l/min
Scan End	3000 m/z	Set Collision Cell RF	150.0 Vpp	Set Divert Valve	Source

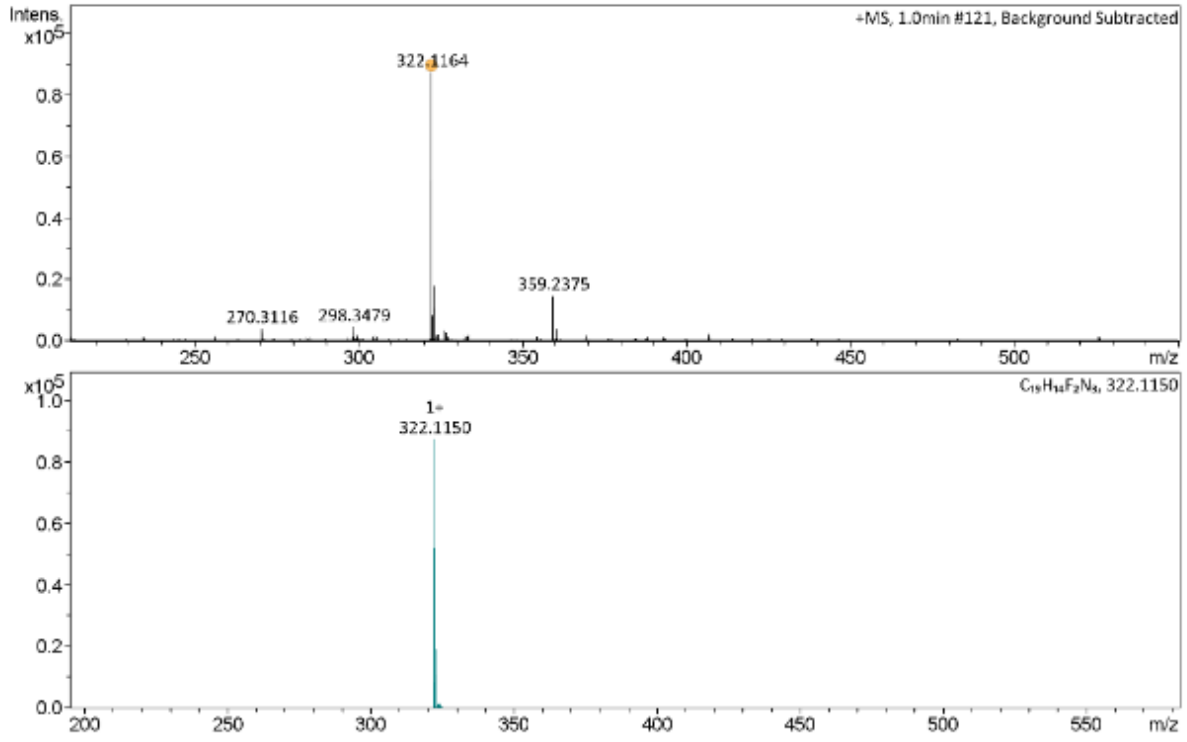

Meas. m/z	#	Ion Formula	m/z	err [ppm]	mSigma	# mSigma	Score	rdb	e⁻ Conf	N-Rule
322.1164	1	C19H14F2N3	322.1150	-4.4	8.8	2	100.00	13.5	even	ok

This material is based upon work supported by the National Science Foundation under CHE-0741793

Mass Spectrometry & Proteomics Facility

Mass Spectrum SmartFormula Report

Analysis Info

Analysis Name	D:\Data\Nonka\Aug,23\SW_080423 - 13s\4J_GB2_01_40368.d	Acquisition Date	8/4/2023 3:01:00 PM
Method	tune_low_lc_pos_bb_6jun.m	Operator	BDAL@DE
Sample Name	4J	Instrument / Ser#	micrOTOF-Q 228888.10195
Comment			

Acquisition Parameter

Source Type	ESI	Ion Polarity	Positive	Set Nebulizer	4.0 Bar
Focus	Not active	Set Capillary	2800 V	Set Dry Heater	180 °C
Scan Begin	50 m/z	Set End Plate Offset	-500 V	Set Dry Gas	7.0 l/min
Scan End	3000 m/z	Set Collision Cell RF	150.0 Vpp	Set Divert Valve	Source

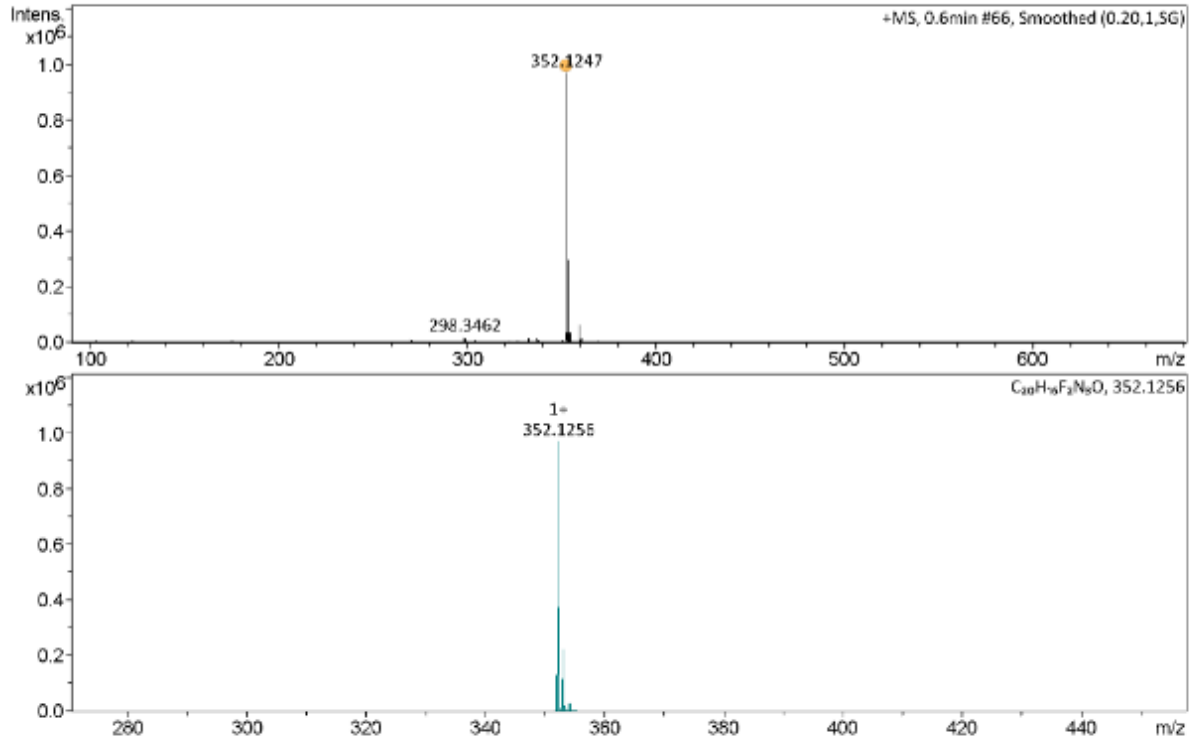

Meas. m/z	#	Ion Formula	m/z	err [ppm]	mSigma	# mSigma	Score	rdb	e⁻ Conf	N-Rule
352.1247	1	C20H16F2N3O	352.1256	2.6	44.5	1	100.00	13.5	even	ok

This material is based upon work supported by the National Science Foundation under CHE-0741793

Mass Spectrometry & Proteomics Facility

Mass Spectrum SmartFormula Report

Analysis Info

Analysis Name	D:\Data\Nonka\Aug,23\SW_080423 - 13s\4K_GB3_01_40370.d	Acquisition Date	8/4/2023 3:05:57 PM
Method	tune_low_lc_pos_bb_6jun.m	Operator	BDAL@DE
Sample Name	4K	Instrument / Ser#	micrOTOF-Q 228888.10195
Comment			

Acquisition Parameter

Source Type	ESI	Ion Polarity	Positive	Set Nebulizer	4.0 Bar
Focus	Not active	Set Capillary	2800 V	Set Dry Heater	180 °C
Scan Begin	50 m/z	Set End Plate Offset	-500 V	Set Dry Gas	7.0 l/min
Scan End	3000 m/z	Set Collision Cell RF	150.0 Vpp	Set Divert Valve	Source

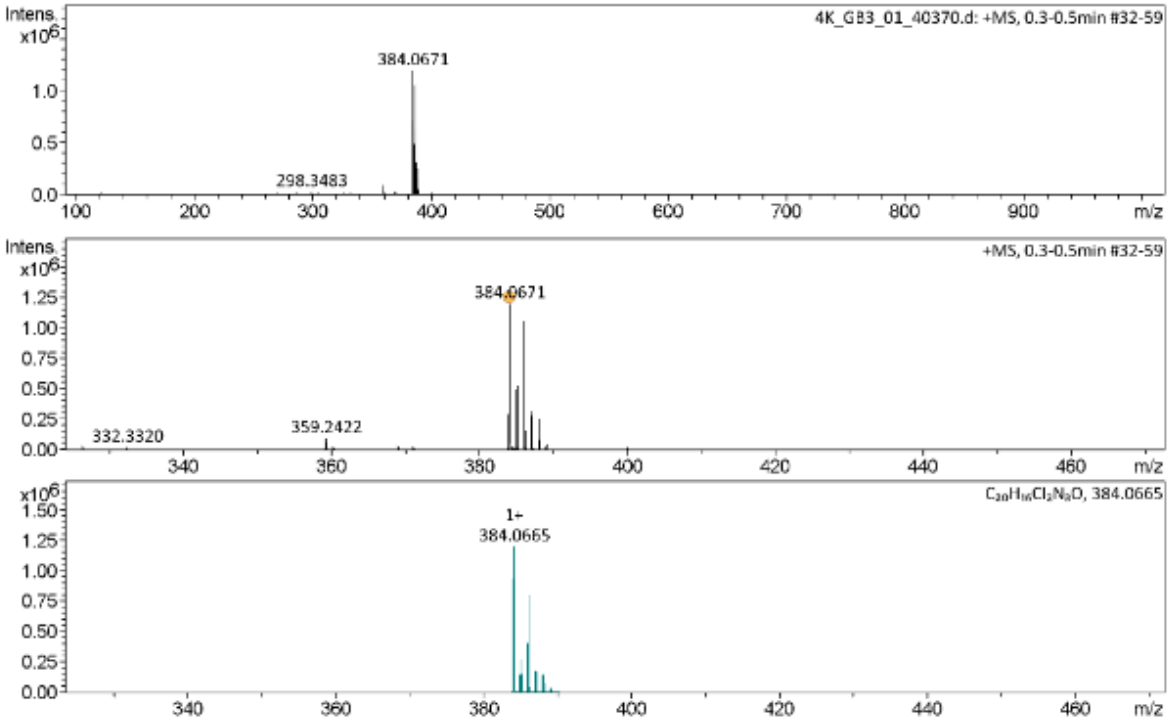

Meas. m/z	#	Ion Formula	m/z	err [ppm]	mSigma	# mSigma	Score	rdb	e⁻ Conf	N-Rule
384.0671	1	C20H16Cl2N3O	384.0665	-1.6	131.3	1	100.00	13.5	even	ok

This material is based upon work supported by the National Science Foundation under CHE-0741793

Mass Spectrometry & Proteomics Facility

Mass Spectrum SmartFormula Report

Analysis Info

Analysis Name	D:\Data\Nonka\Aug,23\SW_080423 - 13s\4L_GB4_01_40371.d	Acquisition Date	8/4/2023 3:08:24 PM
Method	tune_low_lc_pos_bb_6jun.m	Operator	BDAL@DE
Sample Name	4L	Instrument / Ser#	micrOTOF-Q 228888.10195
Comment			

Acquisition Parameter

Source Type	ESI	Ion Polarity	Positive	Set Nebulizer	4.0 Bar
Focus	Not active	Set Capillary	2800 V	Set Dry Heater	180 °C
Scan Begin	50 m/z	Set End Plate Offset	-500 V	Set Dry Gas	7.0 l/min
Scan End	3000 m/z	Set Collision Cell RF	150.0 Vpp	Set Divert Valve	Source

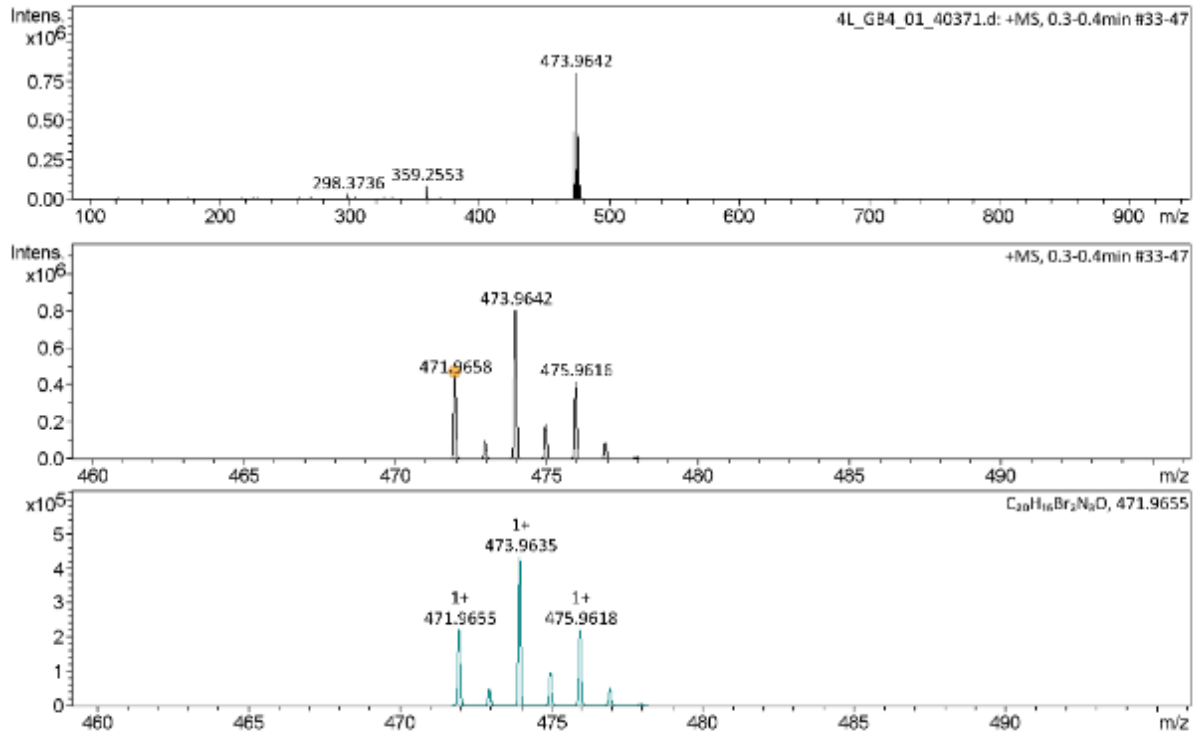

Meas. m/z	#	Ion Formula	m/z	err [ppm]	mSigma	# mSigma	Score	rdb	e⁻ Conf	N-Rule
471.9658	1	C20H16Br2N3O	471.9655	-0.7	13.3	1	100.00	13.5	even	ok

This material is based upon work supported by the National Science Foundation under CHE-0741793

Mass Spectrometry & Proteomics Facility

Mass Spectrum SmartFormula Report

Analysis Info

Analysis Name	D:\Data\Nonka\Aug,23\SW_080423 - 13s\4M_GB5_01_40372.d	Acquisition Date	8/4/2023 3:10:48 PM
Method	tune_low_lc_pos_bb_6jun.m	Operator	BDAL@DE
Sample Name	4M	Instrument / Ser#	micrOTOF-Q 228888.10195
Comment			

Acquisition Parameter

Source Type	ESI	Ion Polarity	Positive	Set Nebulizer	4.0 Bar
Focus	Not active	Set Capillary	2800 V	Set Dry Heater	180 °C
Scan Begin	50 m/z	Set End Plate Offset	-500 V	Set Dry Gas	7.0 l/min
Scan End	3000 m/z	Set Collision Cell RF	150.0 Vpp	Set Divert Valve	Source

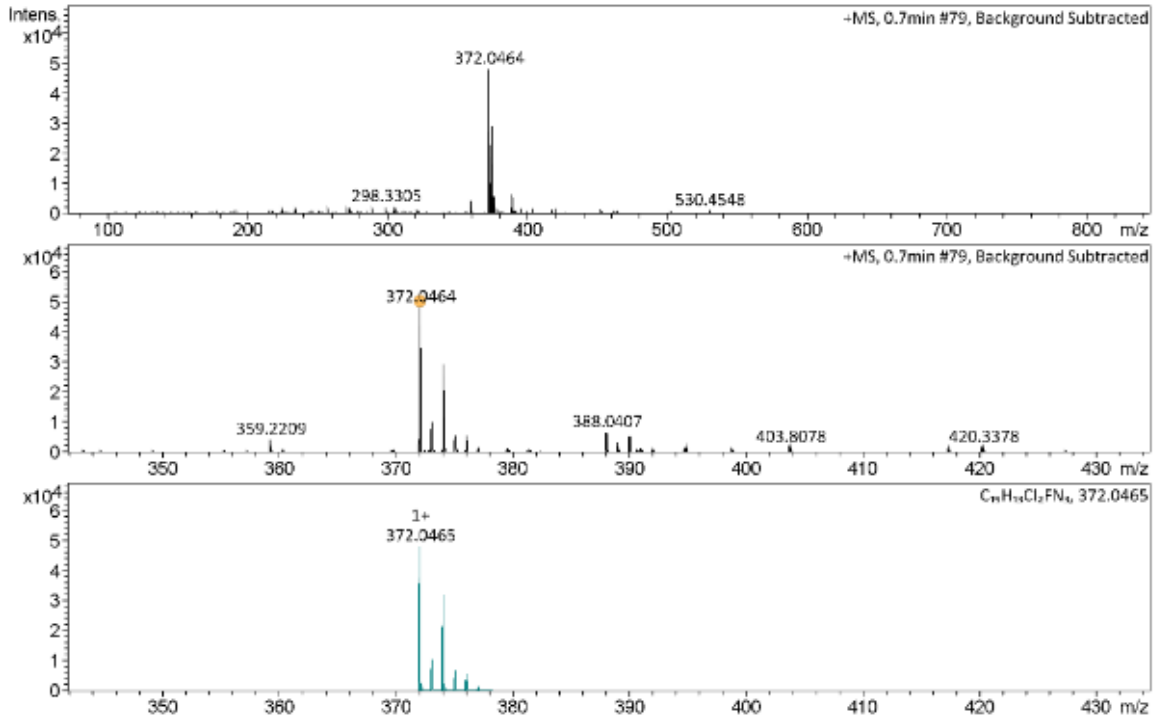

Meas. m/z	#	Ion Formula	m/z	err [ppm]	mSigma	# mSigma	Score	rdb	e⁻ Conf	N-Rule
372.0464	1	C19H13Cl2FN3	372.0465	0.2	24.8	1	100.00	13.5	even	ok

This material is based upon work supported by the National Science Foundation under CHE-0741793

6 4a

Sample Name:	**4a**	*Injection Volume:*	**10.0**
Vial Number:	**RD1**	*Channel:*	**UV_VIS_1**
Sample Type:	**unknown**	*Wavelength:*	**254**
Control Program:	**Banerjee_grad**	*Bandwidth:*	**n.a.**
Quantif. Method:	**Banerjee**	*Dilution Factor:*	**1.0000**
Recording Time:	**7/1/2023 13:57**	*Sample Weight:*	**1.0000**
Run Time (min):	**40.00**	*Sample Amount:*	**1.0000**

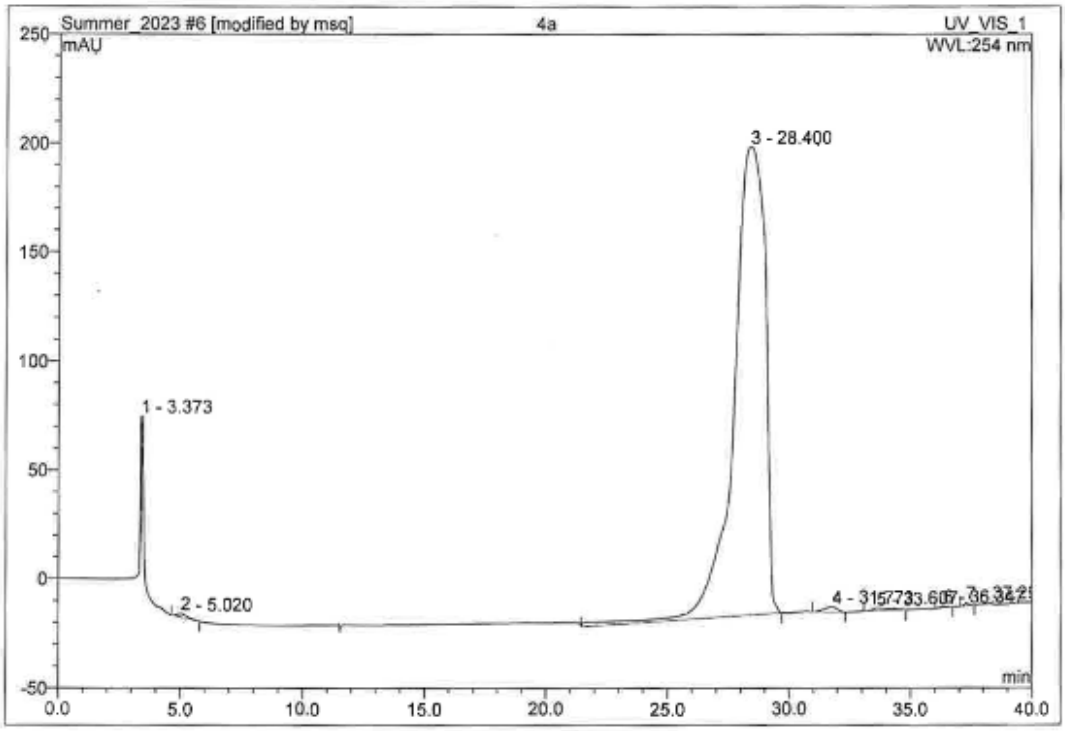

No.	Ret.Time min	Peak Name	Height mAU	Area mAU*min	Rel.Area %	Amount	Type
1	3.37	n.a.	54.825	2.573	0.78	n.a.	BMB
2	5.02	n.a.	1.675	0.807	0.24	n.a.	BMB
3	28.40	n.a.	215.152	323.238	98.04	n.a.	BMB
4	31.77	n.a.	2.359	1.493	0.45	n.a.	BMB
5	33.61	n.a.	1.311	1.095	0.33	n.a.	BMB
6	36.35	n.a.	0.547	0.187	0.06	n.a.	BMB
7	37.29	n.a.	1.430	0.296	0.09	n.a.	BMB
Total:			277.300	329.688	100.00	0.000	

30 4h

Sample Name:	**4h**	*Injection Volume:*	**10.0**
Vial Number:	**RD3**	*Channel:*	**UV_VIS_1**
Sample Type:	**unknown**	*Wavelength:*	**254**
Control Program:	**Banerjee_grad**	*Bandwidth:*	**n.a.**
Quantif. Method:	**Banerjee**	*Dilution Factor:*	**1.0000**
Recording Time:	**7/3/2023 16:41**	*Sample Weight:*	**1.0000**
Run Time (min):	**60.00**	*Sample Amount:*	**1.0000**

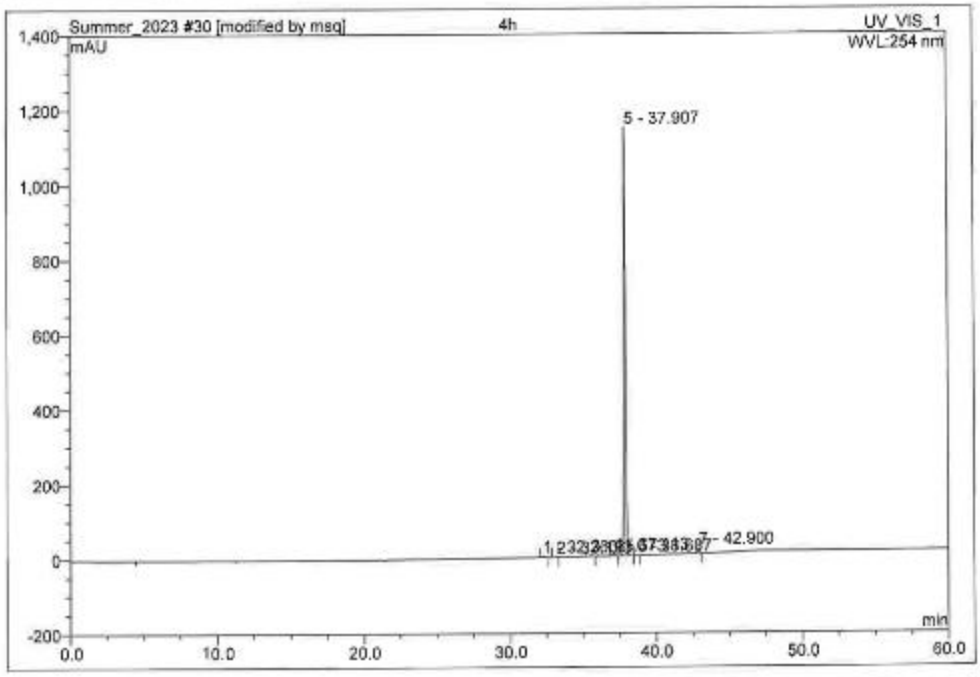

No.	Ret.Time min	Peak Name	Height mAU	Area mAU*min	Rel.Area %	Amount	Type
1	32.26	n.a.	2.757	0.789	0.51	n.a.	BMB
2	33.19	n.a.	0.564	0.107	0.07	n.a.	BMB
3	35.57	n.a.	3.717	0.664	0.43	n.a.	BMB
4	37.11	n.a.	6.510	0.915	0.59	n.a.	BMB
5	37.91	n.a.	1145.289	151.831	97.20	n.a.	BMb
6	38.69	n.a.	1.404	0.212	0.14	n.a.	bMB
7	42.90	n.a.	14.512	1.691	1.08	n.a.	BMB
Total:			1174.752	156.208	100.00	0.000	

default/Integration

25 4i

Sample Name:	**4i**	*Injection Volume:*	**10.0**
Vial Number:	**RD1**	*Channel:*	**UV_VIS_1**
Sample Type:	**unknown**	*Wavelength:*	**254**
Control Program:	**Banerjee_grad**	*Bandwidth:*	**n.a.**
Quantif. Method:	**Banerjee**	*Dilution Factor:*	**1.0000**
Recording Time:	**7/3/2023 9:34**	*Sample Weight:*	**1.0000**
Run Time (min):	**60.00**	*Sample Amount:*	**1.0000**

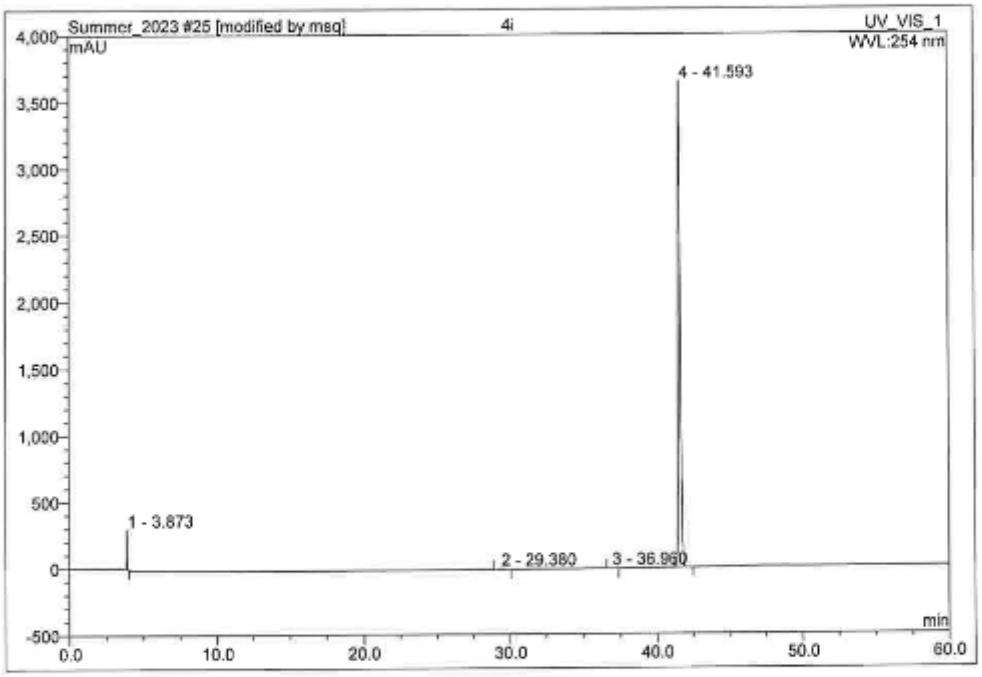

No.	Ret.Time min	Peak Name	Height mAU	Area mAU*min	Rel.Area %	Amount	Type
1	3.87	n.a.	298.734	7.583	1.11	n.a.	BMB
2	29.38	n.a.	2.162	0.889	0.13	n.a.	BMB
3	36.96	n.a.	0.497	0.167	0.02	n.a.	BMB
4	41.59	n.a.	3651.398	674.934	98.74	n.a.	BMB
Total:			3952.791	683.574	100.00	0.000	

26 4j

Sample Name:	**4j**	*Injection Volume:*	**10.0**
Vial Number:	**RD2**	*Channel:*	**UV_VIS_1**
Sample Type:	**unknown**	*Wavelength:*	**254**
Control Program:	**Banerjee_grad**	*Bandwidth:*	**n.a.**
Quantif. Method:	**Banerjee**	*Dilution Factor:*	**1.0000**
Recording Time:	**7/3/2023 10:39**	*Sample Weight:*	**1.0000**
Run Time (min):	**60.00**	*Sample Amount:*	**1.0000**

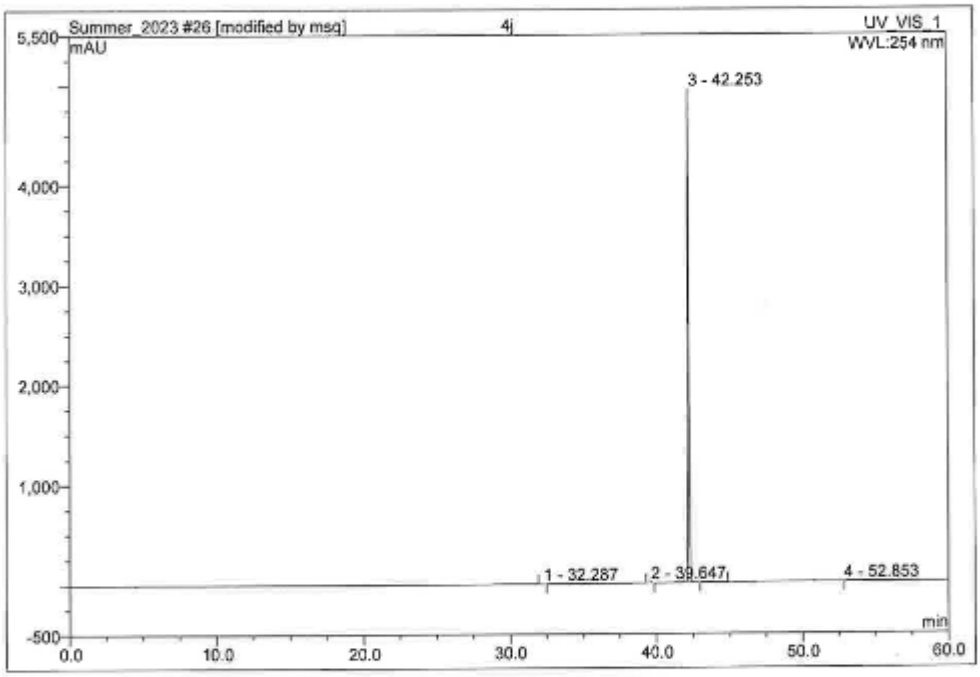

No.	Ret.Time min	Peak Name	Height mAU	Area mAU*min	Rel.Area %	Amount	Type
1	32.29	n.a.	0.905	0.158	0.03	n.a.	BMB
2	39.65	n.a.	5.718	0.748	0.14	n.a.	BMB
3	42.25	n.a.	4941.737	540.457	97.86	n.a.	BMB
4	52.85	n.a.	0.013	10.921	1.98	n.a.	BMB
Total:			4948.372	552.285	100.00	0.000	

27 4k

Sample Name:	**4k**	*Injection Volume:*	**10.0**
Vial Number:	**RD3**	*Channel:*	**UV_VIS_1**
Sample Type:	**unknown**	*Wavelength:*	**254**
Control Program:	**Banerjee_grad**	*Bandwidth:*	**n.a.**
Quantif. Method:	**Banerjee**	*Dilution Factor:*	**1.0000**
Recording Time:	**7/3/2023 11:45**	*Sample Weight:*	**1.0000**
Run Time (min):	**60.00**	*Sample Amount:*	**1.0000**

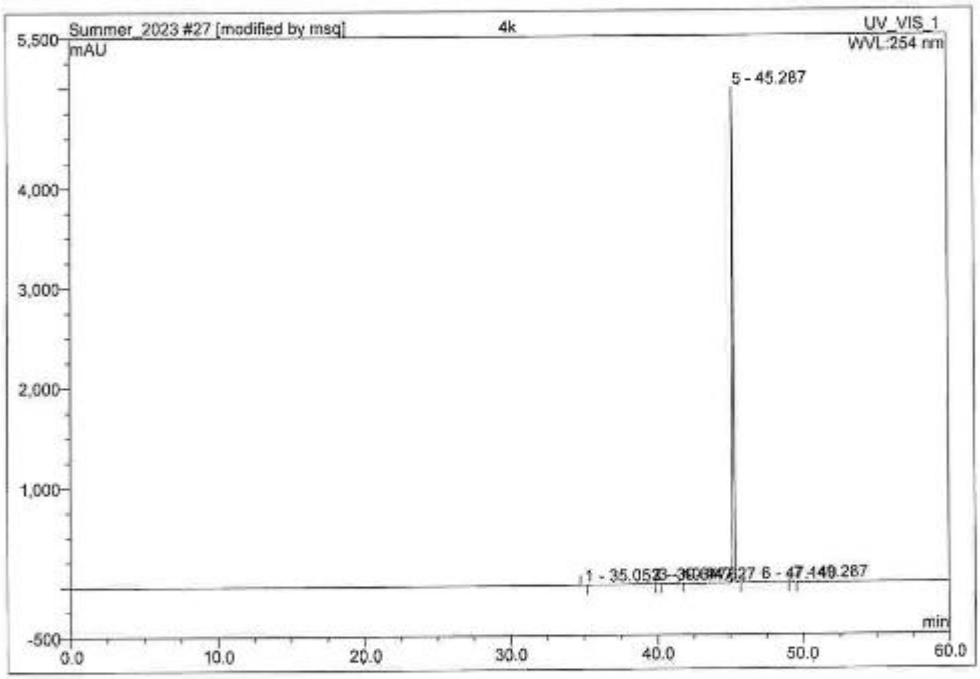

No.	Ret.Time min	Peak Name	Height mAU	Area mAU*min	Rel.Area %	Amount	Type
1	35.05	n.a.	1.524	0.237	0.04	n.a.	BMB
2	39.65	n.a.	3.484	0.451	0.08	n.a.	BMB
3	40.05	n.a.	5.829	0.696	0.12	n.a.	BMB
4	41.63	n.a.	1.462	0.164	0.03	n.a.	BMB
5	45.29	n.a.	4963.549	553.863	99.27	n.a.	BMB
6	47.14	n.a.	1.040	1.642	0.29	n.a.	BMb
7	49.29	n.a.	5.650	0.876	0.16	n.a.	bMB
Total:			4982.537	557.929	100.00	0.000	

Chapter II - ^{1}HNMR and ^{13}CNMR

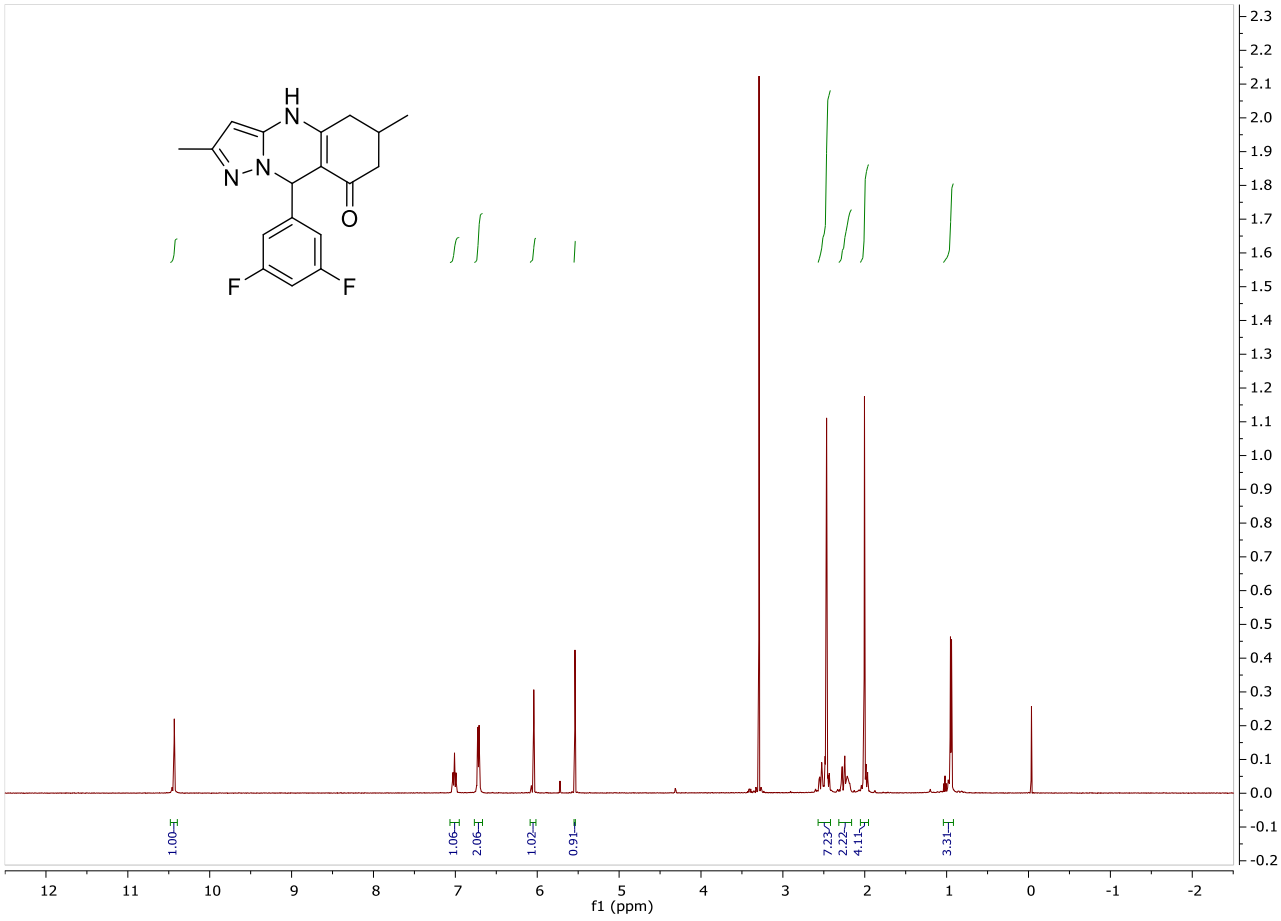

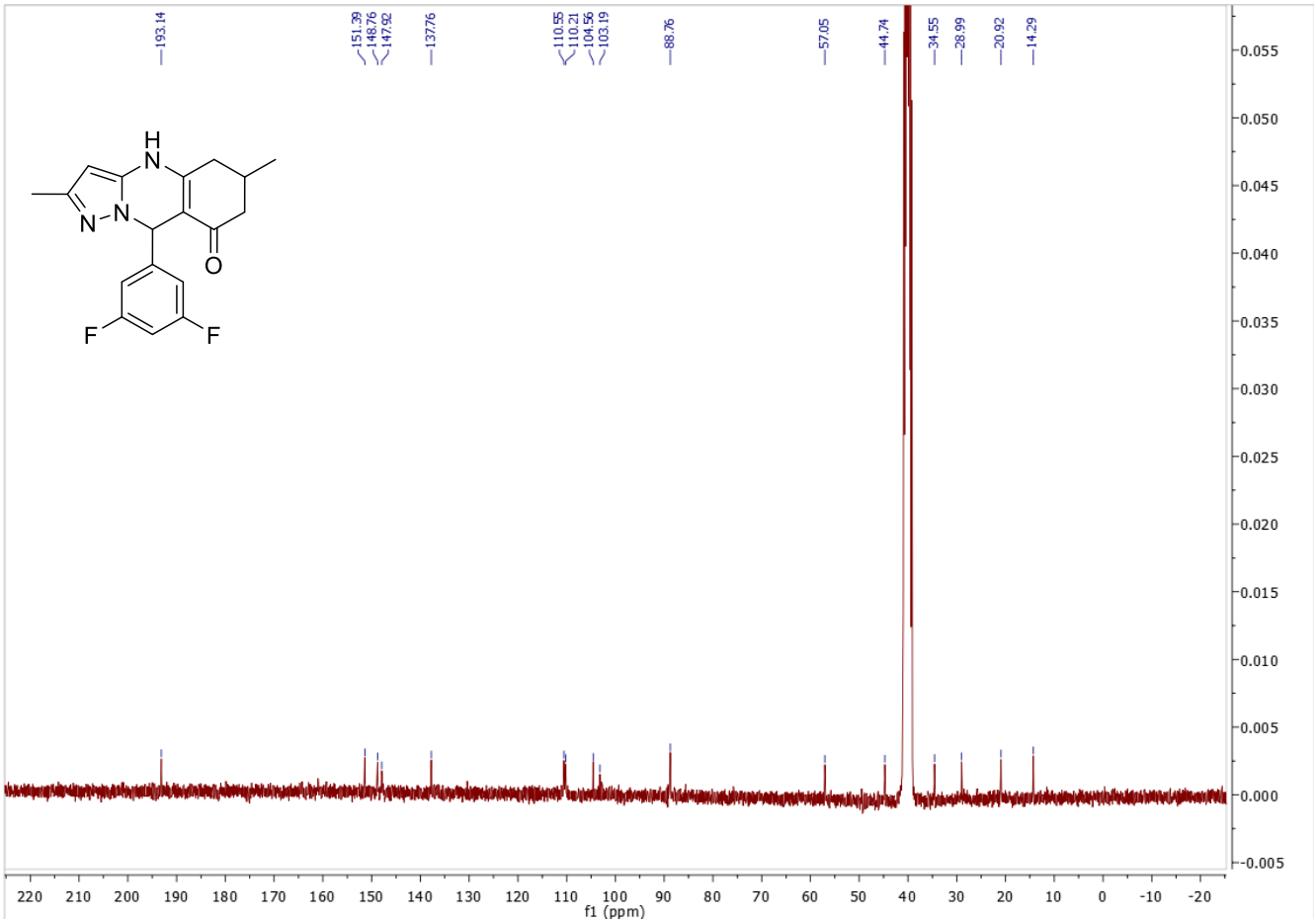
193.14
151.39
148.76
147.92
137.76
110.55
110.21
104.56
103.19
88.76
57.05
44.74
34.55
28.99
20.92
14.29
H
N
N
N
O
F
F
0.055
0.050
0.045
0.040
0.035
0.030
0.025
0.020
0.015
0.010
0.005
0.000
-0.005
220 210 200 190 180 170 160 150 140 130 120 110 100 90 80 70 60 50 40 30 20 10 0 -10 -20
f1 (ppm)

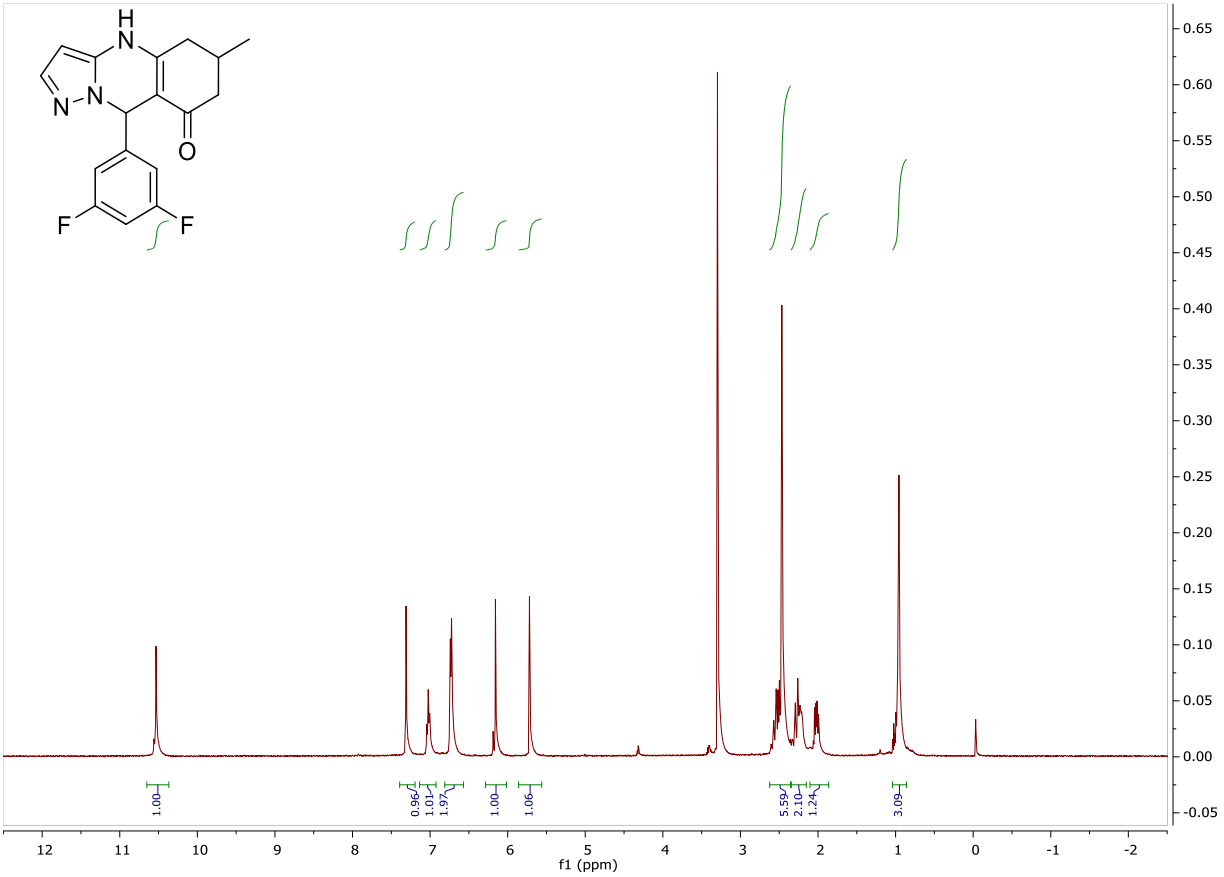
H
N
N
N
O
F
F
1.00
0.96
1.01
1.97
1.00
1.06
5.59
2.10
1.24
3.09
f1 (ppm)

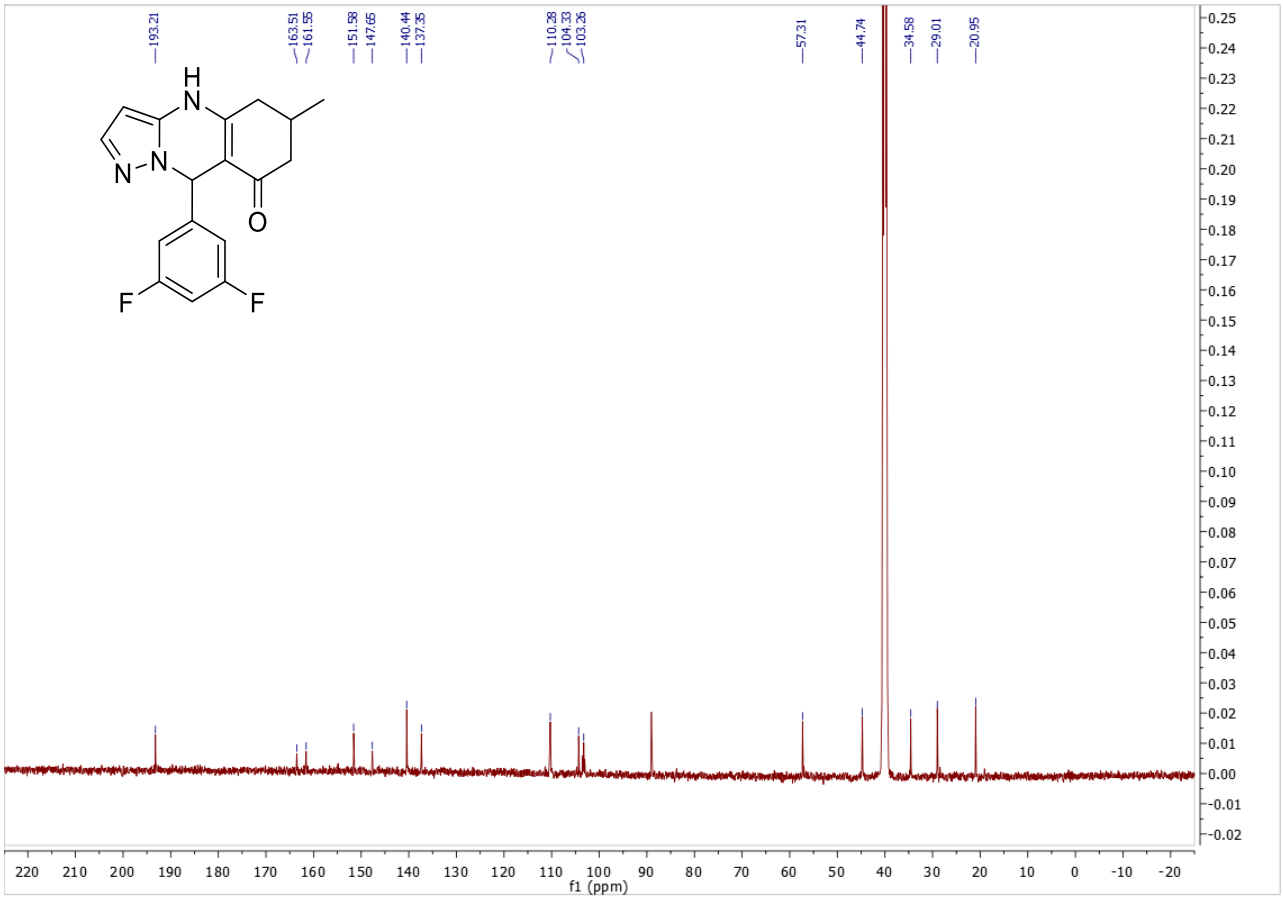
193.21
163.51
161.55
151.58
147.65
140.44
137.35
110.28
104.33
103.26
57.31
44.74
34.58
29.01
20.95
H
N
N
N
O
F
F
f1 (ppm)

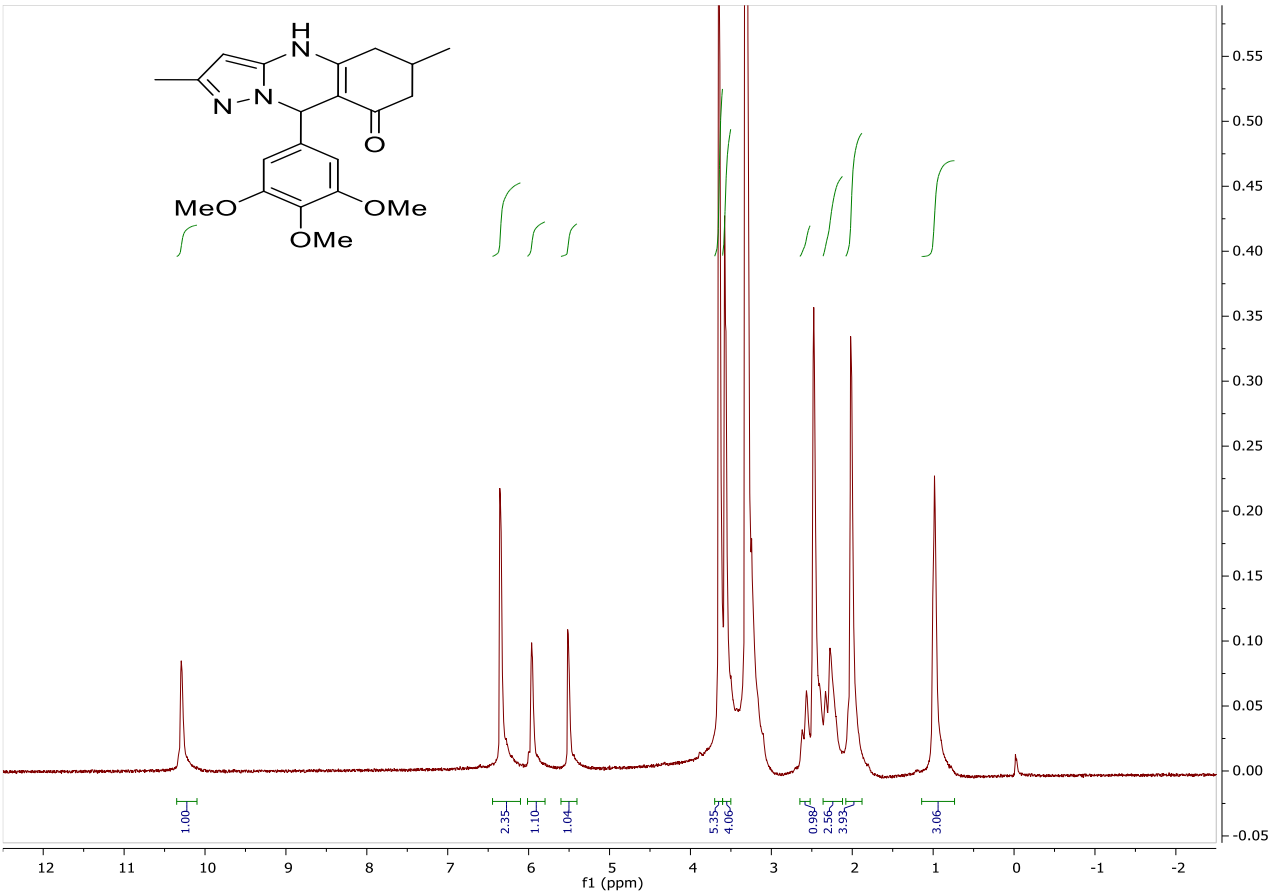
H
N
N
N
O
MeO
OMe
OMe
1.00
2.35
1.10
1.04
5.35
4.06
0.98
2.56
3.93
3.06
f1 (ppm)

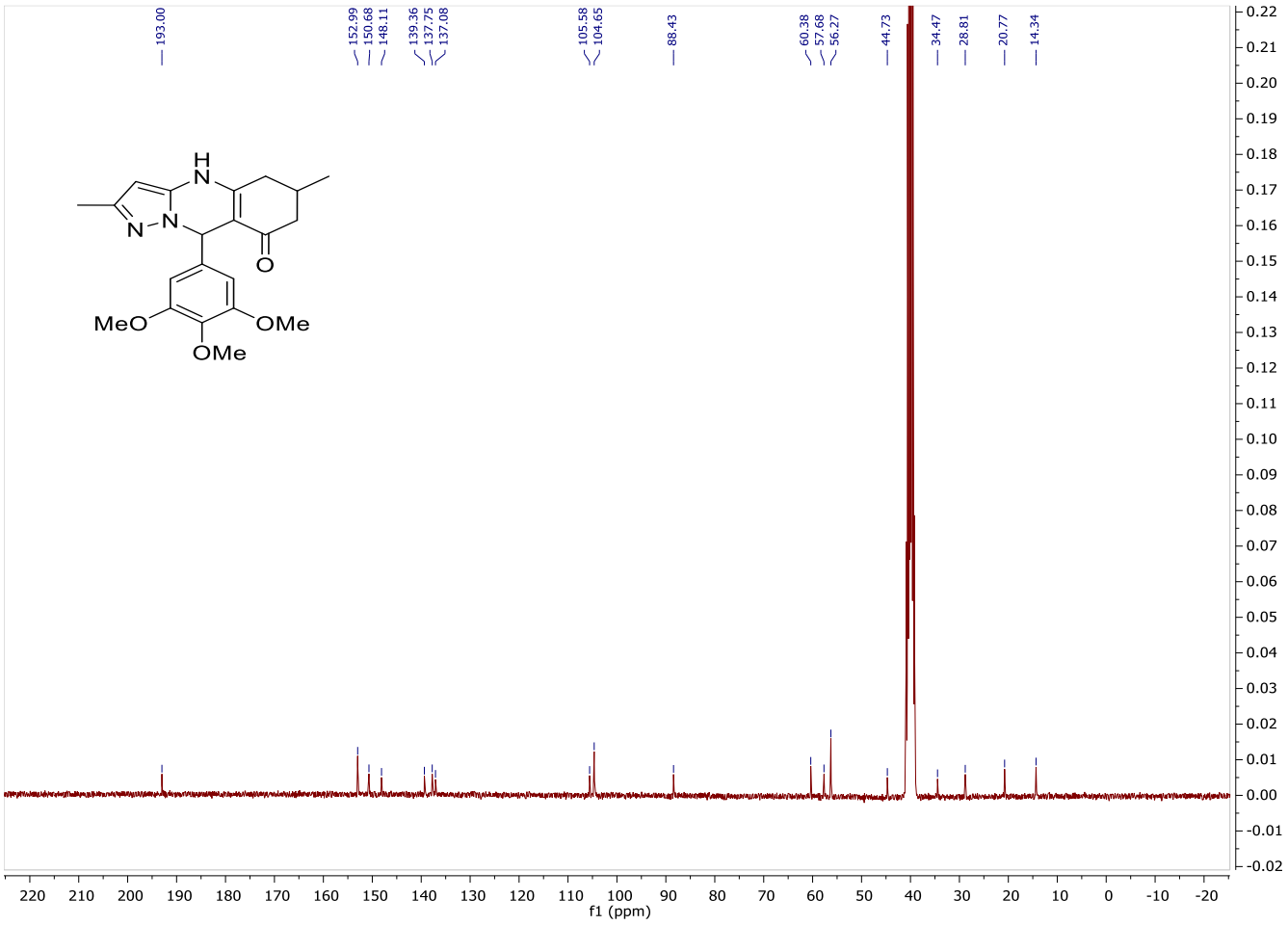
193.00
152.99
150.68
148.11
139.36
137.75
137.08
105.58
104.65
88.43
60.38
57.68
56.27
44.73
34.47
28.81
20.77
14.34
H
N
N
N
O
MeO
OMe
OMe
f1 (ppm)

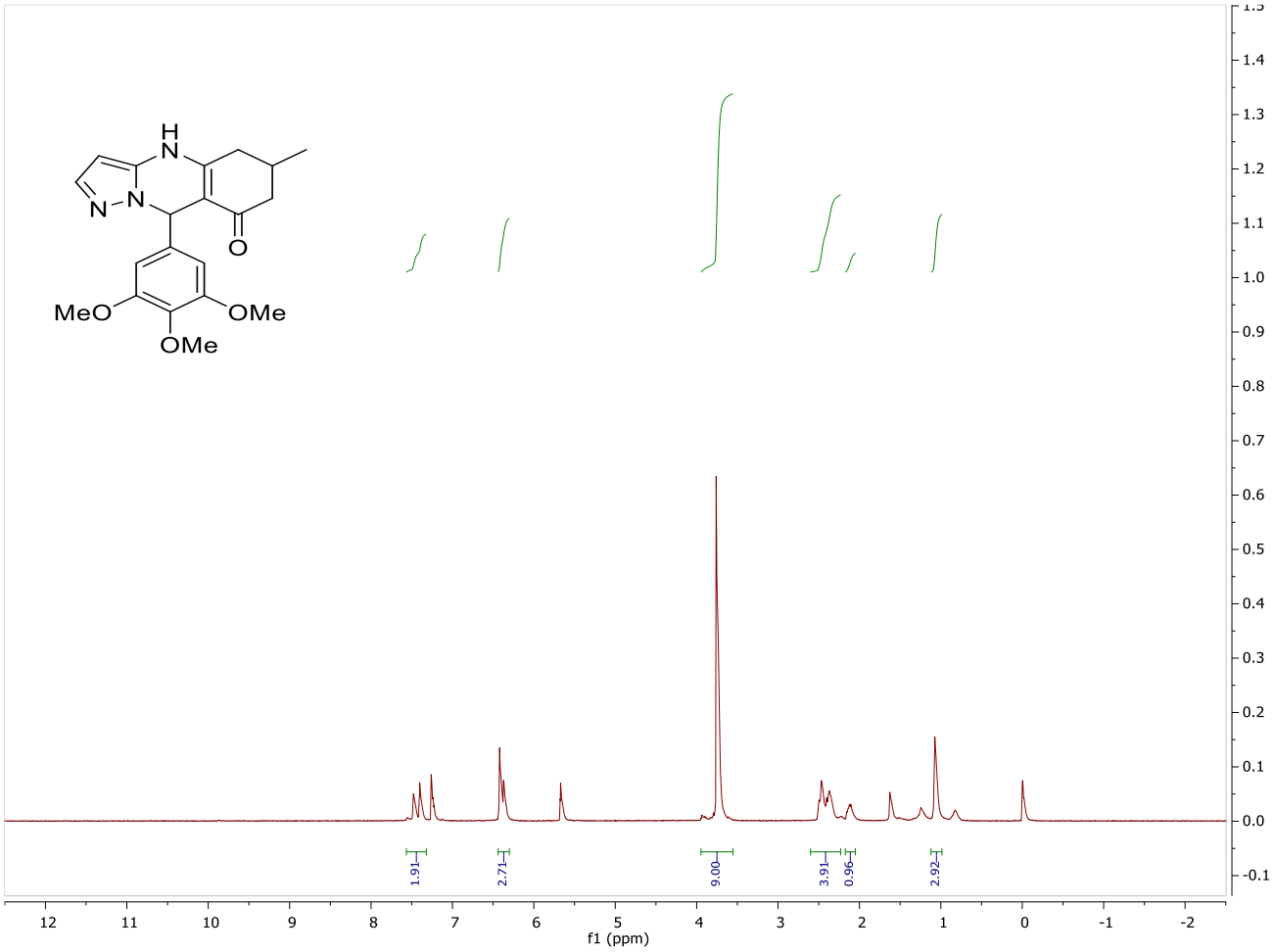
H
N
N
N
O
MeO
OMe
OMe
1.91
2.71
9.00
3.91
0.96
2.92
f1 (ppm)

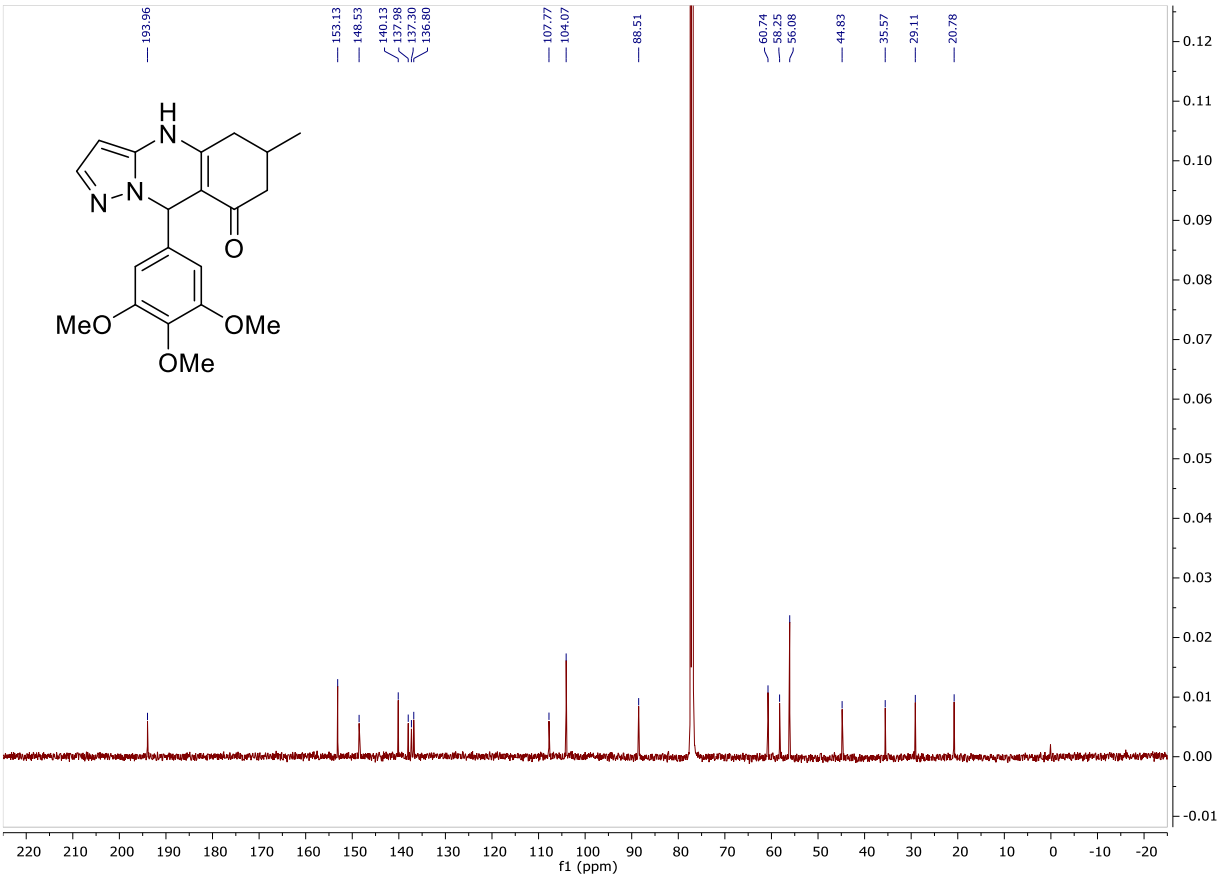
193.96
153.13
148.53
140.13
137.98
137.30
136.80
107.77
104.07
88.51
60.74
58.25
56.08
44.83
35.57
29.11
20.78
H
N
N
N
O
MeO
OMe
OMe
f1 (ppm)

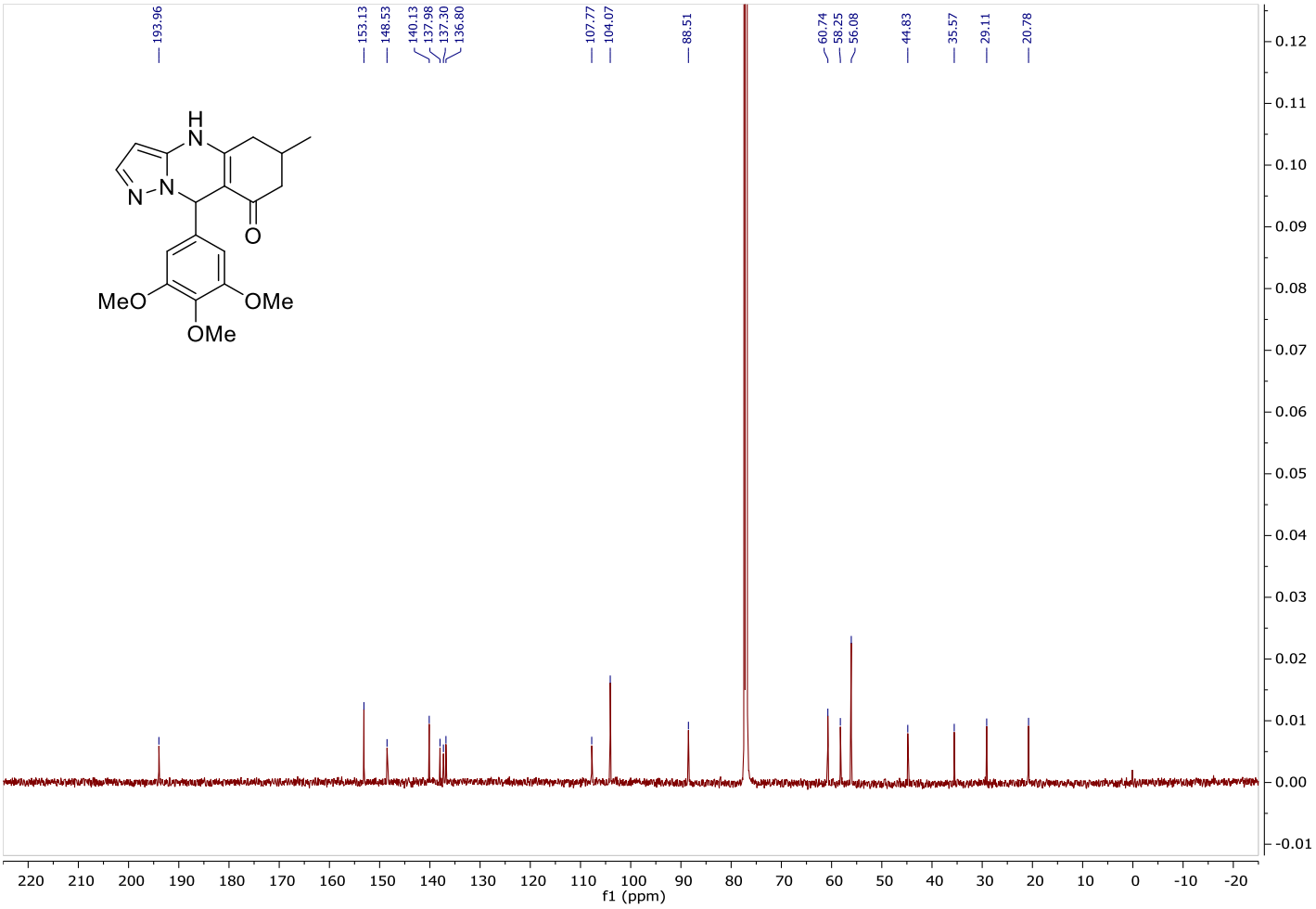
193.96
153.13
148.53
140.13
137.98
137.30
136.80
107.77
104.07
88.51
60.74
58.25
56.08
44.83
35.57
29.11
20.78
H
N
N
N
O
MeO
OMe
OMe
f1 (ppm)

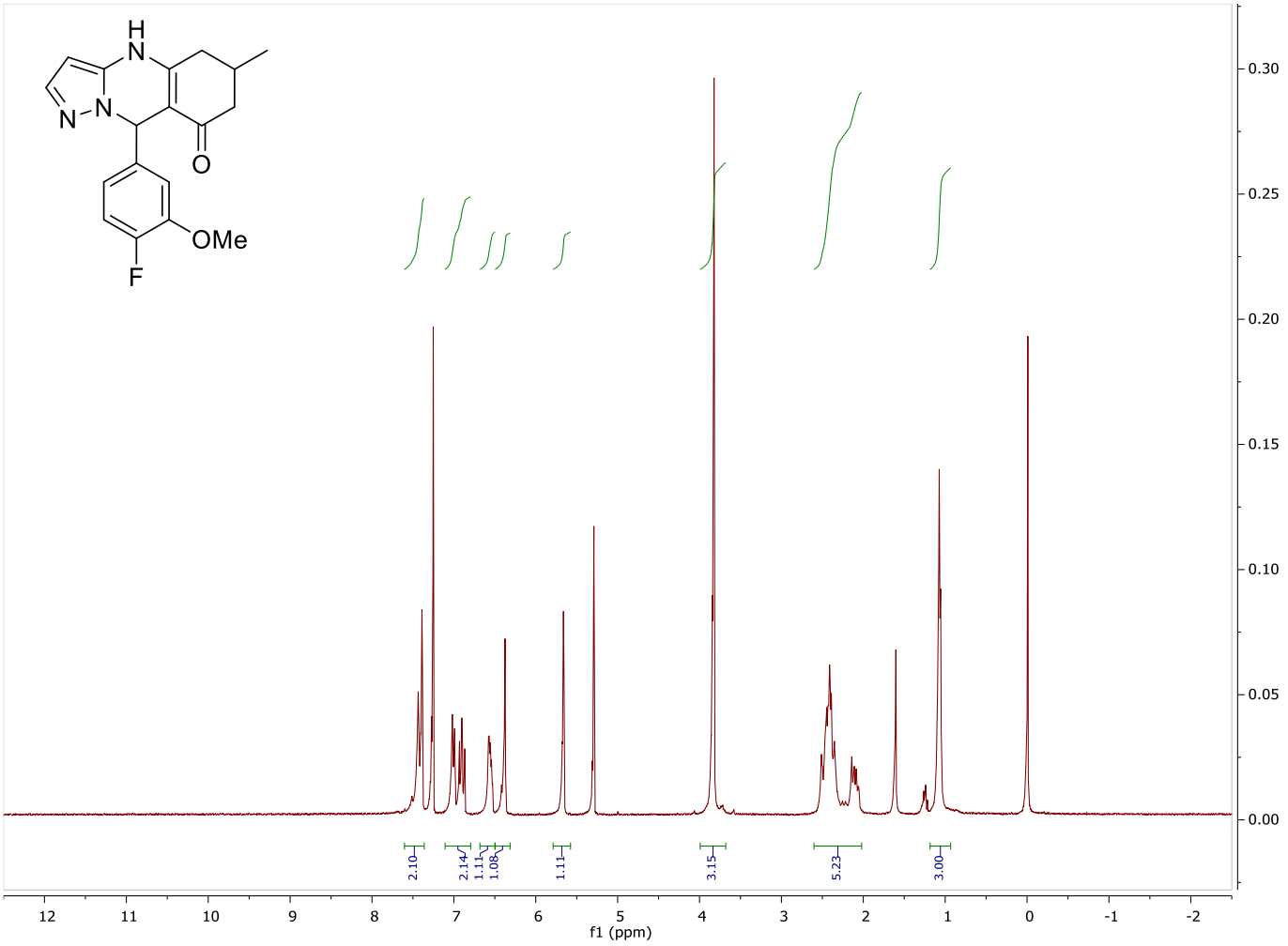
H
N
N
N
O
OMe
F
0.30
0.25
0.20
0.15
0.10
0.05
0.00
2.10
2.14
1.11
1.08
1.11
3.15
5.23
3.00
12
11
10
9
8
7
6
5
4
3
2
1
0
-1
-2
f1 (ppm)

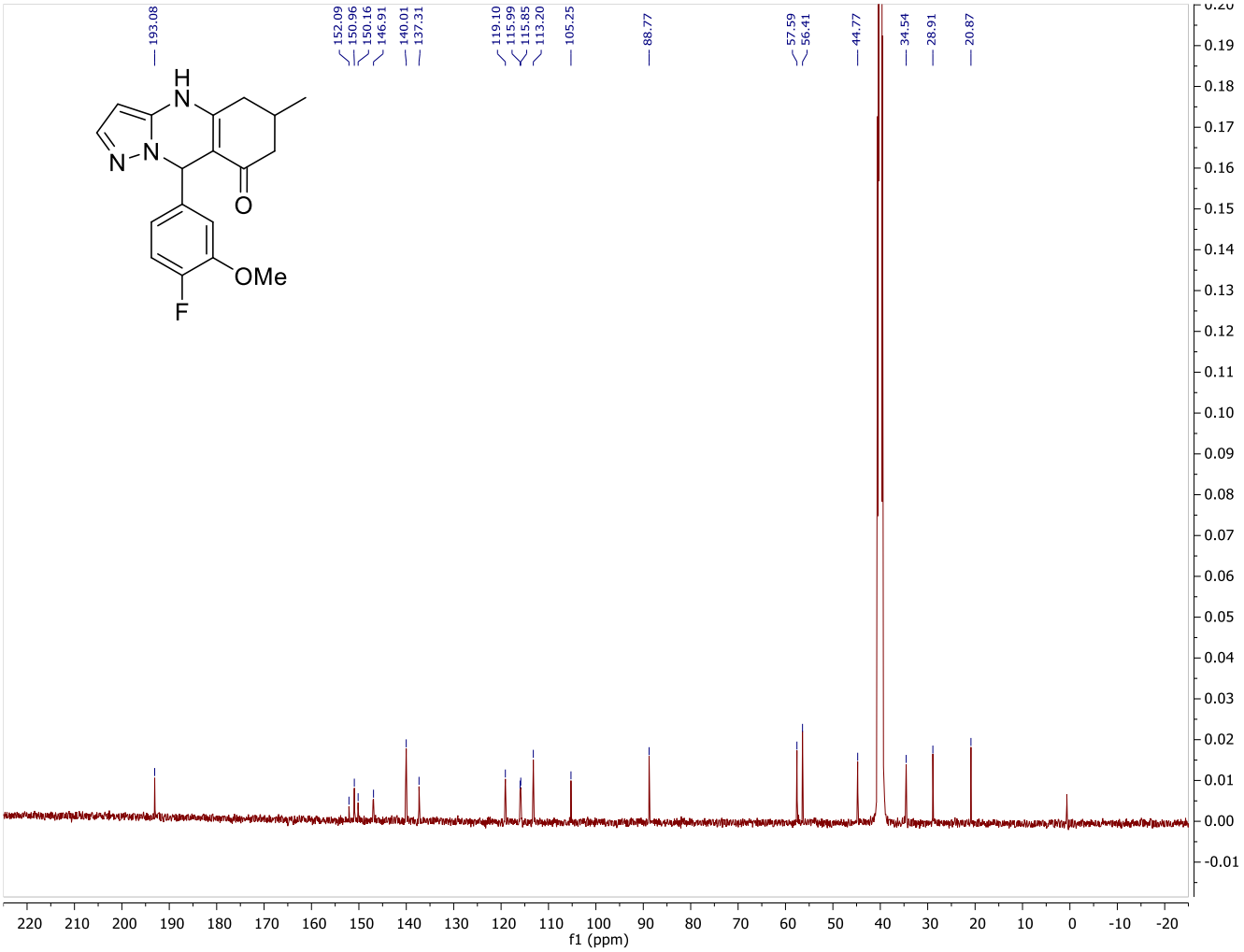
193.08
152.09
150.96
150.16
146.91
140.01
137.31
119.10
115.99
115.85
113.20
105.25
88.77
57.59
56.41
44.77
34.54
28.91
20.87
H
N
N
N
O
OMe
F
f1 (ppm)

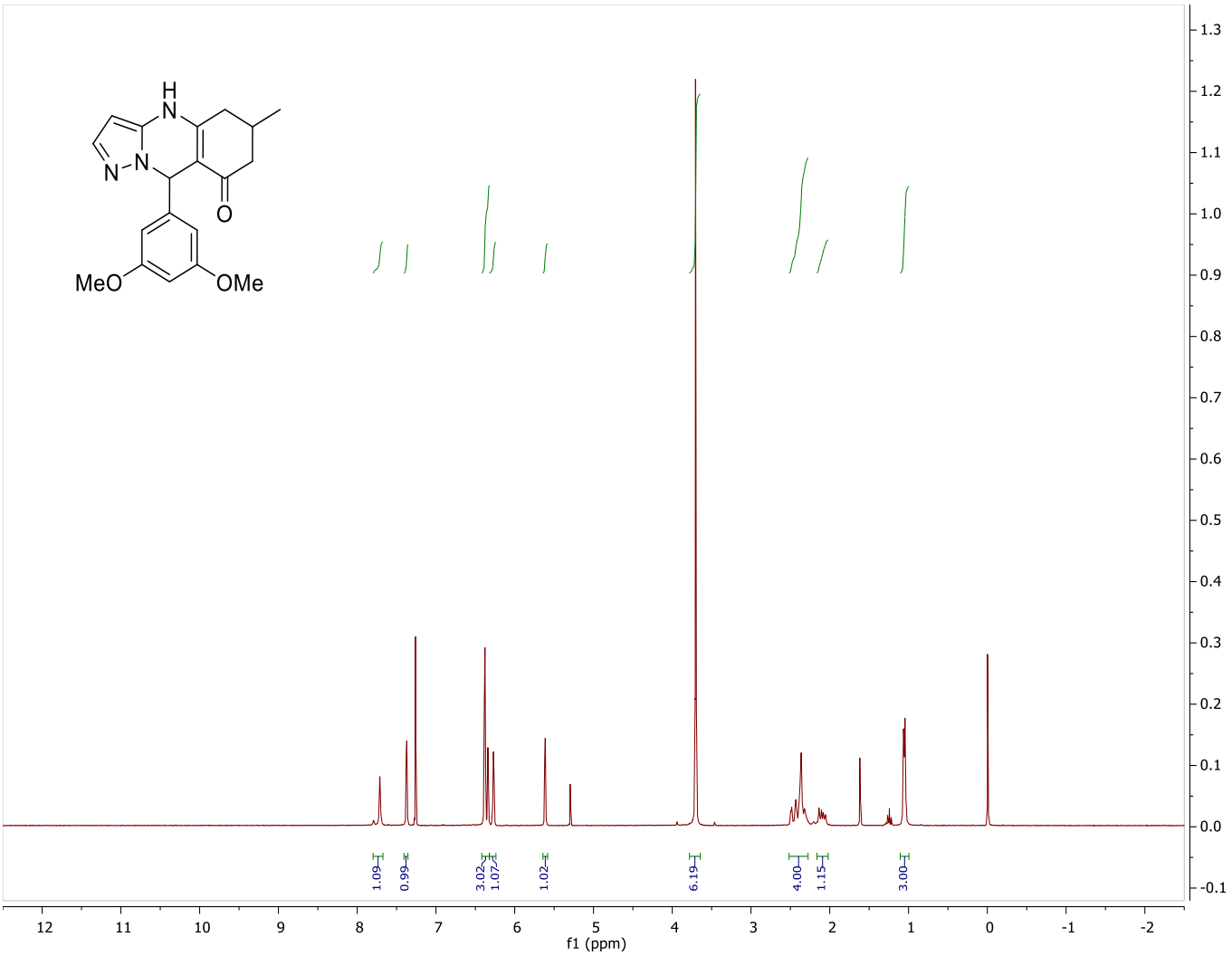
H
N
N
N
O
MeO
OMe
1.09
0.99
3.02
1.07
1.02
6.19
4.00
1.15
3.00
f1 (ppm)

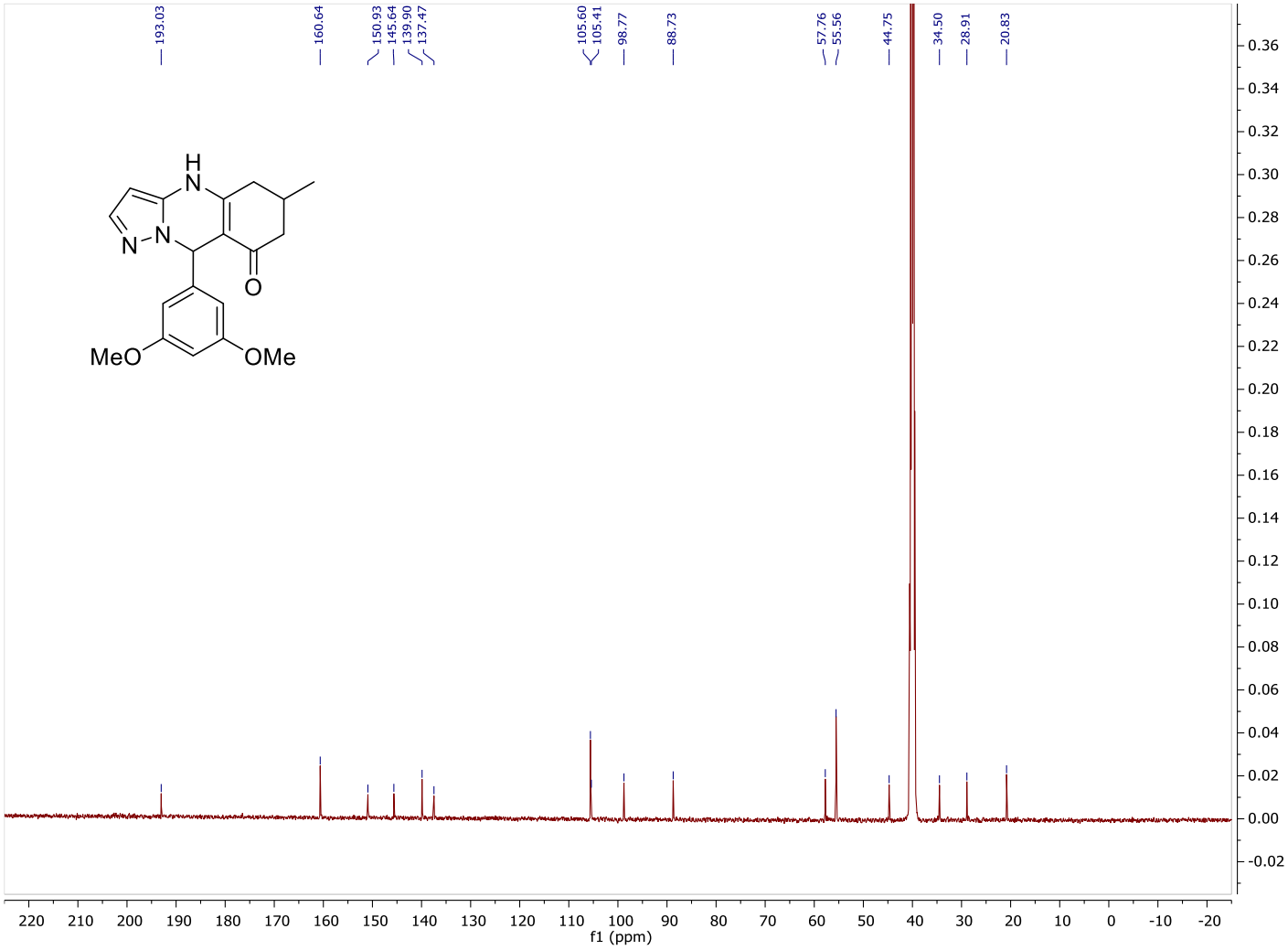
193.03
160.64
150.93
145.64
139.90
137.47
105.60
105.41
98.77
88.73
57.76
55.56
44.75
34.50
28.91
20.83
H
N
N
N
O
MeO
OMe
f1 (ppm)

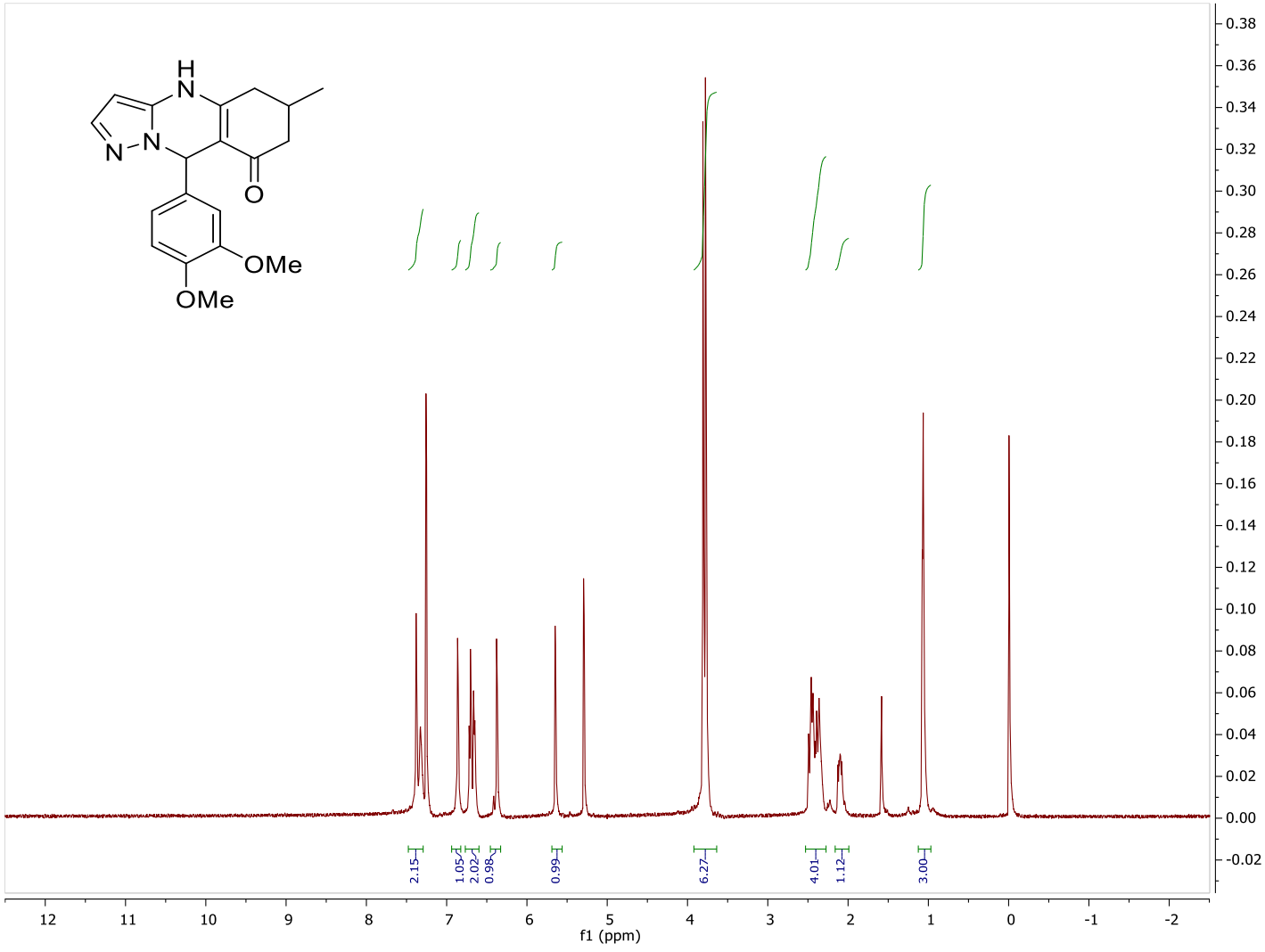
H
N
N
N
O
OMe
OMe
2.15
1.05
2.02
0.98
0.99
6.27
4.01
1.12
3.00
f1 (ppm)

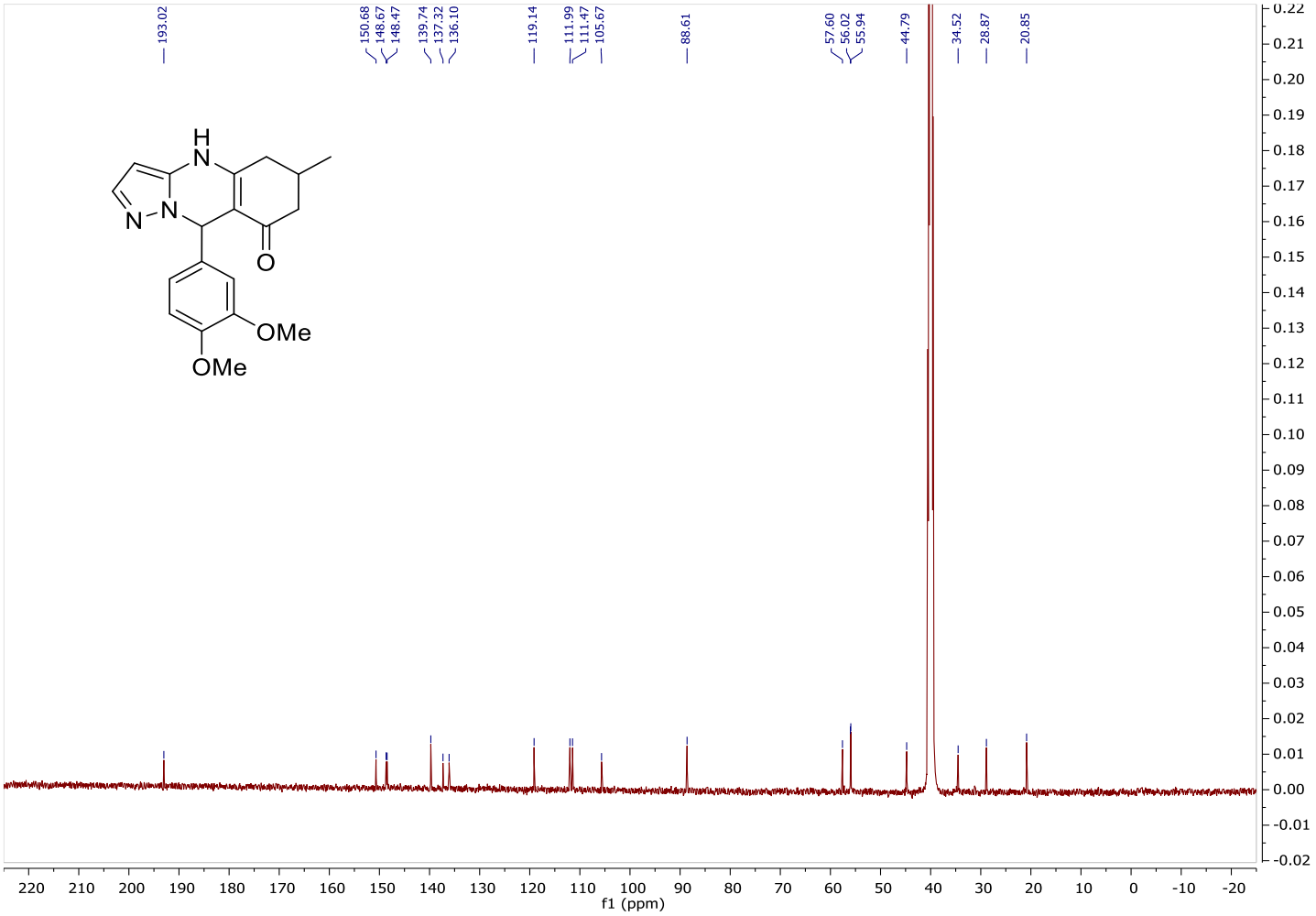
193.02
150.68
148.67
148.47
139.74
137.32
136.10
119.14
111.99
111.47
105.67
88.61
57.60
56.02
55.94
44.79
34.52
28.87
20.85
H
N
N
N
O
OMe
OMe
f1 (ppm)

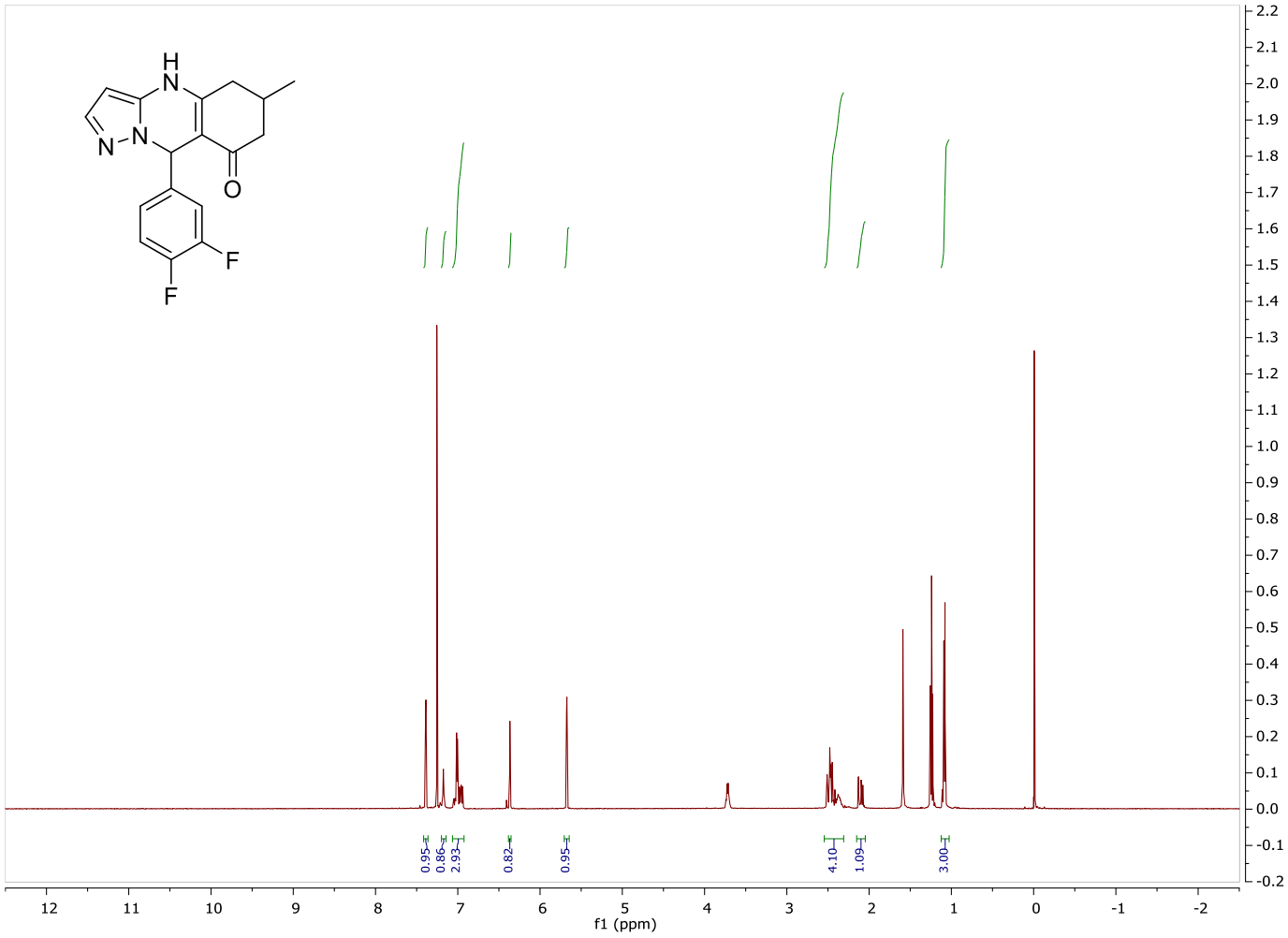
H
N
N
N
O
F
F
0.95
0.86
2.93
0.82
0.95
4.10
1.09
3.00
f1 (ppm)

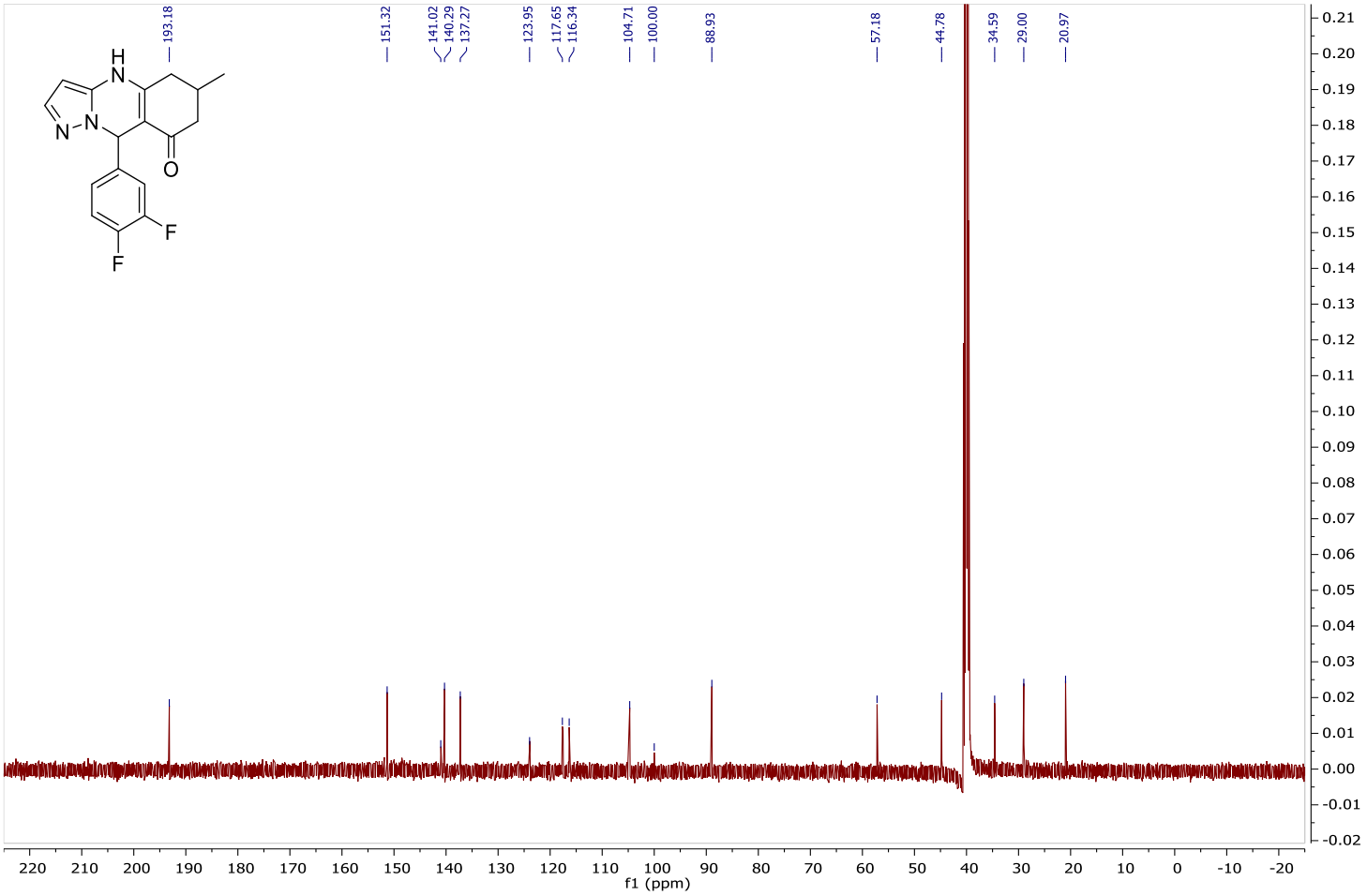
193.18
151.32
141.02
140.29
137.27
123.95
117.65
116.34
104.71
100.00
88.93
57.18
44.78
34.59
29.00
20.97
H
N
N
N
O
F
F
f1 (ppm)

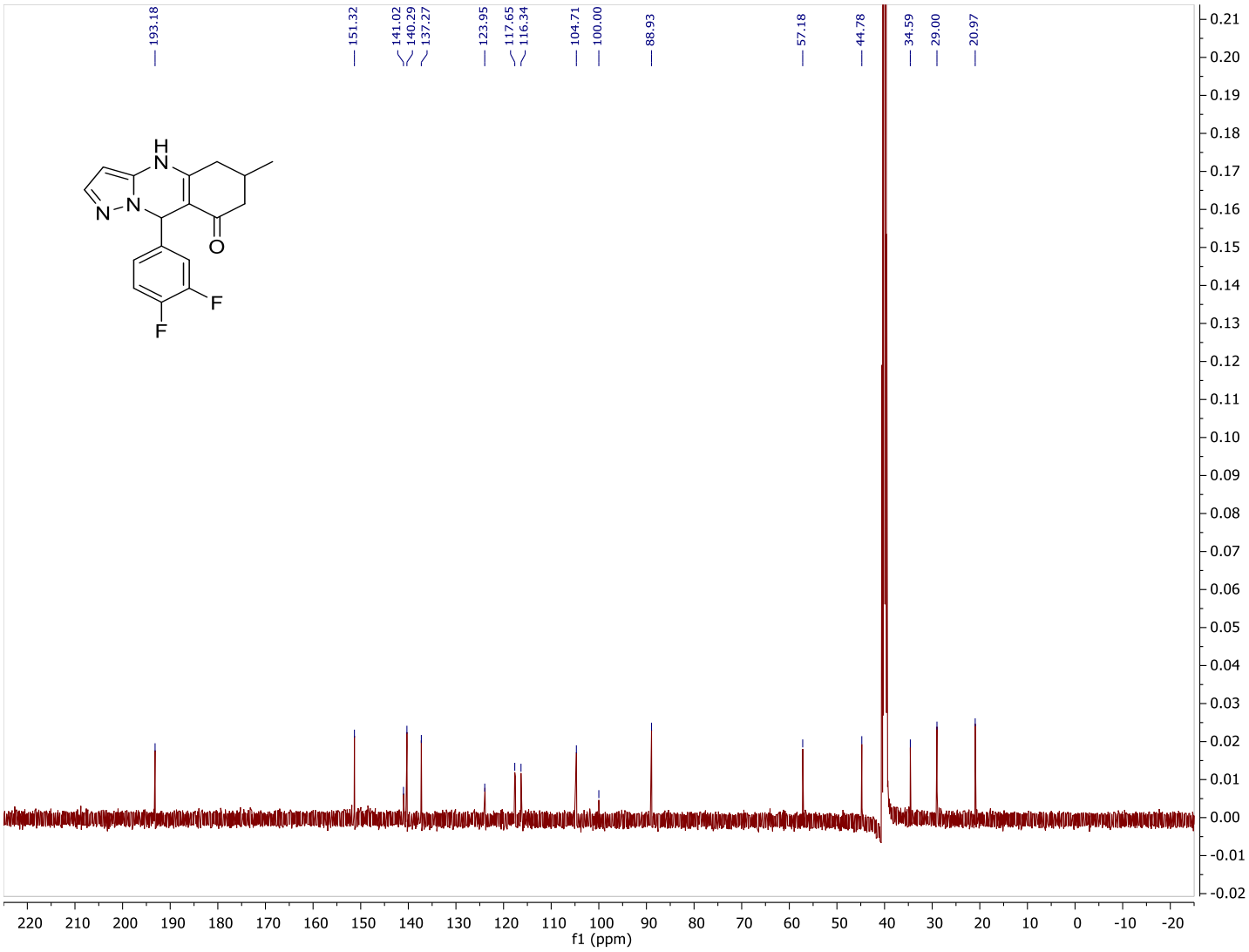
193.18
151.32
141.02
140.29
137.27
123.95
117.65
116.34
104.71
100.00
88.93
57.18
44.78
34.59
29.00
20.97
H
N
N
N
O
F
F
f1 (ppm)

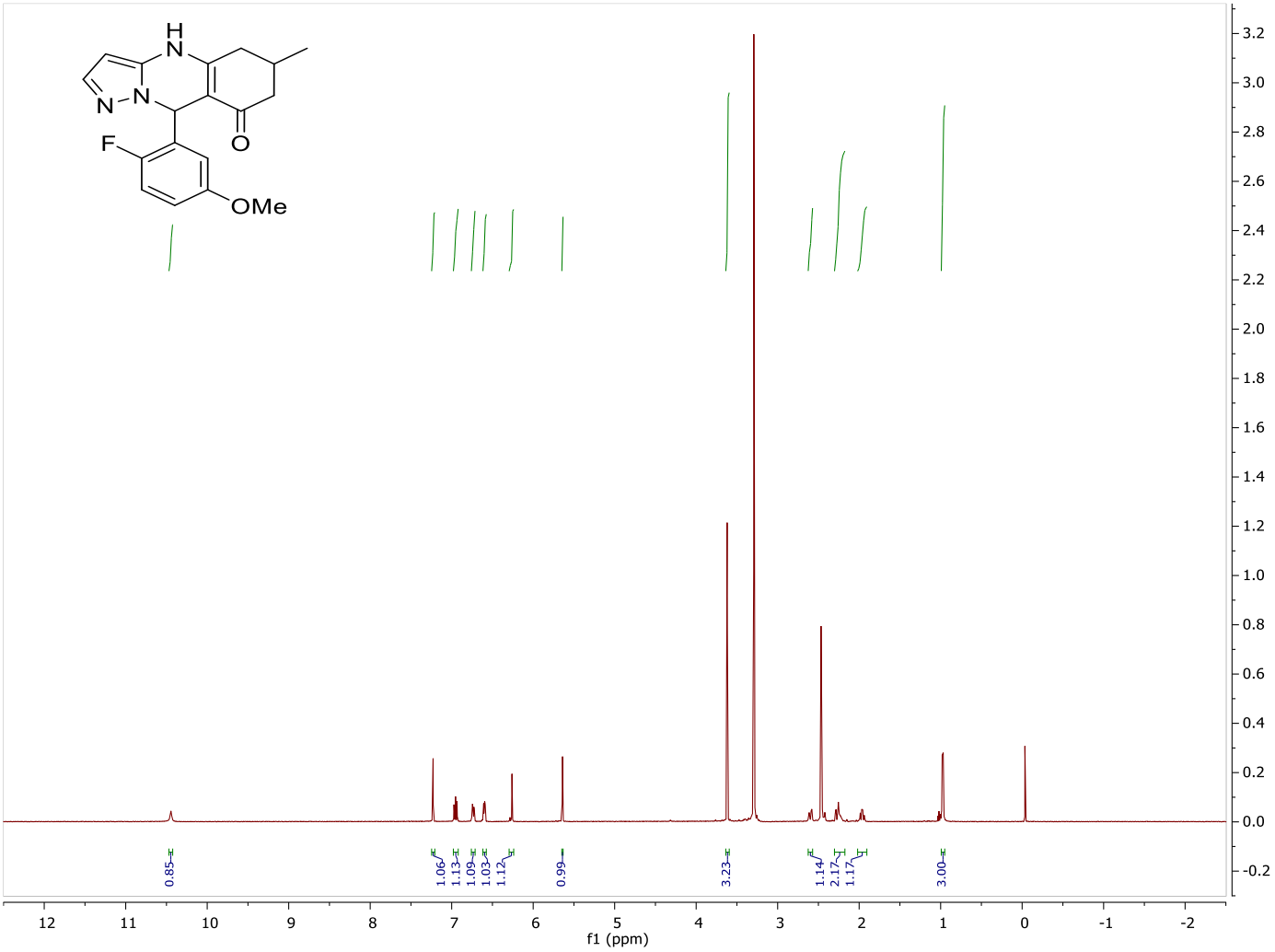
H
N
N
N
F
O
OMe
0.85
1.06
1.13
1.09
1.03
1.12
0.99
3.23
1.14
2.17
1.17
3.00
f1 (ppm)

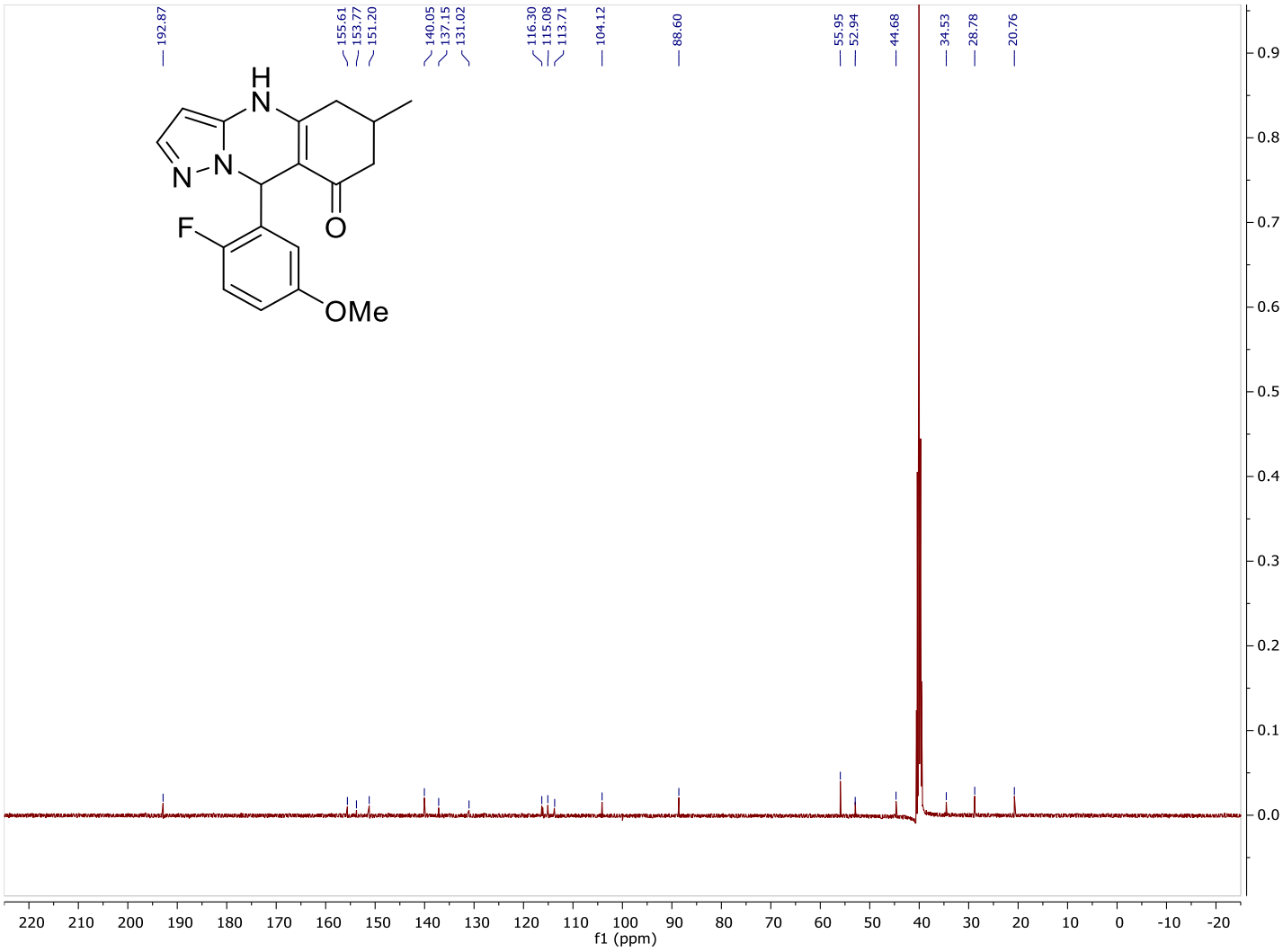
192.87
155.61
153.77
151.20
140.05
137.15
131.02
116.30
115.08
113.71
104.12
88.60
55.95
52.94
44.68
34.53
28.78
20.76
H
N
N
N
F
O
OMe
0.9
0.8
0.7
0.6
0.5
0.4
0.3
0.2
0.1
0.0
220 210 200 190 180 170 160 150 140 130 120 110 100 90 80 70 60 50 40 30 20 10 0 -10 -20
f1 (ppm)

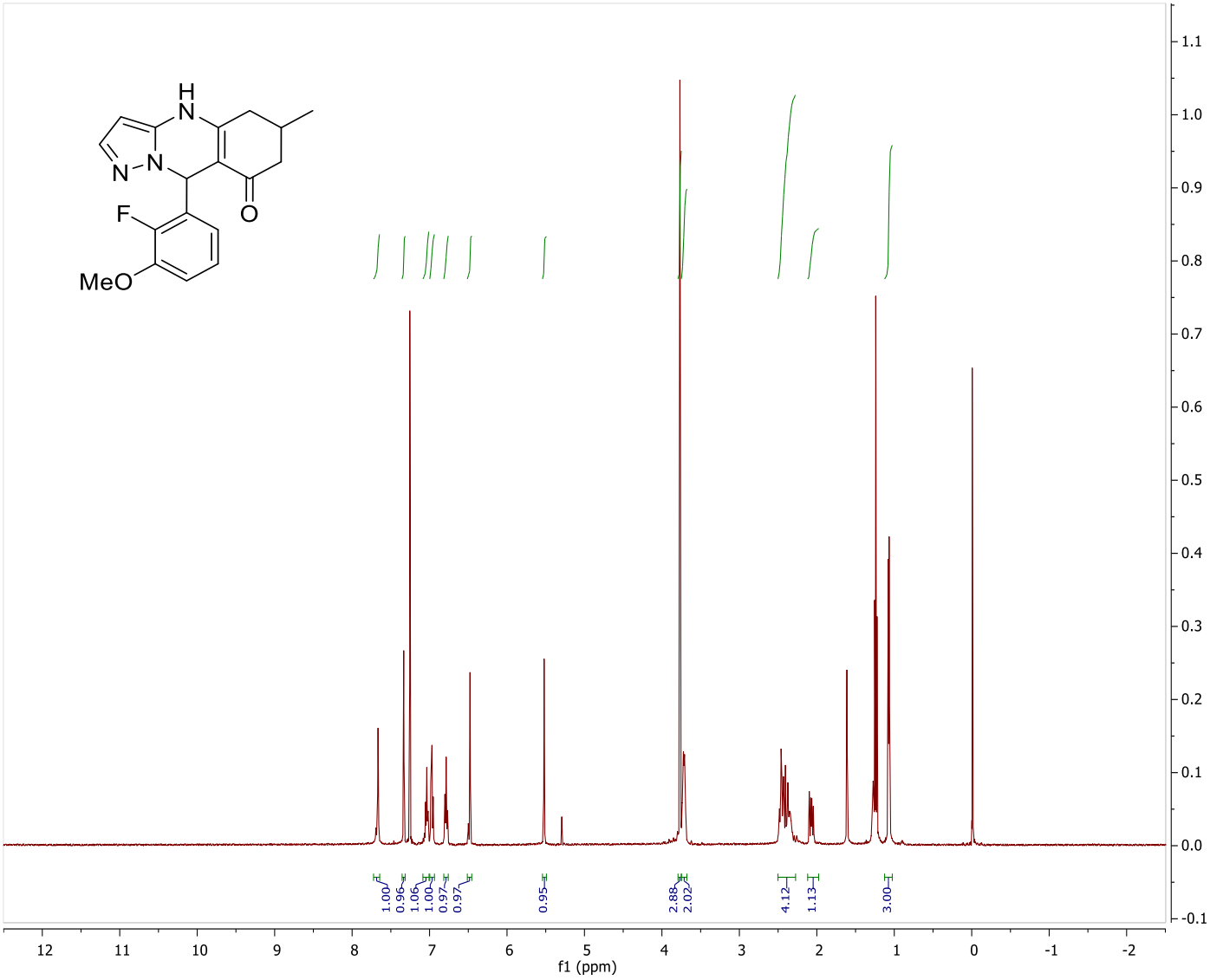
H
N
N
N
F
MeO
O
1.00
0.96
1.06
1.00
0.97
0.97
0.95
2.88
2.02
4.12
1.13
3.00
f1 (ppm)

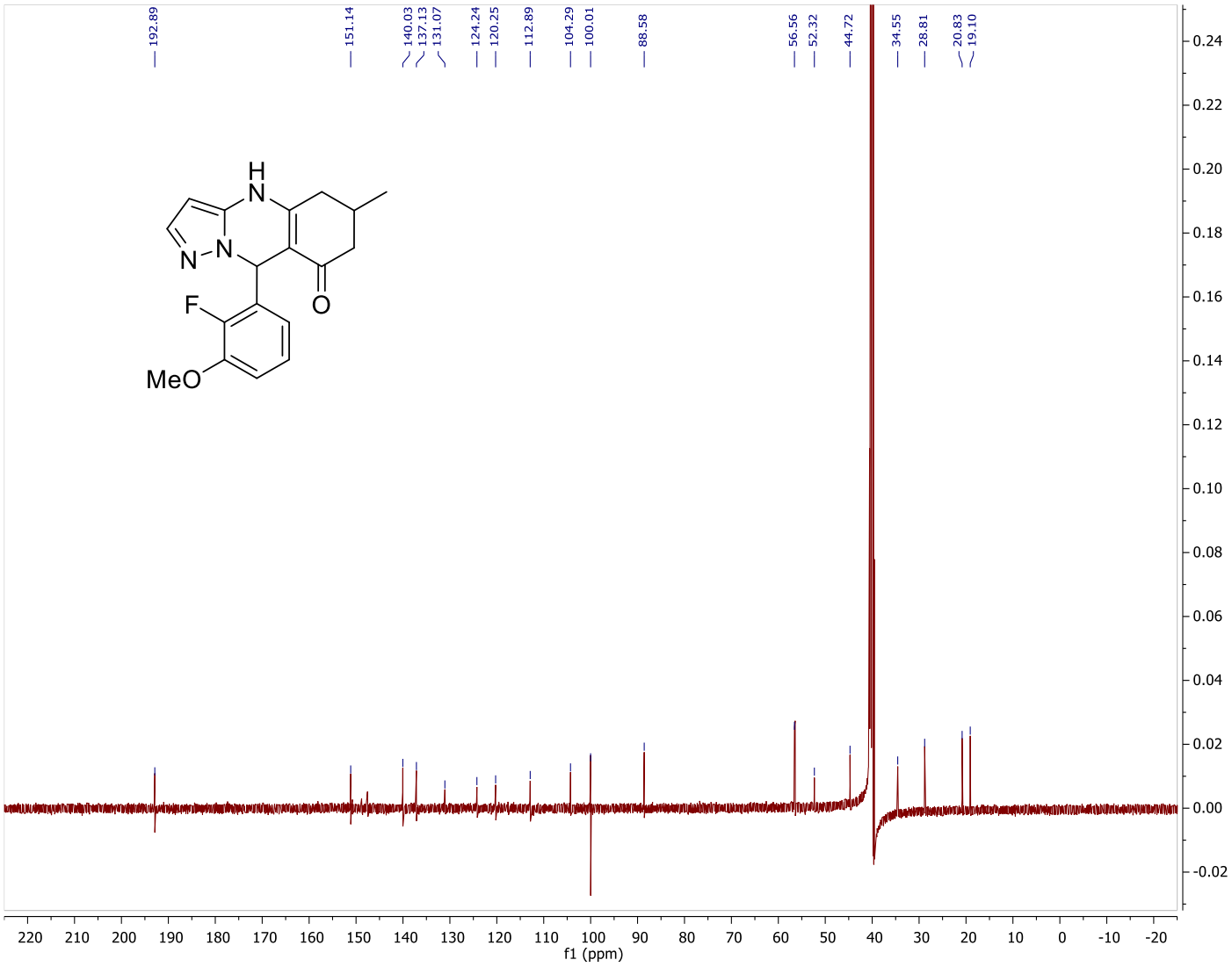
192.89
151.14
140.03
137.13
131.07
124.24
120.25
112.89
104.29
100.01
88.58
56.56
52.32
44.72
34.55
28.81
20.83
19.10
H
N
N
N
F
O
MeO
0.24
0.22
0.20
0.18
0.16
0.14
0.12
0.10
0.08
0.06
0.04
0.02
0.00
-0.02
220 210 200 190 180 170 160 150 140 130 120 110 100 90 80 70 60 50 40 30 20 10 0 -10 -20
f1 (ppm)

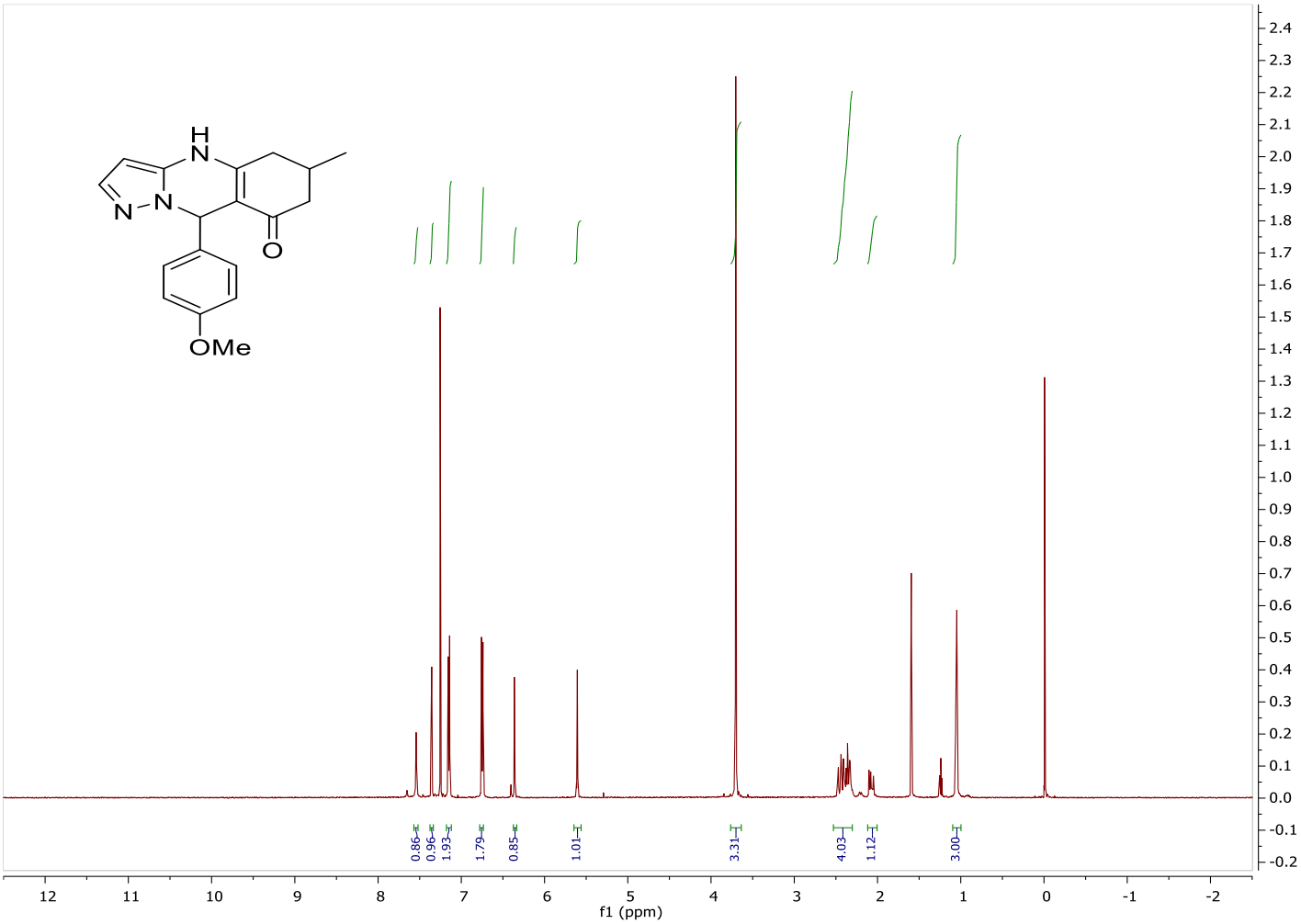
H
N
N
N
O
OMe
0.86
0.96
1.93
1.79
0.85
1.01
3.31
4.03
1.12
3.00
f1 (ppm)

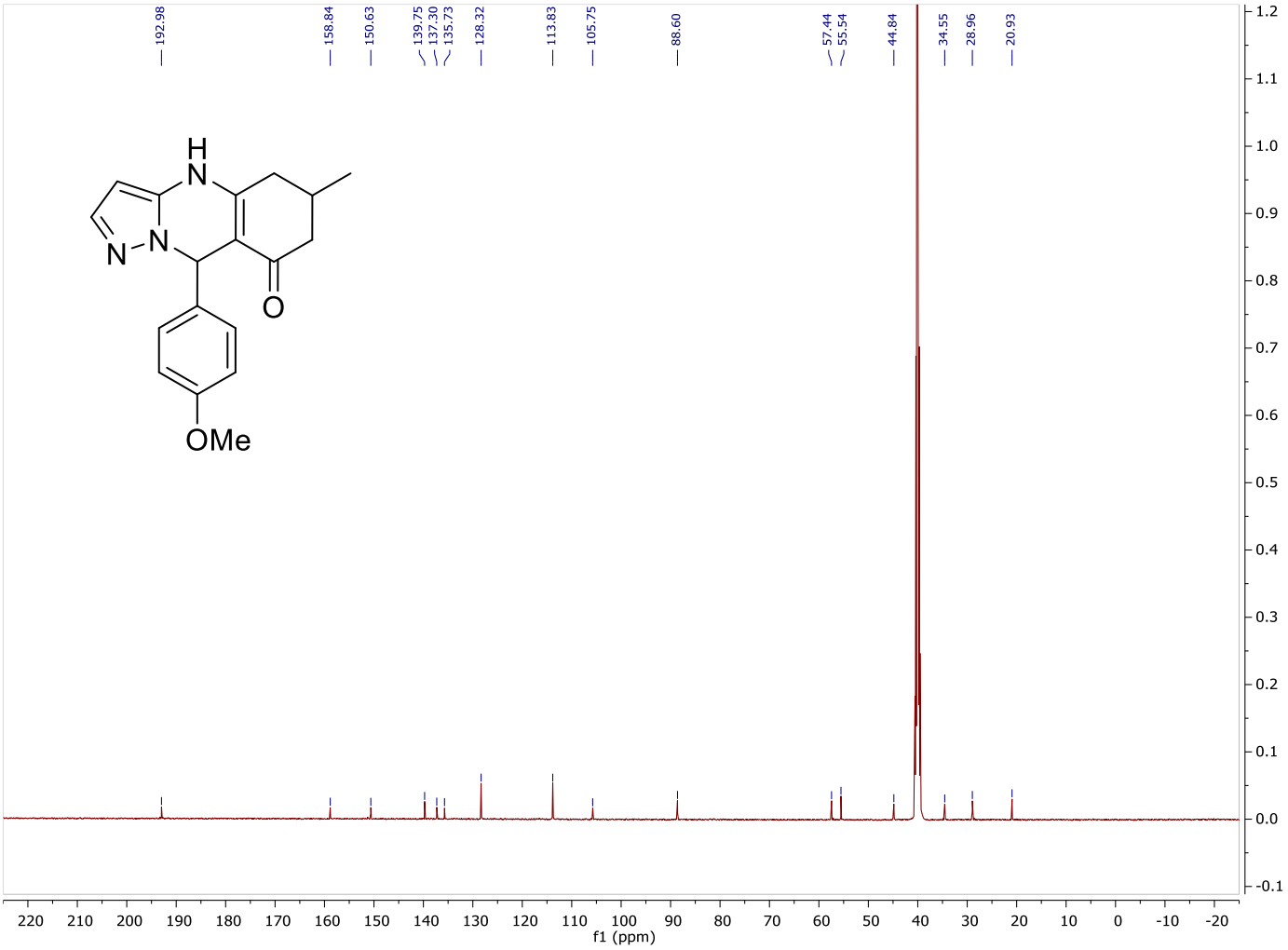
192.98
158.84
150.63
139.75
137.30
135.73
128.32
113.83
105.75
88.60
57.44
55.54
44.84
34.55
28.96
20.93
H
N
N
N
O
OMe
f1 (ppm)

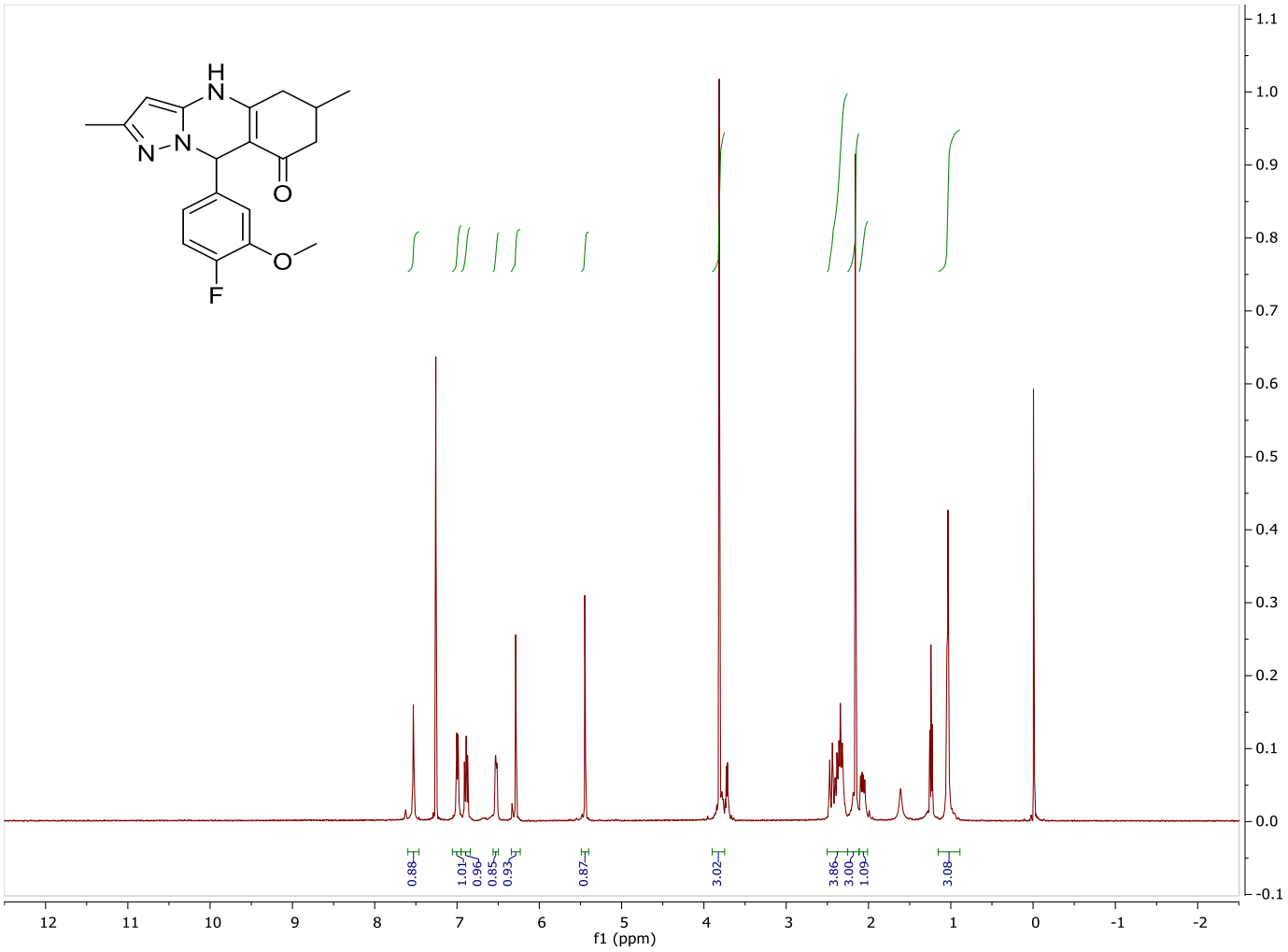
H
N
N
N
O
O
F
0.88
1.01
0.96
0.85
0.93
0.87
3.02
3.86
3.00
1.09
3.08
f1 (ppm)

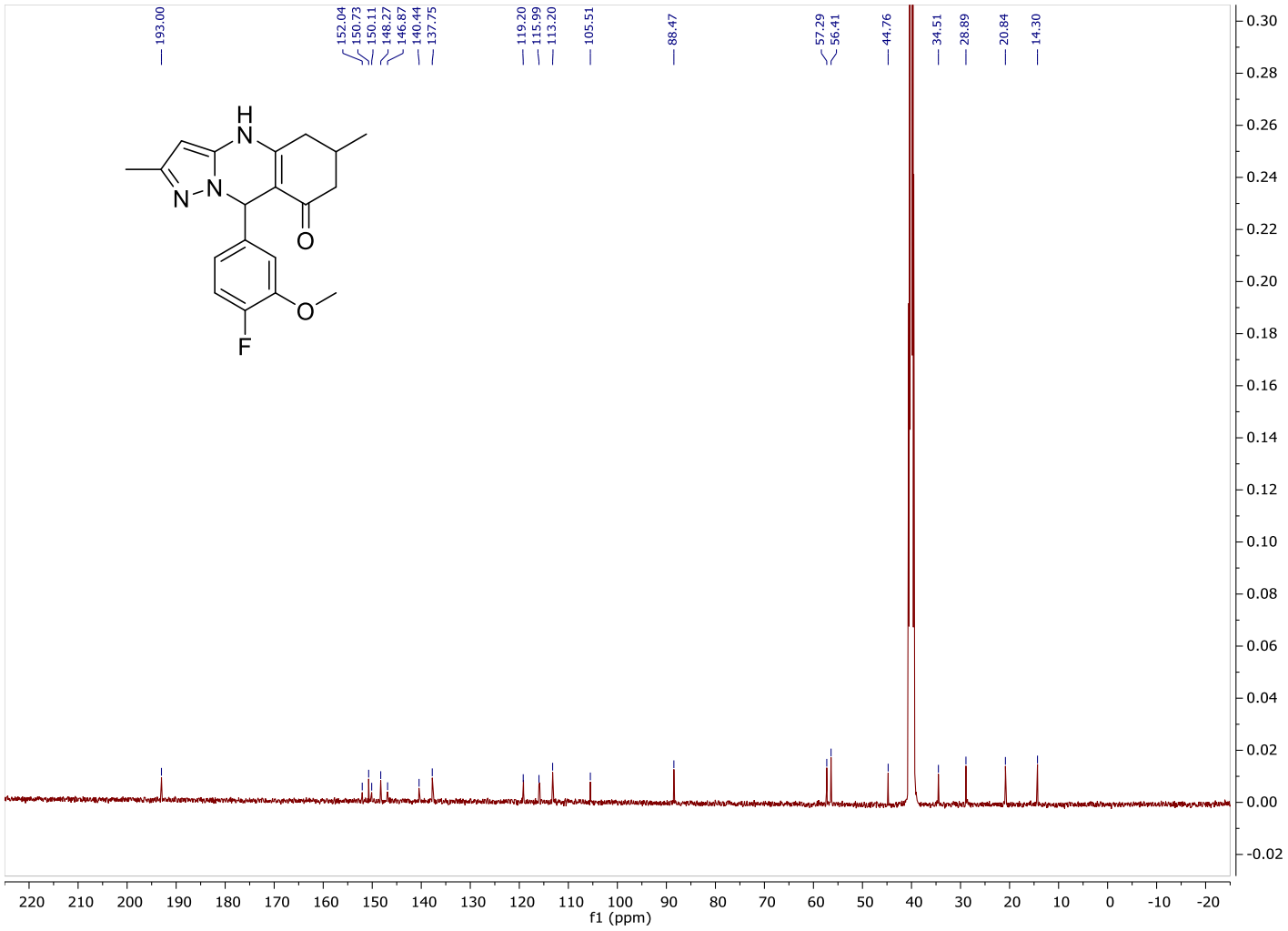
193.00
152.04
150.73
150.11
148.27
146.87
140.44
137.75
119.20
115.99
113.20
105.51
88.47
57.29
56.41
44.76
34.51
28.89
20.84
14.30
H
N
N
N
O
O
F
f1 (ppm)

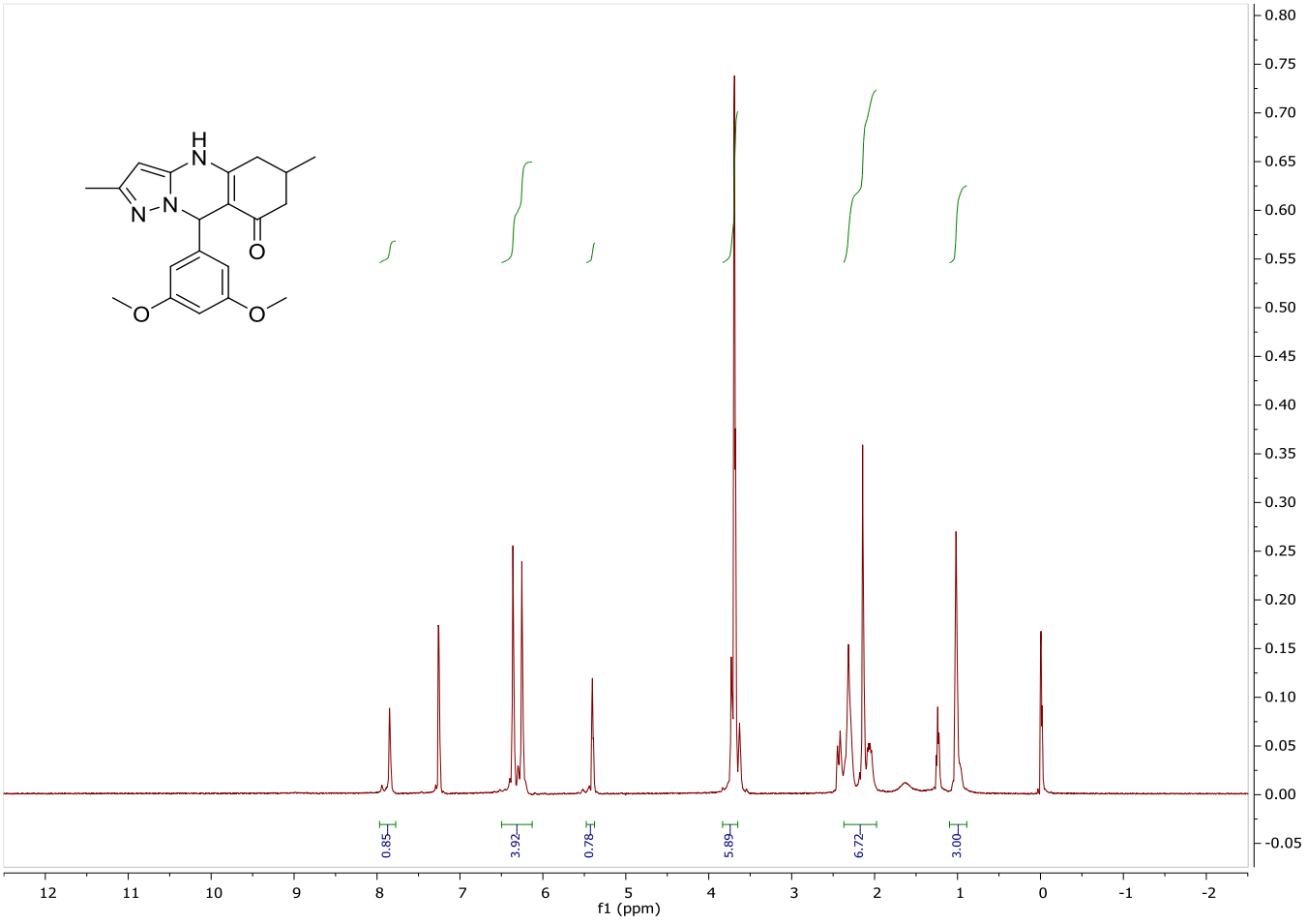
H
N
N
N
O
O
O
0.85
3.92
0.78
5.89
6.72
3.00
12
11
10
9
8
7
6
5
4
3
2
1
0
-1
-2
f1 (ppm)
0.80
0.75
0.70
0.65
0.60
0.55
0.50
0.45
0.40
0.35
0.30
0.25
0.20
0.15
0.10
0.05
0.00
-0.05

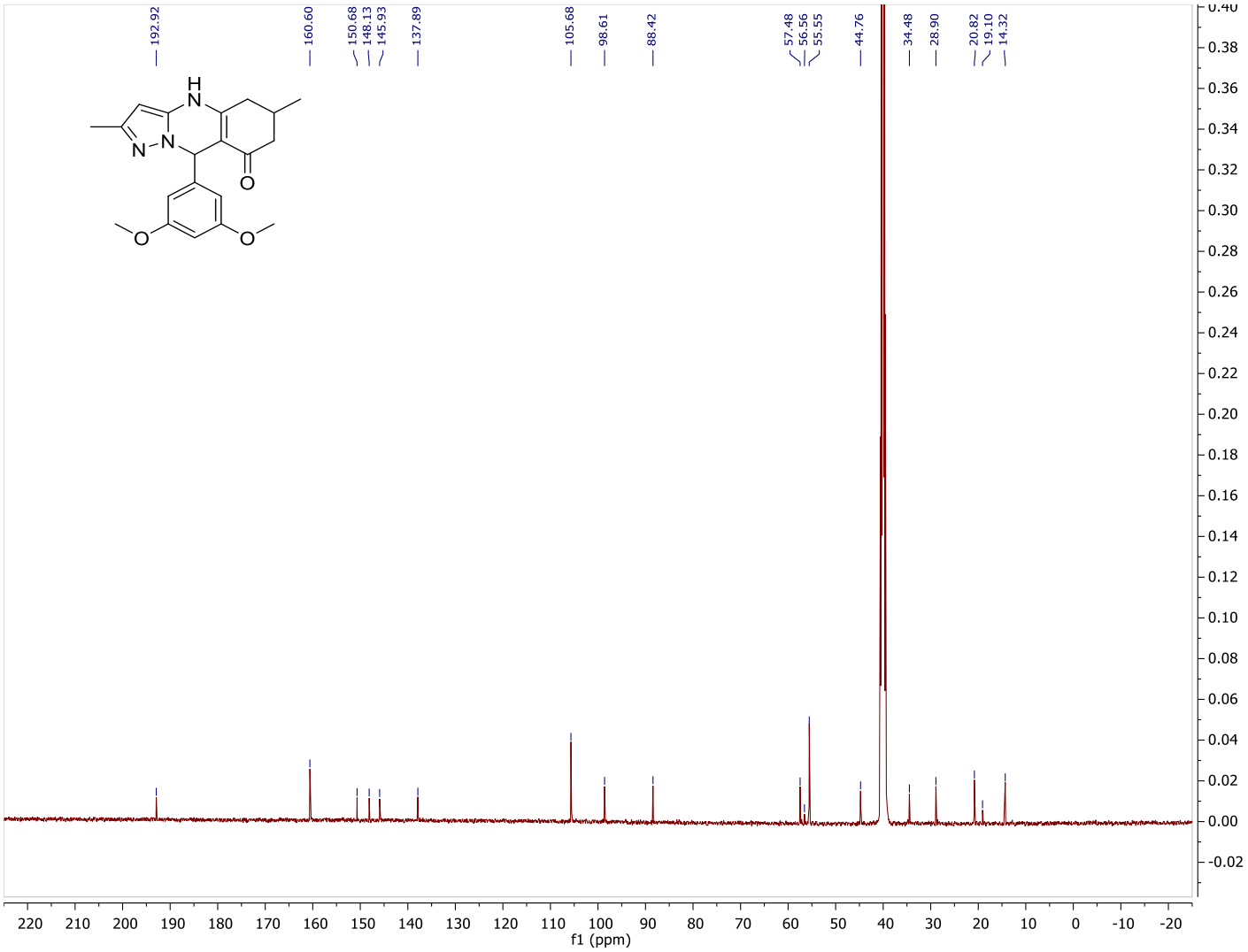
192.92
160.60
150.68
148.13
145.93
137.89
105.68
98.61
88.42
57.48
56.56
55.55
44.76
34.48
28.90
20.82
19.10
14.32
H
N
N
N
O
O
O
f1 (ppm)

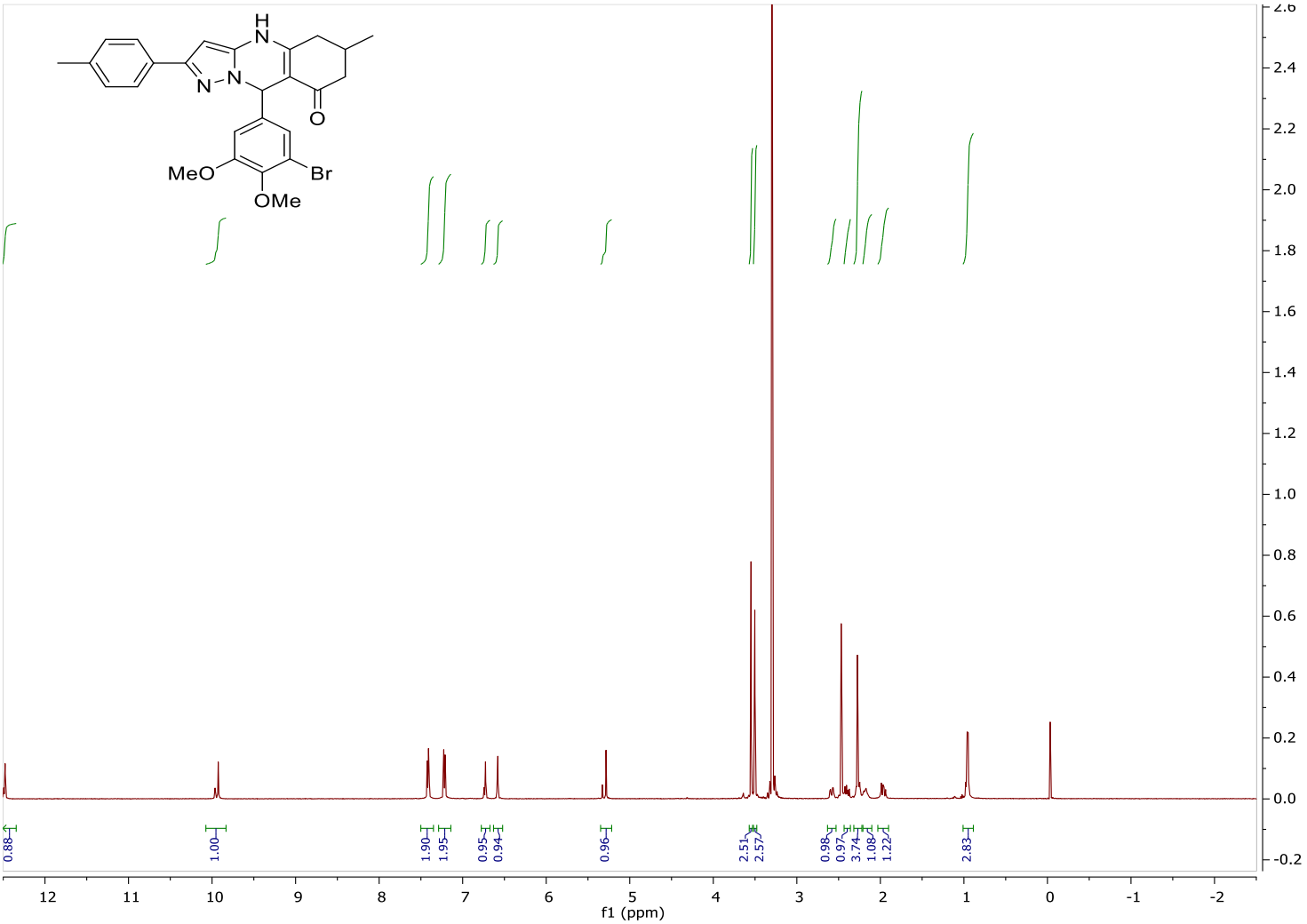
H
N
N
N
O
MeO
Br
OMe
0.88
1.00
1.90
1.95
0.95
0.94
0.96
2.51
2.57
0.98
0.97
3.74
1.08
1.22
2.83
12
11
10
9
8
7
6
5
4
3
2
1
0
-1
-2
f1 (ppm)
2.6
2.4
2.2
2.0
1.8
1.6
1.4
1.2
1.0
0.8
0.6
0.4
0.2
0.0
-0.2

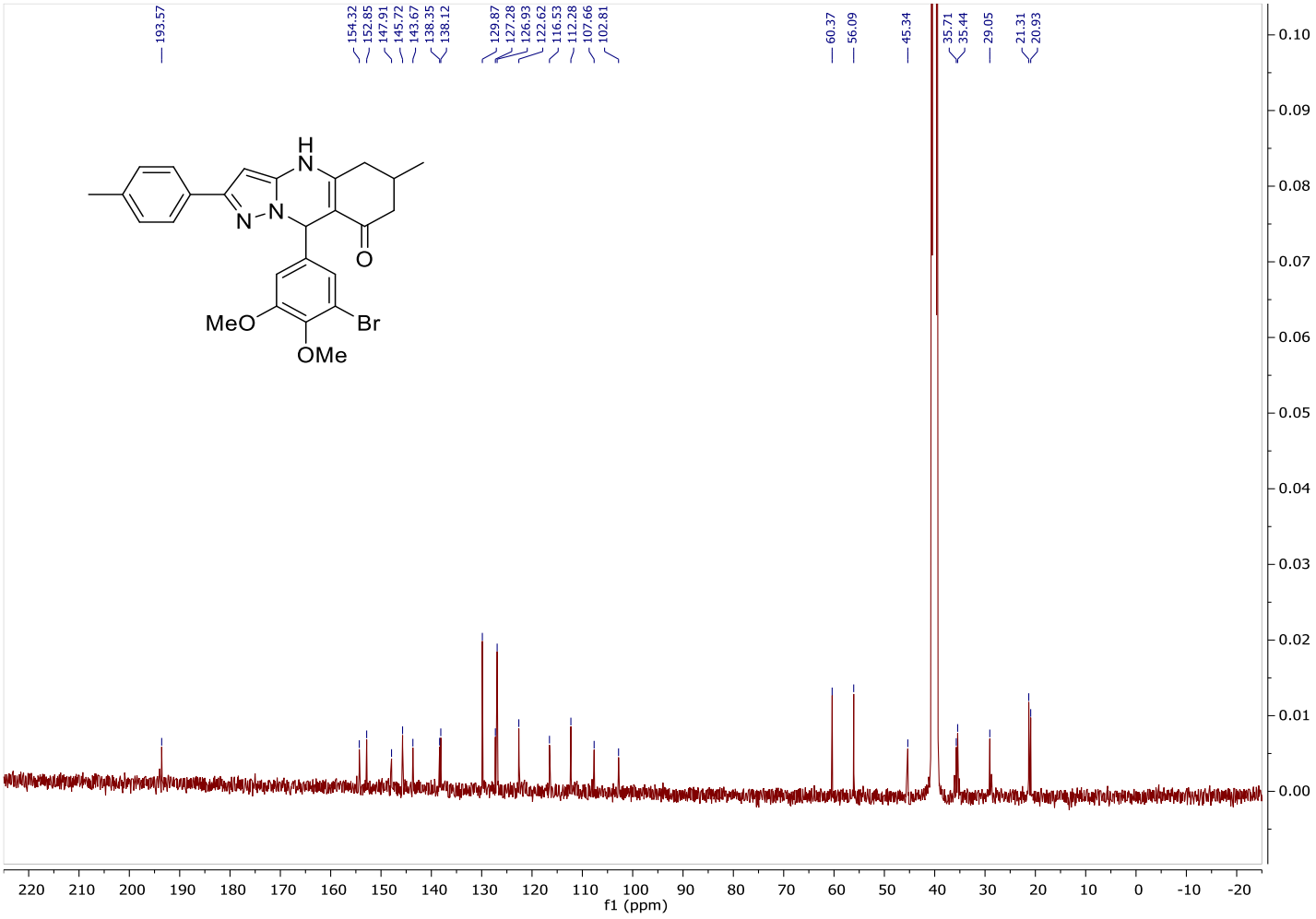
193.57
154.32
152.85
147.91
145.72
143.67
138.35
138.12
129.87
127.28
126.93
122.62
116.53
112.28
107.66
102.81
60.37
56.09
45.34
35.71
35.44
29.05
21.31
20.93
H
N
N
N
O
MeO
Br
OMe
f1 (ppm)

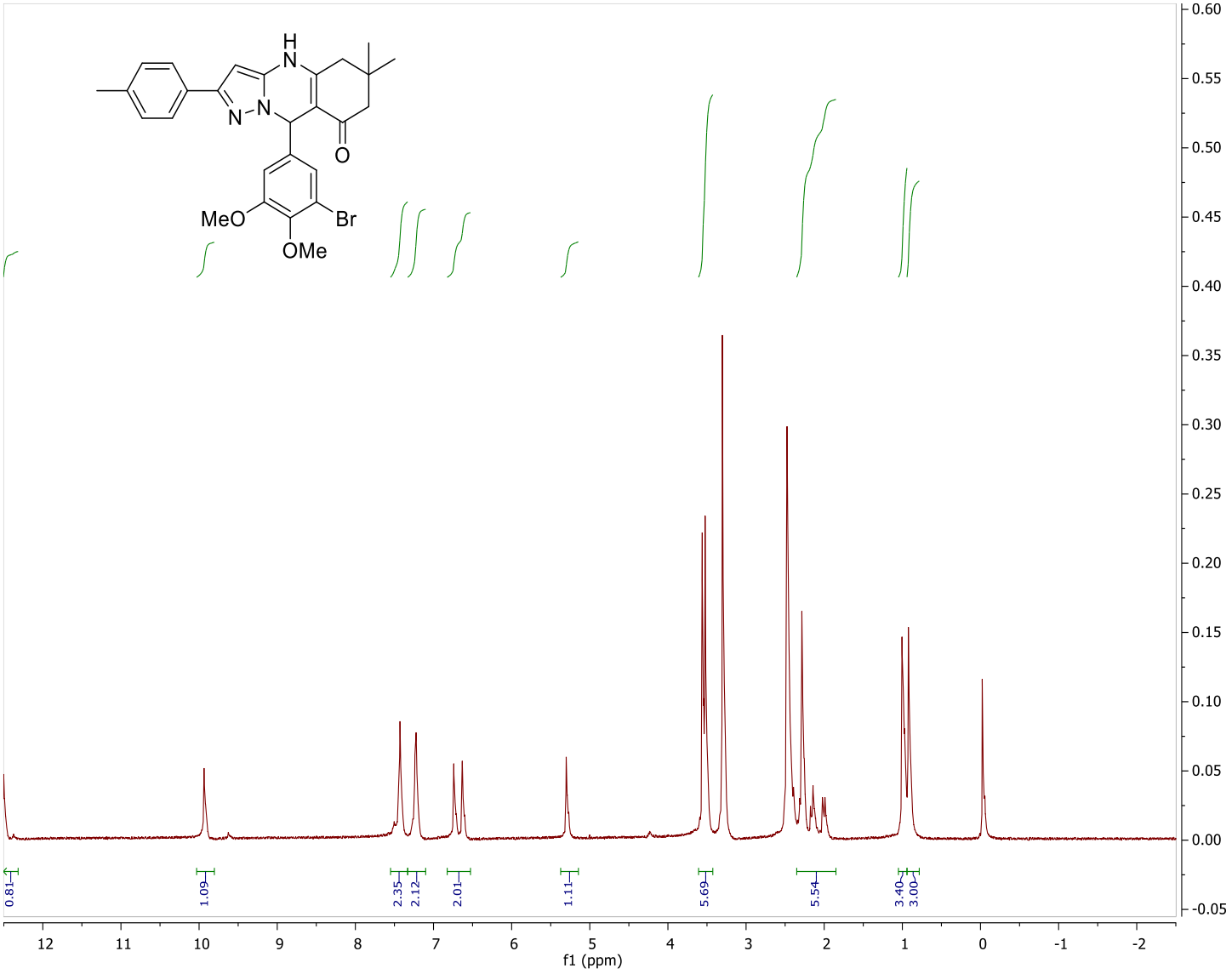
H
N
N
N
O
MeO
Br
OMe
0.81
1.09
2.35
2.12
2.01
1.11
5.69
5.54
3.40
3.00
12
11
10
9
8
7
6
5
4
3
2
1
0
-1
-2
f1 (ppm)
0.60
0.55
0.50
0.45
0.40
0.35
0.30
0.25
0.20
0.15
0.10
0.05
0.00
-0.05

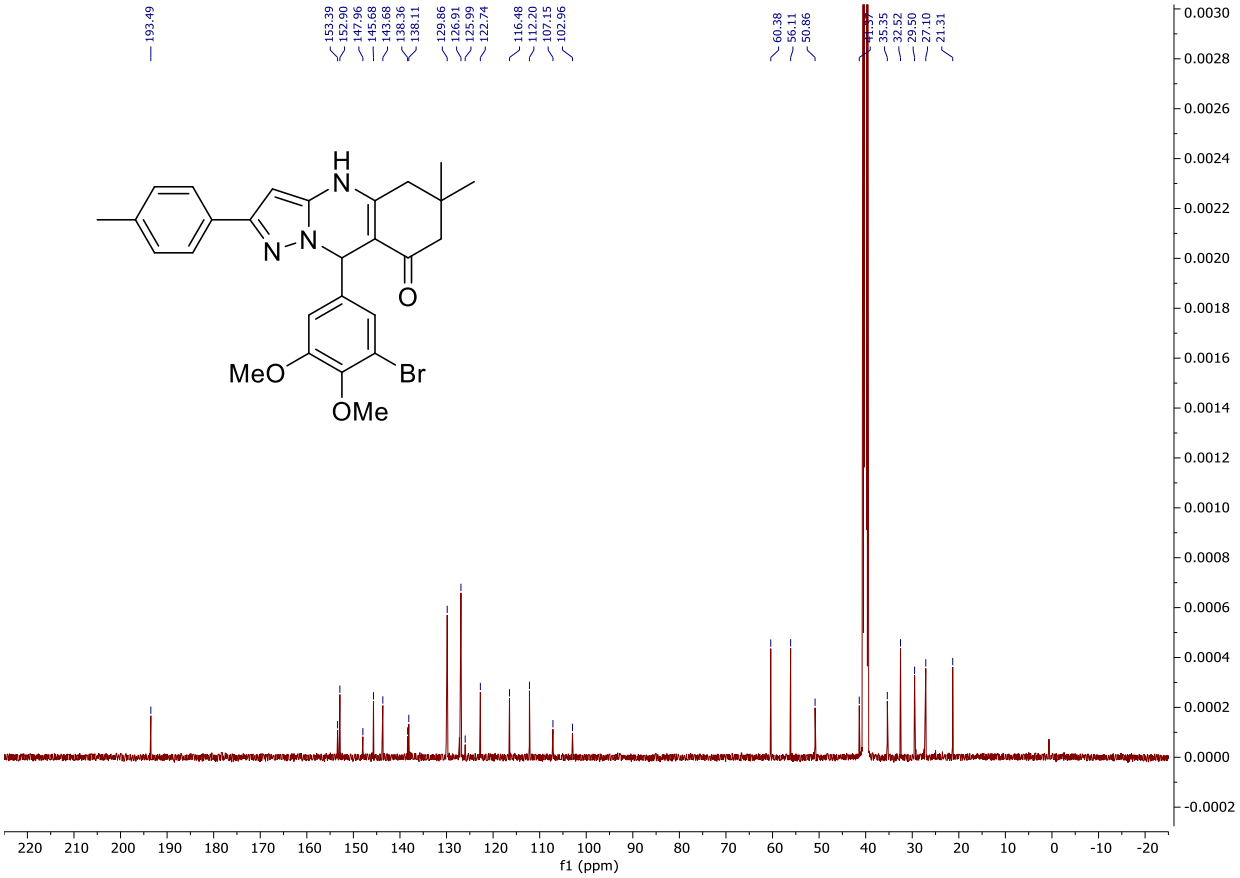
193.49
153.39
152.90
147.96
145.68
143.68
138.36
138.11
129.86
126.91
125.99
122.74
116.48
112.20
107.15
102.96
60.38
56.11
50.86
41.39
35.35
32.52
29.50
27.10
21.31
H
N
N
N
O
MeO
Br
OMe
f1 (ppm)

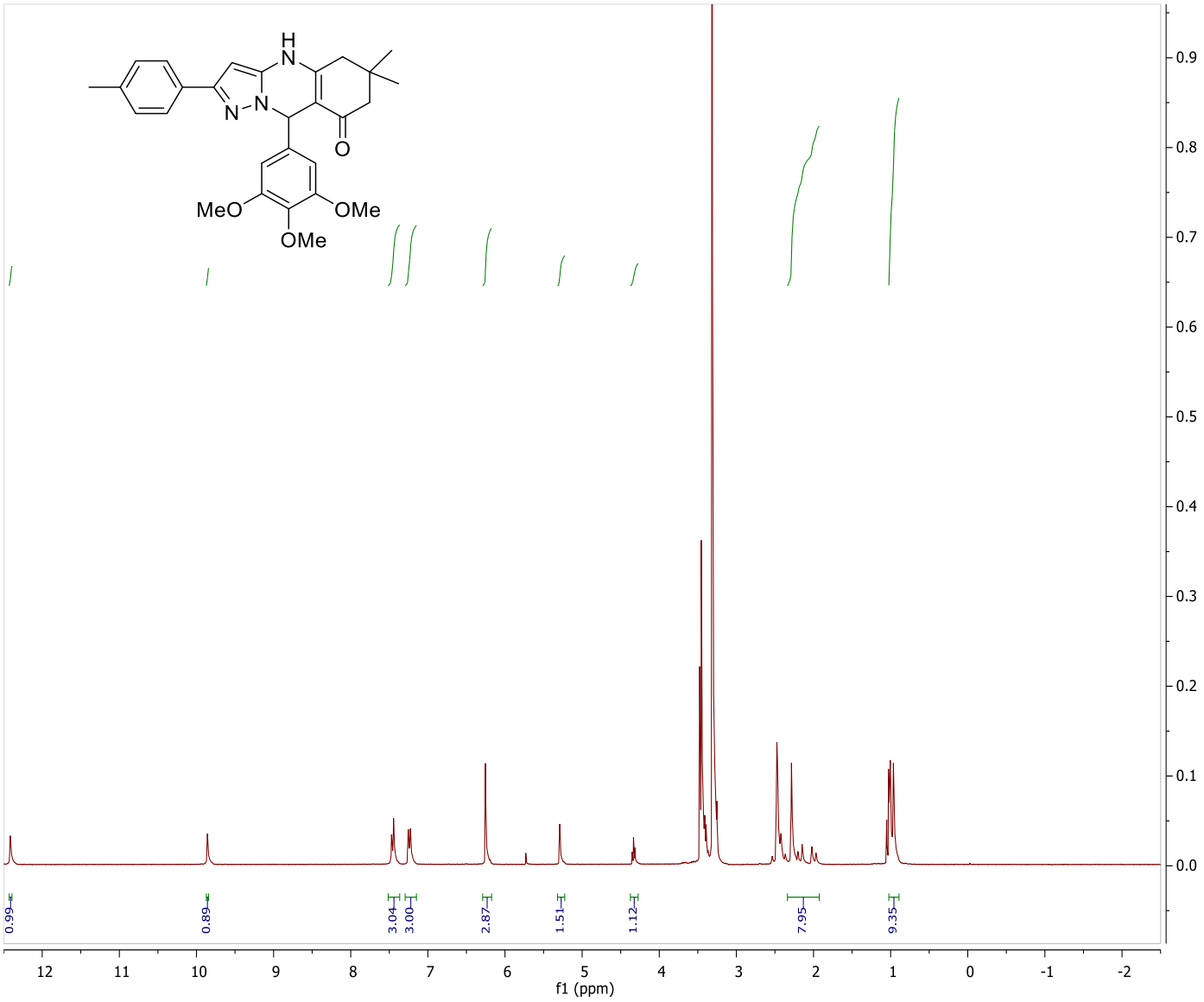
H
N
N
N
O
MeO
OMe
OMe
0.99
0.89
3.04
3.00
2.87
1.51
1.12
7.95
9.35
12
11
10
9
8
7
6
5
4
3
2
1
0
-1
-2
f1 (ppm)
0.9
0.8
0.7
0.6
0.5
0.4
0.3
0.2
0.1
0.0

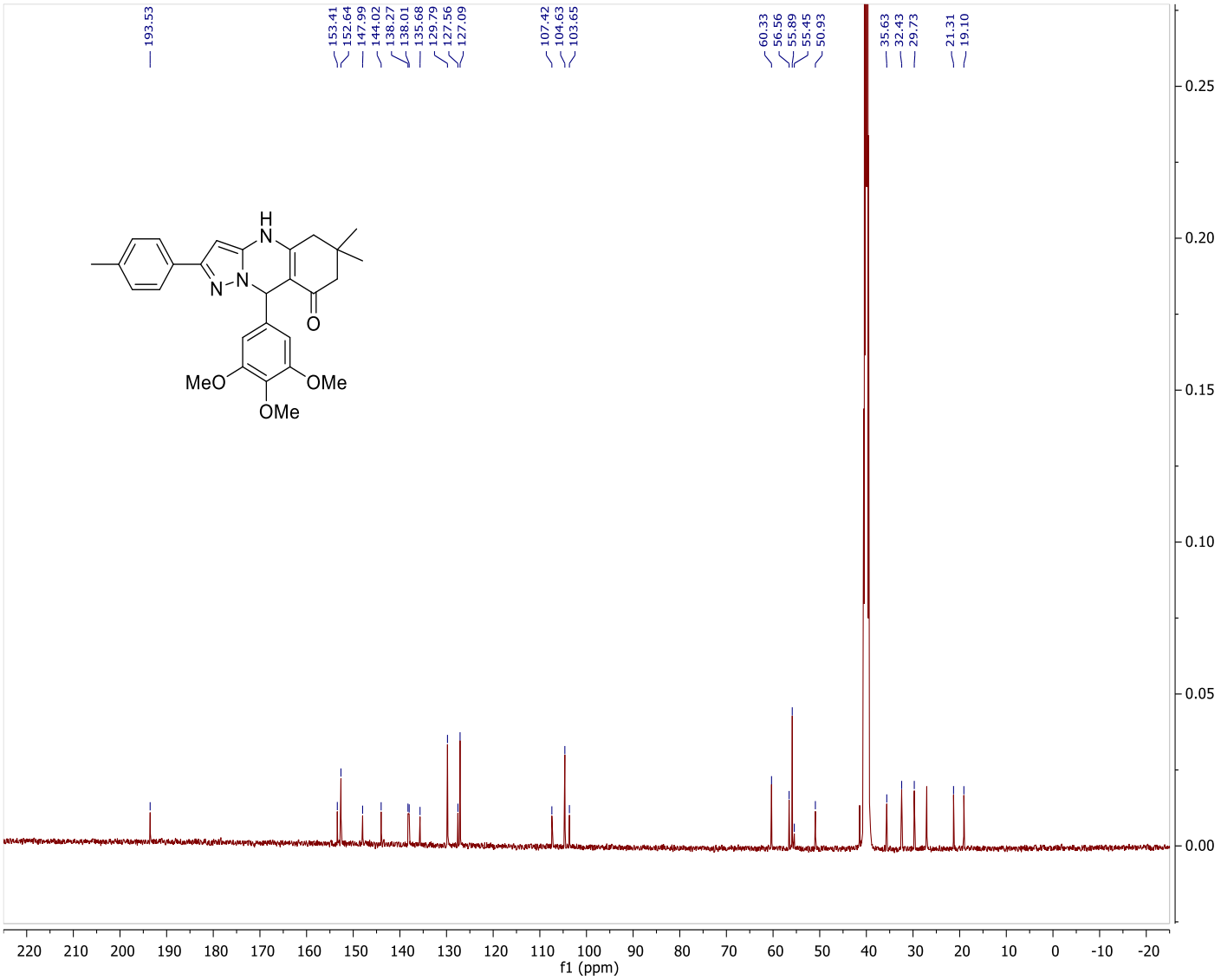
193.53
153.41
152.64
147.99
144.02
138.27
138.01
135.68
129.79
127.56
127.09
107.42
104.63
103.65
60.33
56.56
55.89
55.45
50.93
35.63
32.43
29.73
21.31
19.10
H
N
N
N
O
MeO
OMe
OMe
0.25
0.20
0.15
0.10
0.05
0.00
220 210 200 190 180 170 160 150 140 130 120 110 100 90 80 70 60 50 40 30 20 10 0 -10 -20
f1 (ppm)

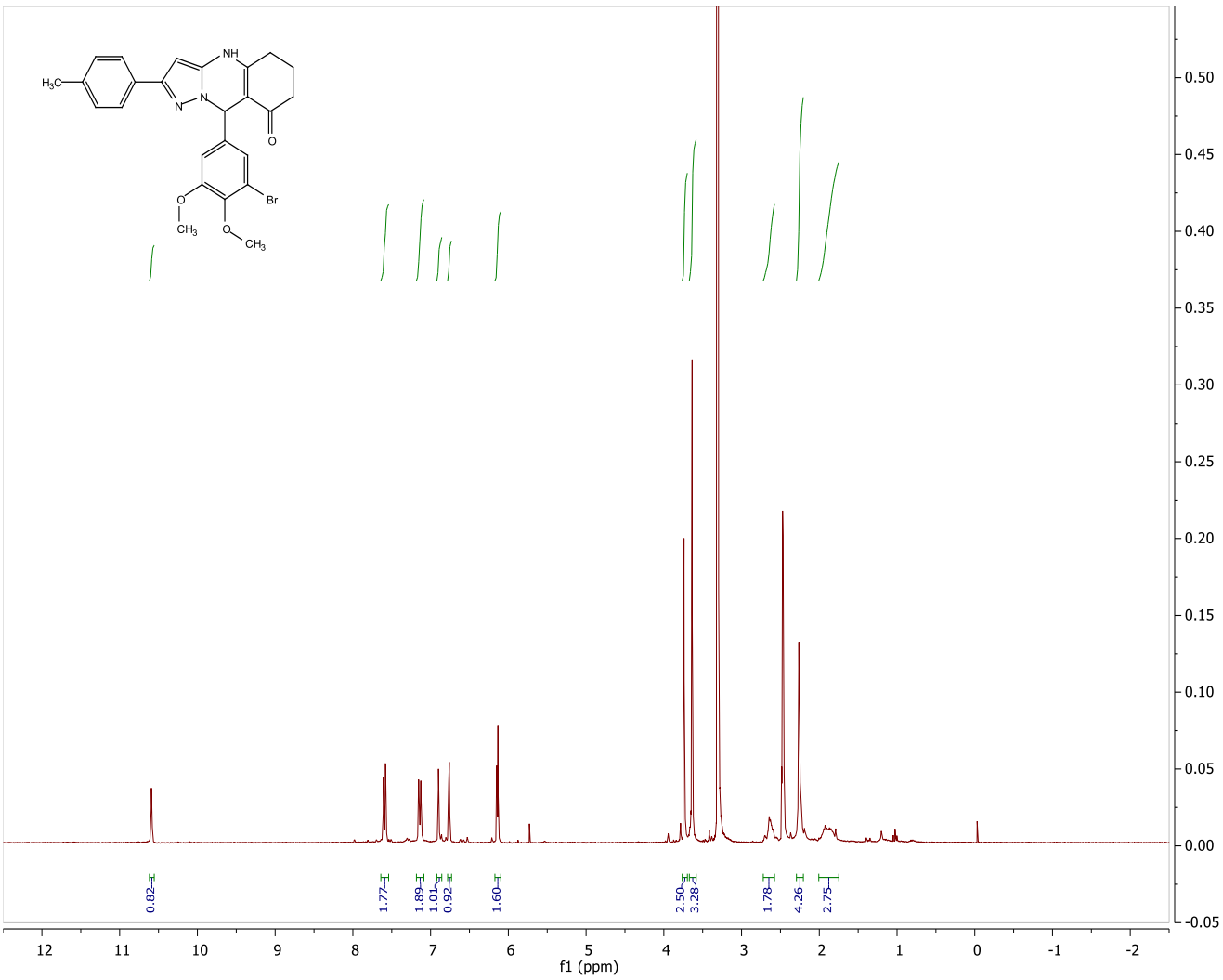
NH
H3C
N
N
O
Br
O
CH3
O
CH3
0.82
1.77
1.89
1.01
0.92
1.60
2.50
3.28
1.78
4.26
2.75
12
11
10
9
8
7
6
5
4
3
2
1
0
-1
-2
f1 (ppm)
0.50
0.45
0.40
0.35
0.30
0.25
0.20
0.15
0.10
0.05
0.00
-0.05

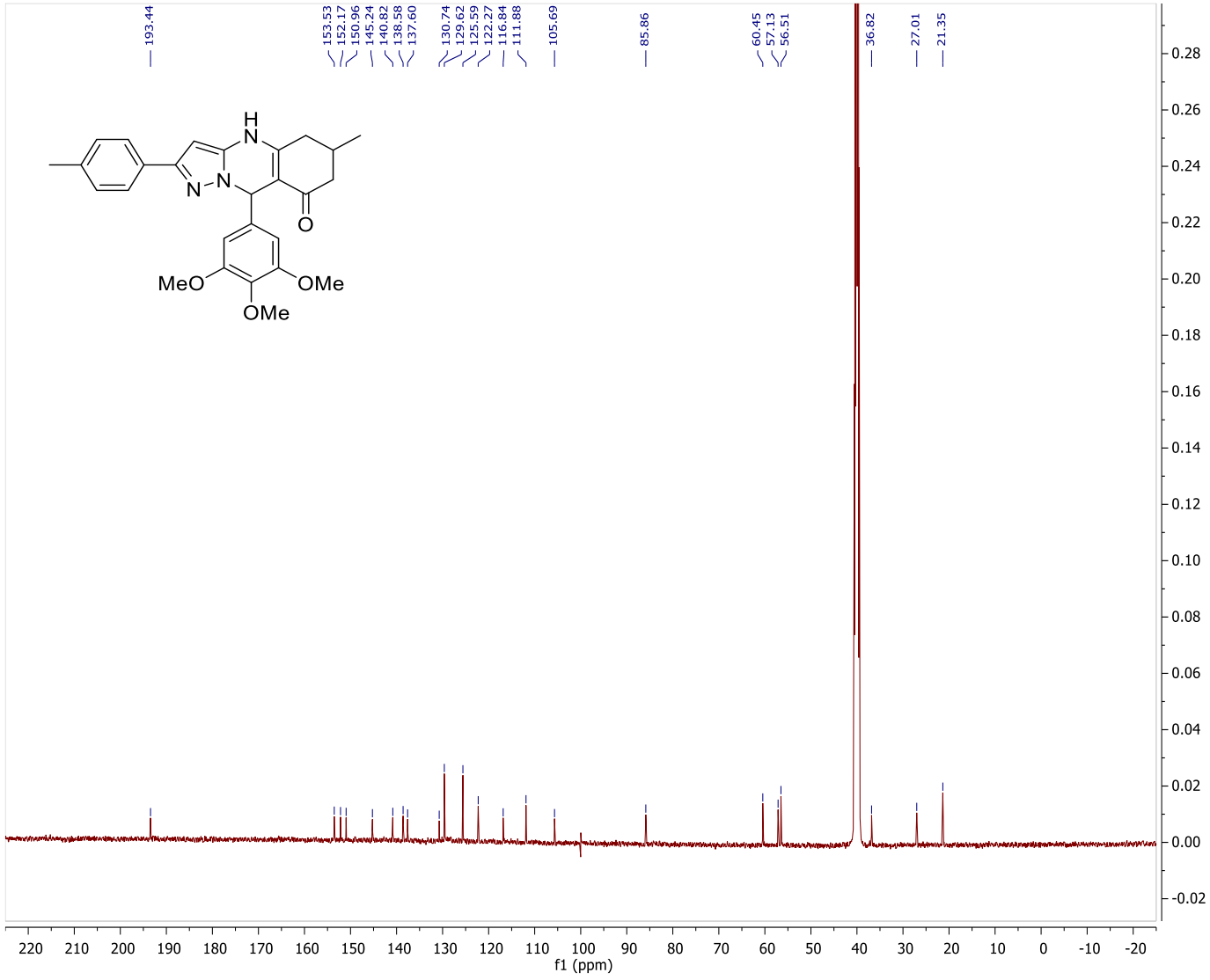
193.44
153.53
152.17
150.96
145.24
140.82
138.58
137.60
130.74
129.62
125.59
122.27
116.84
111.88
105.69
85.86
60.45
57.13
56.51
36.82
27.01
21.35
H
N
N
N
O
MeO
OMe
OMe
0.28
0.26
0.24
0.22
0.20
0.18
0.16
0.14
0.12
0.10
0.08
0.06
0.04
0.02
0.00
-0.02
220 210 200 190 180 170 160 150 140 130 120 110 100 90 80 70 60 50 40 30 20 10 0 -10 -20
f1 (ppm)

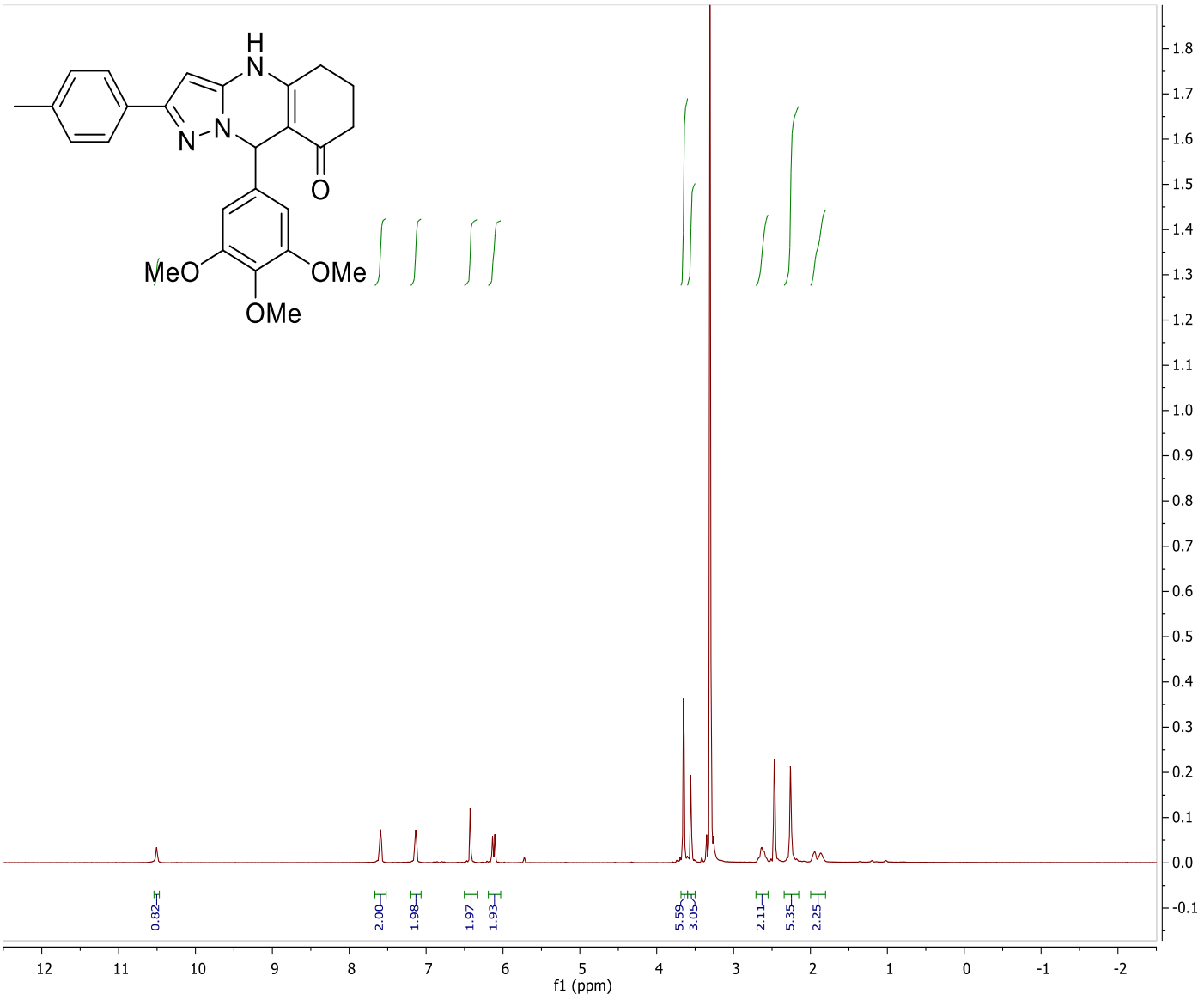
H
N
N
N
O
MeO
OMe
OMe
0.82
2.00
1.98
1.97
1.93
5.59
3.05
2.11
5.35
2.25
f1 (ppm)

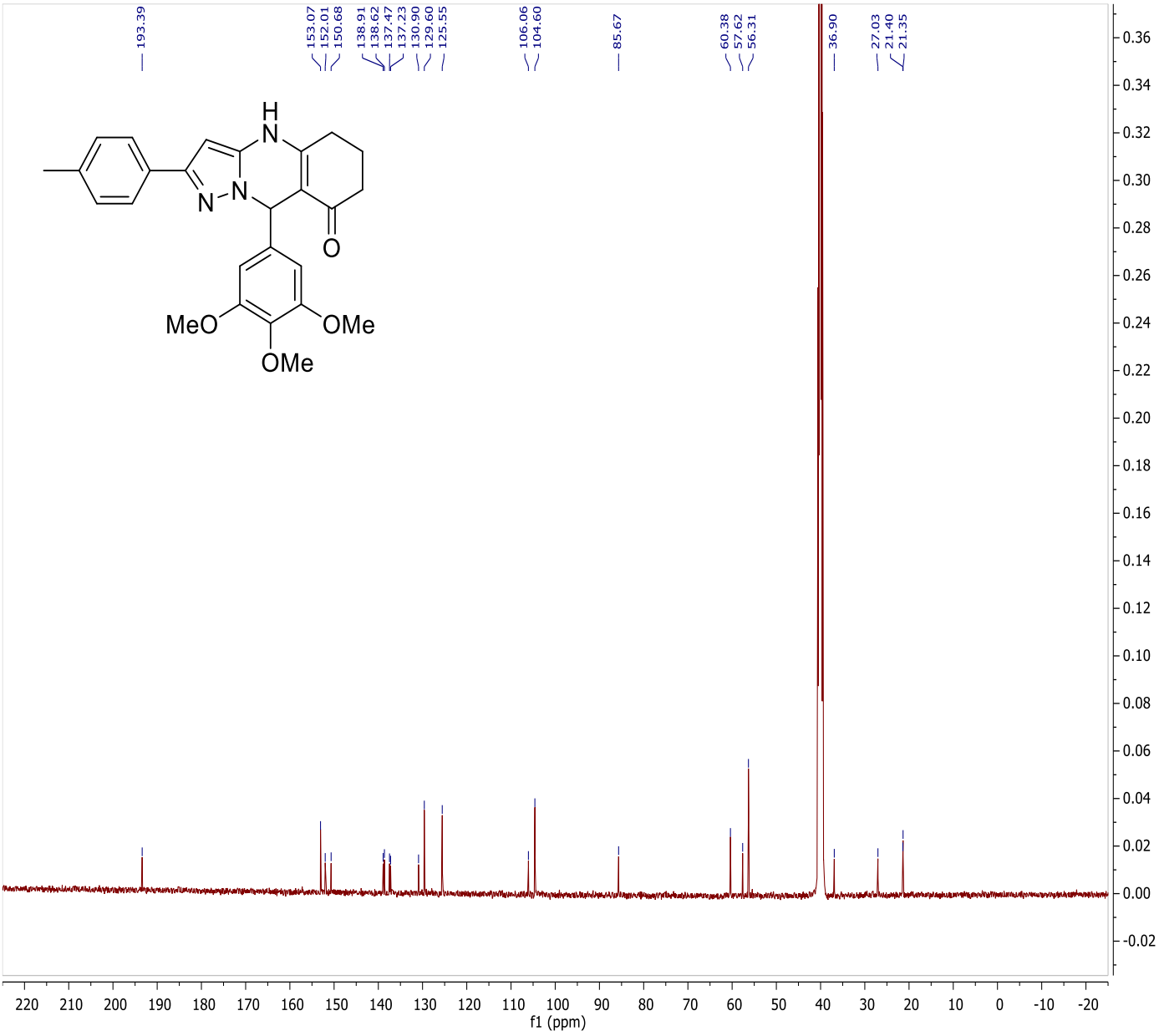
193.39
153.07
152.01
150.68
138.91
138.62
137.47
137.23
130.90
129.60
125.55
106.06
104.60
85.67
60.38
57.62
56.31
36.90
27.03
21.40
21.35
H
N
N
N
O
MeO
OMe
OMe
f1 (ppm)

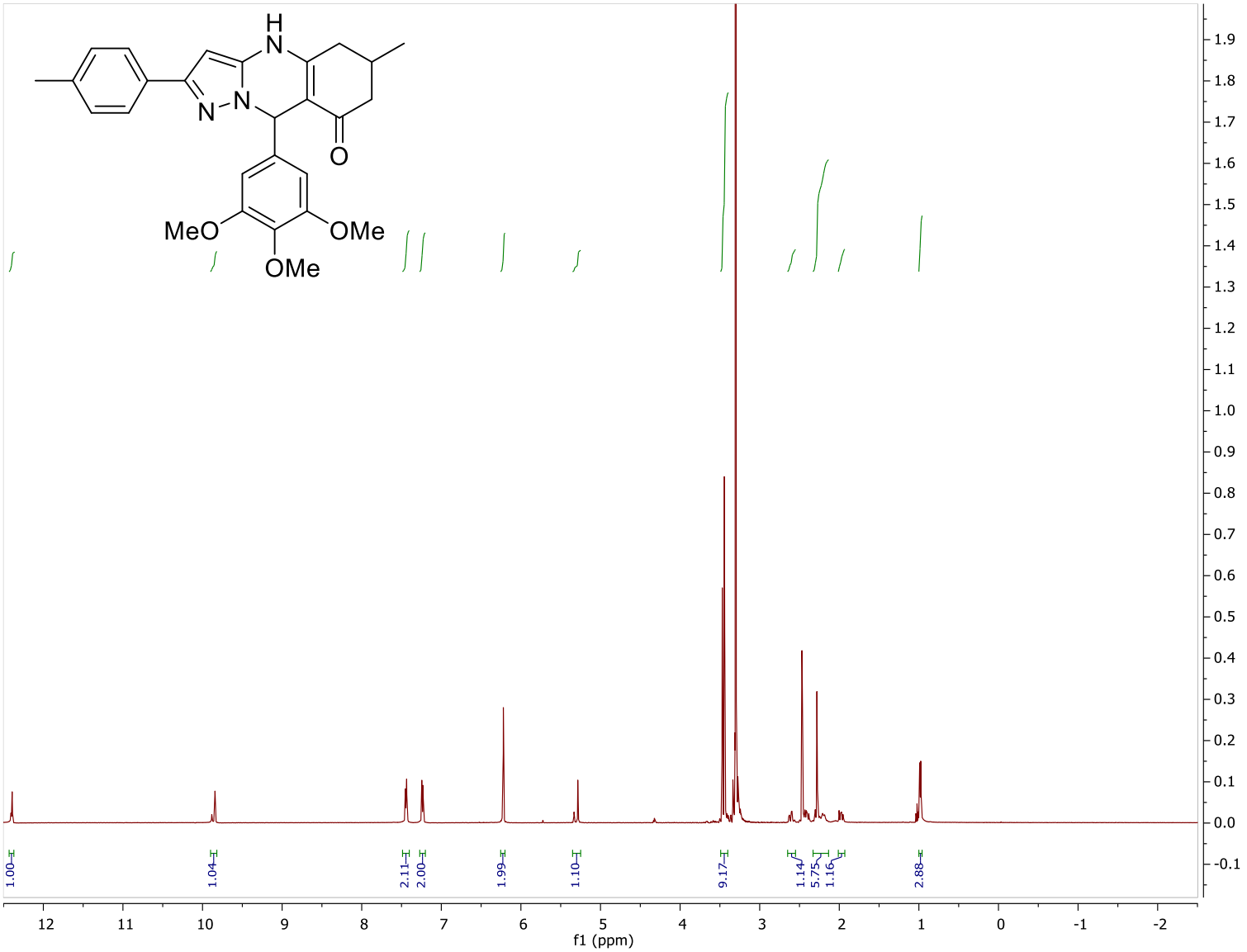
H
N
N
N
O
MeO
OMe
OMe
1.00
1.04
2.11
2.00
1.99
1.10
9.17
1.14
5.75
1.16
2.88
f1 (ppm)

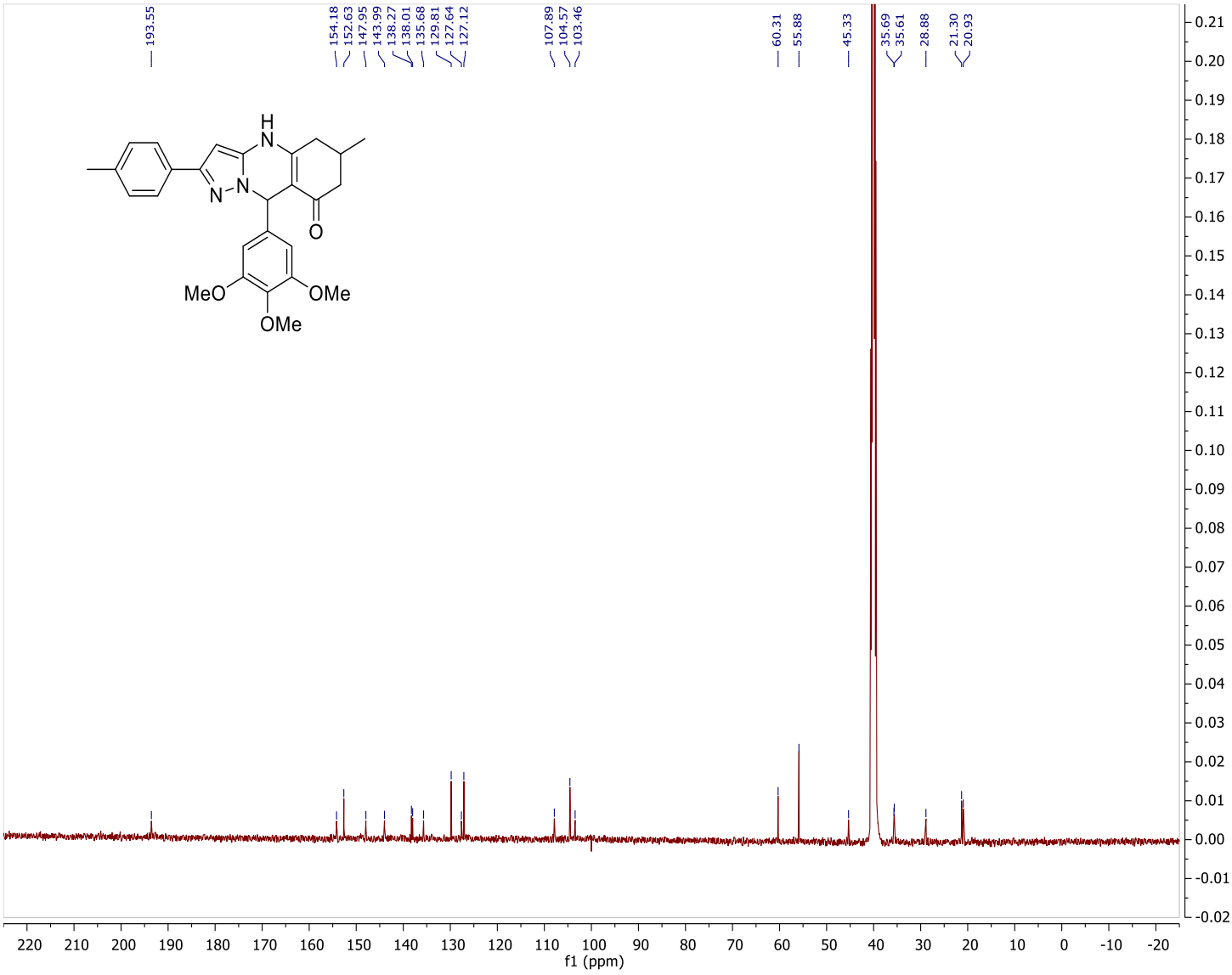
193.55
154.18
152.63
147.95
143.99
138.27
138.01
135.68
129.81
127.64
127.12
107.89
104.57
103.46
60.31
55.88
45.33
35.69
35.61
28.88
21.30
20.93
H
N
N
N
O
MeO
OMe
OMe
f1 (ppm)

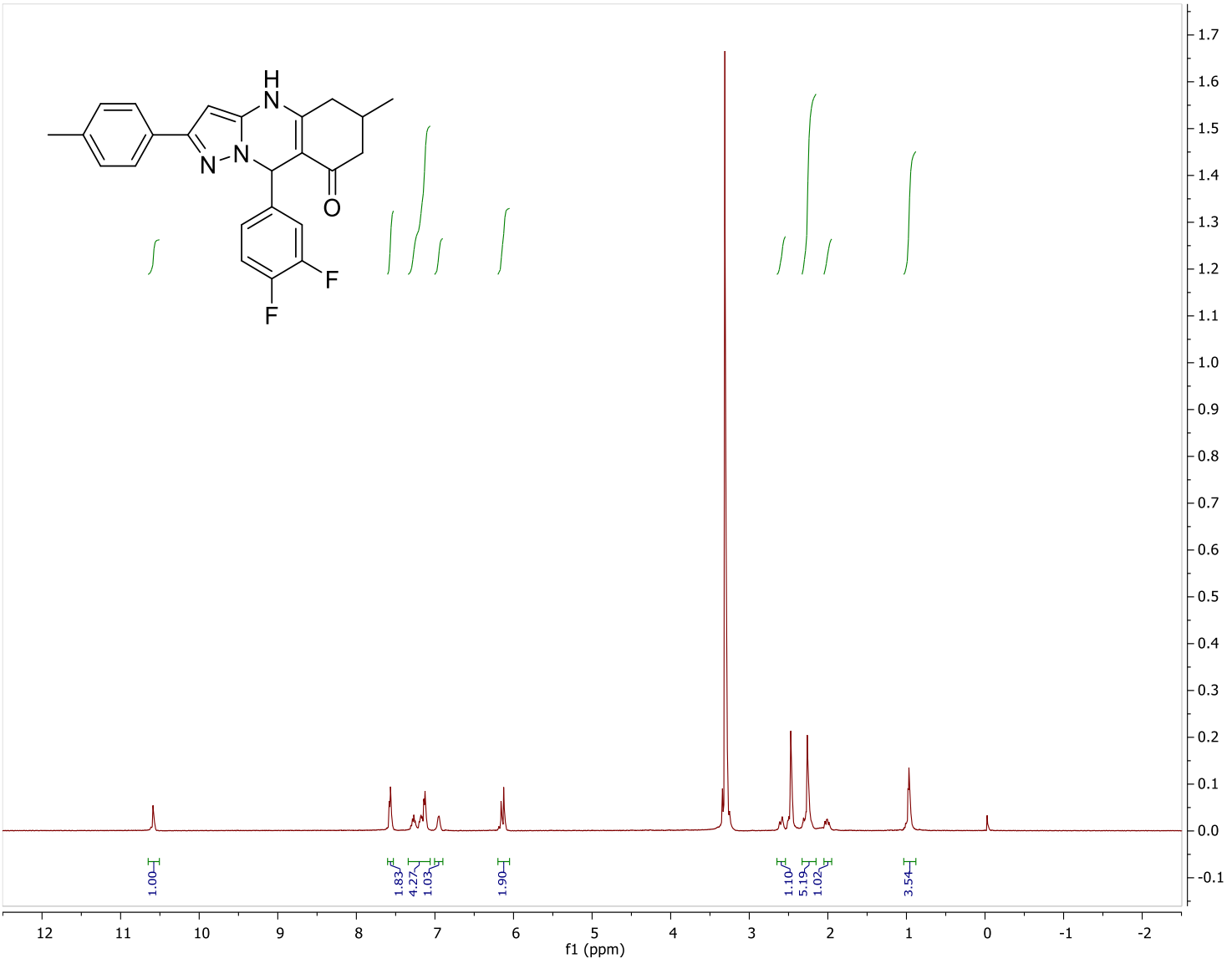
H
N
N
N
O
F
F
1.00
1.83
4.27
1.03
1.90
1.10
5.19
1.02
3.54
f1 (ppm)

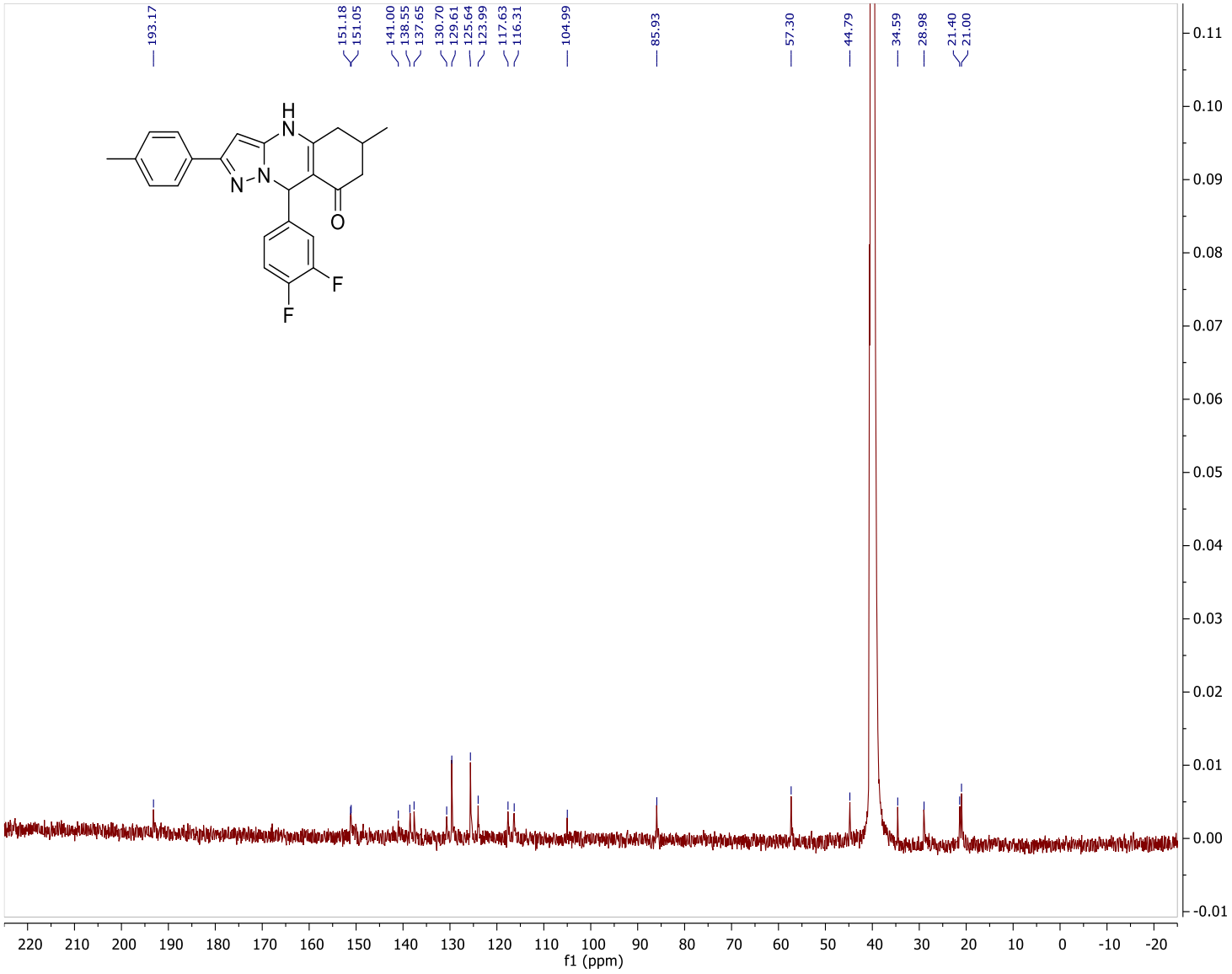
193.17
151.18
151.05
141.00
138.55
137.65
130.70
129.61
125.64
123.99
117.63
116.31
104.99
85.93
57.30
44.79
34.59
28.98
21.40
21.00
H
N
N
N
O
F
F
0.11
0.10
0.09
0.08
0.07
0.06
0.05
0.04
0.03
0.02
0.01
0.00
-0.01
220 210 200 190 180 170 160 150 140 130 120 110 100 90 80 70 60 50 40 30 20 10 0 -10 -20
f1 (ppm)

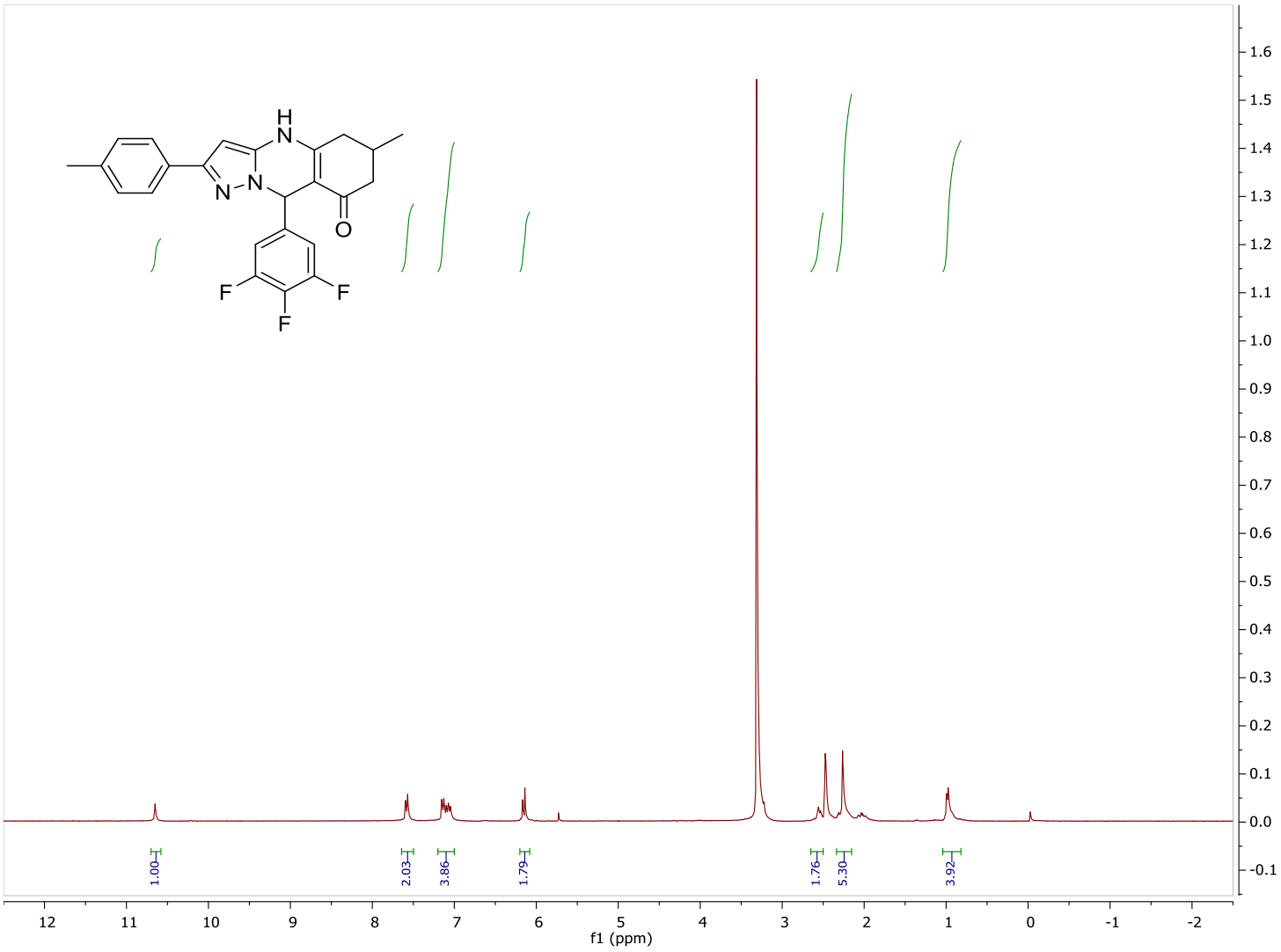
H
N
N
N
O
F
F
F
1.00
2.03
3.86
1.79
1.76
5.30
3.92
12
11
10
9
8
7
6
5
4
3
2
1
0
-1
-2
f1 (ppm)
1.6
1.5
1.4
1.3
1.2
1.1
1.0
0.9
0.8
0.7
0.6
0.5
0.4
0.3
0.2
0.1
0.0
-0.1

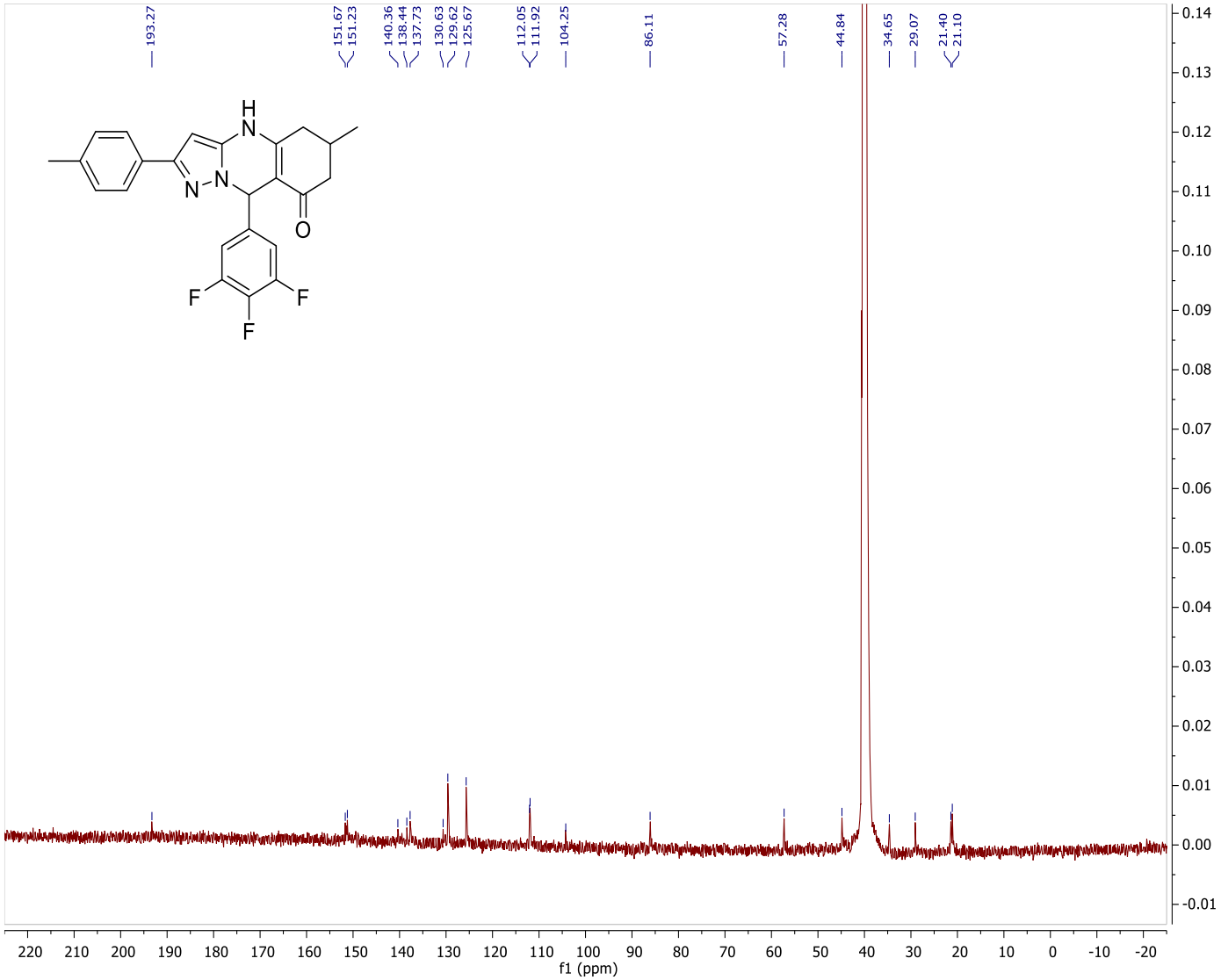
193.27
151.67
151.23
140.36
138.44
137.73
130.63
129.62
125.67
112.05
111.92
104.25
86.11
57.28
44.84
34.65
29.07
21.40
21.10
H
N
N
N
O
F
F
F
f1 (ppm)